POR-2036-V2(EX)
(WT-2036-V2)(EX)
EXTRACTED VERSION

OPERATION DOMINIC, FISH BOWL SERIES

Project Officers Report—Project 8A.2

Optical Phenomenology of High-Altitude Nuclear Detonations

D. F. Hansen, Project Officer
M. P. Shuler, Jr.
C. W. Wyckoff
W. P. Boquist
J. H. Campbell
W. T. Foreman
G. H. Hetley, Jr.
Edgerton, Germeshausen & Grier, Inc.
Boston, Massachusetts

9 October 196

NOTICE:
This is an extracted version of POR-2036 (WT-2036), Volume 2, OPERATION DOMINIC, Fish Bowl Series, Project 8A.2.

Extracted version prepared for
Director
DEFENSE NUCLEAR AGENCY
Washington, DC 20305-1000

1 September 1985

87

Destroy this report when it is no longer needed. Do not return to sender.

PLEASE NOTIFY THE DEFENSE NUCLEAR AGENCY ATTN: TITL, WASHINGTON, DC 20305 1000, IF YOUR ADDRESS IS INCORRECT, IF YOU WISH IT DELETED FROM THE DISTRIBUTION LIST, OR IF THE ADDRESSEE IS NO LONGER EMPLOYED BY YOUR ORGANIZATION.

DNA PRINTING PLANT

UNCLASSIFIED
SECURITY CLASSIFICATION OF THIS PAGE

AD-A995-489

REPORT DOCUMENTATION PAGE

1a. REPORT SECURITY CLASSIFICATION UNCLASSIFIED	1b. RESTRICTIVE MARKINGS
2a. SECURITY CLASSIFICATION AUTHORITY	3. DISTRIBUTION/AVAILABILITY OF REPORT Approved for public release; distribution is unlimited.
2b. DECLASSIFICATION/DOWNGRADING SCHEDULE	
4. PERFORMING ORGANIZATION REPORT NUMBER(S)	5. MONITORING ORGANIZATION REPORT NUMBER(S) POR-2036-V2(EX) (WT-2036-V2)(EX)
6a. NAME OF PERFORMING ORGANIZATION Edgerton, Germeshausen & Grier, Inc. 6b. OFFICE SYMBOL (*If applicable*)	7a. NAME OF MONITORING ORGANIZATION Defense Atomic Support Agency
6c. ADDRESS (*City, State, and ZIP Code*) Boston, MA	7b. ADDRESS (*City, State, and ZIP Code*) Washington, DC
8a. NAME OF FUNDING/SPONSORING ORGANIZATION 8b. OFFICE SYMBOL (*If applicable*)	9. PROCUREMENT INSTRUMENT IDENTIFICATION NUMBER
8c. ADDRESS (*City, State, and ZIP Code*)	10. SOURCE OF FUNDING NUMBERS PROGRAM ELEMENT NO. / PROJECT NO. / TASK NO. / WORK UNIT ACCESSION NO.

11 TITLE (*Include Security Classification*) OPERATION DOMINIC; FISH BOWL SERIES; PROJECT OFFICER'S REPORT--PROJECT 8A.2; Optical Phenomenology of High-Altitude Nuclear Detonations, Extracted Version

12. PERSONAL AUTHOR(S) D. F. Hansen, M. P. Shuler, Jr., C. W. Wyckoff, W. P. Boquist, J. H. Campbell, W. T. Foreman, G. H. Hetley, Jr.

13a. TYPE OF REPORT	13b. TIME COVERED FROM ____ TO ____	14. DATE OF REPORT (*Year, Month, Day*)	15. PAGE COUNT
		641009	470

16. SUPPLEMENTARY NOTATION This report has had sensitive military information removed in order to provide an unclassified version for unlimited distribution. The work was performed by the Defense Nuclear Agency in support of the DoD Nuclear Test Personnel Review Program.

17. COSATI CODES		
FIELD	GROUP	SUB-GROUP
18	3	
20	6	

18. SUBJECT TERMS (*Continue on reverse if necessary and identify by block number*)
Dominic, Star Fish, King Fish, Fish Bowl, Check Mate, Tight Rope, Optical Phenomenology, Blue Gill

19. ABSTRACT (*Continue on reverse if necessary and identify by block number*)

This report describes the optical coverage of the five Fish Bowl high-altitude bursts. The basic information on these bursts was obtained with an extensive group of sophisticated photographic and spectrographic instruments. In the burst area, these instruments were placed in land-based and airborne recording stations. The southern conjugate area instruments which were used for investigating auroral phenomena were on land-based stations. A verifying temporal and spatial framework which was used for the identification of various observed phenomena was provided for each event by means of qualitative phenomenology and descriptions of each event illustrated by a selection of photographs of graphical presentations of final values of various geometric parameters. These parameters are fireball diameter versus time, fireball and cloud rise rates, motion of internal and external shock waves, debris motions, and location and dimensions of auroras in the southern magnetic conjugate area. A radiance versus time history is given for each event. Also presented are identification of atomic and molecular species obtained from spectral measurements which extend from microseconds to many minutes after detonations.

20. DISTRIBUTION/AVAILABILITY OF ABSTRACT ☒ UNCLASSIFIED/UNLIMITED ☐ SAME AS RPT. ☐ DTIC USERS	21. ABSTRACT SECURITY CLASSIFICATION UNCLASSIFIED
22a. NAME OF RESPONSIBLE INDIVIDUAL MARK D. FLOHR	22b. TELEPHONE (*Include Area Code*) 202-325-7559 / 22c. OFFICE SYMBOL DNA/ISCM

DD FORM 1473, 84 MAR — 83 APR edition may be used until exhausted. All other editions are obsolete.

SECURITY CLASSIFICATION OF THIS PAGE
UNCLASSIFIED

POR-2036-V2 (EX)
(WT-2036-V2) (EX)
EXTRACTED VERSION

OPERATION DOMINIC

FISH BOWL SERIES

PROJECT OFFICER'S REPORT - PROJECT 8A.2

Optical Phenomenology of High-Altitude Nuclear Detonations

D. F. Hansen, Project Officer
M. P. Shuler, Jr.
C. W. Wyckoff
W. P. Boquist
J. H. Campbell
W. T. Foreman
G. H. Hetley, Jr.
Edgerton, Germeshausen & Grier, Inc.
Boston, Massachusetts

9 October 1964

NOTICE

This is an extract of POR-2036 (WT-2036), Volume 2, OPERATION DOMINIC, FISH BOWL SERIES, Project 8A.2.

Extracted version prepared for
Director
DEFENSE NUCLEAR AGENCY
Washington, DC 20305-1000

1 September 1985

FOREWORD

Classified material has been removed in order to make the information available on an unclassified, open publication basis, to any interested parties. The effort to declassify this report has been accomplished specifically to support the Department of Defense Nuclear Test Personnel Review (NTPR) Program. The objective is to facilitate studies of the low levels of radiation received by some individuals during the atmospheric nuclear test program by making as much information as possible available to all interested parties.

The material which has been deleted is either currently classified as Restricted Data or Formerly Restricted Data under the provisions of the Atomic Energy Act of 1954 (as amended), or is National Security Information, or has been determined to be critical military information which could reveal system or equipment vulnerabilities and is, therefore, not appropriate for open publication.

The Defense Nuclear Agency (DNA) believes that though all classified material has been deleted, the report accurately portrays the contents of the original. DNA also believes that the deleted material is of little or no significance to studies into the amounts, or types, of radiation received by any individuals during the atmospheric nuclear test program.

OPERATION DOMINIC

FISH BOWL SERIES

PROJECT OFFICERS REPORT—PROJECT 8A.2

OPTICAL PHENOMENOLOGY OF HIGH-ALTITUDE NUCLEAR DETONATIONS

D. F. Hansen, Project Officer
M. P. Shuler, Jr.
C. W. Wyckoff
W. P. Boquist
J. H. Campbell
W. T. Foreman
G. H. Hetley, Jr.

Edgerton, Germeshausen & Grier, Inc.
160 Brookline Avenue
Boston, Massachusetts

CONTENTS

TABLES

FIGURES

CHAPTER 3

STAR FISH PRIME PHOTOGRAPHIC RESULTS

Star Fish Prime was detonated at 0900:09.0290Z on July 9, 1962. For the convenience of the reader some general information on Star Fish Prime as well as its warhead configuration and yield have been extracted from Reference 12 and given below. Where superseded by later information the DASA Data Center information has been changed to incorporate the later values.

The actual position and height of burst as determined by Sandia Corporation are given below. The predicted values are shown for comparison:

	Planned	Actual
Latitude	16° 28' 14.16" N	16° 28' 06.56" N
Longitude	169° 37' 31.44" W	169° 37' 48.37" W
Altitude	400.000 km	400.094 km

Positions of the instrumentation pods with respect to the re-entry vehicle at the time of detonation are presented in Table 3.1. They were taken from Reference 13. The x-axis is positive East, the y-axis is positive true North and the z-axis is positive upward.

3.1 INSTRUMENTATION

3.1.1 Camera Parameters. More than 130 cameras and spectrographs were used on Star Fish Prime. The parameter settings for the cameras used are given in Tables 3.2 through 3.4.

A table is devoted to each of the two aircraft stations and the Johnston Island Station. For the most part the tables are self-explanatory, but a few comments are in order. The station position designator is a number assigned to a camera mount position for bookkeeping purposes and has no real significance here. Film types are abbreviated according to standard nomenclature which may be found in **Section** 2.6. A five-digit perforation number was assigned to each data record. This number is important for reference purposes in that it identifies a single record from among the more than 900 other Project 8A.2 Fish Bowl records. Throughout the report, references are frequently made to specific records by the perforation number only. The perforation number is coded for easy identification of event, station, and instrument. The code is given in **Section** 2.6. The last two digits of the number refer to a specific instrument.

For each camera, the film type, either black and white or color, was chosen mainly on the basis of sensitivity. Star Fish Prime was predicted to have low radiance levels for most **phenomena**; therefore, high-sensitivity films were used for the most part.

It was expected that Star Fish Prime optical phenomena would be of enormous geometric proportions. For this reason photographic coverage from the two aircraft and Johnston Island,

as indicated by the elevation and azimuth columns of the tables, was quite diverse.

Except for the KFC-600 camera, no neutral-density filters were used on any cameras on Star Fish Prime. Again, this was a matter of maximizing the sensitivity of the camera-film combination for the expected low light levels. At the very early framing times of the KFC-600 cameras the predicted radiance levels required that these cameras be attenuated in sensitivity. A Wratten 12 color filter was used with the KFC-600 cameras to eliminate a blue light leak in the Kerr cells when in the closed position.

On the fast-framing cameras, which in all cases were pointed at the burst, the longest possible focal length lenses were used. This choice was an obvious one considering the fact that at early times the debris was confined to a very narrow subtense and remained bright for only a brief span of time. The numbers and shutter sector openings of all cameras were set for maximum possible exposures, while the frame rates were chosen on the basis of providing the best possible time resolution for fast cameras, and a wide selection of exposures to cover a large dynamic range of possible radiance levels.

Several Robot cameras at each station were equipped with interference filters in an attempt to photograph the disturbed air in the wavelengths of the ionized nitrogen molecule, N_2^+, and the auroral atomic lines of [OI].

3.1.2 Aircraft Positions. Star Fish Prime posed a difficult problem in positioning of the two aircraft shared jointly by Projects 8A.1 and 8A.2. It was highly desirable from the standpoint of Project 8A.2 that one aircraft have a minimum slant range to the burst in order to have large image sizes of the burst at early times. On the other hand, aircraft close to the burst would not be in position to photograph the full extent of the optical phenomena. Project 8A.1 had special requirements on the aircraft locations which were dictated by their project objectives. The objectives of both projects were compatible to the extent that a compromise solution was effected which was satisfactory to both projects. The aircraft positions are given in Table 3.5. Aircraft 53120 was located to provide minimum slant range to the burst. The minimum range was determined by the camera elevation angles provided in the aircraft camera mounts. The 45-degree elevation angle used on Aircraft 53120 for Star Fish was the highest elevation angle possible for the majority of those fast cameras which were expected to view the burst point. An eastern position was selected for this aircraft,

because it was felt that constraints imposed on beta particles and debris by the geomagnetic field would limit the observable phenomena to a general north-south plane centered on the burst, with the growth of the aurora in the east-west direction limited to distances well inside the radial distance of the aircraft from the burst. Thus, it was thought that the eastern aircraft, even at minimum slant range, would remain outside or at least on the fringe of the optically excited area and be in a position to record some of its extent, especially the penetration of debris into the atmosphere in the downward direction.

Aircraft 53120 had little success in recording any of the large optical phenomena which occurred. The reasons were twofold: first the predicted radiance levels were much larger than those which actually occurred, so that a majority of films were either underexposed or obtained no records. Secondly, the debris pancake was not observed as expected. Indeed, if it occurred at all, it was of very peculiar shape because of the asymmetric manner in which debris emanated from the explosion.

The other aircraft, Aircraft 53144, was located north of the burst point at the maximum permissible slant range. The camera mounts for the high-speed cameras had a minimum elevation angle of 25 degrees. From this vantage point it was expected that the debris and beta-ray deposition history at the northern conjugate point could be observed in addition to the early time history of the burst itself. While this proved true to some extent, an unexpected additional deposition of debris and beta-rays occurred far north of this aircraft. This unexpected deposition was due to the high altitude to which debris rose above the 400-kilometer burst point. This unexpected deposition was not recorded by the northern aircraft.

The concept of stationing the aircraft 90 degrees or more apart on concentric circles centered on the burst was particularly important from the standpoint of viewing asymmetries of the detonation. This concept was used on all five events, with a greater degree of success on the succeeding events than was achieved in Star Fish Prime.

Aircraft 53144 was located due north (magnetic) of the burst point at H-Hour, and in line with the above concept, Aircraft 53120 was 90 degrees due east (magnetic). The easterly position was selected

rather than a westerly one in order to minimize the flying time from Hickam to the zero-hour position.

The tracks of the aircraft for the first few minutes after zero time are shown in Figure 3.1. The flight patterns of both aircraft consisted of chords of a circle centered on the burst. The length of the chords was governed mainly by the fields of view of the longer focal length cameras.

Both aircraft maintained their circular flight pattern for approximately 1 hour in order for Project 8A.1 to make measurements on long-term infrared effects in the atmosphere. Because of the short time history of the ultraviolet and visible optical effects, the Project 8A.2 mission was completed a few minutes after the detonation.

In the case where long-focal-length lenses are employed, the problem is one of properly aiming them at the predicted burst point. The pointing techniques used by Project 8A.2 on all events are described in Section 2.5. From Johnston Island these techniques were sufficiently accurate to guarantee that mispointing would not be a cause of loss of data if the detonation occurred near the predicted burst point. Pointing from aircraft involved not only setting proper elevation and azimuth angles for cameras, but also the positioning of the aircraft at a precise geographical point at a precise

time, with the proper aircraft heading and attitude. This navigational task is difficult and can be a source of large pointing errors. Focal lengths of lenses used on the aircraft were chosen with rough estimates of these potential errors in mind. Even this allowance was not sufficient in some cases to overcome the large accidental errors in position which actually occurred such as happened to Aircraft 60376 on Check Mate. On Star Fish Prime, the position, heading, and attitude of the two aircraft were within the estimated capabilities of the aircraft. A minor loss of camera records from aircraft occurred, which in retrospect was found to be caused by the errors in camera pointing angles and not navigational errors.

The second major cause of loss of camera data, that of error in burst position, was not a source of difficulty on Star Fish Prime. Normally, the maximum focal length of a lens is chosen so that the field of view of a camera will encompass the 2σ error box plus the predicted radius of the fireball (or other phenomenon of interest) at the time of film run-out for that particular camera. This did not cover the situation on Star Fish Prime which was quite different in its phenomenology from that of the other Fish Bowl events. In general, the use of focal lengths on Star Fish Prime was:to use the longest

possible focal lengths on the fastest cameras, to use the shortest possible focal lengths for the slowest cameras, and to use a graduated set of focal lengths for intermediate-speed cameras. On Star Fish Prime the error in burst position was easily encompassed by the most narrow field of view which was employed.

Table 3.6 provides a summary of pointing information pertinent to Johnston Island (Station J-820). It gives the actual and predicted elevation and azimuth angles to the burst point from the J-820 station as stated in Reference 14. The slant range to the burst from the station was slightly over 401 kilometers.

The positions of the stations with respect to the predicted burst point are indicated in Figure 3.2. Ground ranges and bearing angles are shown nominally for purposes of illustration. In reality the curvature of the earth was taken into account in the pointing of the aircraft.

Figures 3.3 through 3.5 show the fields of view relative to predicted and actual air zero for a number of cameras on each of the two aircraft and Johnston Island. The fields of view are in a plane perpendicular to the optical axes of the cameras passing through the predicted burst point.

At every station the task of pointing was primarily that of aiming the optical axes of the cameras at predicted air zero. In the case of the aircraft where the optical axes and predicted air zero are not coincident (Figures 3.3 and 3.4) the error was primarily due to misalignment or roll of the aircraft. As a result of such errors the Photo-Sonics 4C cameras aboard the aircraft suffered considerable loss of data records, while the Photo-Sonics 10B cameras with their wider fields of view were able to encompass both the predicted and actual burst points.

Where the optical axes of cameras are not coincident with predicted air zero (Figure 3.5) the error is one of aiming the cameras. In comparison with the aircraft pointing errors the Johnston Island angular errors are small; however, because of the longer focal length lenses and narrow fields of view, the angular errors were significant. However, no data was lost at that station due to pointing.

3.2 RECORD SUMMARIES

Summaries of the Project 8A.2 records for Star Fish Prime are presented in Tables 3.7 through 3.9. The summaries present in brief form pertinent comments on the films obtained from the two aircraft and Johnston Island stations.

The statistical success in useful camera records achieved by Project 8A.2 on Star Fish Prime is summarized by Table 3.10. Inappropriate camera parameters are the reasons given for either failure to obtain records or for poor records. This information is somewhat misleading, in that in most cases the failure was a result of the brightness of the various phenomena on Star Fish Prime being so low that they did not record, or barely recorded. Most of the cameras were operating at maximum sensitivity settings, so that the failures could not have been avoided. The overall success in obtaining useful records from the two aircraft and Johnston Island was 50 percent.

3.3 PICTORIAL HISTORY

Star Fish Prime was essentially a nuclear detonation in a vacuum. The optical features of this event had little resemblance to the other Fish Bowl events. Optical stations located at Johnston Island recorded little except X-ray-induced air fluorescence and the very early debris expansion. The remainder of the optical phenomena were of such enormous proportions that little evidence of their existence was seen from Johnston Island. The two aircraft optical stations, even though they were located at considerable distances from ground zero, suffered an almost similar fate;

Aircraft 53144 situated north of the northern conjugate point was able to add to its records only the northern conjugate beta-ray deposition. It was only from the very-long-range optical stations such as the Project 8A. 2 Mauna Loa station that the full extent of the Star Fish Prime phenomena could be recorded.

The earliest Project 8A. 2 records were obtained from Johnston Island with a 2500-frame-per-second Photo-Sonics 4C camera using a 500-millimeter lens. Figures 3. 6 through 3. 10 are a sequence of five photographs of weapon debris expansion taken by that camera. Figure 3. 6 was taken at approximately 300 microseconds after zero time. The small bright object at eight o' clock from the burst point is the Thor booster which evidently had been heated to a faint incandescence by the X-rays, since the observable debris has not yet reached the booster. The protuberance in the expanding debris in the direction of the booster may be due to fuel which is trailing out behind the Thor as it descends.

In Figure 3. 7 the booster has been struck by the debris, at 1. 1 milliseconds, and more fuel is seen surrounding the missile. Vapor trails from rockets that have just left Johnston Island obscure the left edge of the expanding debris. As observed from

beneath the burst, the expansion is quite symmetrical. At 1.9 milliseconds a concentration of debris in the form of a ring has appeared in Figure 3.8. The expansion velocity of this ring is 1.6 meters/microsecond. The outermost debris which can be seen only faintly in the photograph is moving at a velocity of 2 meters/microsecond.

Figures 3.9 and 3.10 show the debris at 2.7 and 3.5 milliseconds, respectively. The bright central core of the explosion contains that debris which is moving mainly in the upward and downward directions.

Further expansion of the debris is shown in Figures 3.11 through 3.15. These pictures were taken from Johnston Island with a 70-mm Photo-Sonics 10B camera. This camera also used a 500-millimeter focal length lens but operated at a framing rate of 360 frames per second. Figure 3.11 shows the explosion at 4 milliseconds. At 6.8 milliseconds, Figure 3.12, the bright rim of debris is 21.8 kilometers in diameter. An instrumentation pod is first recorded at this time on the original film record but was difficult to reproduce in the photographic print. This pod has been heated to incandescence and is the small bright spot very close to the center of the explosion. In Figure 3.13 a second pod has

appeared. This picture was taken 9.6 milliseconds after the detonation. Two other small illuminated objects appear at this time; they are followed at a later time by other objects, none of which have been identified.

Figure 3.14 shows the third pod appearing at 15.1 milliseconds. The outer rim of debris has disappeared beyond the field of view of the camera at this time. The luminous V-shaped debris formation seen in both this and the previous figure occurs along a line between the booster and the center of the explosion. It represents conical flow of the debris around the booster.

Figure 3.15 shows the explosion at 20.5 milliseconds; only slow-moving debris remains in the vicinity of the burst. The Thor booster and the three pods are very bright in comparison to the debris.

Pictures taken from the aircraft stations show the vertical expansion of the bomb debris and the vertical distribution of the instrumentation pods. Aircraft 53120 was located to the east of the burst. From that vantage point, the debris expansion appeared elliptical, Figure 3.16, with the major axis inclined slightly from the horizontal. The inclination was upward toward the north and downward toward the south. The photographs in Figures 3.16 through 3.19 were taken by a Photo-Sonics 10B camera.

At 3.7 milliseconds, the Thor Booster was still shrouded within the slow-moving component of debris and could not be observed from the east. This situation lasted until 9.2 milliseconds. However, Pod S-1 was observed at 6.5 milliseconds when the fast-moving component of debris swept by it. By 9.2 milliseconds the fast components of debris had gone well beyond Pod S-2, Figure 3.17, and at 14.7 milliseconds had begun to collide with Pod S-3 which is faintly visible, Figure 3.18. At 20.2 milliseconds, Figure 3.19, the three pods and booster are seen as an almost vertical array of points.

From the northern aircraft (A/C 53144) the pictorial history is much the same as from the eastern aircraft, with one exception. The northern magnetic conjugate point was between the aircraft and the burst, and as a result beta-ray deposition in the area around the conjugate point was photographed from the northern aircraft. Figures 3.20 through 3.25 show the growth of the beta-ray deposition area as seen from that aircraft. Beta-ray induced air fluorescence was not observed until 6.9 millisecond, Figure 3.21, but thereafter the lateral expansion of the beta-ray deposition area kept pace with the lateral expansion of debris from the burst point. The apparent greater lateral extent of the deposition area is caused by perspective, since the region of beta-ray deposition is much closer to the aircraft.

A later sequence of four photographs taken by a Traid camera from Aircraft 53144 is shown in Figures 3.26 and 3.27. The region of beta-ray deposition is seen to be continually growing in lateral extent throughout the time period extending to 0.16 second . By 1 second the beta-ray excited region has begun to fade in brightness, Figure 3.27. Faint upward-going streamers are apparent both at 1 and 2.5 seconds indicating that bomb debris has also deposited at the northern conjugate point.

Photographs taken from Mauna Loa, 1300 kilometers from the burst, show the enormous proportions of the Star Fish Prime display. A sequence of eight photographs taken by a 100-frame-per-second Mitchell camera, Figures 3.28 through 3.31, follows the full expansion of the bomb debris until it is deposited in the atmosphere. The sea horizon is slightly obscured by a ridge of the mountain; hence, the beta-ray deposition area to the north of the burst is not seen. It is the illuminated area to the right of the burst point and inclined downward at approximately 30 degrees along the geomagnetic field lines. The moon is apparent in the photographs at 1:30 o'clock with respect to the burst point.

At 85 milliseconds the debris is seen to be entering the sensible atmosphere. The remainder of the record appeared much

the same as the picture taken at 145 milliseconds which shows the peak brightness that was associated with the debris deposition.

Much longer exposure times were required to photograph the later time history of Star Fish Prime. Eight long-time exposures, taken with a Robot camera from Mauna Loa, varying in duration from 30 seconds to 4 minutes are shown in Figures 3.32 through 3.37. The first five photographs, covering the time period up to 150 seconds, were made with the burst point oriented in the field of view approximately the same as the previous sequence of eight Mitchell pictures. These five photographs show the development of auroral streamers which rise out of the regions wherein the debris had been deposited. An exceedingly large hemispherical red envelope expanded to fill the field of view by 150 seconds.

The following two pictures of this sequence, Figures 3.35 and 3.36, taken at 210 and 240 seconds, respectively, show the red airglow well north of the burst area. The pictures were taken with a slight tilt to the camera. (The reader may get the proper orientation by observing the clouds in the foreground.) At 210 seconds faint yellow streamers were seen in the middle of the red airglow. The geographic position of these streamers was well north of French Frigate Shoals. The streamers arise from beta rays emitted by debris which has risen to a great height over the burst point. No such streamers are observed at 240 seconds.

The final picture of this sequence, Figure 3.37, was a 4-minute time exposure beginning at 8 minutes after the detonation. The camera is facing slightly west of south. Star trails are visible as well as instrumentation in the foreground. The streamers represent beta particles following the geomagnetic field lines toward the southern magnetic conjugate area.

3.4 RESULTS

3.4.1 Geometric Measurements. Star Fish Prime had few phenomena, other than those related to debris motion, for which geometric measurements had any real significance. With fast-framing cameras on Johnston Island and the two aircraft, the expansion of debris at early times was well documented (Figures 3.6 through 3.25). The early time records from Johnston Island show a radial symmetry to the expansion in the horizontal plane, but the aircraft records show rather gross asymmetries in the vertical plane. Both groups of records show a distribution of several velocity components to the debris expansion. The velocities of these different components could be accurately determined by the use of a microphotometer. Similarly, estimates of the quantities of debris moving in various directions could also be made by a microphotometric analysis of the records. Neither of these

analyses have been performed. The time available for preparation of this report was devoted mainly to higher priority measurements on other events. The few measurements of debris velocities which could easily be performed by comparator techniques were obtained.

Figure 3.8 of the pictorial history shows a distinct ring-shaped structure near the outer edge of the expanding debris. The velocity of this ring was measured to be 1.6 meters/microsecond. Debris ahead of the ring, only faintly seen in the photograph, was moving at 2 meters/microsecond.

The boundary of the debris photographed does not necessarily coincide with the farthest extent of the debris. One reason is that the emission of light by the outermost debris may be too faint to record. Another is that the outermost debris may have cooled to the point where it is a neutral unexcited gas, in which case it does not radiate.

The first reason, and possibly the second, is substantiated by photographs taken from Mauna Loa (Figures 3.28 through 3.31) by a Mitchell camera operating at 100 frames per second. The exposure times were considerably longer than those used with the fast-framing cameras at Johnston Island and aboard the aircraft. In the Mauna Loa photographs the debris has the apparent shape

of an expanding toroid or ellipse. The horizontal axis of the apparent toroid, or ellipse, is inclined slightly upward toward the north. Whatever the shape of the debris, a measurement of the radial motion along the slightly inclined axis in the southern direction should give true values of the velocity of expansion in that direction. Measurements along the slightly inclined vertical axis could be in error if the geometric figure is a toroid and not an ellipse or sphere.

Debris moving to the south along the inclined horizontal axis had a constant velocity of 3.5 meters/microsecond for the time period up to 50 milliseconds (see Figure 3.38), at which time it began to decelerate.

The bright object which persists in the Mauna Loa records is the Thor booster which has been heated to incandescence by the debris. The burst point is some 23 kilometers above the booster, or close to the small bright cloud of debris in Figure 3.28 (Frame Thus, the burst point does not coincide with intersection of the axis of the apparent toroid (or ellipse). In fact, measurements of the radial distance and velocity of debris in the downward direction indicate (Figure 3.38) that both the distance traveled and the velocity were identical to the horizontal values until approximately 30 milliseconds, when a rapid deceleration of the downward-movin

debris began. These measurements are substantiated by the behavior of the radiance-time curve for the sky brightness over Johnston Island.

Since the debris retained a constant velocity in the downward direction until 30 milliseconds, and in the horizontal direction until 60 milliseconds, it could be concluded that the light emitted during these times is due solely to the internal energy of the debris and not to collisions with the rarefied air, and that after those times the collisions of debris with the atmospheric constituents began to dominate the emission process.

If the radial velocity measurements are believed, then an alternate conclusion can be drawn that the true shape of the debris expansion was spherical, at least for the 3.5 meters/microsecond component and in the bottom hemisphere centered on the burst. The conclusion can also be drawn that an upper hemisphere existed but was not seen. The failure to observe the upper hemisphere may be explained by postulating that the debris in the lower hemisphere was only seen through weak collisions with the rarefied atmosphere and not by its internal energy. The collisions postulated in this explanation are not sufficient to decelerate the bulk of the debris until it enters the denser region of the atmosphere (at 30 milliseconds in the downward direction and 60 milliseconds

in the inclined horizontal).

An inference to be drawn from the curves in Figure 3.38 is that bomb debris from Star Fish Prime never reached an altitude lower than about 230 kilometers. Such a conclusion must then explain the apparent penetration to lower altitudes as seen in later time photographs from Mauna Loa (see Figure 3.31, Frame 14). A sketch by the reader of the spherical geometry involved will show a possible explanation. Debris stopped at 230 kilometers but well beyond a line between ground zero and air zero could appear from Mauna Loa to be at a lower altitude than it really was. Other photographs (Figure 3.32 and Figure 3.33) tend to substantiate the 230-kilometer altitude. Filamentary streamers caused by beta rays from the debris originate at high altitudes in these pictures. The large glowing white area, indicative of the region where the bulk of debris was deposited, resides mainly above the 230-kilometer altitude.

3.4.2 Brightness Temperature, Visible Power, and Visible Yield. The very early time history (up to 300 microseconds) of Star Fish Prime was not recorded photographically by Project 8A.2. For the most part this was a result of the extremely small images caused by the long slant ranges to the burst. From photoelectric measurements performed by another EG&G project on Mauna Loa

(Reference 15) the brightness temperature for the first 70 microseconds has been obtained.

The attenuation of the atmosphere over the 5 air masses in the path was included in the calculation. Brightness temperatures derived from the two independent measurements are shown in Figure 3.39. The agreement between the two measurements is extremely good. An average value of brightness temperature from these two measurements has been used to compute the radiance in the bandwidth 4000Å to 6500Å assuming a blackbody spectral energy distribution.

The resultant radiance values have been combined with the photographically measured values (see Figure 3.40) to give a radiance vs time history of the debris from 2 microseconds to 30 milliseconds. The radiance values for the debris pertain to the central debris cloud seen in Figures 3.7 through 3.25. The small peak at 4 milliseconds is not explained.

An upper limit to the total power radiated as a function of time in the visible spectral region was obtained

and

assuming that the sphere determined by this radius was uniformly bright and had the radiance given by Figure 3.40. The visible power vs. time obtained by using these assumptions is given in Figure 3.41. The total visible yield for various periods of time after detonation were obtained by integrating the visible power versus time. The values are given in Table 3.11.

Under the assumptions used in the determination of this value it must be taken as an upper limit to the true value.

3.4.3 Sky Glow and Beta-Ray Glow. Slow-speed motion-picture cameras located at Johnston Island found little to record on Star Fish Prime other than a general sky glow over the island. There is essentially no geometric feature of interest in the motion pictures, except perhaps for some faint filamentary streamers passing overhead in the general North-South direction. The photometric-time history does show interesting detail.

The radiance vs. time history of the sky glow over Johnston Island, as observed by a Mitchell camera framing at 100 frames/second and a Traid camera at 12 frames/second is shown in

Figure 3.42. The sky glow beginning at the earliest recorded time (5 msec) is probably due to excited metastable states of atomic oxygen created by the X-ray energy deposition at a much earlier time. The decay proceeds monatonically until 30 milliseconds at which time a sudden increase occurs in the sky glow. The rise is coincident with the deceleration of the downward moving debris as seen in Figure 3.38, confirming the conclusion that the debris did not penetrate below an altitude of 230 kilometers. The later peak in the sky glow beginning at 12 seconds is not explained.

The beta-ray-induced air fluorescence in the vicinity of the northern conjugate point (see Figures 3.21 through 3.25) was also subjected to photometric analysis. The radiance vs. time curve for this phenomena is shown in Figure 3.42. A peak occurs at 16 milliseconds which is not yet explainable. It is much too early to be the arrival of debris at the 230-kilometer altitude because of the increased range from the burst to the northern conjugate point. If it were debris, a velocity four times as great as 3.5 meters/microsecond would be required. No combination of geometry and the rate of fission frament beta-decay has been found which will explain this peak.

TABLE 3.1 INSTRUMENT POD POSITIONS IN BRAVO COORDINATE SYSTEM, STAR FISH PRIME

Pod	ΔX	ΔY	ΔZ	Slant Range	Slant Range
	feet	feet	feet	feet	kilometers
S-1	-195	1,542	-28,599	28,641	8.730
S-2	1,971	1,331	-49,126	40,196	12.252
S-3	2,682	3,536	-76,651	76,779	23.403

TABLE 3.2 SUMMARY OF STAR FISH PRIME CAMERA PARAMETERS, AIRCRAFT 53120

INSTRUMENT AND STATION POSITION		FILM TYPE	FILM NUMBER	AIMING ANGLES IN DEGREES ELEV	AZIMUTH	FILTERS ND	COLOR	FOCAL LENGTH MM	LENS F/N	FRAMES PER SECOND	SHUTTER SECTOR, DEGREES	EXPOSURE TIME	MARKER RATE CPS
RAPATRONIC	W7	TXA	93103	45	-	-	WR12	490	18	*(A)	-	5MUSEC	-
KFC-600	W6	TXA	93104	45	-	3	WR12	301	9	50000	-	1MUSEC	-
CLOUD	W10	DXN	93109	45	-	-	-	105	3.7	0.5	-	0.5SEC	-
CLOUD	W13	EDER	93110	45	-	-	-	105	3.7	0.5	-	0.5SEC	-
ROBOT	W15	RXP	93111	55	-	-	3914A	45	2.8	1	-	0.25SEC	-
ROBOT	W16	RXP	93112	55	-	-	4278A	45	2.8	1	-	0.25SEC	-
ROBOT	W17	RXP	93113	55	-	-	4709A	45	2.8	1	-	0.25SEC	-
ROBOT	W21	EDER	93114	86.5	-	-	-	45	2.8	1	-	0.25SEC	-
ROBOT	W22	RXP	93115	86.5	-	-	5577A	45	2.8	1	-	0.20SEC	-
ROBOT	W23	RXP	93116	86.5	-	-	6300A	45	2.8	1	-	0.25SEC	-
TRAID	W8	DXN	93117	45	-	-	-	25	2.3	16	160	0.023SEC	200
TRAID	W9	KDII	93118	45	-	-	-	25	2.3	16	160	0.023SEC	200
TRAID	W18	DXN	93119	55	-	-	-	25	2.3	16	160	0.023SEC	200
TRAID	W19	EDER	93120	55	-	-	-	25	2.3	16	160	0.023SEC	200
MAURER	W1	DXN	93121	19	-	-	-	80	2.8	5.5	-	0.002SEC	-
MAURER	W2	EDER	93122	19	-	-	-	38	4.5	5.5	-	0.002SEC	-
FAIRCHILD HS-100	11R	KDII	93123	45	-	-	-	13	1.5	1000	-	-	200
GSAP	W11A	KDII	93124	45	-	-	-	9.5	2.2	16	133	-	-
PHOTO-SONICS 4C	W12	DXN	93125	45	-	-	-	150	2.8	2500	30	33MUSEC	200
PHOTO-SONICS 10R	W5	DXN	93127	45	-	-	-	180	2.5	360	60	67MUSEC	200
PHOTO	PANEL	PX	93131	-	-	-	-	25	16	1	160	30MSEC	CLOCK
PHOTO	PANEL	PX	93132	-	-	-	-	25	16	0.2	160	30MSEC	CLOCK

*(A) SINGLE EXPOSURE AT 510 MUSEC.
N.B. MUSEC = MUS = MICROSECOND

TABLE 3.3 SUMMARY OF STAR FISH PRIME CAMERA PARAMETERS, AIRCRAFT 53144

INSTRUMENT AND STATION POSITION		FILM TYPE	FILM NUMBER	AIMING ANGLES IN DEGREES ELEV	AZIMUTH	FILTERS NO	COLOR	FOCAL LENGTH MM	LENS F/N	FRAMES PER SECOND	SHUTTER SECTOR, DEGREES	EXPOSURE TIME	MARKER RATE CPS
RAPATRONIC	W7	TXA	93203	25	-	-	WR12	490	22	*(A)	-	5MUSEC	-
KFC-600	W6	TXA	93204	25	-	3.0	WR12	301	9	200000	-	0.5MUSEC	-
CLOUD	W10	DXN	93209	25	-	-	-	105	3.7	0.5	-	0.5SEC	CLOCK
CLOUD	W13	DXN	93210	25	-	-	-	105	3.7	0.5	-	0.5SEC	CLOCK
ROBOT	W15	RXP	93211	50	-	-	3914A	45	2.8	1	-	0.25SEC	-
ROBOT	W16	RXP	93212	50	-	-	4287A	45	2.8	1	-	0.25SEC	-
ROBOT	W17	RXP	93213	50	-	-	4709A	45	2.8	1	-	0.25SEC	-
ROBOT	W21	EDER	93214	86.5	-	-	-	45	2.8	1	-	0.25SEC	-
ROBOT	W22	RXP	93215	86.5	-	-	5577A	45	2.8	1	-	0.25SEC	-
ROBOT	W23	RXP	93216	86.5	-	-	6300A	45	2.8	1	-	0.25SEC	-
TRAID	W8	OXN	93217	30	-	-	-	18.5	2.2	16	160	0.023SEC	200
TRAID	W9	KOII	93218	25	-	-	-	18.5	2.2	16	160	0.023SEC	200
TRAID	W18	OXN	93219	55	-	-	-	18.5	2.2	16	160	0.023SEC	200
MAURER	W1	DXN	93221	19	10 AFT	-	-	38	4.5	5.5	-	0.002SEC	-
MAURER	W2	DXN	93222	19	10 FWD	-	-	38	4.5	5.5	-	0.002SEC	-
FAIRCHILD HS-100	W11	KDII	93223	25	-	-	-	13	1.5	1000	-	0.2MSEC	200
GSAP	W11	KOII	93224	25	-	-	-	9.5	2.3	16	-	0.2MSEC	-
PHOTO-SONICS 4C	W12	OXN	93225	25	-	-	-	250	4	2500	30	33MUSEC	200
PHOTO-SONICS 4C	W14	OXN	93226	25	-	-	-	85	3.5	2500	30	33MUSEC	200
PHOTO-SONICS 10B	W5	OXN	93227	25	-	-	-	180	2.5	360	60	67MUSEC	200
PHOTO PANEL CAMERA	PANEL	PX	93231	-	-	-	-	25	16	1	160	30MSEC	CLOCK
PHOTO PANEL CAMERA	PANEL	PX	93232	-	-	-	-	25	16	0.2	160	30MSEC	CLOCK

*(A) SINGLE EXPOSURE AT 200 MUSEC.
N.B. MUSEC = MUS = MICROSECOND

TABLE 3.4 SUMMARY OF STAR FISH PRIME CAMERA PARAMETERS, JOHNSTON ISLAND

INSTRUMENT AND STATION POSITION		FILM TYPE	FILM NUMBER	AIMING ANGLES IN DEGREES ELEV	AZIMUTH	FILTERS ND	COLOR	FOCAL LENGTH MM	LENS F/N	FRAMES PER SECOND	SHUTTER SECTOR, DEGREES	EXPOSURE TIME	MARKER RATE CPS
KFC-600	A1	PX	93304	85.28	199	2.0	WR12	302	9	1000000	-	0.1MUSEC	-
PHOTO-SONICS 4C	A2	DXN	93324	85.28	199	-	-	360	5.5	2500	72	80MUSEC	200
PHOTO-SONICS 4C	A3	DXN	93323	85.28	199	-	-	500	5	2500	72	80MUSEC	200
PHOTO-SONICS 108	A4	DXN	93325	85.28	199	-	-	500	5	360	60	67MUSEC	200
RAPATRONIC	A5	TX	93303	85.28	199	2.0	WR12	490	22	*(A)	-	5MUSEC	-
MAURER	A7	DXN	93319	85.28	199	-	-	150	2.8	5.5	-	0.002SEC	-
MAURER	A8	EDER	93320	85.28	199	-	-	80	2.8	5.5	-	0.002SEC	-
TRAID	A9	DXN	93317	85.28	199	-	-	35	2.3	16	160	0.023SEC	10
MITCHELL	A10	EDER	93327	85.28	199	-	-	35	2.3	100	170	4.7MSEC	100
FAIRCHILD HS-100	A12	KDII	93321	85.28	199	-	-	13	1.5	900	-	0.22MSEC	100
GSAP	A13	KDII	93322	85.28	199	-	-	9.5	2.2	16	133	0.024SEC	-
KC-1	A14	TXA	93332	90	199	-	-	153	6.3	0.1	-	3.4SEC	-
CLOUD	C1	EDER	93310	82	12	-	-	105	*(B)	*(C)	-	*(D)	CLOCK
CLOUD	C2	DXN	93309	60	12	-	-	105	*(B)	*(C)	-	*(D)	CLOCK
TRAID	C3	XR	93318	60	12	-	-	18.5	2.2	16	160	0.023SEC	10
BELL AND HOWELL	C4	EDER	93329	60	12	-	-	25	2	12	160	0.037SEC	10
MITCHELL LS	C5	DXN	93328	55	12	-	-	25	2.3	2.5	170	0.19SEC	10
MITCHELL HS	C6	DXN	93326	75	12	-	-	35	2.3	100	170	4.7MSEC	10
ROBOT	C7	RXP	93311	75	12	-	4278A	45	2.8	0.33	-	1.2SEC	-
ROBOT	C8	RXP	93312	75	12	-	4709A	45	2.8	0.33	-	1.2SEC	-
ROBOT	C9	RXP	93313	75	12	-	5228A	45	2.8	0.33	-	1.2SEC	-
ROBOT	C10	RXP	93314	75	12	-	6300A	45	2.8	0.33	-	1.2SEC	-
ROBOT	C11	RXP	93315	75	12	-	3914A	45	2.8	0.33	-	1.2SEC	-
ROBOT	OUTSIDE	EDER	93334	VARIABLE		-	-	45	2.8	0.33	-	1.2SEC	-

*(A) SINGLE EXPOSURE AT 938 MUSEC.
*(B) F/22 FROM ZERO TO 120SEC, F/3.7 AFTERWARD.
*(C) 0.2 FPS FROM ZERO TO 600SEC, 0.033 FPS THEREAFTER.
*(D) 4.6SEC FROM ZERO TO 600SEC, 30 SEC THEREAFTER.
N.B. MUSEC = MUS = MICROSECOND

TABLE 3.5 STAR FISH PRIME H-HOUR AIRCRAFT POSITIONS

	Planned Values		Actual Values	
	Aircraft 53144	Aircraft 53120	Aircraft 53144	Aircraft 53120
Latitude	22° 42' N	15° 52' N	22° 43' N	15°53' N
Longitude	168° 29' W	166° 21' W	168°24' W	166° 21' W
Magnetic Heading	089° 30'	180° 35'	089°	181°
Altitude (feet)	37,500	37,500	35,900	41,000
Slant Range to Burst (km)	844.2	549.4	823.2	534.5
Elevation Angle to Burst (w/o Refraction Correction)	25°	45°	25° 00'	44° 51'
True Azimuth (Burst to Aircraft)	190°	280°	190° 43'	280° 55'

TABLE 3.6 POINTING INFORMATION FOR JOHNSTON ISLAND, STAR FISH PRIME

Station Location: Latitude 16° 44' 04.79'' N
Longitude 169° 31' 36.59'' W

	Elevation Angle (w/o Refraction Correction)	True Azimuth Angle	Slant Range To Burst (meters)
Planned	85° 16' 48''	199° 48' 14''	401,275
Actual	85° 13' 17.08''	200° 30' 36.57''	401,402

TABLE 3.7 SUMMARY OF STAR FISH PRIME FILM RECORDS, AIRCRAFT 53120

FILM NUMBER	FILM TYPE	CAMERA	RESULTS
93104	PX	KFC-600	NO RECORD.
93109	DXN	CLOUD	SEVEN EXPOSED FRAMES. BURST APPEARS IN FIRST FRAME.
93110	EDER	CLOUD	TWO EXPOSED FRAMES. BURST IN FIRST FRAME.
93111	RXP	ROBOT	FOUR FRAMES. BURST APPEARS IN FIRST FRAME. 3914A FILTER.
93112	RXP	ROBOT	SERIES OF FRAMES SHOWING BURST DEVELOPMENT. 4278 A FILTER
93113	RXP	ROBOT	SIMILAR TO 93112. 4709A FILTER.
93114	EDER	ROBOT	SIXTEEN FRAMES.
93115	RXP	ROBOT	SEVERAL EXPOSURES. NO DISCERNIBLE STRUCTURE. 5577A FILTER.
93116	RXP	ROBOT	LONG SERIES OF EXPOSED FRAMES. NO DISCERNIBLE STRUCTURE. 6300A FILTER.
93117	DXN	TRAID	VIEW OF BURST AREA SHOWING DEBRIS EXPANDING. STREAMERS APPEAR OVER BURST AREA IN NORTH-SOUTH DIRECTION. INCLINATION IS DOWN TOWARD NORTH AND UP TOWARD SOUTH.
93118	KDII	TRAID	FIRST FRAME STRONGLY EXPOSED WITH BLUISH WHITE COLOR. SECOND FRAME SHOWS GREEN. REMAINING FRAMES ARE BLUISH IN COLOR.
93119	DXN	TRAID	BURST SHOWS IN FIRST FRAME. VERY SHORTLY, STREAMERS DEVELOP APPARENTLY ALONG FIELD LINES.
93120	EDER	TRAID	FIRST THREE FRAMES SHOW BURST AND GREEN GLOW. COLOR THEN CHANGES TO BLUE FOR ABOUT ONE HUNDRED FRAMES.
93121	DXN	MAURER	GENERAL BRIGHTENING IN FIELD OF VIEW. NO DISCERNIBLE STRUCTURE. ABOUT 30 SECONDS OF RECORD.
93122	EDER	MAURER	NO RECORD.
93123	KDII	RED DEVIL	FIRST FRAME SHOWS BURST WITH ASYMMETRICAL EXPANSION. VIOLET COLOR OVER ENTIRE FRAME. FOURTEEN USABLE FRAMES.
93124	KDII	GSAP	APPROXIMATELY FIFTY EXPOSED FRAMES. NO DISCERNIBLE STRUCTURE.
93125	DXN	PS-4C	NO RECORD.
93127	DXN	PS-10B	BURST APPEARS IN FIRST FRAME OFF-CENTER. ASYMMETRIC EXPANSION SHOWS CLEARLY. ALSO MAJOR EXPANSION AXIS IS TILTED WITH RESPECT TO HORIZON. WELL-EXPOSED RECORD FOR ABOUT THIRTY FRAMES. SKY BRIGHTNESS APPARENT FOR LONG TIME.

TABLE 3.8 SUMMARY OF STAR FISH PRIME FILM RECORDS, AIRCRAFT 53144

FILM NUMBER	FILM TYPE	CAMERA	RESULTS
93203	TX	RAPATRONIC	SMALL IMAGE OF EXPANDING DEBRIS AT EARLY TIMES.
93204	PX	KFC-600	NO RECORD
93209	DXN	CLOUD	TWO FRAMES EXPOSED. FIRST FRAME SHOWS STAR IMAGE OF BURST. SECOND FRAME ONLY SLIGHTLY EXPOSED.
93210	DXN	CLOUD	SIX DATA FRAMES. FIRST HEAVILY EXPOSED. SUCCEEDING FRAMES SHOW BURST AREA.
93211	RXP	ROBOT	ABOUT FIFTEEN USABLE FRAMES. FIRST TEN SHOW AURORAL STRUCTURE CLEARLY.
93212	RXP	ROBOT	ABOUT FIFTEEN TO TWENTY USABLE FRAMES. FIRST TEN FRAMES RESEMBLE 93211.
93213	RXP	ROBOT	ONLY ONE WELL-EXPOSED FRAME SHOWING AURORAL STRUCTURE.
93214	EDER	ROBOT	ABOUT EIGHT TO TEN GOOD FRAMES. FIRST FRAME OVEREXPOSED. REMAINDER SHOW GREEN AND BLUE-GREEN AURORAL STRUCTURE.
93215	RXP	ROBOT	APPROXIMATELY FIFTY USABLE FRAMES. AURORAL STRUCTURE APPARENT.
93216	RXP	ROBOT	APPROXIMATELY ONE HUNDRED EXPOSED FRAMES. LESS STRUCTURE THAN IN 93216.
93217	DXN	TRAID	NO RECORD.
93218	KDII	TRAID	FIPST FPAME OVEREXPOSED. SECOND FRAME GREEN. SUCCEEDING FRAMES BLUISH. ABOUT SEVENTY-FIVE FRAMES.
93219	DXN	TRAID	LONG RECORD. AURORAL STREAMER APPEARS IN MIDDLE OF FRAME.
93221	DXN	MAURER	FIRST FRAME SHOWS CONFINEMENT OF SOME DEBRIS TO BURST AREA. BRIGHT REGION APPEARS IN BOTTOM OF FRAME. APPROXIMATELY TEN USABLE FRAMES
93222	DXN	MAURER	COMPANION INSTRUMENT TO 93221. CONTAINS APPROX-IMATELY SAME RECORD.
93223	KDII	FAIRCHILD PS-180	FIRST FRAME SHOWS BURST ASYMMETRY. BACKGROUND CONTAINS GENERAL VIOLET-PINKISH GLOW. TWELVE USABLE FRAMES.
93224	KDII	GSAP	FIRST FRAME SHOWS GENERAL GREEN SKY GLOW WITH CENTRAL WHITE BURST REGION SURROUNDED BY PINKISH REGION. MORE THAN FIFTY USABLE FRAMES.
93225	DXN	PS-4C	WIDE FIELD OF VIEW PICTURE OF BURST AREA SHOWING EARLY TIME DEVELOPMENT OF BURST. BRIGHT REGION DEVELOPS AT BOTTOM OF FRAME. RECORD APPROXIMATELY 20 MSEC LONG.
93226	DXN	PS-4C	BURST APPEARS IN VERY BOTTOM OF FIELD OF VIEW. BURST SHOWS CENTRAL CORE WITH OUTER SHELL. BRIGHT SPOT (PRESUMABLY BOOSTER) APPEARS. RECORD APPROX-IMATELY 15 MSEC LONG.
93227	DXN	PS-10B	GOOD RECORD OF BURST AREA SHOWING ASYMMETRY AND TILT OF BURST. DEBRIS EXPANSION SEEN CLEARLY. BRIGHT AREA APPEARS IN BOTTOM OF FRAME AND GROWS IN SIZE, EVENTUALLY COVERING ENTIRE FRAME. AURORAL STREAMERS FORM IN BRIGHT AREA. RECORD APPROXIMATELY 1/2 SECOND LONG.

TABLE 3.9 SUMMARY OF STAR FISH PRIME FILM RECORDS, JOHNSTON ISLAND

FILM NUMBER	FILM TYPE	CAMERA	RESULTS
93303	TX	RAPATRONIC	NO RECORD.
93304	PX	KFC-600	NO RECORD.
93309	DXN	CLOUD	TIME EXPOSURES OF SKY JUST NORTH OF BURST AREA. DEVELOPMENT AND MOTION OF STREAMERS APPEARS. RECORD ARCS FOR SEVERAL MINUTES.
93310	EDER	CLOUD	DEVELOPED AS BLACK AND WHITE. TO BE REHALOGENATED.
93311	RXP	ROBOT	BURST APPEARS IN FIRST FRAME. TOTAL RECORD FOUR FRAMES. 4278A FILTER.
93312	RXP	ROBOT	NO RECORD. 4709A FILTER.
93313	RXP	ROBOT	VIEW OF SKY NORTH OF BURST. FIVE FRAMES SHOW EXPOSURE. 5228A FILTER.
93314	RXP	ROBOT	VIEW OF SKY NORTH OF BURST. LONG RECORD. 6300A FILTER.
93315	RXP	ROBOT	APPROXIMATELY TWELVE EXPOSED FRAMES. NO STRUCTURE 3914A FILTER.
93317	DXN	TRAID	WIDE FIELD OF VIEW PICTURE OF BURST SHOWING DEBRIS EXPANSION. STREAMERS GOING IN NORTH-SOUTH DIRECTION DEVELOP AFTER SEVERAL SECONDS. RECORD ABOUT 2-3 MINUTES LONG.
93318	XR	TRAID	FORTY EXPOSED FRAMES, UNINTERESTING RECORD. SHOWS NO FIREBALL OR AURORA STRUCTURE.
93319	DXN	MAURER	BURST AREA REGION. APPROXIMATELY TWENTY DATA FRAMES.
93320	EDER	MAURER	SINGLE GREEN-COLORED FRAME FOLLOWED BY SIX BLUE FRAMES. NO STRUCTURE. ROCKET TRAILS SHOW.
93321	KDII	FAIRCHILD HS-100	GOOD RECORD SHOWING BURST FOLLOWED BY DEBRIS MOTION. ROCKET TRAIL PARTIALLY OBSCURES FIELD OF VIEW.
93322	KDII	GSAP	FIRST THREE FRAMES SHOW BURST. FIRST FRAME OVEREXPOSED. SECOND FRAME SHOWS GREEN BACKGROUND. CAMERA JAMMED INTERMITTENTLY. ABOUT THIRTY USABLE FRAMES.
93323	DXN	PS-4C	GOOD HIGH-SPEED RECORD OF BURST EXPANSION. GENERAL BURST SHAPE IS DENSE CENTRAL CORE SURROUNDED BY EXPANDING SHELL.
93324	DXN	PS-4C	SIMILAR TO 93323 EXCEPT LESS MAGNIFICATION.
93325	DXN	PS-10B	FIRST FRAME OVEREXPOSED. SUCCEEDING EIGHT OR TEN FRAMES GIVE GOOD RECORD OF EXPANDING DEBRIS. RECORD CONTINUES FOR LONG TIME.
93326	DXN	MITCHELL HS	VIEW OF SKY NORTH OF BURST. SHOWS TRACE OF STREAMERS BEGINNING. CAMERA JAMMED AFTER FOUR HUNDRED AND THIRTY-SIX FRAMES.
93327	EDER	MITCHELL HS	BURST AREA PICTURES. SHOWS BLUE SKY INITIALLY. BACKGROUND CHANGES TO GREEN AND BACK TO BLUE.
93328	DXN	MITCHELL LS	VIEW OF SKY NORTH OF BURST. TWO FILAMENTARY STREAMERS DEVELOP HALFWAY THROUGH RECORD.
93329	EDER	B AND H	NORTHERN SKY VIEWS. GREEN SKY BACKGROUND PREDOMINATES.
93332	TXA	KC-1B	FIRST FRAME SHOWS BURST POINT. THIRTY-EIGHT FRAMES OF AURORAL STREAMERS OVER JOHNSTON ISLAND.
93334	EDER	ROBOT	SEVERAL FRAMES SHOWING STREAMERS IN SOUTHERN SKY.

TABLE 3.10 STATISTICAL SUMMARY OF STAR FISH PRIME CAMERA RECORDS FROM THE BURST AREA

Station	J-820	Aircraft 53120	Aircraft 53144	Totals
Number of Cameras	24	20	20	64
Number of Useful Records	13	9	10	32
Reasons for No Records:				
Mechanical failure	0	0	0	0
Inappropriate camera parameters	3	4	2	9
Error in shot location	0	0	0	0
Reasons for Poor Records:				
Inappropriate camera parameters	8	7	8	23
Error in shot location	0	0	0	0
Other	0	0	0	0
Percent Success	54	45	50	—
Overall Success: 50 percent				

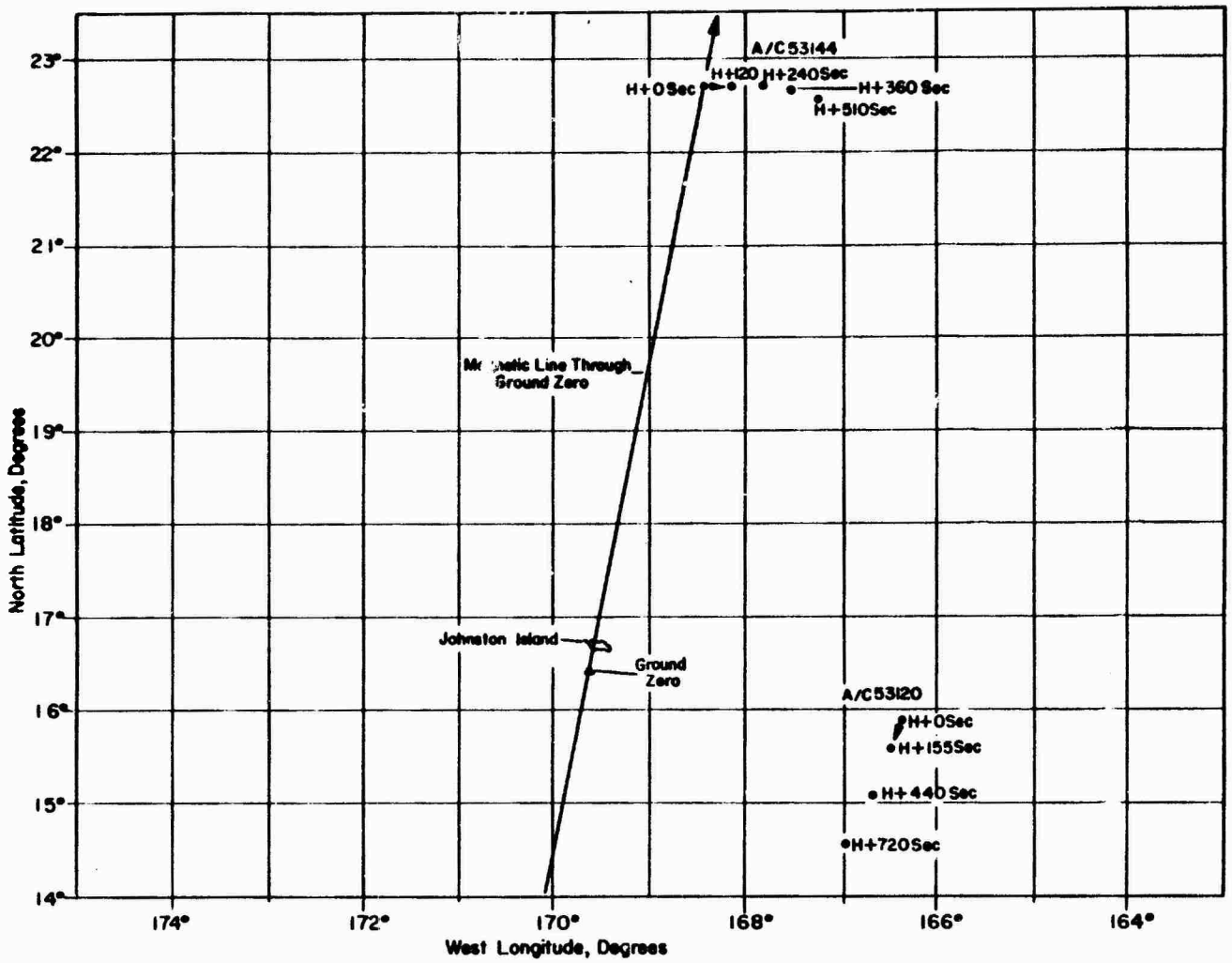

Figure 3.1 Aircraft flight paths from H-hour to + 12 minutes, Star Fish Prime.

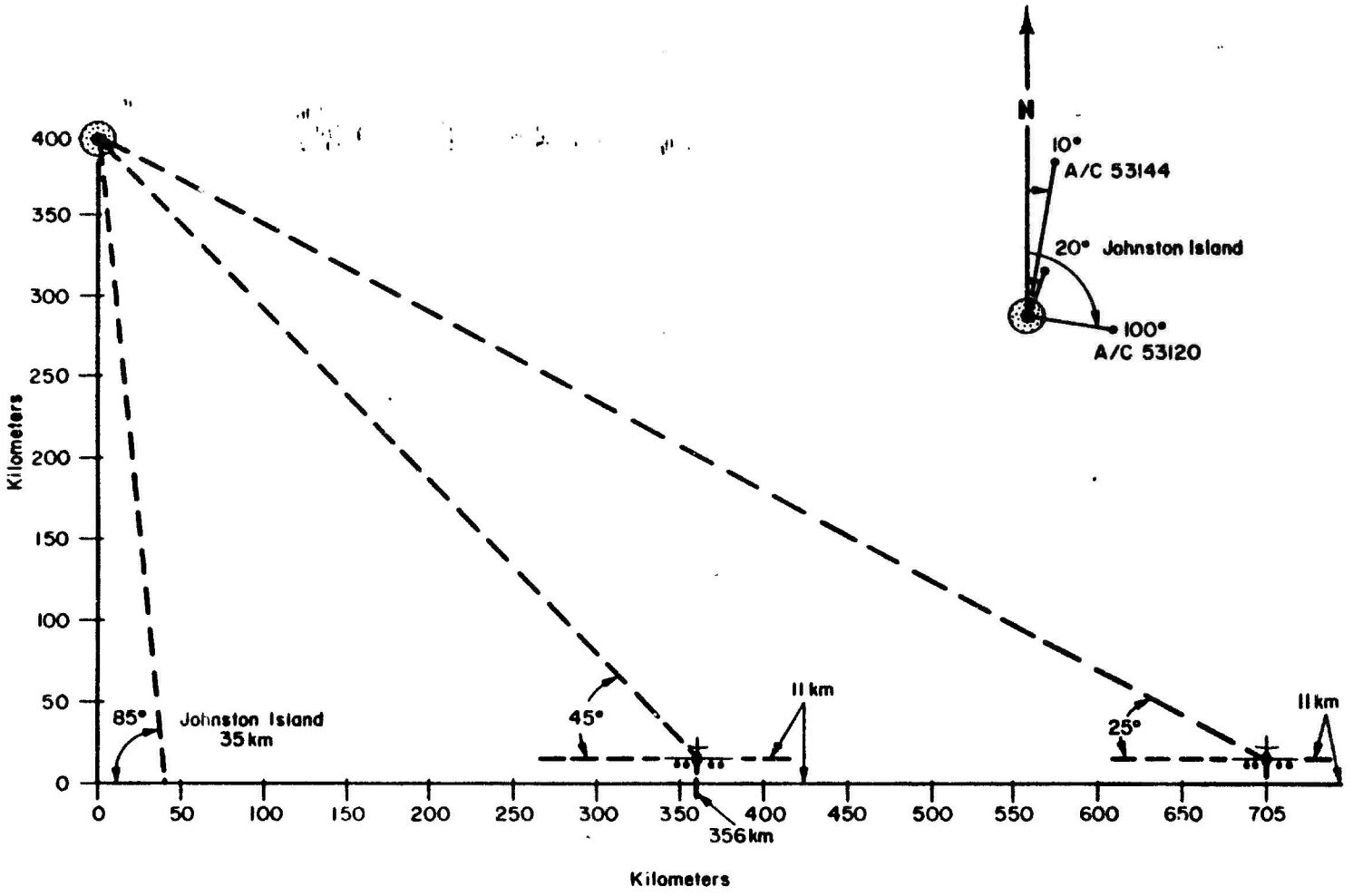

Figure 3.2 Project 8A.2 station positions with respect to Star Fish Prime predicted air zero. Bearing angles shown are from ground zero to the stations.

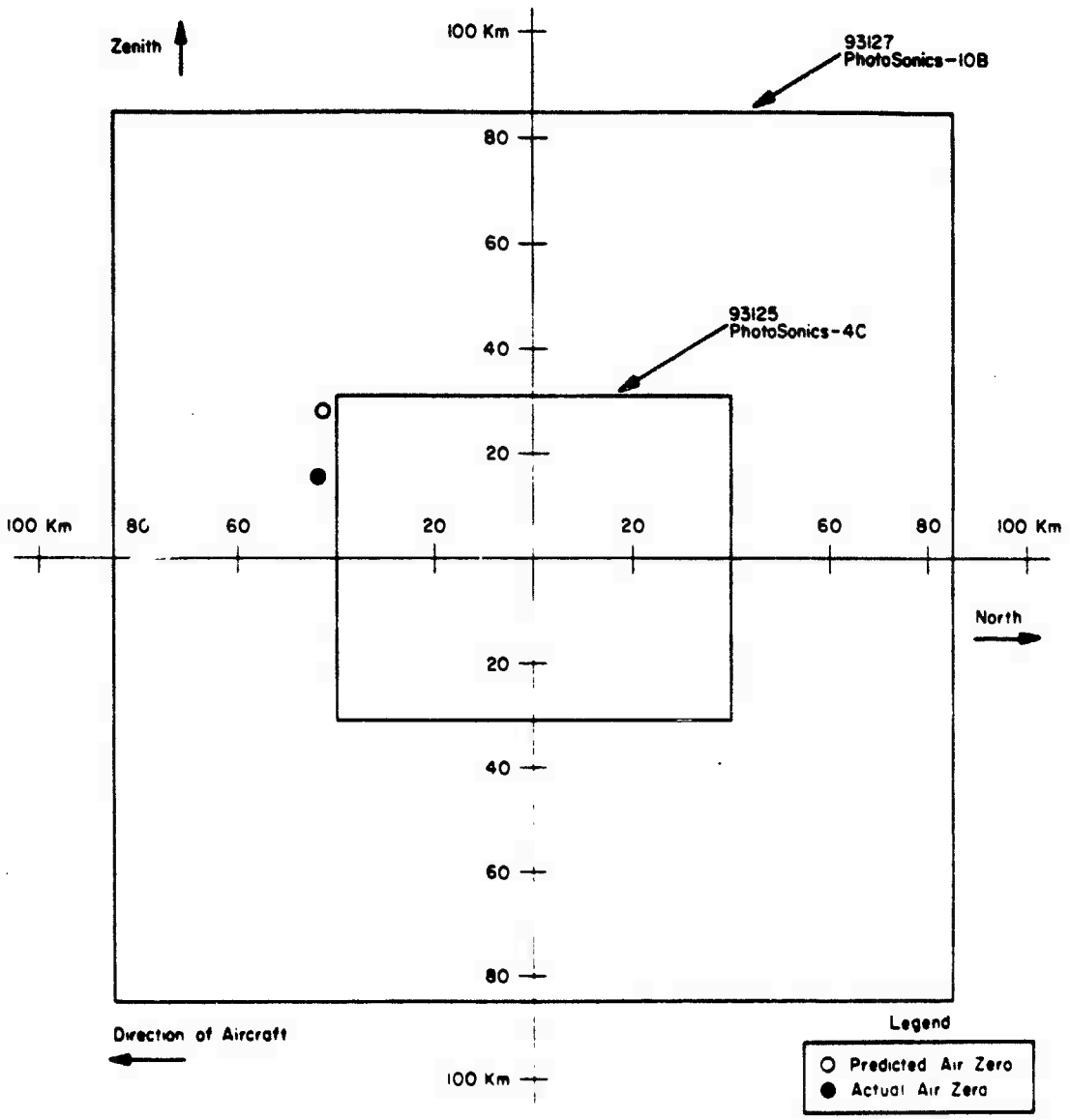

Figure 3.3 Fields of view for two Aircraft 53120 cameras with predicted and actual air zero indicated.

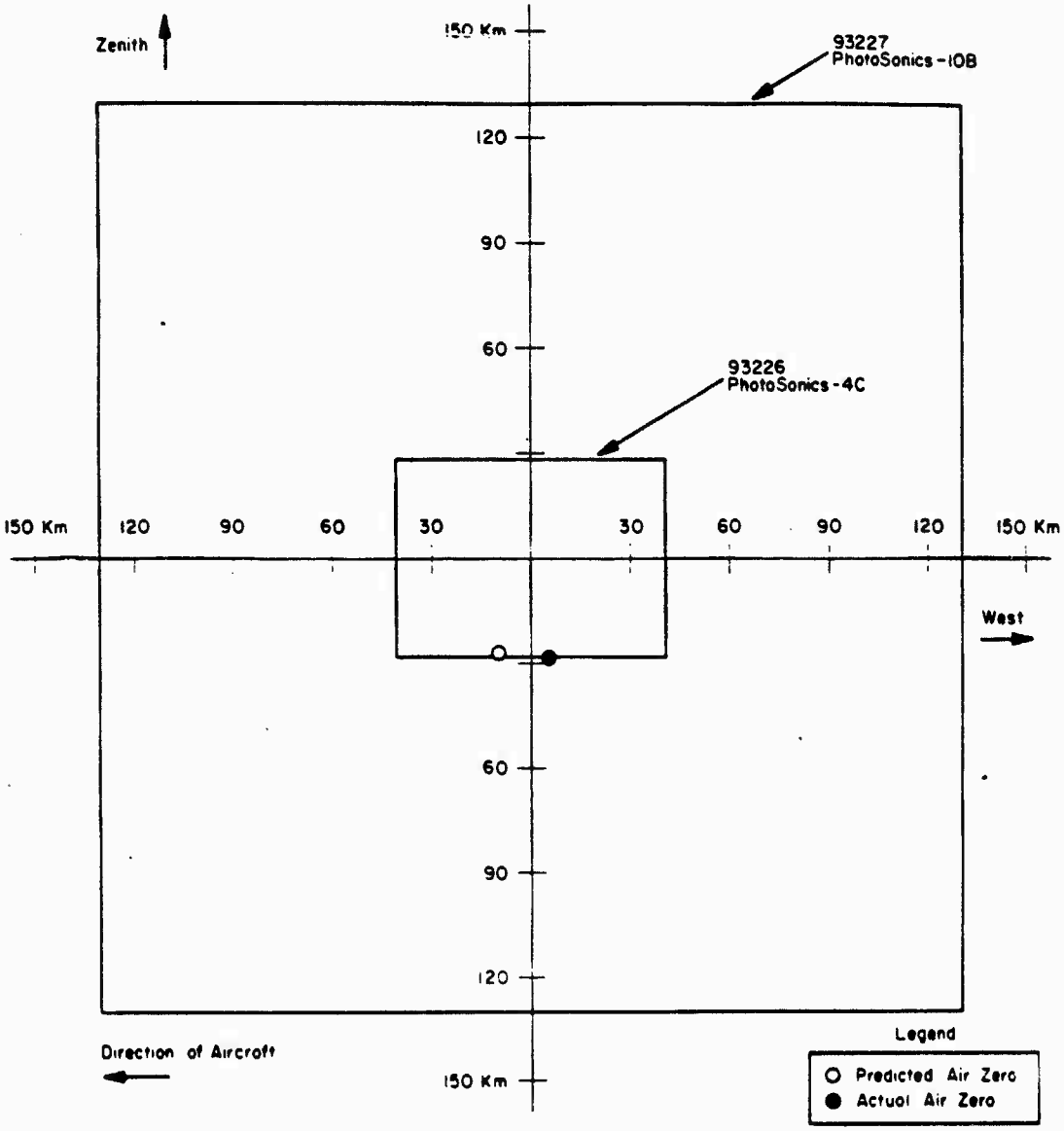

Figure 3.4 Fields of view for two Aircraft 53144 cameras with predicted and actual air zero indicated.

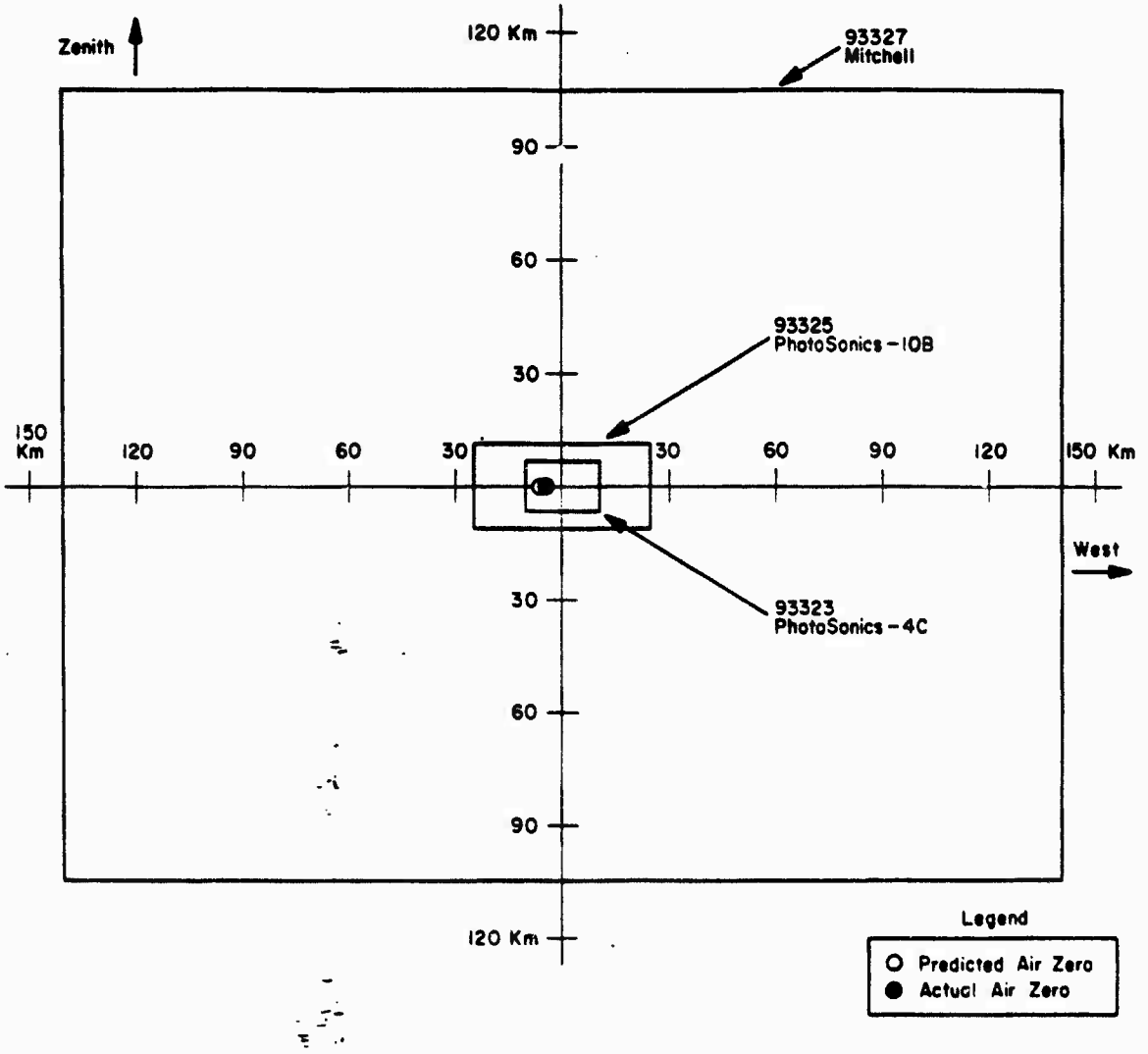

Figure 3.5 Fields of view for three Johnston Island cameras with predicted and actual air zero indicated.

Figure 3.6 Star Fish Prime; bomb debris at 0.3 msec, taken from Johnston Island. Film 93323, Frame 0.

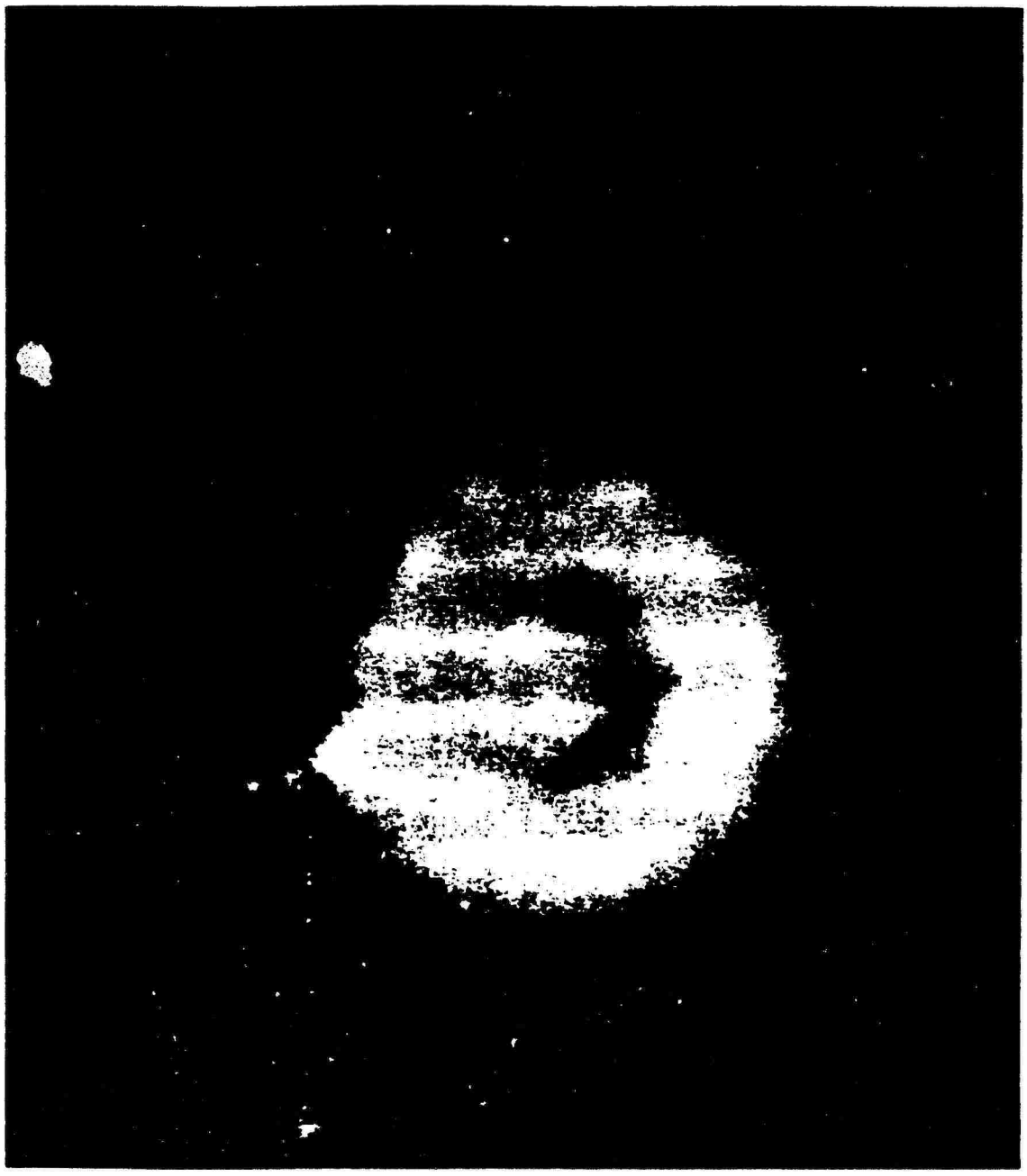

Figure 3.7 Star Fish Prime; bomb debris and Thor booster at 1.1 msec, taken from Johnston Island. Film 93323, Frame 2.

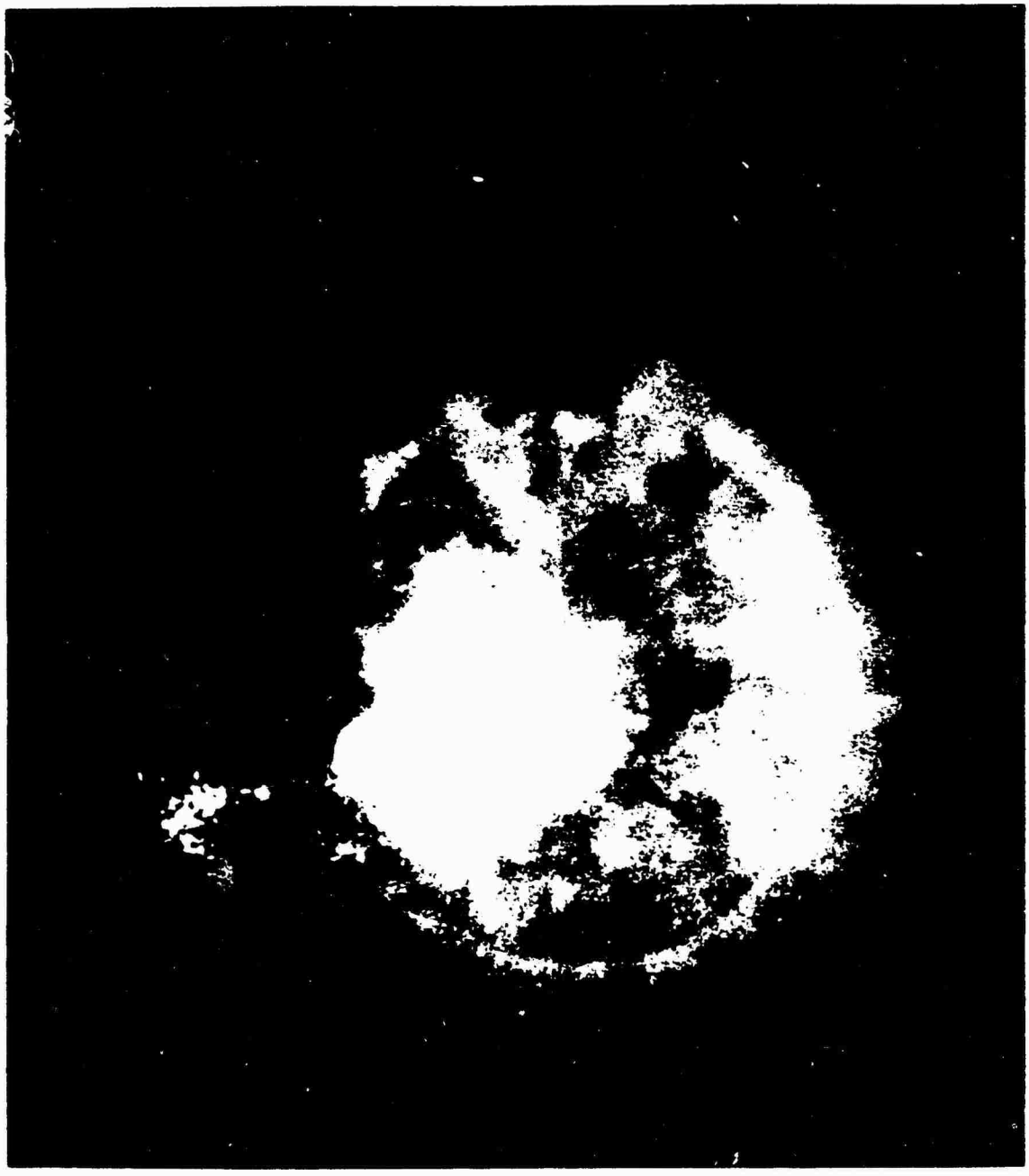

Figure 3.8 Star Fish Prime; bomb debris and Thor booster at 1.9 msec, taken from Johnston Island. Film 93323, Frame 4.

Figure 3.9 Star Fish Prime; bomb debris and Thor booster at 2.7 msec, taken from Johnston Island. Film 93323, Frame 6.

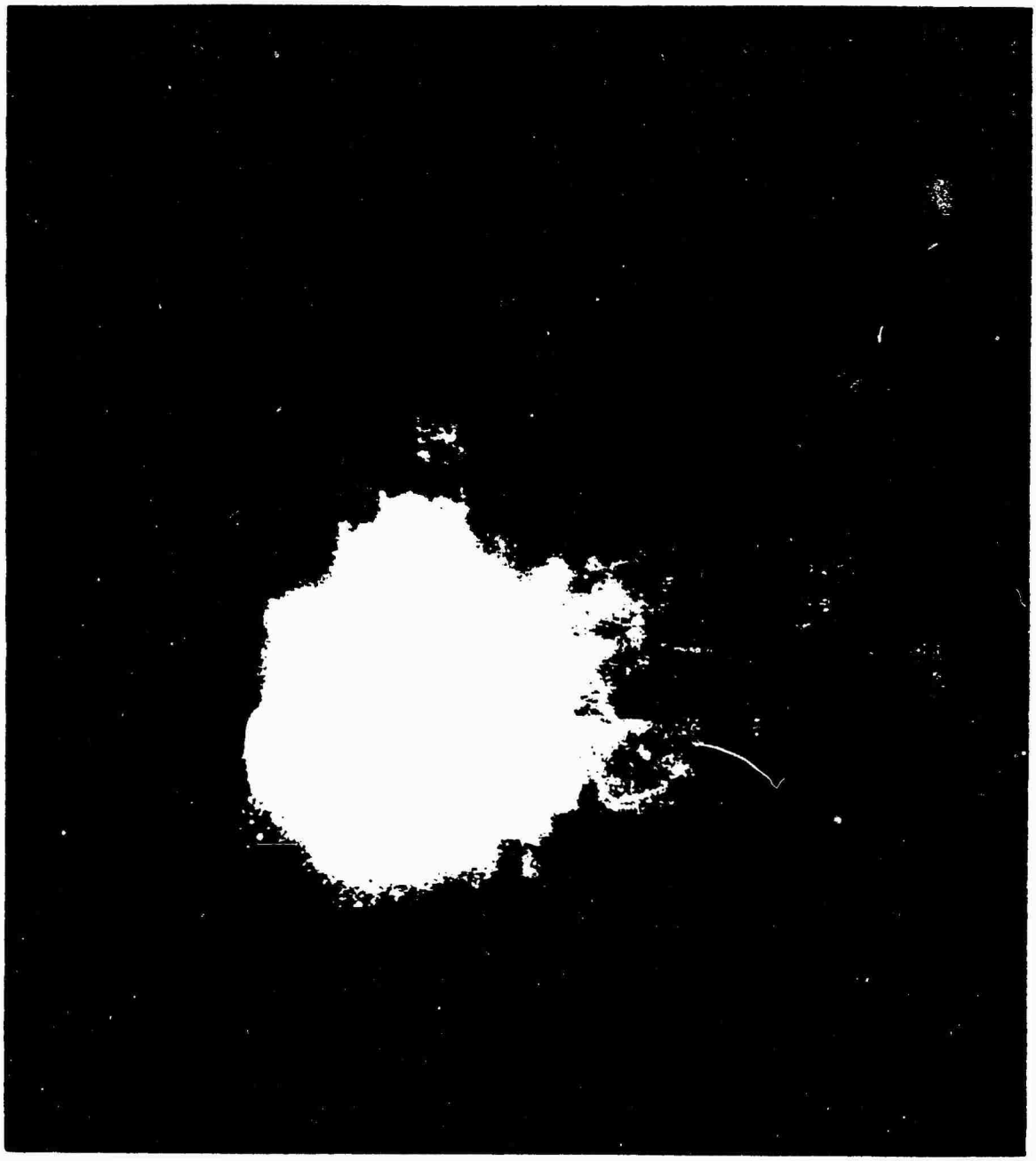

Figure 3.10 Star Fish Prime; bomb debris and Thor booster at 3.5 msec, taken from Johnston Island. Film 93323, Frame 8.

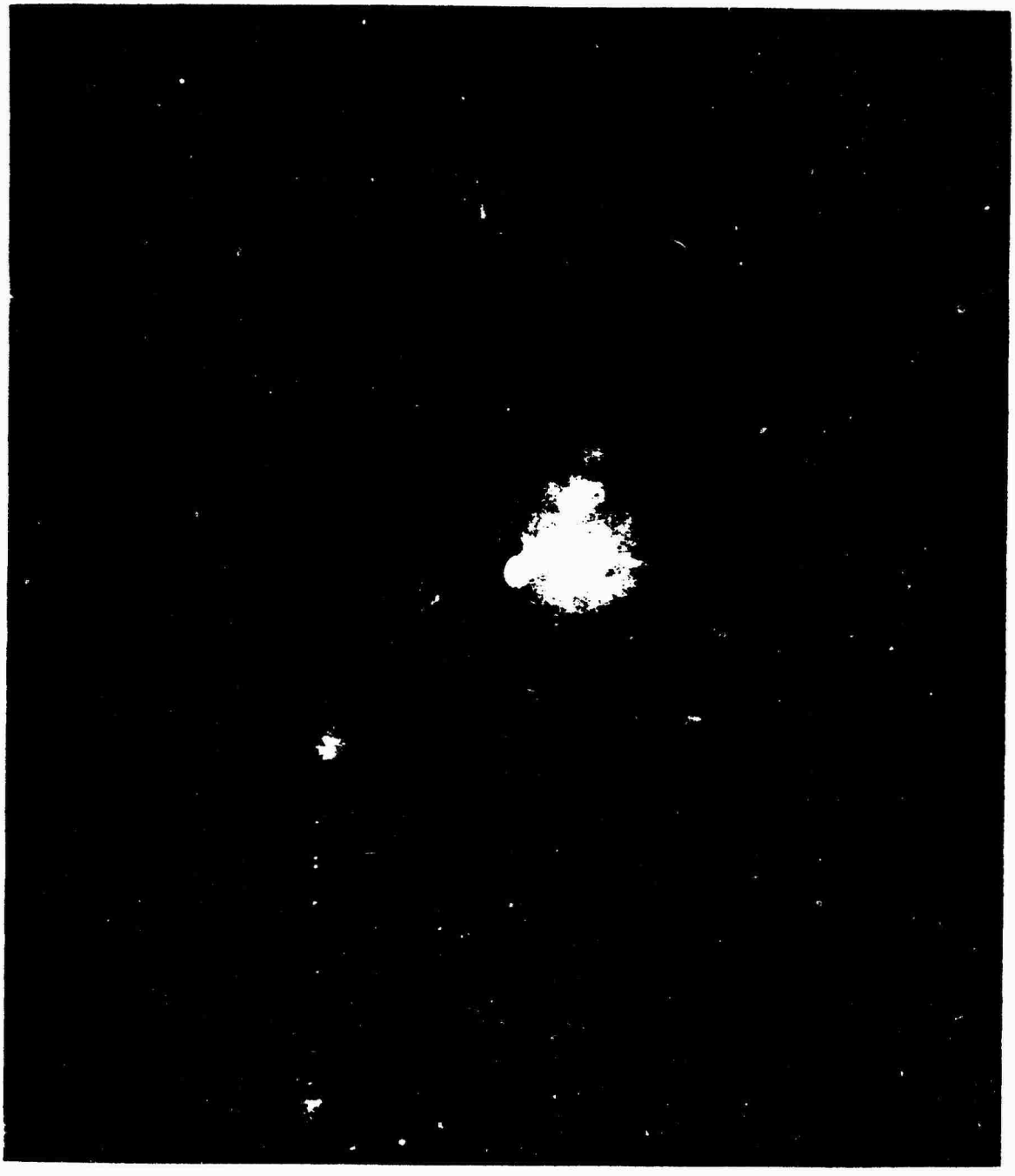

Figure 3.11 Star Fish Prime; bomb debris and Thor booster at 4.0 msec, taken from Johnston Island. Film 93325, Frame 1.

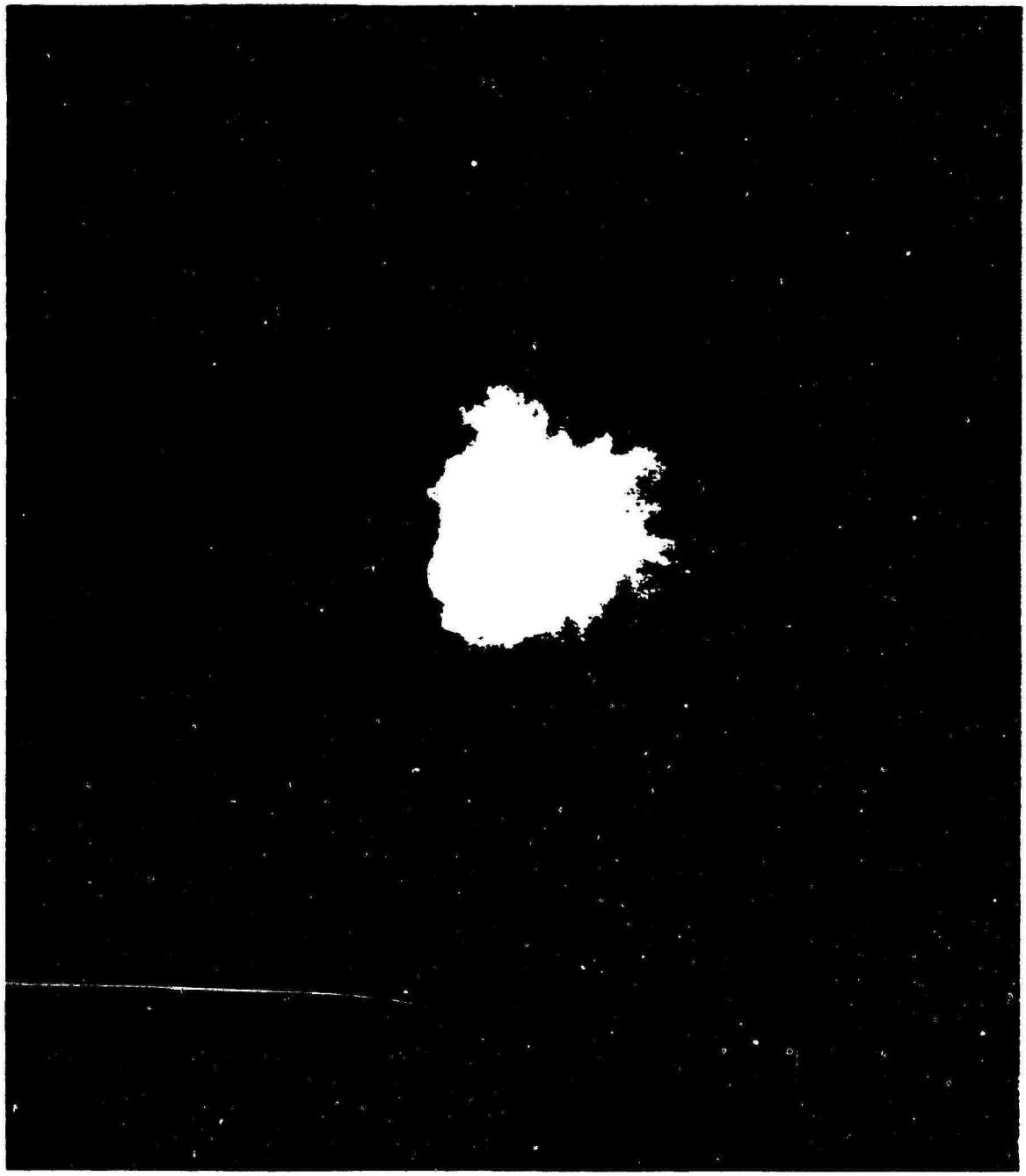

Figure 3.12 Star Fish Prime; bomb debris, Thor booster, and Pod S-1 at 6.8 msec, taken from Johnston Island. Film 93325, Frame 2.

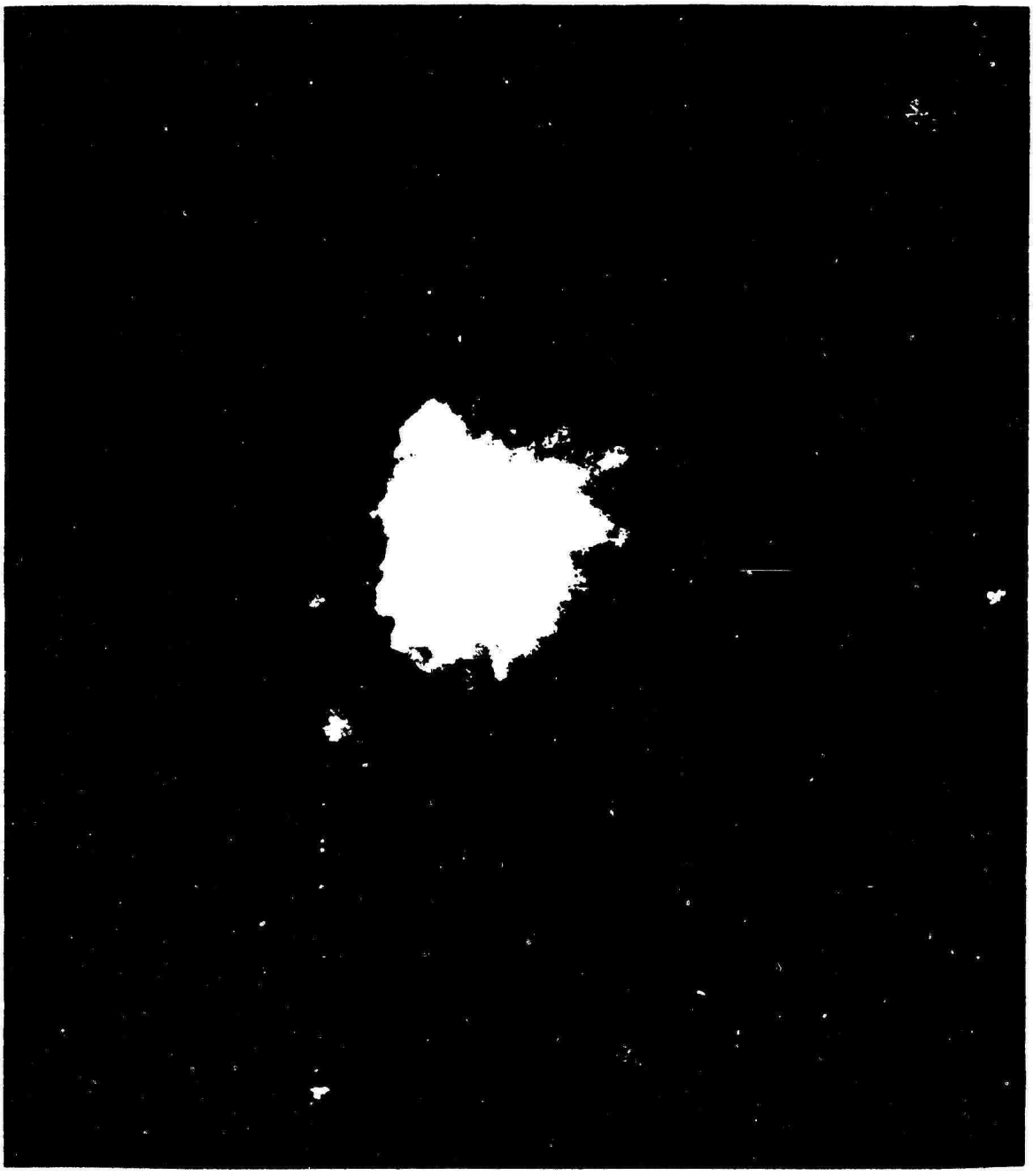

Figure 3.13 Star-Fish Prime; bomb debris, Thor booster, and Pods S-1 and S-2 at 9.6 msec, taken from Johnston Island. Film 93325, Frame 3.

Figure 3.14 Star Fish Prime: bomb debris, Thor booster, and Pods S-1, S-2, and S-3 at 15.1 msec, taken from Johnston Island. Film 93325, Frame 5.

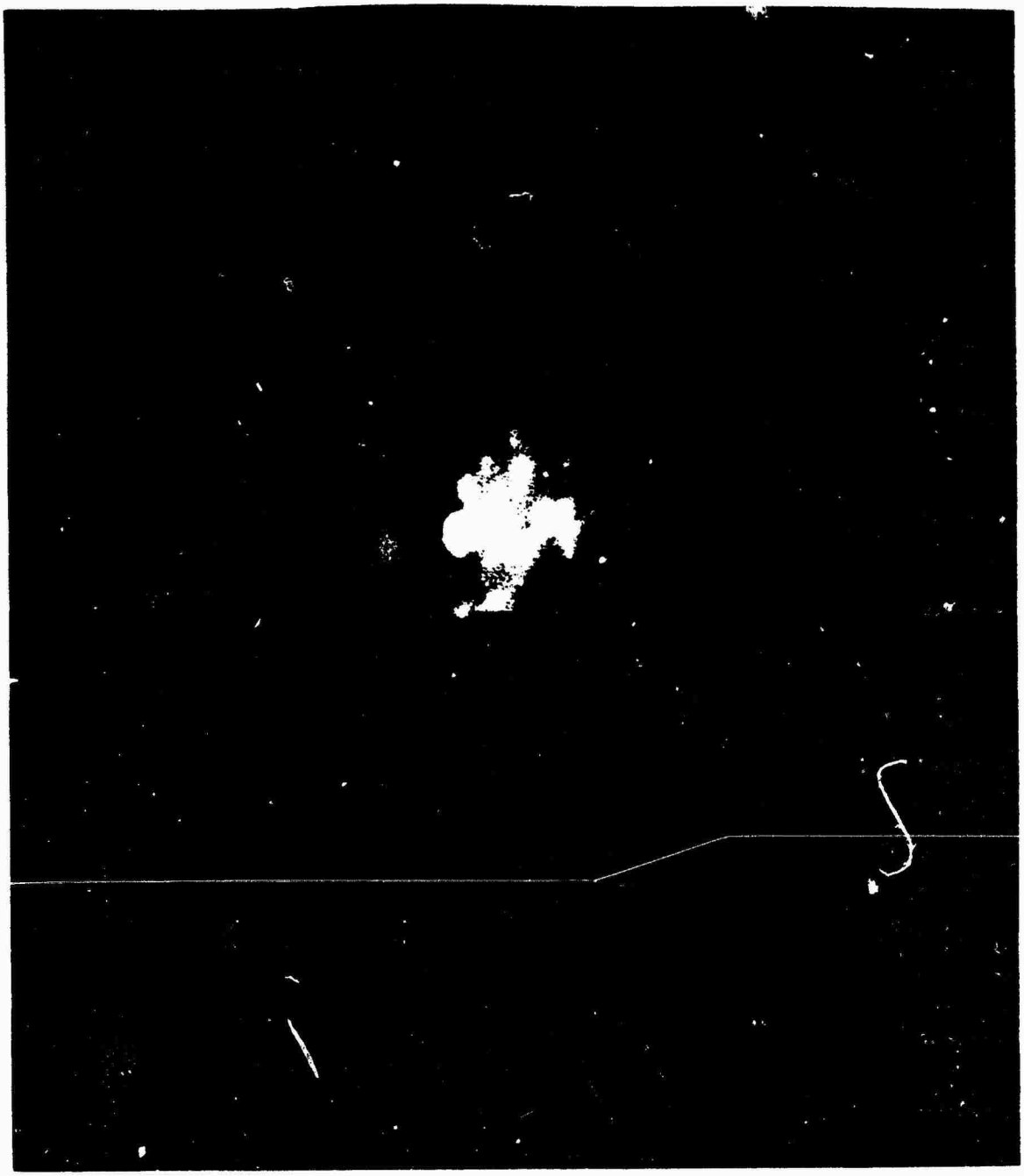

Figure 3.15 Star Fish Prime; bomb debris, Thor booster, and Pods S-1, S-2, and S-3 at 20.5 msec, taken from Johnston Island. Film 93325, Frame 7.

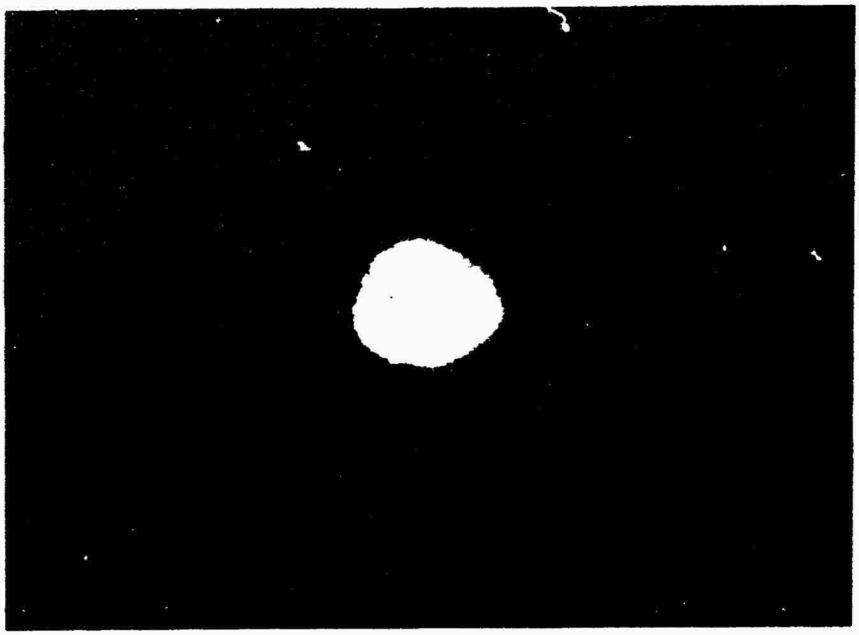

3.7 msec

6.5 msec

Figure 3.16 Star Fish Prime; bomb debris expansion and Pod S-1, taken from Aircraft 53120. Film 93127, Frames 1 and 2.

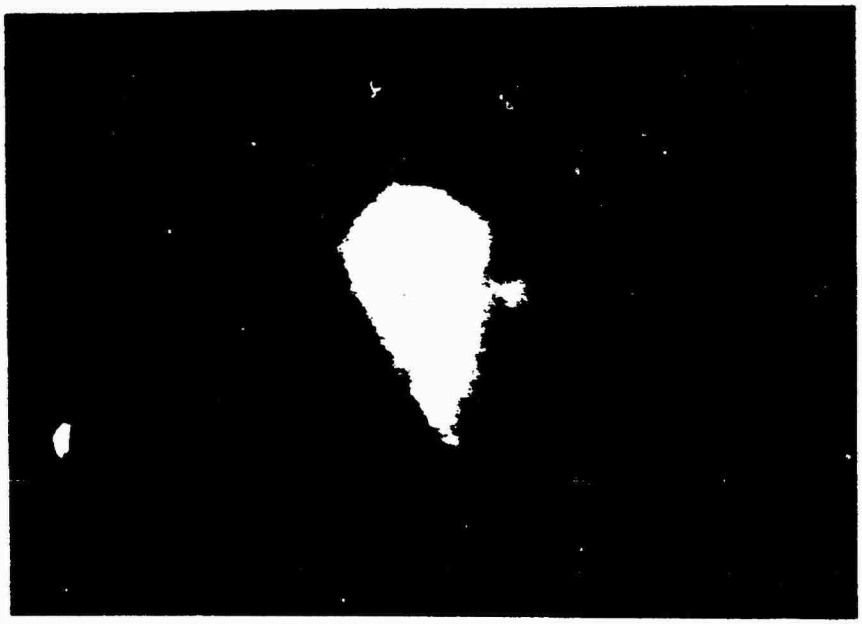

9.2 msec

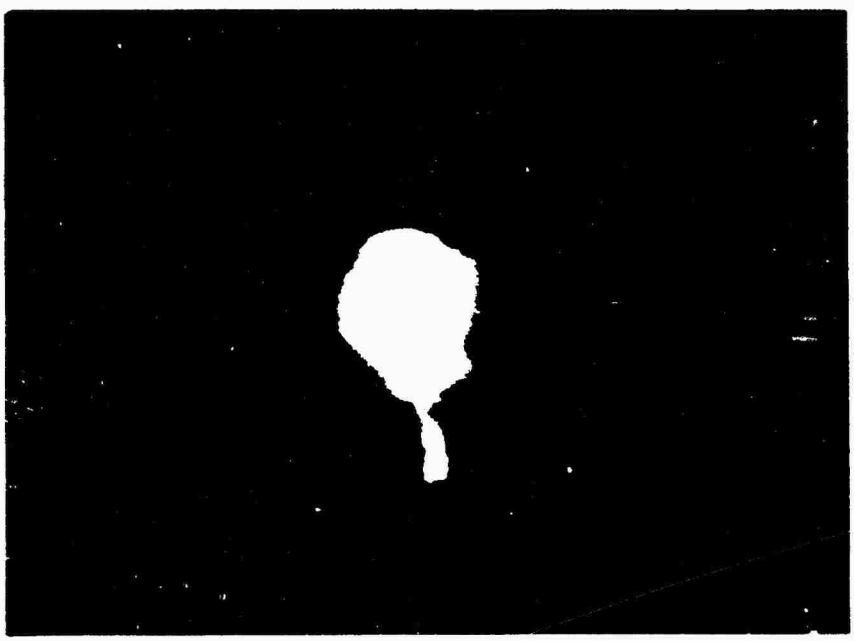

12.0 msec

Figure 3.17 Star Fish Prime; bomb debris expansion, Thor booster, and Pods S-1 and S-2, taken from Aircraft 53120. Film 93127, Frames 3 and 4.

Figure 3.18 Star Fish Prime; bomb debris, Thor booster, and Pods S-1, S-2, and S-3 at 14.7 msec, taken from Aircraft 53120. Film 93127, Frame 5.

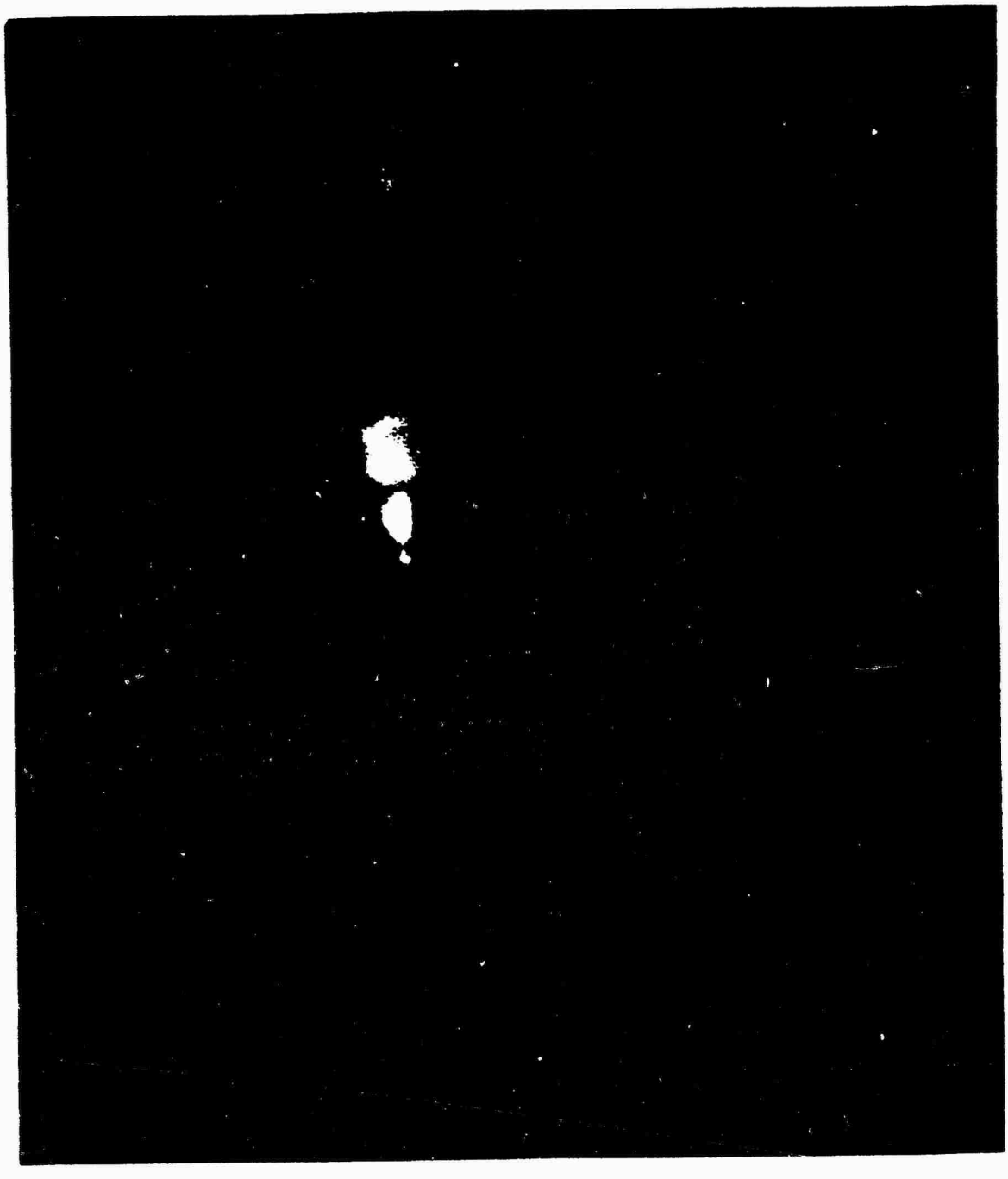

Figure 3.19 Star Fish Prime; bomb debris, Thor booster, and Pods S-1, S-2, and S-3 at 20.2 msec, taken from Aircraft 53120. Film 93127, Frame 7.

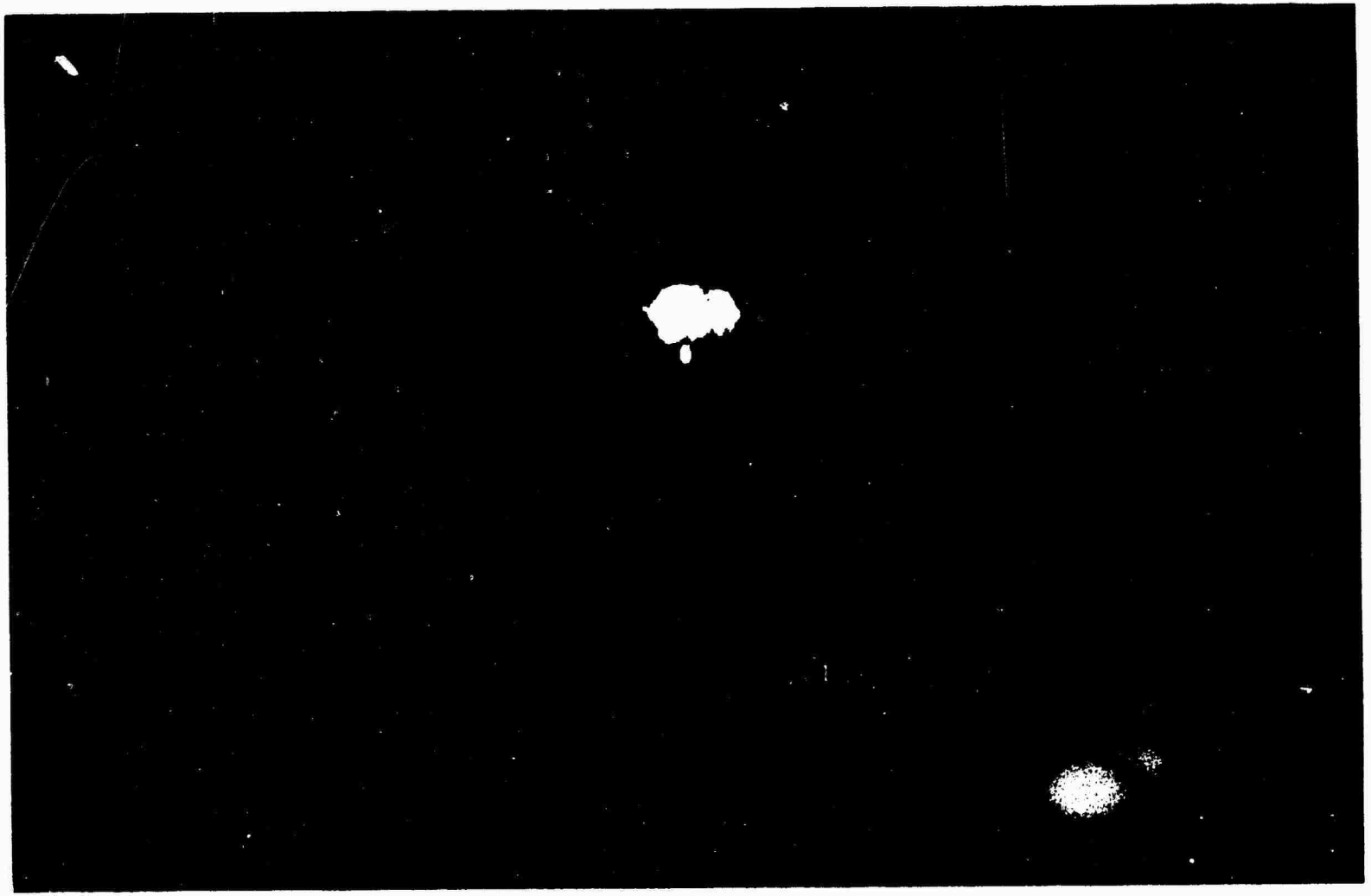

Figure 3.20 Star Fish Prime; bomb debris, Thor booster, and Pods S-1 and S-2 at 4.1 msec, taken from Aircraft 53144. Film 93227, Frame 1.

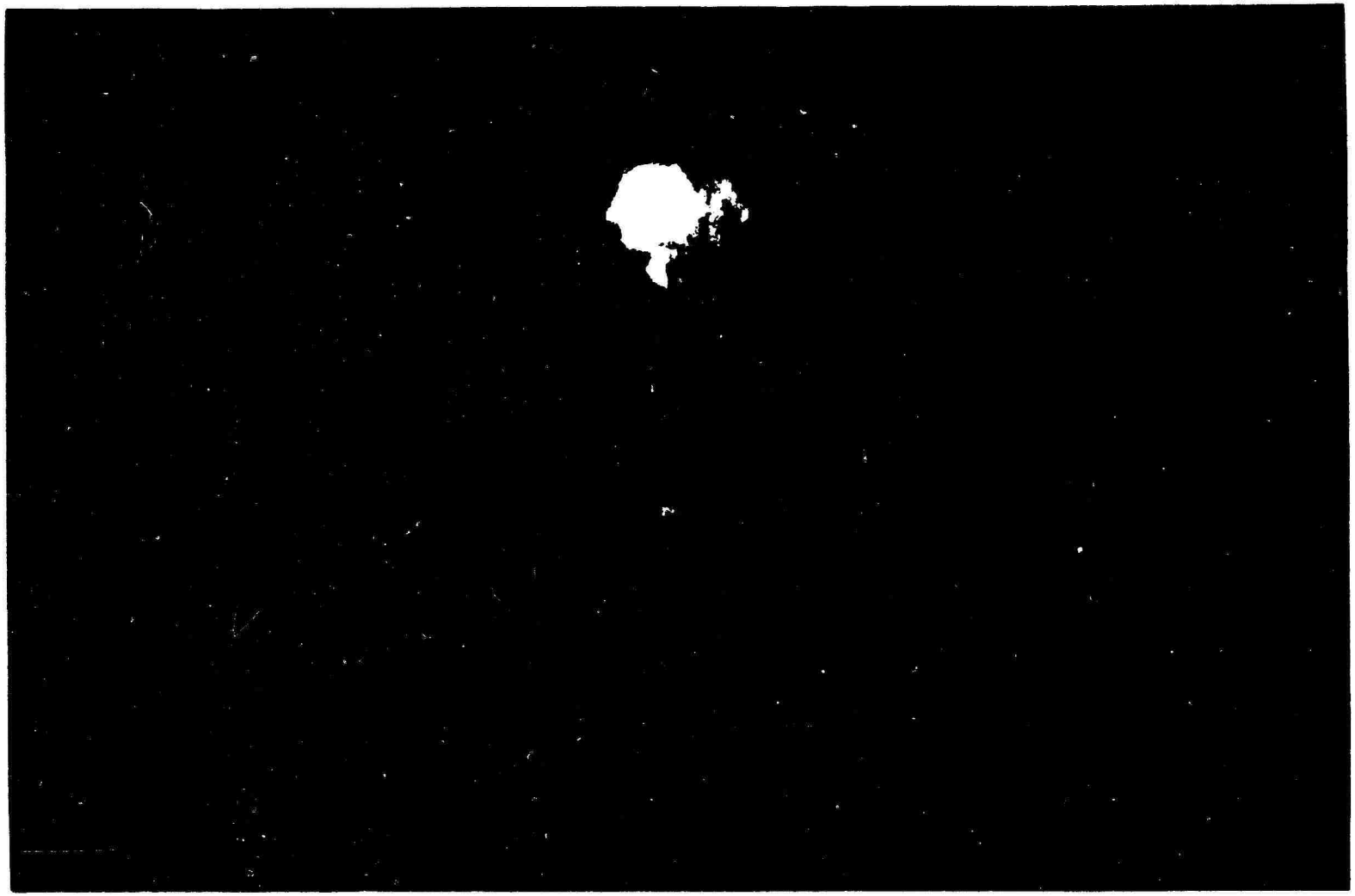

Figure 3.21 Star Fish Prime; bomb debris, Thor booster, Pods S-1 and S-2, and beta-ray aurora at 6.9 msec, taken from Aircraft 53144. Film 93227, Frame 2.

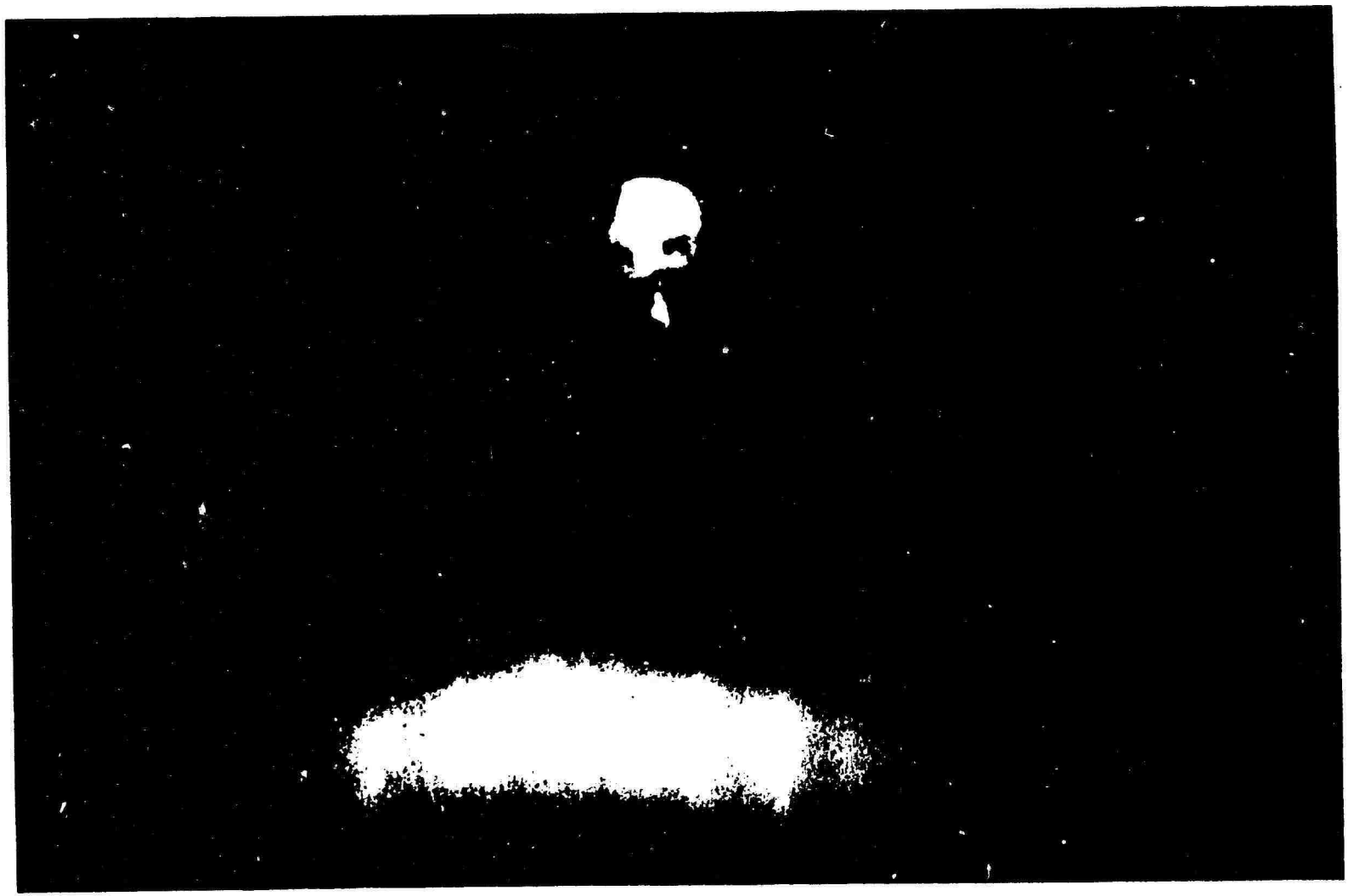

Figure 3.22 Star Fish Prime; bomb debris, Thor booster, Pods S-1, S-2, and S-3, and beta-ray aurora at 9.6 msec, taken from Aircraft 53144. Film 93227, Frame 3.

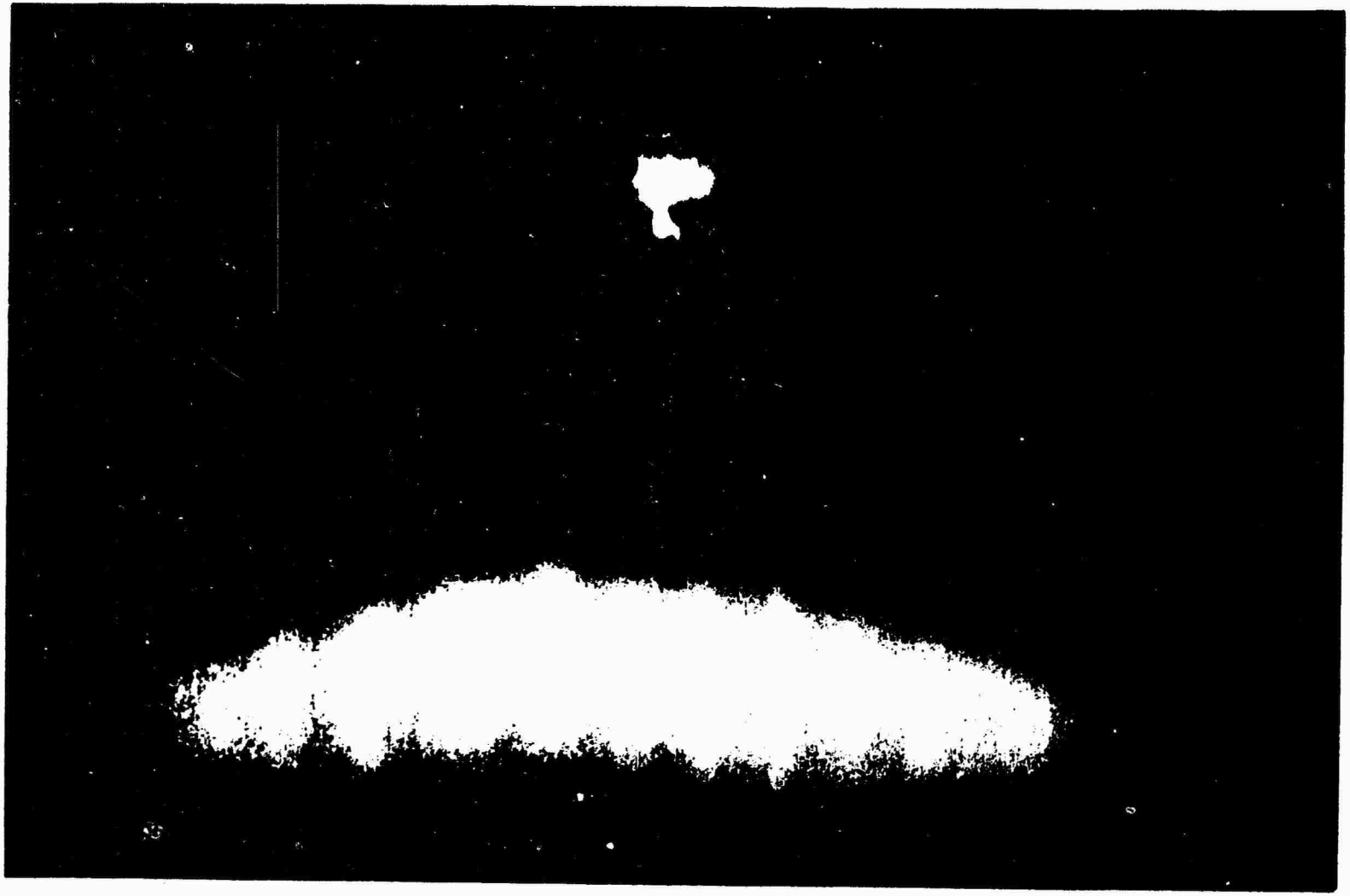

Figure 3.23 Star Fish Prime; bomb debris, Thor booster, Pods S-1, S-2, and S-3, and beta-ray aurora at 12.4 msec, taken from Aircraft 53144. Film 93227, Frame 4.

Figure 3.24 Star Fish Prime; bomb debris, Thor booster, Pods S-1, S-2, and S-3, and beta-ray aurora at 15.1 msec, taken from Aircraft 53144. Film 93227, Frame 5.

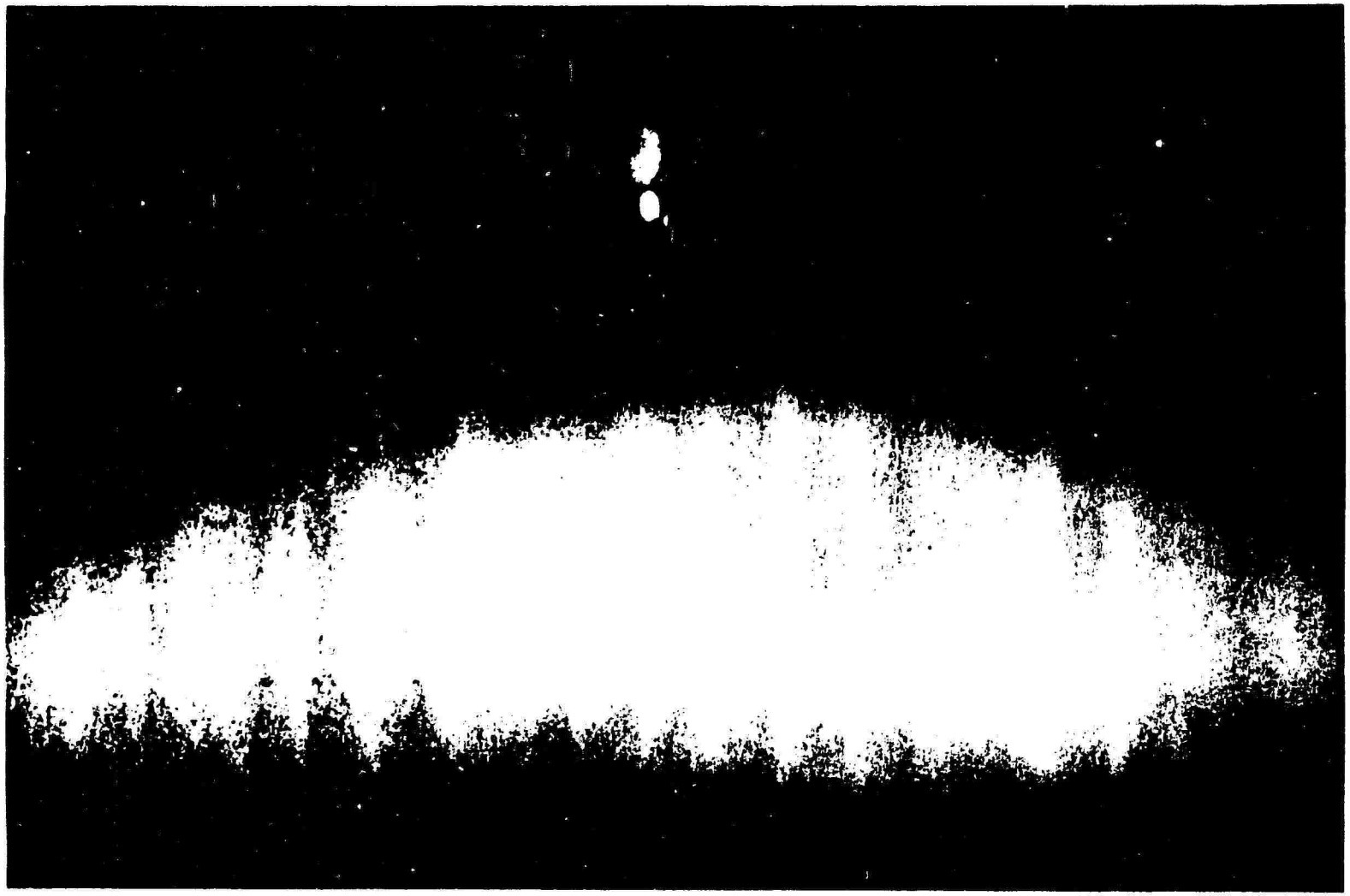

Figure 3.25 Star Fish Prime; bomb debris, Thor booster, Pod S-3, and beta-ray aurora at 17.9 msec, taken from Aircraft 53144. Film 93227, Frame 6.

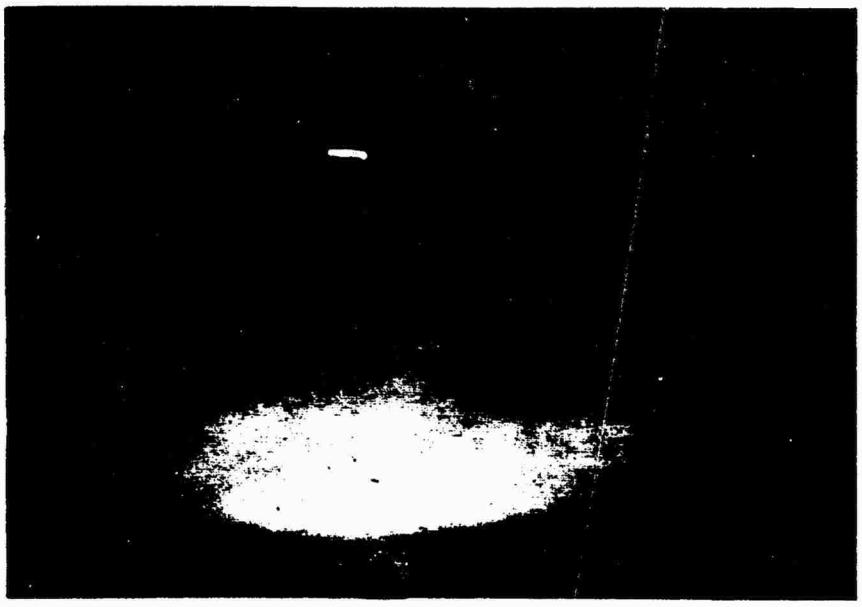

0.09 sec

0.16 sec

Figure 3.26 Star Fish Prime; northern beta-ray induced aurora, taken from Aircraft 53144. Film 93218, Frames 1 and 2.

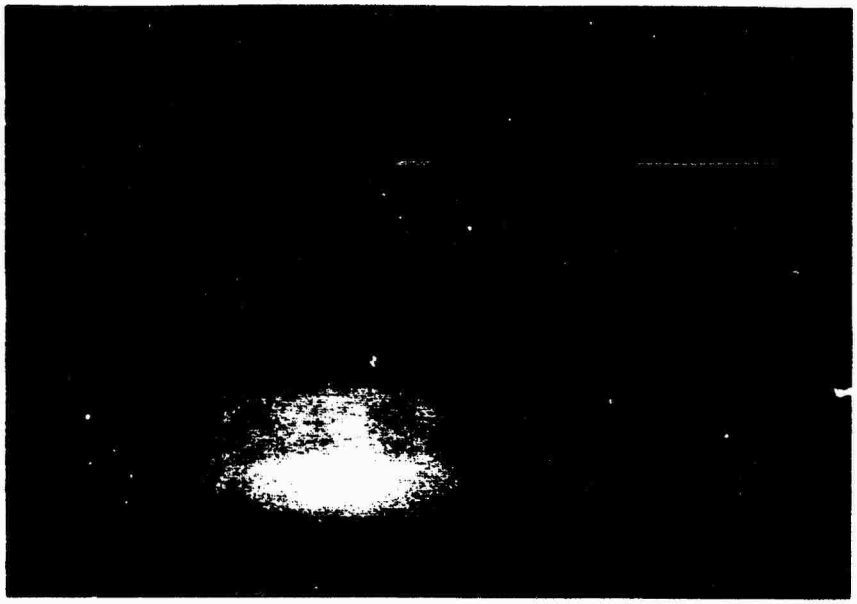

1.0 sec

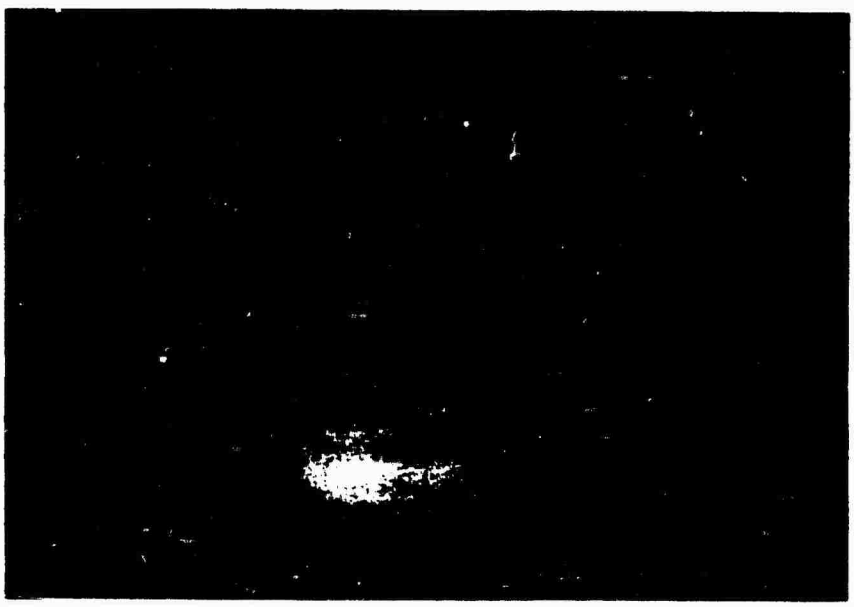

2.5 sec

Figure 3.27 Star Fish Prime; northern beta-ray induced aurora, taken from Aircraft 53144. Film 93218, Frames 15 and 40.

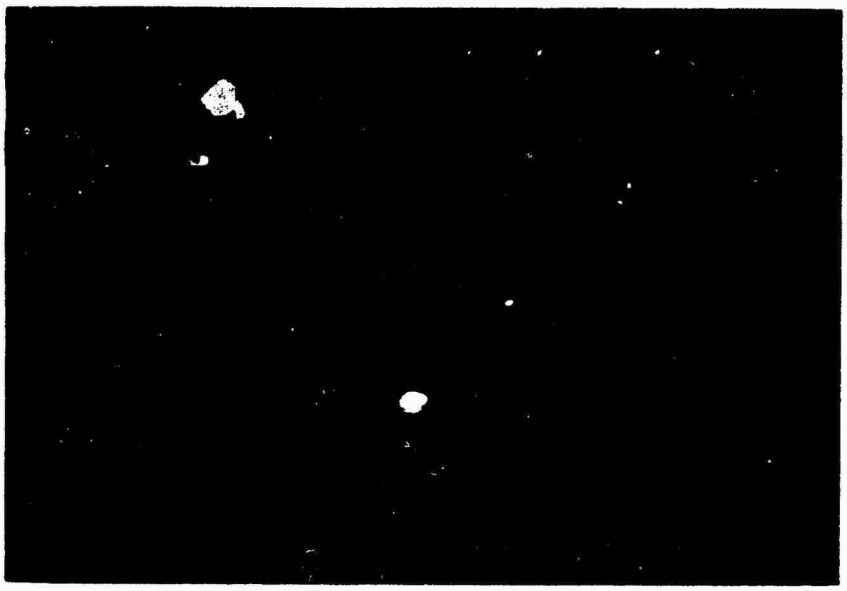

5 msec

15 msec

Figure 3.28 Star Fish Prime; bomb debris expansion, taken from Mauna Loa. Film 93701, Frames 0 and 1.

25 msec

35 msec

Figure 3.29 Star Fish Prime; bomb debris expansion, taken from Mauna Loa. Film 93701, Frames 2 and 3.

45 msec

55 msec

Figure 3.30 Star Fish Prime; bomb debris expansion, taken from Mauna Loa. Film 93701, Frames 4 and 5.

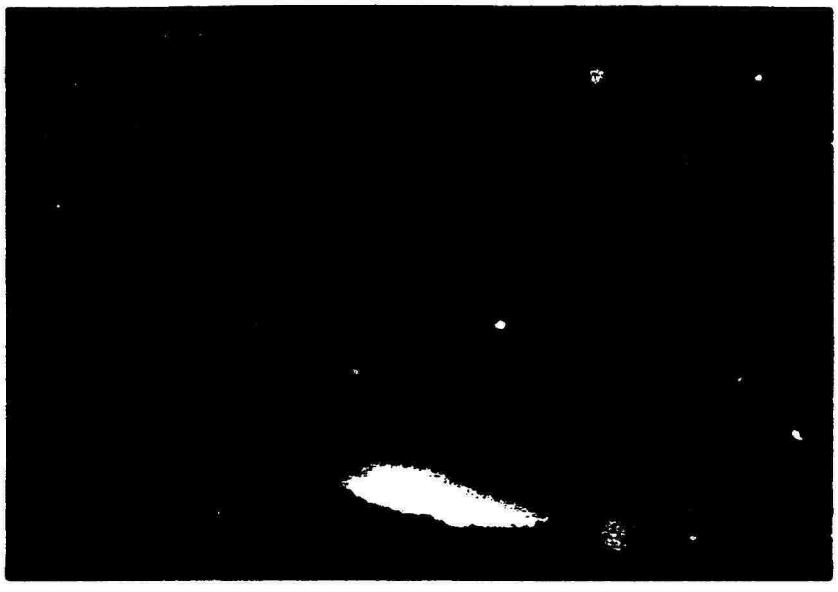

85 msec

145 msec

Figure 3.31 Star Fish Prime; bomb debris collision with atmosphere, taken from Mauna Loa. Film 93701, Frames 8 and 14.

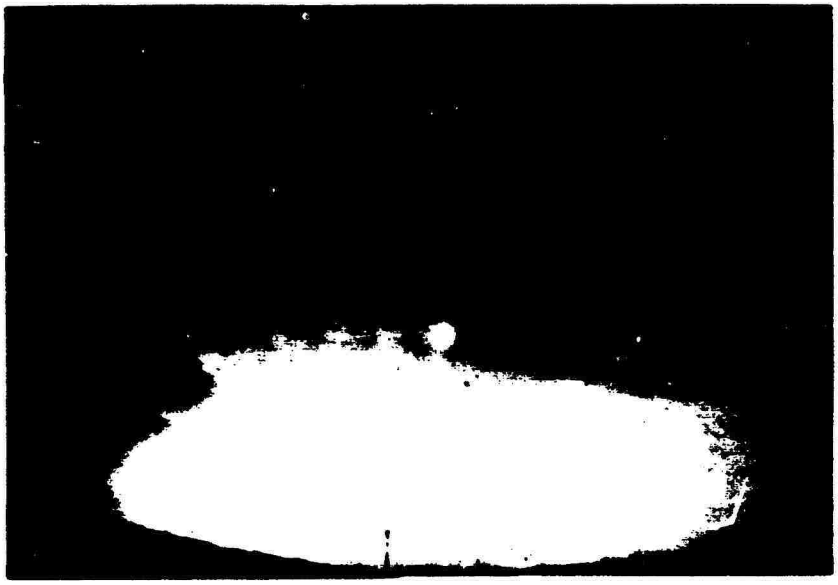

30 sec

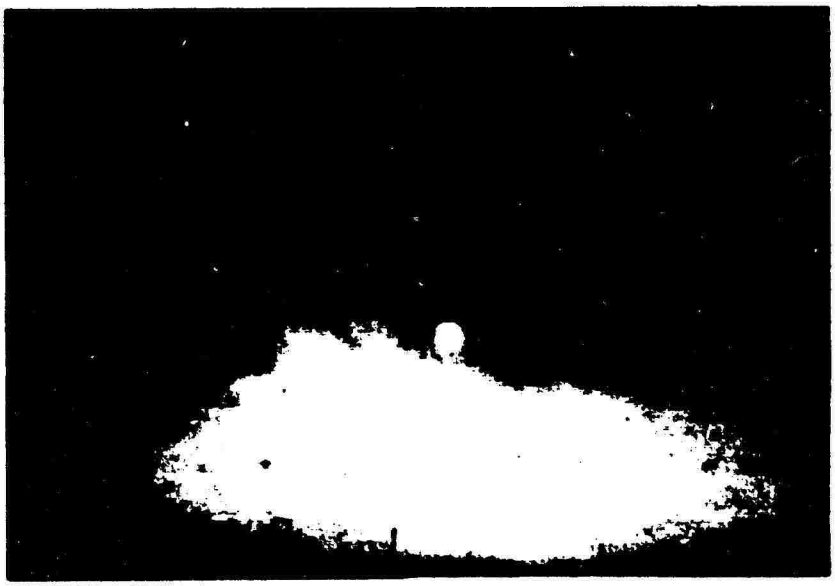

60 sec

Figure 3.32 Star Fish Prime; auroral streamers developing from debris and excited atmosphere below burst, taken from Mauna Loa. Film 93707, Frames 1 and 2.

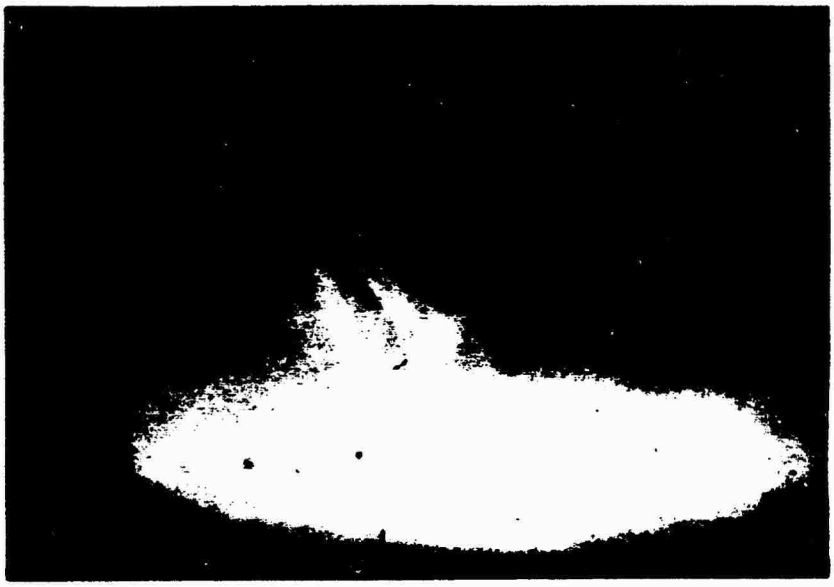

90 sec

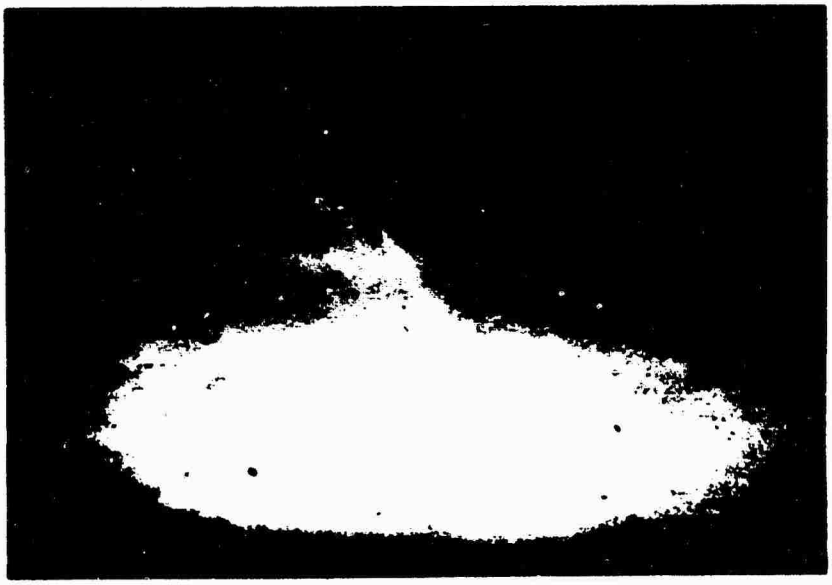

120 sec

Figure 3.33 Star Fish Prime; auroral streamers developing from debris and excited atmosphere below burst, taken from Mauna Loa. Film 93707, Frames 3 and 4.

Figure 3.34 Star Fish Prime; auroral streamers developing from debris and excited atmosphere below burst at 150 seconds, taken from Mauna Loa. Film 93707, Frame 5.

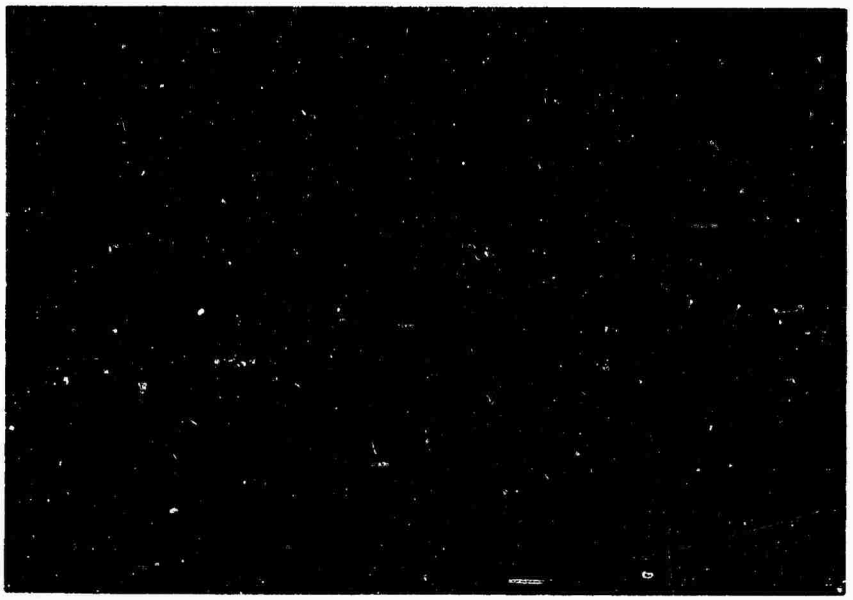

Figure 3.35 Star Fish Prime; auroral display north of French Frigate Shoals at 210 seconds, taken from Mauna Loa. Film 93707, Frame 6.

Figure 3.36 Star Fish Prime; auroral display north of French Frigate Shoals at 240 seconds, taken from Mauna Loa. Film 93707, Frame 7.

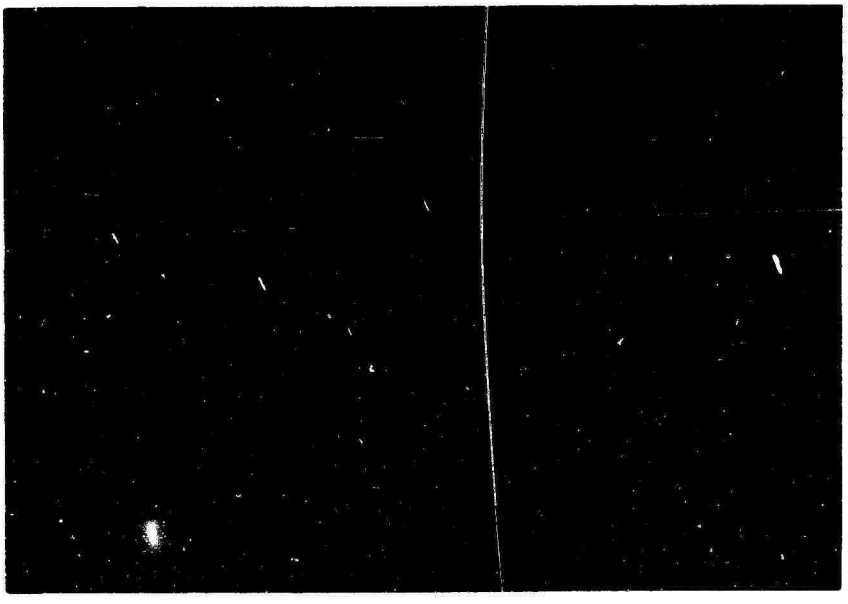

Figure 3.37 Star Fish Prime; auroral display looking south from Mauna Loa at 13 minutes. Film 93707, Frame 17.

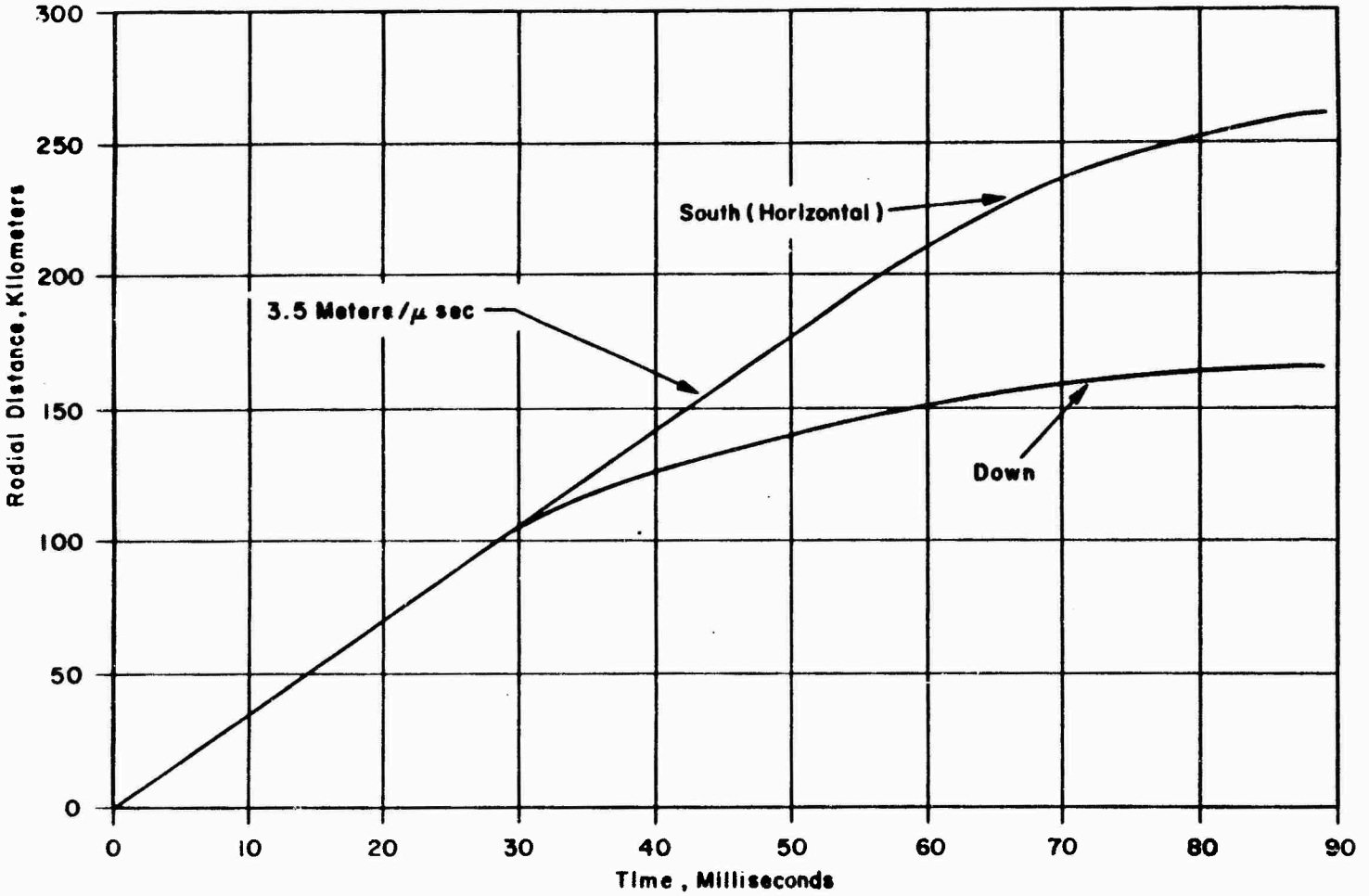

Figure 3.38 Star Fish Prime; radial distance versus time for the bomb debris in the horizontal and downward directions.

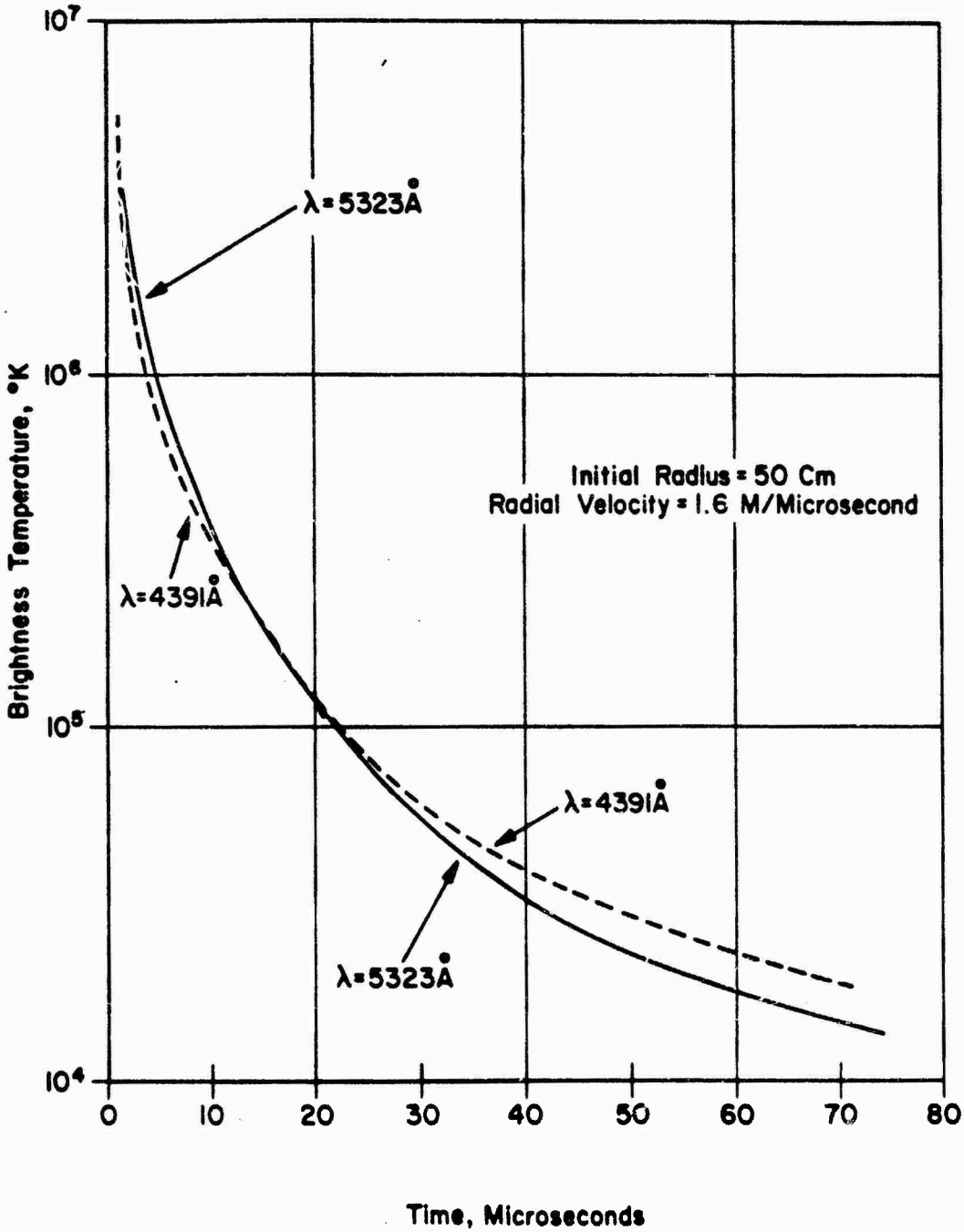

Figure 3.39 Star Fish Prime; brightness temperature versus time, from 1 to 70 μsec.

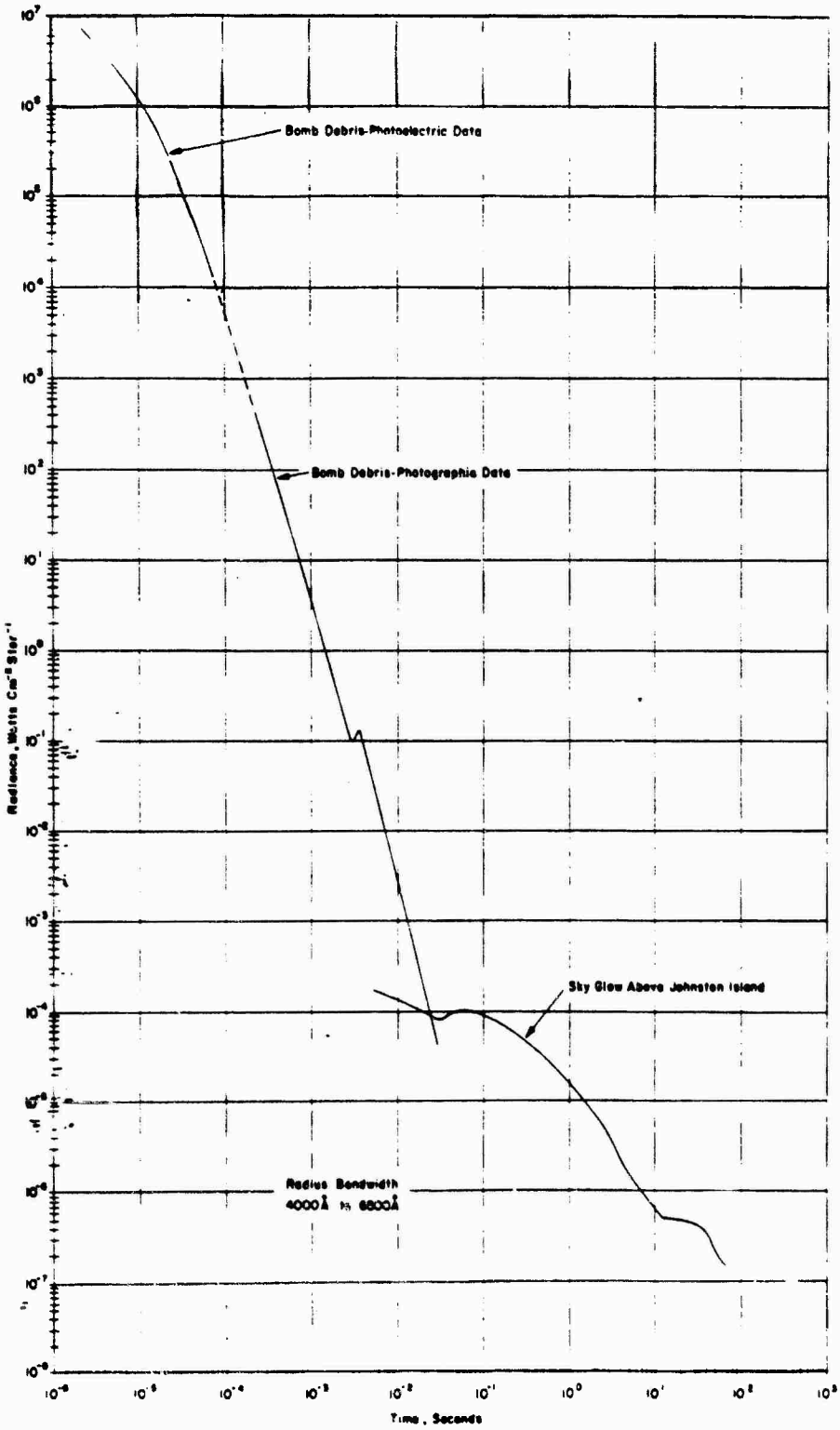

Figure 3.40 Star Fish Prime; radiance versus time of bomb debris and sky over Johnston Island.

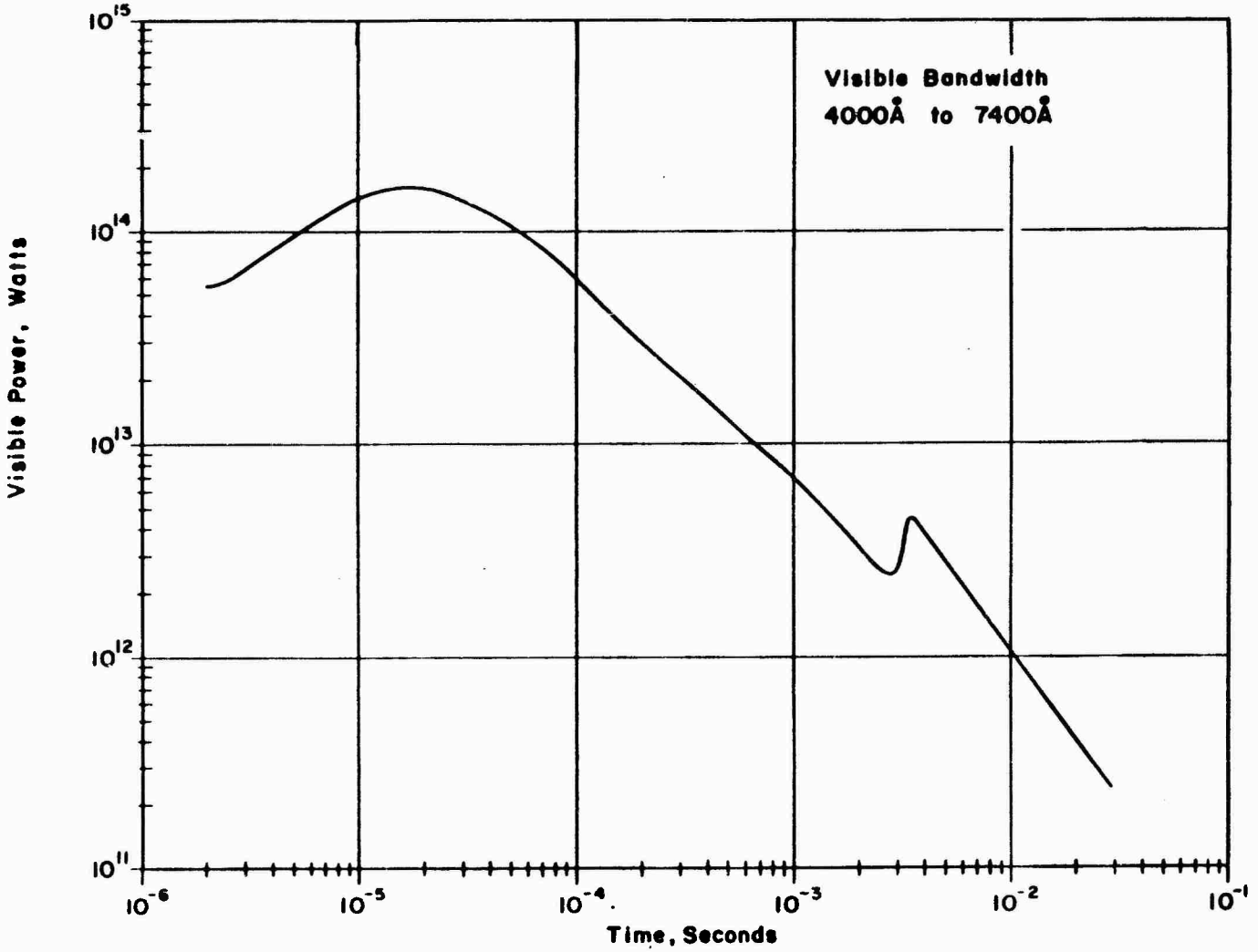

Figure 3.41 Star Fish Prime; visible power versus time curves.

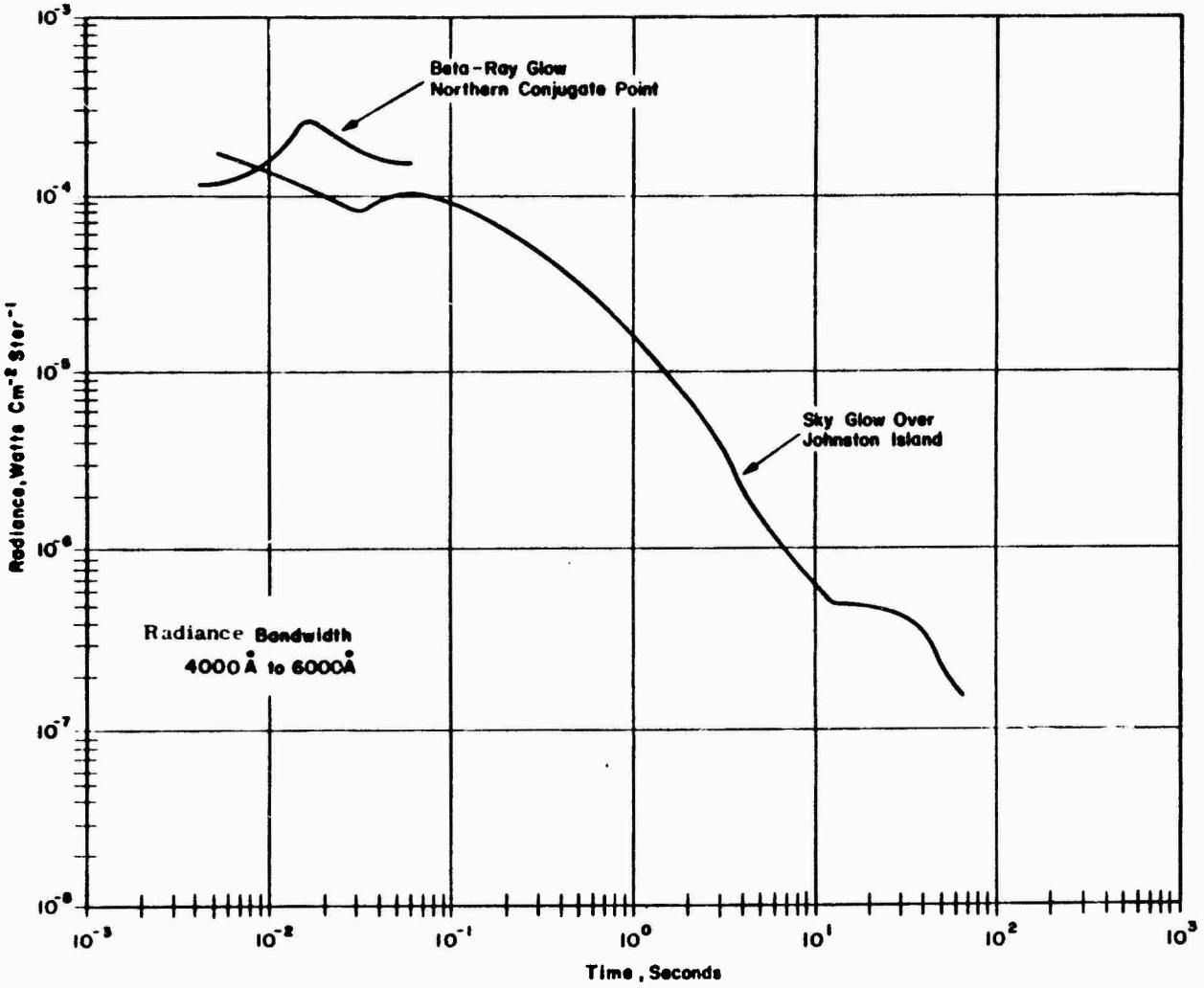

Figure 3.42 Star Fish Prime; radiance versus time for sky glow and beta-ray glow.

CHAPTER 4

CHECK MATE PHOTOGRAPHIC RESULTS

Check Mate was detonated at 0830:00.0029Z on 20 October 1962. The following information on the warhead and vehicle has been extracted from Reference 16.

The predicted burst position and the actual burst position measured by Sandia Corporation were:

	Predicted	Actual
Latitude	16° 06' 42.12'' N	16° 04' 20.57'' N
Longitude	169° 39' 40.32'' N	169° 36' 35.95'' N

4.1 INSTRUMENTATION

4.1.1 Camera Parameters. Tables 4.1 through 4.3 present the camera parameters used for Check Mate. This event was the first after the interim between Phases I and II of Fish Bowl and the first following the loss of Aircraft 53144 and the outfitting of its replacement, Aircraft 60376. The instrument additions were a result of experience obtained on Star Fish Prime, while the instrument changes resulted from both experience and procurement difficulties. The additions were made in order to more fully cover the earliest time phases of the events and to extend coverage in space and time. In general the new instruments used in the aircraft were functional copies of those they replaced.

Excellent results were obtained on Star Fish Prime using color film, and results from the first trials of XR film on several of the Christmas Island atmospheric shots exceeded expectations. Both of these film types were used in greater quantities on Check Mate. In general no neutral density (ND) filters were used because of the low yield of the weapon and the expected low brightness levels. Because of the great-circle probable error expected with the Strypi vehicle, wider fields of view were employed by using short-focal-length lenses. The low expected brightnesses led to use of maximum lens apertures and exposure times.

4.1.2 Aircraft Positions. The planned and actual positions for both aircraft at burst time are summarized in Table 4.4. These positions represent a slight change from the original concept of aircraft placement as a result of experience gained in examining the Star Fish Prime records. The two aircraft were still used to obtain views generally along and perpendicular to the magnetic field lines, but now they were placed away from exact perpendicularity and parallelism. In this way any wide-sweeping phenomena would be seen over larger areas. One aircraft was placed north of the event, and the other was placed in the southeast quadrant. Since Aircraft 53120 more nearly contained the

originally planned instrumentation, it was placed in the primary (northern) position. The exact choice of position for Aircraft 60376 was made difficult because of the danger zones south of Johnston Island. In fact, the final choice was not made until the afternoon of D-day. The late changes in this position, coupled with a failure of the aircraft search radar, led to the incorrect positioning of this station, with the consequent loss of some data records.

Figure 4.1 presents an elevation view of the relationship of the aircraft and the predicted burst point. Also shown is a plan view of the locations with respect to ground zero. The zero positions of Aircraft 53120 and 60376, and their tracks while recording data after the burst, are given in Figure 4.2.

4.1.3 Instrument Pointing. Because of the expected errors in burst location and the possibilities of large debris expansion, the fields of view of the various instruments were chosen to cover large sky areas. Figures 4.3 through 4.5 show representative fields of view as they appear projected onto a plane containing the burst point. The smallest areas belong to high-speed cameras which are used to photograph the earliest phases of the event when it is relatively small, and the larger areas are used to insure coverage of the full expansion and rising motion of the later stages of the explosion.

Table 4.5 summarizes the pointing information pertinent to the Johnston Island Station.

4.2 CAMERA RECORD SUMMARY

The camera results obtained on Check Mate for the two aircraft stations and the Johnston Island station are summarized in Tables 4.6 through 4.8. Table 4.9 gives a short statistical summary of the results in terms of success and failure. Except for Aircraft 60376, very good records were obtained. The main reason for the loss of data records in that instance was the error in positioning mentioned in Paragraph 4.1.2. Because of the pronounced asymmetry of the Check Mate burst, the loss of these records has hindered a complete understanding of this event.

4.3 PICTORIAL HISTORY

Check Mate produced spectacular visible displays. The characteristic feature of the Check Mate photographic records is debris motion. Because a strongly absorbing fireball was not formed, this motion could be followed from its initial stages, microseconds after the burst, to its final slow dispersal, 9 minutes later. Although some shock waves were present, they were notable by their lack of intensity compared to shots at lower altitudes.

The appearance of Check Mate during the first 279 milliseconds is illustrated in Figures 4.6 through 4.21, taken from Johnston Island with a Photo-Sonics 10B camera running at 360 frames/second. At 1.4 milliseconds, Figure 4.6, the debris is a small circle in the photograph, surrounded by a much larger region of X-ray-excited air.

In Figure 4.7, the debris has expanded into a ring leaving a small circular hot spot marking the original burst position. This structure is seen more clearly in Figures 4.8 and 4.9.

At 12.5 milliseconds, Figure 4.10, instabilities are clearly seen in the expanding debris
They are probably present in the previous picture but cannot be resolved clearly. Although the debris is concentrated in the ring, small amounts of it are distributed in the region between the ring and its center. The next sequence of photographs, Figures 4.11 through 4.16, shows the growth of the instabilities from 15.3 milliseconds to 29.2 milliseconds in steps of 2.8 milliseconds. The individual waves or perturbations grow into jets of material which move faster than the main body of debris.

Figures 4.17 through 4.21 follow the debris expansion from 60 to 279 milliseconds.

In this sequence, the jets continue their expansion, and the debris becomes dispersed.

Figures 4.22 and 4.23 contain four views of the expanding debris taken from Johnston Island with a Photo-Sonics 4C camera operating at 2500 frames/second using high-speed Ektachrome film. This sequence shows the early stages of the instabilities in the expanding debris. A clear distinction between the white debris and the bluish X-ray deposition region can be seen.

Figure 4.24, a view of Check Mate, showing both the expanding debris and the X-ray deposition region at 28 milliseconds, was taken from Aircraft 53120 north of the burst with a Photo-Sonics 4C camera operating at 2500 frames/second. Comparison of this picture with Figures 4.15 and 4.16, which were taken from Johnston Island at approximately the same time, shows that the same features were seen from these two vantage points.

Figures 4.25 and 4.26, covering the period of 43 to 696 milliseconds, were taken from Aircraft 53120 located north of the burst with a Photo-Sonics 10B camera using high speed Ektachrome film. The X-ray deposition region maintains the same

size, although it decreases in intensity, and finally is not visible. The debris expands and passes beyond the X-ray region. The fast-moving jets which grew from the original instabilities are seen clearly, and a few jets can be followed throughout the entire sequence.

The views of Check Mate taken from Aircraft 60376 located to the southeast of the burst show a new and interesting feature of the expanding debris. Figures 4.27 through 4.34 are 8 pictures taken with a Photo-Sonics 10B camera running at 360 frames/second, and covering the interval from 4.2 milliseconds to 24 milliseconds in approximately 3-millisecond intervals. The new feature is the existence of two expanding debris rings of approximately the same diameter and the same velocity of expansion. Further, the central spot can clearly be seen to be a well-defined mass of hot material.

Another interesting feature of this sequence is the large conical protuberance which appears, starting in Figure 4.30. The decrease in size in the direction away from the center of the burst is undoubtedly caused by the perspective introduced by the camera. The long axis of the protuberance is approximately in the direction of the geomagnetic field. Charged particles, possibly electrons,

are suggested as the cause. If these are electrons, the decrease in intensity which is so noticeable in Figure 4.34 is hard to explain, since the electron emission rate from the radioactive debris would not change greatly in this short interval.

Figures 4.35 and 4.36 show an eight-picture sequence of Check Mate. They were taken by a Maurer camera from Aircraft 53120, located north of the burst. The last three pictures show the development of a weak converging shock which causes the center of the debris to brighten. The details of this shock can be seen more clearly in the four pictures in Figures 4.37 and 4.38 which were taken from Johnston Island with a Maurer camera. This shock is not seen as a clearly localized ring, but only as a region of gas glowing more than its surroundings.

Although, at 3 to 5 seconds, only the debris could be seen from Johnston Island, the next six pictures, Figures 4.39 through 4.44, from Aircraft 60376 located southeast of the burst, show a region of emitting air surrounding the debris. This region expands faster than the debris and is undoubtedly a shock wave. Figure 4.45 shows the same region taken on high-speed Ektachrome film with a Beattie-Coleman camera from the same aircraft. The red color is attributed to the red auroral line at λ6300 Å.

The red shock is no longer visible in the two pictures in Figure 4.46, taken with the same Beattie-Coleman camera. Only the debris is seen as it begins to move along the geomagnetic field.

At these late times, the debris also shows a large upward movement. Between Figure 4.47, taken at 8 seconds, and Figure 4.48, taken at 16 seconds, the debris has moved upward

Both pictures were taken with a Cloud camera from Aircraft 53120, located north of the burst. A faint beta-ray aurora can be seen in both pictures, the shape being determined by the camera perspective.

The next three pictures in Figures 4.49 through 4.51 were taken by a Traid camera from Aircraft 53120. They show the influence of the geomagnetic field on the motion of Check Mate debris. The central spot of earlier photographs has moved to the top of the debris circle and then formed a distinct wedge opening in the debris. Continued upward motion accentuates this separation, and two arms formed in the debris mass.

This peculiar behavior can be seen in more detail in Figures 4.52 and 4.53. This series of four pictures was taken from Johnston Island with a Cloud camera. The alignment of debris filaments

along the field lines and the formation of two branches of the debris are evident.

The final sequence of 8 photographs, taken with a Minolta camera (Figures 4.54 through 4.56), shows the debris from Check Mate rising above the horizon at Mauna Loa and then extending along the geomagnetic field lines.

4.4 RESULTS

4.4.1 Geometric Measurements. Check Mate had two main geometric features: the large region of X-ray-heated air, which essentially remained constant in size until it began to fade, and the expanding ring of debris (see Figures 4.25 and 4.35).

The burst point was centered on the horizontal diameter, but not on the vertical diameter.

At times less than 10 to 15 milliseconds, the weapon debris was concentrated in the form of a cylindrical ring whose diameter could be easily measured. After these times, the unstable material distorted into a shape in which no single feature could be followed from frame to frame. Instead, it was necessary to follow the outside edge of the bulk of the debris, the edge being a subjective definition in the mind of the film reader. Figure 4.57 gives the so-defined debris radius in the interval 0 to 60 milliseconds. The debris undergoes a large deceleration during the first 10 milliseconds, its velocity

decreasing from 1000 km/sec to 130 km/sec. The debris velocity then decreases slightly to an approximately constant value of 100 km/sec which it maintains to approximately 60 milliseconds. Gradual deceleration continues, and an average velocity of 31 km/sec is found over the interval 100 to 200 milliseconds. Over the interval 200 to 300 milliseconds, the expanding debris has an average velocity of 16 km/sec. Figure 4. 58 gives the radius as a function of time from about 400 microseconds to 300 milliseconds.

The radial expansion of the debris out to tens of seconds is given in Figure 4. 59. At these times, when the debris has no clearly defined outer surface, radius should be taken to mean the radius of a circle drawn around the debris so as to include at least 95 percent of the visible material. This radius of the main debris body does not get larger than about 30 km after 5 to 10 seconds. After about 20 seconds, the debris no longer has a circular shape, but begins to elongate into an elliptical shape.

The rise of the Check Mate debris as a function of time is presented in Figure 4.60. The bottom, center, and top of the debris ring as seen from Aircraft 53120 could be followed out to

approximately 20 to 25 seconds. At that time an opening or cleft began to develop in the debris (see Figures 4. 49 and 4. 50). From that time on, the points indicated in the legend to Figure 4. 60 were followed. The whole mass of debris had an upward velocity of about 2 km/sec initially.

The points in Figure 4. 60 have been corrected for aircraft roll and for camera aspect. Even so, the sudden decrease in motion which apparently occurred around 40 to 50 seconds seemed suspicious. To further examine the rise of Check Mate, an attempt to triangulate the positions of several recognizable points on the debris cloud was undertaken. The preliminary results are shown in Figure 4. 61. There are still some unexplainable features to the motion, but it is clear that the apparent stabilization of Check Mate debris actually represents its capture by the magnetic field line. Since it was moving along a constant angular ray from the aircraft camera, its upward motion was not detected.

4. 4. 2 Shock Waves. Only two shock waves have been located in the Check Mate photographs. The first is a converging shock which forms 1 or 2 seconds after the burst, reaches the

center around 4 seconds, and then reflects and moves out to the periphery of the debris. It can be seen in Figures 4. 37 and 4. 38 as a tenuous blue ring. Because of the absence of low material density near the center of the debris, the shock was not clearly visible and was therefore hard to measure. This difficulty of measurement was particularly severe after the shock had reflected and was moving out. Although a continuous history of this shock was not obtained, visual examination of the motion-picture records showed that the two branches of this shock shown in Figure 4. 59 were in reality continuous. This examination also confirmed that the shock moved out rapidly following its reflection.

The second shock was an outward-going red shock which apparently originated outside of the main debris body. It can be seen clearly in the sequence of photographs in Figures 4. 39 through 4. 45. These pictures were taken from Aircraft 60376 located to the east of the burst. No clear evidence of its existence has been found in the records from Johnston Island and Aircraft 53120.

4.4.3 Radiometric Measurements. A radiometric history of Check Mate is presented in Figure 4.62. As with the geometric measurements, there are only two distinct features: the X-ray-heated air and the debris. The radiance of the debris was difficult to obtain for the same reasons that made geometric measurements difficult; i.e., the shapeless appearance of the debris. However, three general debris regions were measured: the debris core, an area near the mean radius of the debris ring, and an area near one-half the mean radius. The radiance of all these regions decreased in a monotonic way, and there are no unusual features.

TABLE 4.1 SUMMARY OF CHECK MATE CAMERA PARAMETERS, AIRCRAFT 53120

INSTRUMENT AND STATION POSITION		FILM TYPE	FILM NUMBER	AIMING ANGLES IN DEGREES ELEV	AZIMUTH	FILTERS ND	COLOR	FOCAL LENGTH MM	LENS F/N	FRAMES PER SECOND	SHUTTER SECTOR, DEGREES	EXPOSURE TIME	MARKER RATE CPS
MAURER	W1	EDER	94121	30	0	-	-	80	2.8	5	-	0.002SEC	-
MAURER	W2	XR	94122	19	0	-	-	38	4.5	5	-	0.002SEC	-
PHOTO-SONICS 10 B	W5	EDER	94127	30	0	-	-	180	2.5	360	60	0.1MSEC	200
KFC-600	W6	XR	94104	30	0	2.0	WR12	250	9.5	100D0O	-	1MUSEC	-
RAPATRONIC	W7	XR	94103	30	0	-	-	490	22	*(A)	-	5MUSEC	-
TRAID	W8	DXN	94117	30	0	-	-	25	2.3	16	160	30MSEC	50
TRAID	W9	EDER	94118	30	0	-	-	25	2.3	16	160	30MSEC	50
CLOUD	W10	DXN	94109	25	0	-	-	105	3.7	75	-	1SEC	CLOCK
FAIRCHILD HS-100	W11B	KDII	94123	30	0	-	-	13	1.5	10D0	-	200MUSEC	50
GSAP N-6	W11B	KDII	94124	45	0	-	-	9.5	2.2	16	-	5.8MSEC	-
PHOTO-SONICS 4C	W12	DXN	94125	30	0	-	-	108	2.8	250D	72	80MUSEC	200
CLOUD	W13	EDER	94110	25	0	-	-	105	3.7	D.5	-	1SEC	CLOCK
ROBOT	W15	RXP	94111	50	0	-	3914A	45	2.8	1	-	0.125SEC	-
ROBOT	W16	RXP	94112	50	0	-	4278A	45	2.8	1	-	D.25SEC	-
ROBOT	W17	RXP	94113	50	0	-	4709A	45	2.8	1	-	0.25SEC	-
TRAID	W18	EDER	94119	55	0	-	-	25	2.3	16	16D	30MSES	50
TRAID	W19	XR	94120	55	0	-	-	25	2.3	16	160	30MSEC	50
ROBOT	W21	EDER	94114	70	0	-	-	45	2.8	1	-	250MSEC	-
ROBOT	W22	RXP	94115	70	0	-	5577A	45	2.8	1	-	250MSEC	-
ROBOT	W23	RXP	94116	70	0	-	6300A	45	2.8	1	-	250MSEC	-
PHOTO PANEL CAMERA	PANEL	PX	94131	-	-	-	-	25	16	1	-	-	CLOCK
PHOTO PANEL CAMERA	PANEL	PX	94132	-	-	-	-	25	16	0.2	-	-	CLOCK

*(A) SINGLE EXPOSURE AT 963 MICROSECONDS.
N.B. MUSEC = MUS = MICROSECOND

TABLE 4.2 SUMMARY OF CHECK MATE CAMERA PARAMETERS, AIRCRAFT 60376

INSTRUMENT AND STATION POSITION		FILM TYPE	FILM NUMBER	AIMING ANGLES IN DEGREES ELEV	AZIMUTH	FILTERS NO	COLOR	FOCAL LENGTH MM	LENS F/N	FRAMES PER SECOND	SHUTTER SECTOR, DEGREES	EXPOSURE TIME	MARKER RATE CPS
BEATTIE-COLEMAN	W1	EDER	94221	30	0	-	-	105	3.5	*(A)	-	*(B)	-
BEATTIE-COLEMAN	W2	DXN	94222	30	0	-	-	105	3.5	*(A)	-	*(B)	-
RAPATRONIC	W3	XR	94205	30	0	-	WR12	490	22	*(E)	-	5MUSEC	-
PHOTO-SONICS 10 B	W5	DXN	94227	30	0	-	-	180	2.5	360	60	90MUSEC	200
RAPATRONIC	W6	XR	94204	30	0	-	WR12	490	22	*(F)	-	5MUSEC	-
RAPATRONIC	W7	XR	94203	30	0	-	WR12	490	22	*(G)		5MUSEC	-
FLIGHT RESEARCH-CINE	W8	EDER	94217	30	0	-	-	35	2.3	20	130	18MSEC	10
FLIGHT RESEARCH-CINE	W9	XR	94218	30	0	-	-	35	2.5	20	130	18MSEC	10
RAPATRONIC	W10	XR	94223	30	0	-	WR12	482	22	*(H)	-	5MUSEC	-
BEATTIE-COLEMAN	W11	EDER	94209	30	AFT 10	-	-	105	3.5	*(C)	-	*(D)	-
PHOTO-SONICS 4C	W12	XR	94226	30	0	-	-	108	2.8	2500	72	80MUSEC	200
BEATTIE-COLEMAN	W13	XR	94210	30	FWD 10	-	-	105	3.5	*(C)	-	*(D)	-
PHOTO-SONICS 4C	W14	DXN	94225	30	0	-	-	150	2.8	2500	72	80MUSEC	200
FLIGHT RESEARCH-CINE	W15	EDER	94219	50	0	-	-	35	2.3	20	130	18MSEC	10
FLIGHT RESEARCH-CINE	W16	DXN	94220	50	0	-	-	35	2.3	20	130	18MSEC	10
FLIGHT RESEARCH-PULSED	W17	RXP	94211	50	0	-	3914A	35	2.3	1	130	0.36SEC	-
FLIGHT RESEARCH-PULSED	W18	RXP	94212	50	0	-	4278A	35	2.3	1	130	0.36SEC	-
FLIGHT RESEARCH-PULSED	W19	RXP	94213	50	0	-	4709A	35	2.3	1	130	0.36SEC	-
FLIGHT RESEARCH-PULSED	W20	RXP	94214	50	0	-	5577A	35	2.3	1	130	0.36SEC	-
FLIGHT RESEARCH-PULSED	W21	RXP	94215	50	0	-	6300A	35	2.3	1	130	0.36SEC	-
PHOTO PANEL CAMERA	PANEL	PX	94231	-	-	1.0	-	25	5.6	1	160	30MSEC	CLOCK
PHOTO PANEL CAMERA	PANEL	PX	94232	-	-	1.0	-	25	5.6	0.2	160	30MSEC	CLOCK

*(A) 1 FR/SEC, 0.5 FR/SEC, 0.2 FR/SEC, 0.1 FR/SEC UP TO + 10 SEC, +60 SEC, +180 SEC +1800 SEC, RESPECTIVELY.
*(B) 0.5 SEC, 1.5 SEC, 4.5 SEC, 9.5 SEC, UP TO +10 SEC, +60 SEC, +180 SEC, +1800 SEC, RESPECTIVELY.
*(C) SINGLE EXPOSURE AT 14 MUSEC.
*(D) SINGLE EXPOSURE AT 52.4 MUSEC.
*(E) SINGLE EXPOSURE AT 103.4 MUSEC.
*(F) SINGLE EXPOSURE AT 256.2 MUSEC.
*(G) 1 FR/SEC, 0.2 FR/SEC, 0.1 FR/SEC UP TO +10 SEC, +180 SEC, +1800 SEC, RESPECTIVELY.
*(H) 0.5 SEC, 4.5 SEC, 9.5 SEC, UP TO +10 SEC, +180 SEC, +1800 SEC, RESPECTIVELY.
N.B. MUSEC = MUS = MICROSECOND

TABLE 4.3 SUMMARY OF CHECK MATE CAMERA PARAMETERS, JOHNSTON ISLAND

INSTRUMENT AND STATION POSITION		FILM TYPE	FILM NUMBER	AIMING ANGLES IN DEGREES ELEV	AZIMUTH	FILTERS ND	COLOR	FOCAL LENGTH MM	LENS F/N	FRAMES PER SECOND	SHUTTER SECTOR, DEGREES	EXPOSURE TIME	MARKER RATE CPS
KFC-600	A1	XR	94304	64.28	191.75	2.0	WR12	254	9.5		-	0.1MUSEC	-
PHOTO-SONICS 4C	A2	EDER	94324	64.28	191.75	-	-	108	2.8	2500	72	80MUSEC	200
PHOTO-SONICS 4C	A3	DXN	94323	64.28	191.75	-	-	250	4.0	2500	72	80MUSEC	200
PHOTO-SONICS 10B	A4	DXN	94325	64.28	191.75	-	-	250	4.0	360	60	0.46MSEC	50
RAPATRONIC	A5	XR	94303	64.28	191.75	-	-	490	22	*(A)	-	5MUSEC	-
MAURER	A7	XR	94319	65.13	192	-	-	150	2.8	5.5	-	0.05SEC	-
MAURER	A8	EDER	94320	65.13	192	-	-	150	2.8	5.5	-	0.05SEC	-
TRAIO	A9	OXN	94317	65.13	192	-	-	35	2.3	16	160	0.028SEC	10
MITCHELL	A10	DXN	94326	65.13	192	-	-	35	2.3	100	170	4.7MSEC	100
FAIRCHILD HS-100	A12	KDI	94321	65.13	192	-	-	13	1.5	900	-	0.22MSEC	100
GSAP	A13	KDII	94322	65.13	192	-	-	9.5	2.2	16	133	0.023SEC	-
KC-18	A14	TXA	94332	79	192	-	-	153	6.3	0.2	-	5SEC	-
CLOUD	C1	EDER	94309	65.13	192	-	-	105	3.7	*(B)	-	*(C)	-
CLOUD	C2	EOER	94310	40	12	-	-	105	3.7	*(B)	-	*(C)	-
TRAID	C3	XR	94318	65.13	192	-	-	25	2.3	16	160	0.028SEC	10
MPTCHELL	C4	EDER	94327	65.13	192	-	-	35	2.3	100	170	4.7MSEC	100
BELL AND HOWELL	C5	XR	94329	39.83	192	-	-	25	2.0	12	170	0.039SEC	10
MITCHELL LS	C6	EDER	94328	65.13	192	-	-	18.5	2.3	2.5	170	0.19SEC	10
ROBOT	C7	RXP	94311	65	192	-	4278A	45	2.8	*(B)	-	*(C)	-
ROBOT	C8	RXP	94312	65	192	-	4709A	45	2.8	*(B)	-	*(C)	-
ROBOT	C9	RXP	94313	65	192	-	5228A	45	2.8	*(B)	-	*(C)	-
ROBOT	C11	RXP	94314	65	192	-	6300A	45	2.8	*(B)	-	*(C)	-
ROBOT	C12	RXP	94315	65	192	-	3914A	45	2.8	*(B)	-	*(C)	-
DYNAFAX	D1	IRA	94335	65.13	192	-	-	915	9.0	25000	-	5MUSEC	-
DYNAFAX	O2	IRA	94336	65.13	192	-	-	76	2.8	25000	-	5MUSEC	-
ROBOT	OUTSIDE	EOER	94334	TRAINABLE		-	-	45	2.8	*(B)	-	*(C)	-

*(A) SINGLE EXPOSURE AT 963 MICROSECONDS.
*(B) 0.2 FR/SEC FROM -30 SEC TO +120 SEC, THEN 0.033 FR/SEC TO END.
*(C) 5-SEC EXPOSURE FROM -30 SEC TO +120 SEC, THEN 30 SEC EXPOSURE TO END.
N.B. MUSEC = MUS = MICROSECOND

Page 113 deleted.

TABLE 4.6 SUMMARY OF CHECK MATE FILM RECORDS, AIRCRAFT 53120

FILM NUMBER	FILM TYPE	CAMERA	RESULTS
94103	XR	RAPATRONIC	NO RECORD.
94104	XR	KFC-600	FIRST FRAME SHOWS NO RECORD. FRAMES TWO THROUGH SIX SHOW EXPANDING SPOT IMAGE.
94109	DXN	CLOUD	SHOWS JETTING FIREBALL, AURORA, AND FIREBALL RISE. RECORD PERSISTS FOR ABOUT FORTY FRAMES.
94110	EDER	CLOUD	ONLY FIRST FRAME EXPOSED. NO USEFUL INFORMATION.
94111	RXP	ROBOT	FIFTEEN-FRAME RECORD, AURORA SEEN IN THREE FRAMES.
94112	RXP	ROBOT	39-FRAME RECORD SHOWING AURORA IN FIRST FRAME.
94113	RXP	ROBOT	24-FRAME RECORD SIMILAR TO OTHER ROBOT SEQUENCES.
94114	EDER	ROBOT	GREEN SKY AT BURST TIME, THEN BLUE SKY FOR ONE OR TWO FRAMES.
94115	RXP	ROBOT	ONLY TWO RECORD FRAMES. NO STRUCTURE.
94116	RXP	ROBOT	NO RECORD.
94117	DXN	TRAID	EXCELLENT RECORD OF BURST AND AURORAL STREAMERS. APPROXIMATELY 120 FEET OF RECORD.
94118	EDER	TRAID	20 FEET SHOWING A PINK FIREBALL WITH A RISING BLUE CORE. REGION OF X-RAY DEPOSITION APPEARS GREEN.
94119	EDER	TRAID	BURST OCCURRED BELOW FIELD OF VIEW BUT LATER RISES INTO VIEW. BLUE AURORA AND BLUE DEBRIS SEEN.
94120	XR	TRAID	VERY FAINT IMAGE OF LATE DEBRIS FOR A FEW FEET.
94121	EDER	MAURER	ABOUT THIRTY-FIVE FRAMES SHOWING DEBRIS AND CONTRACTING RINGS.
94122	XR	MAURER	SHOWS TWELVE TO FIFTEEN FRAMES OF DEBRIS GROWTH.
94123	KDII	FAIRCHILD HS-100	CENTRAL BRIGHT CORE, DEBRIS EXPANSION, AND ASYMMETRICAL SHOCK OBSERVED.
94124	KDII	GSAP	200-FRAME RECORD SHOWING BLUE AURORA, GREEN SKY, PINK DEBRIS RING AND BLUE CENTRAL CORE.
94125	DXN	PS-40	BEAUTIFUL RECORD FOR 412 FEET SHOWING DEBRIS EXPANSION, FIREBALL JETTING, AND TURBULENCE.
94127	EDER	PS-10B	LONG RECORD OF DEBRIS EXPANSION.

TABLE 4.7 SUMMARY OF CHECK MATE FILM RECORDS, AIRCRAFT 60376

FILM NUMBER	FILM TYPE	CAMERA	RESULTS
94203	XR	RAPATRONIC	NO RECORD.
94204	XR	RAPATRONIC	NO RECORD.
94205	XR	RAPATRONIC	NO RECORD.
94209	EDER	BC	SINGLE OVEREXPOSED FRAME.
94210	XR	BC	NO RECORD.
94211	RXP	FR-PULSED	NO SIGNIFICANT RECORD.
94212	RXP	FR-PULSED	3- TO 4-MINUTE RECORD SHOWS RISE AND ELONGATION OF BURST.
94213	RXP	FR-PULSED	RECORD OF LESS THAN ONE MINUTE SHOWS RAPIDLY DYING BURST.
94214	RXP	FR-PULSED	BURST FAINTLY RECORDED
94215	RXP	FR-PULSED	4-MINUTE RECORD. HOWEVER, BURST DOES NOT APPEAR CLEARLY.
94217	EDER	FR-CINE	50-FOOT RECORD SHOWS WHITE BURST AGAINST GREEN SKY. DEVELOPMENT OF PERSISTENT BLUE CORE. AND SOUTHERN AURORA.
94218	XR	FR-CINE	RECORD PARTIALLY OBSCURED BY INTERNAL MASK. 35 FEET SHOWING EXPANDING DEBRIS AND SURROUNDINGS.
94219	EDER	FR-CINE	BURST OCCURS IN LOWER RIGHT HAND CORNER OF FRAME AND RISES SLOWLY INTO VIEW.
94220	DXN	FR-CINE	VERY LONG RECORD IN WHICH BURST OCCURS INITIALLY BELOW FIELD OF VIEW. MOVING GRADUALLY INTO FIELD.
94221	EDER	BC	38 FRAMES.
94222	DXN	BC	GOOD RECORD SHOWING FIREBALL JETTING. FIREBALL RISE. SHOCK. AND AURORAL EFFECTS.
94223	XR	RAPATRONIC	NO RECORD.
94225	DXN	PS-4C	500 FEET OF RECORD BUT NOT VERY USEFUL BECAUSE BURST OCCURS IN SPROCKET HOLES.
94226	XR	PS-4C	NO USEFUL RESULTS. IMAGE IN SPROCKET HOLES.
94227	DXN	PS-10B	100 FEET OF RECORD SHOWING BURST ON RIGHT SIDE OF FRAME.

TABLE 4.8 SUMMARY OF CHECK MATE FILM RECORDS, JOHNSTON ISLAND

FILM NUMBER	FILM TYPE	CAMERA	RESULTS
94303	XR	RAPATRONIC	GOOD PICTURE OF BURST.
94304	XR	KFC-600	NO RECORD.
94309	EDER	CLOUD	ABOUT TWENTY-EIGHT FRAMES SHOWING DEVELOPMENT AND EXPANSION OF DEBRIS ALONG FIELD LINES.
94310	EDER	CLOUD	NO RECORD.
94311	RXP	ROBOT	ONLY ONE FRAME SHOWING BURST.
94312	RXP	ROBOT	ONLY ONE GOOD EXPOSURE SHOWING WISH-BONE OR HORSESHOE SHAPE OF DEBRIS CLOUD.
94313	RXP	ROBOT	ABOUT THIRTY FRAMES SHOWING BREAK-UP OF SPHERE INTO TWO DISTINCT DEBRIS MASSES.
94314	RXP	ROBOT	ABOUT THIRTY-ONE GOOD FRAMES OF BURST SEQUENCE. DIFFERS SLIGHTLY FROM 94315.
94315	RXP	ROBOT	GOOD SERIES OF THIRTY PHOTOS SHOWING DEVELOPMENT OF TWO SEPARATE MASSES.
94317	DXN	TRAID	RECORD SHOWS DISINTEGRATION OF CENTRAL MASS INTO TWO STREAKS AT LATE TIMES.
94318	XR	TRAID	SHOWS DEBRIS EXPANSION. PARTIALLY OBSCURED BY ROCKET TRAILS.
94319	XR	MAURER	GOOD SEQUENCE OBTAINED OF LATE DEBRIS DISTRIBUTION. ABOUT THIRTY FRAMES.
94320	EDER	MAURER	THIRTY-FIVE FRAMES SHOWING LATE DEBRIS EXPANSION AND CONTRACTING SHOCKS.
94321	KDI	FAIRCHILD HS-100	RECORD SHOWS EXPANDING SHOCK AND DEBRIS RING AS WELL AS JETS AND TURBULENCE.
94322	KDII	GSAP	200-FRAME RECORD SIMILAR TO RECORDS OBTAINED BY OTHER CAMERAS. EARLY GREEN GLOW OBSERVED.
94323	DXN	PS-4C	GOOD RECORD OF BURST EXTENDING TO END OF FILM.
94324	EDER	PS-4C	WHITE DEBRIS RING FOLLOWED BY TURBULENT EFFECTS.
94325	DXN	PS-10B	APPROXIMATELY 200 FEET. SHOWS INSTABILITIES IN EXPANDING SHELL.
94326	DXN	MITCHELL	BURST WELL CENTERED IN FRAME. SHOWS DEBRIS EXPANSION.
94327	EDER	MITCHELL	WHITE BURST AGAINST BLUE SKY EARLY, GREEN SKY LATER, PINK HALO APPEARS AROUND DEBRIS RING.
94328	EDER	MITCHELL	GREEN OVERALL EXPOSURE INITIALLY FOLLOWED BY HORSESHOE-SHAPED DEBRIS RING ALONG FIELD LINES.
94329	XP	B AND H	ABOUT THIRTY FRAMES SHOWING DEBRIS.
94332	TXA	KC-1	GOOD IMAGES OF LATE DEBRIS.
94334	EDER	ROBOT	BEAUTIFUL 12-FRAME RECORD OF FORMATION OF HORSE-SHOE CLOUD.
94335	IRA	DYNAFAX	VERY MUCH UNDEREXPOSED.
94336	IRA	DYNAFAX	EXCELLENT RECORD OF EARLY DEBRIS.

TABLE 4.9 STATISTICAL SUMMARY OF CHECK MATE RECORDS FROM THE BURST AREA

Station	Aircraft 53120	Aircraft 60376	Johnston Island	Totals
Number of Cameras	20	20	26	66
Number of Useful Records	17	11	23	51
Reasons for No Records:				
Mechanical failure	1	2	0	3
Inappropriate camera parameters	1	1	2	4
Error in shot or aircraft location	1	6	0	7
Reasons for Poor Records:				
Inappropriate camera parameters	1	3	4	8
Error in shot or aircraft location	0	0	0	0
Other	0	0	0	0
Percent Success	85	55	88	—
Overall Success: 77 percent				

Page 118 deleted.

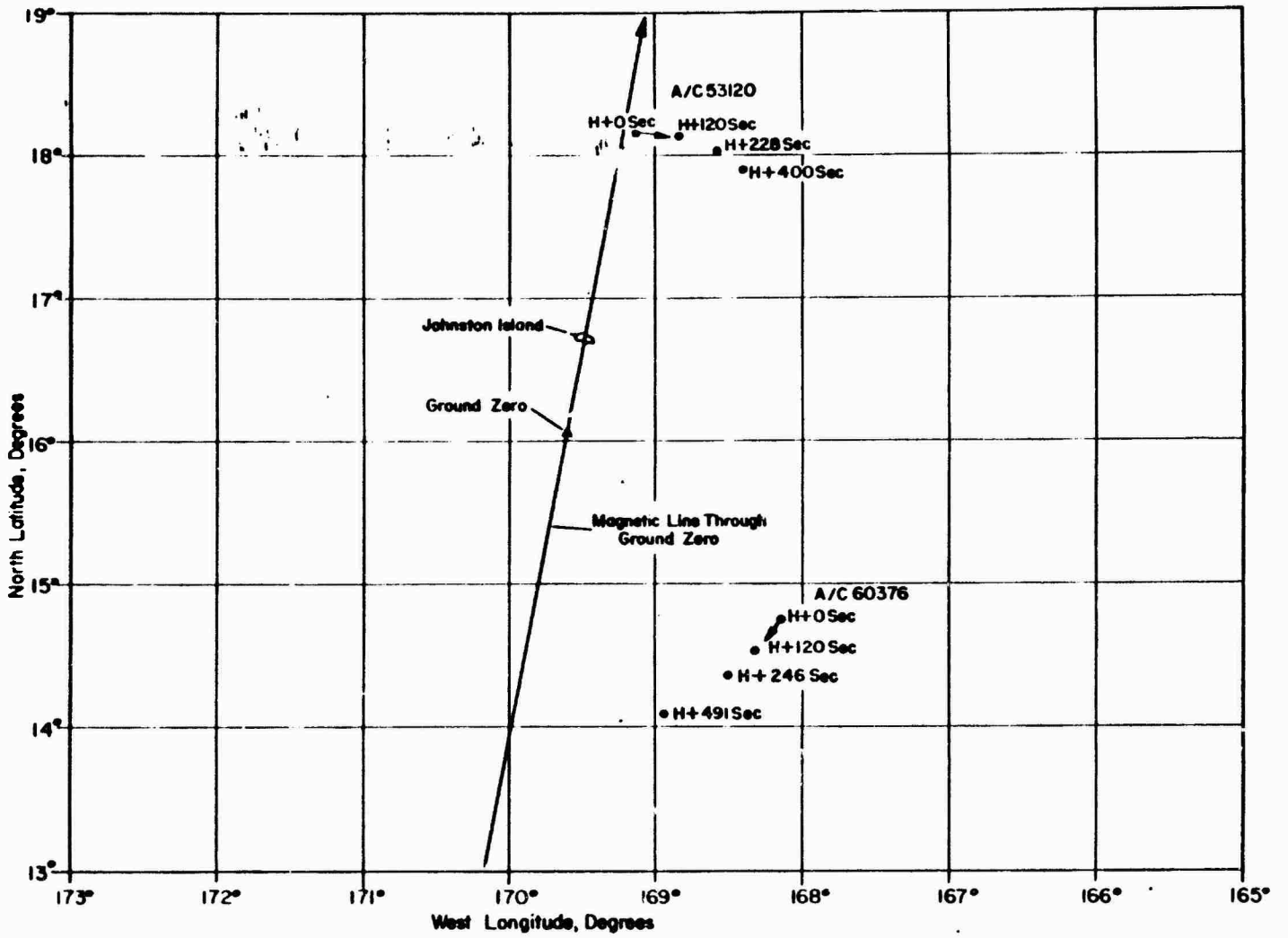

Figure 4.2 Aircraft flight paths from H-hour to +8 minutes, Check Mate.

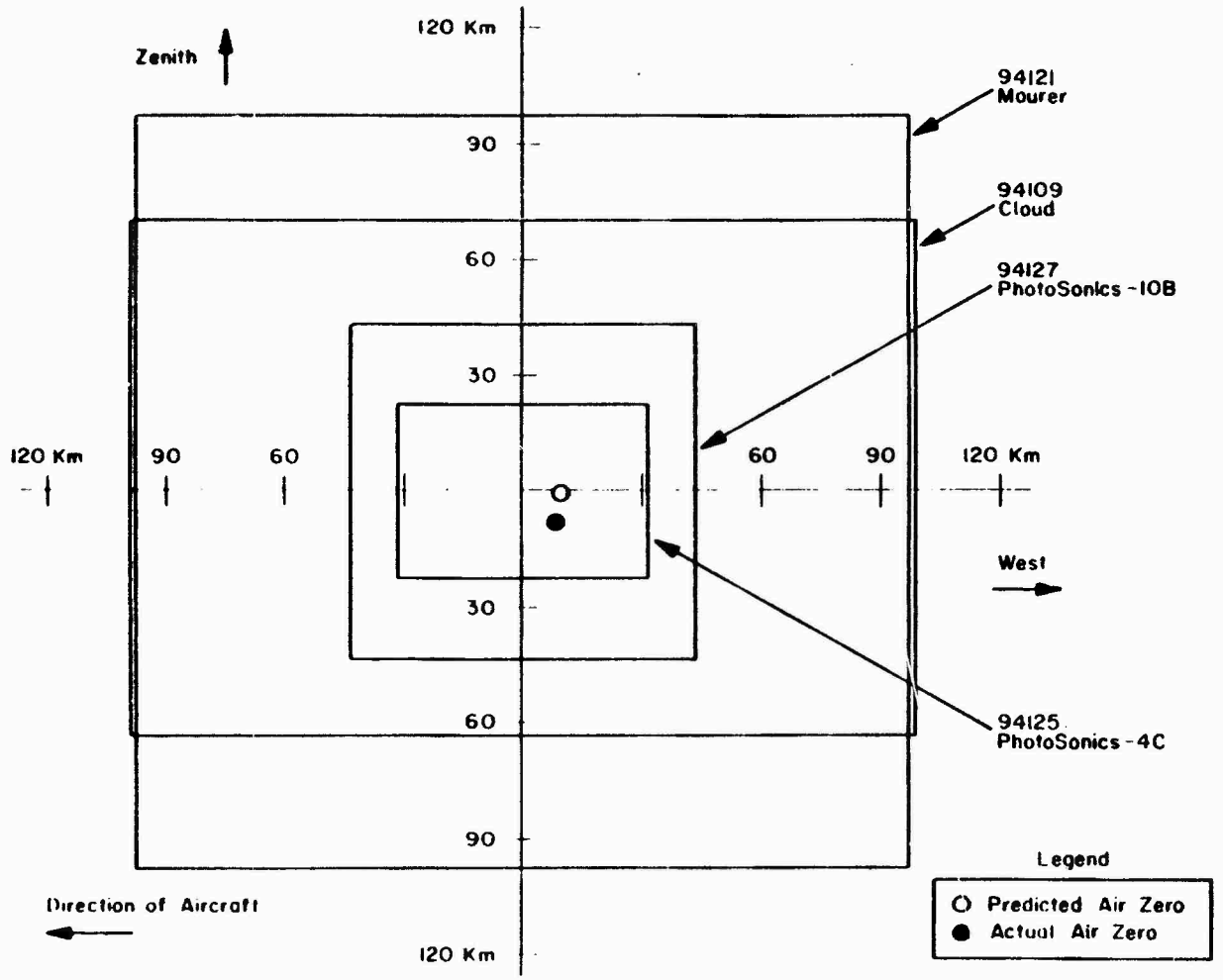

Figure 1.3 Fields of view for four Aircraft 53120 cameras with predicted and actual air zero indicated.

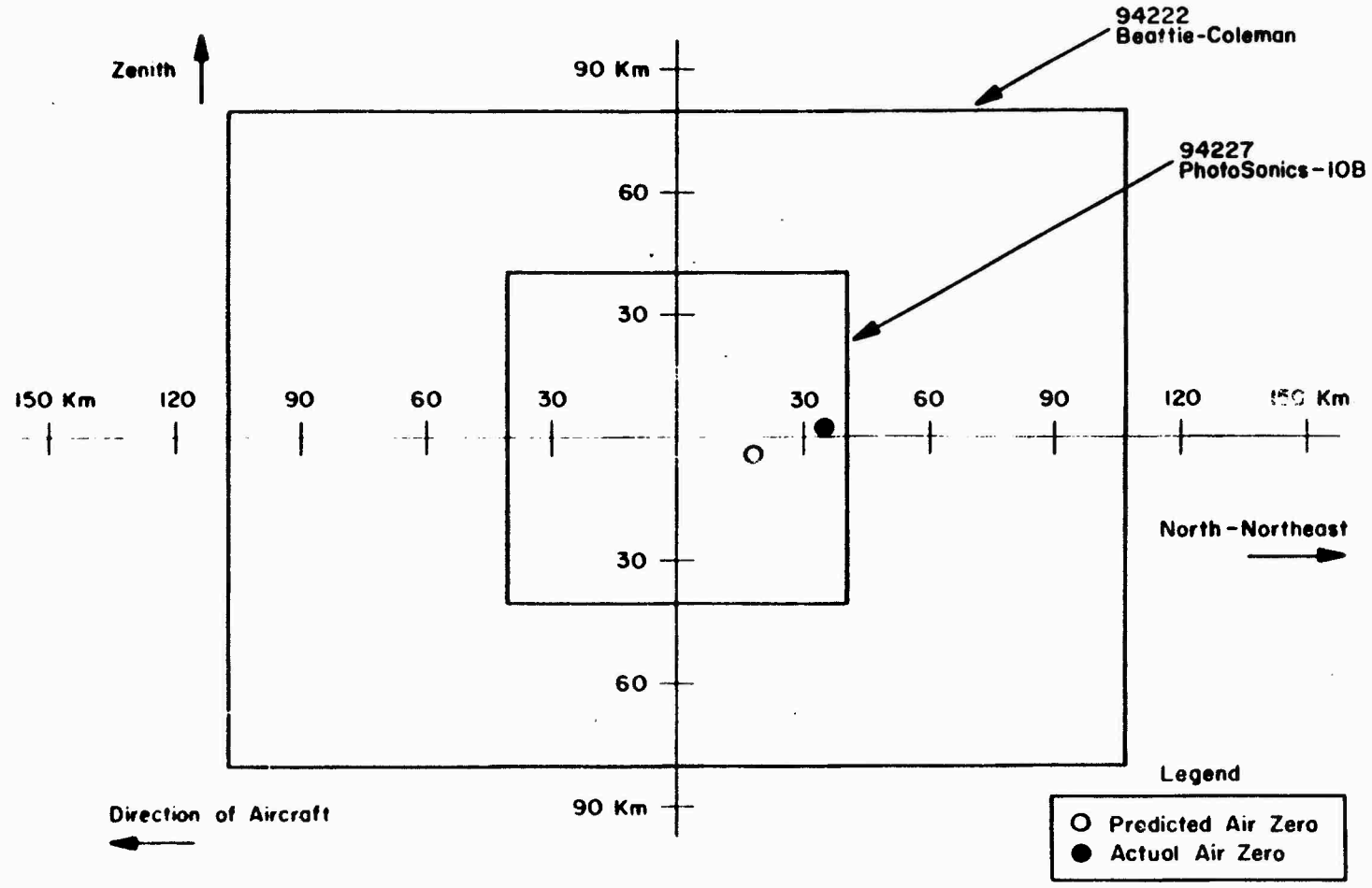

Figure 4.4 Field of view for four Aircraft 60376 cameras with predicted and actual air zero indicated.

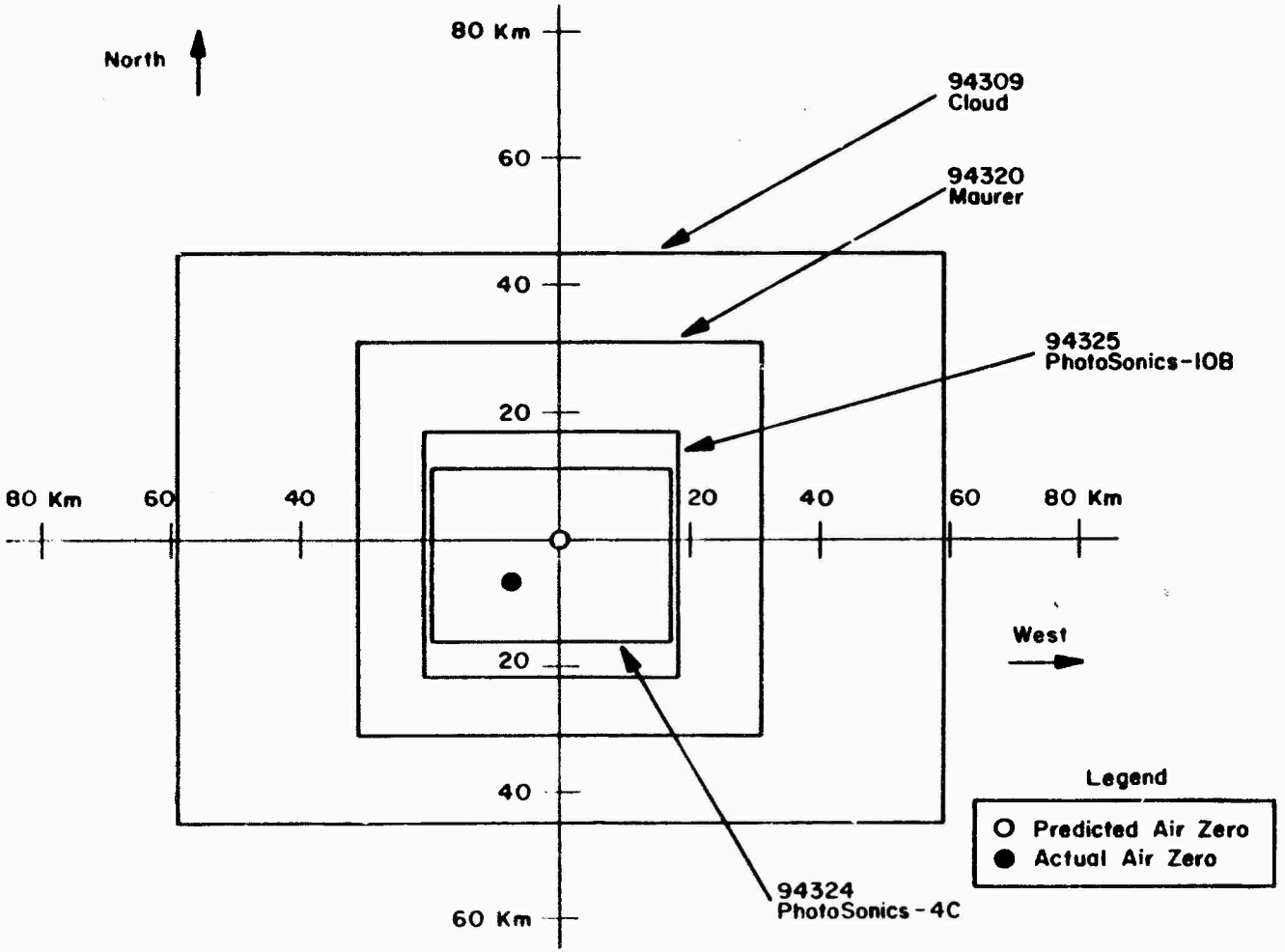

Figure 4.5 Fields of view for two Johnston Island cameras with predicted and actual air zero indicated.

Pages 123 through 155 deleted.

3.0 sec

4.6 sec

Figure 4.38 Check Mate; converging shock inside debris, taken from Johnston Island. Film 94320, Frames 16 and 25.

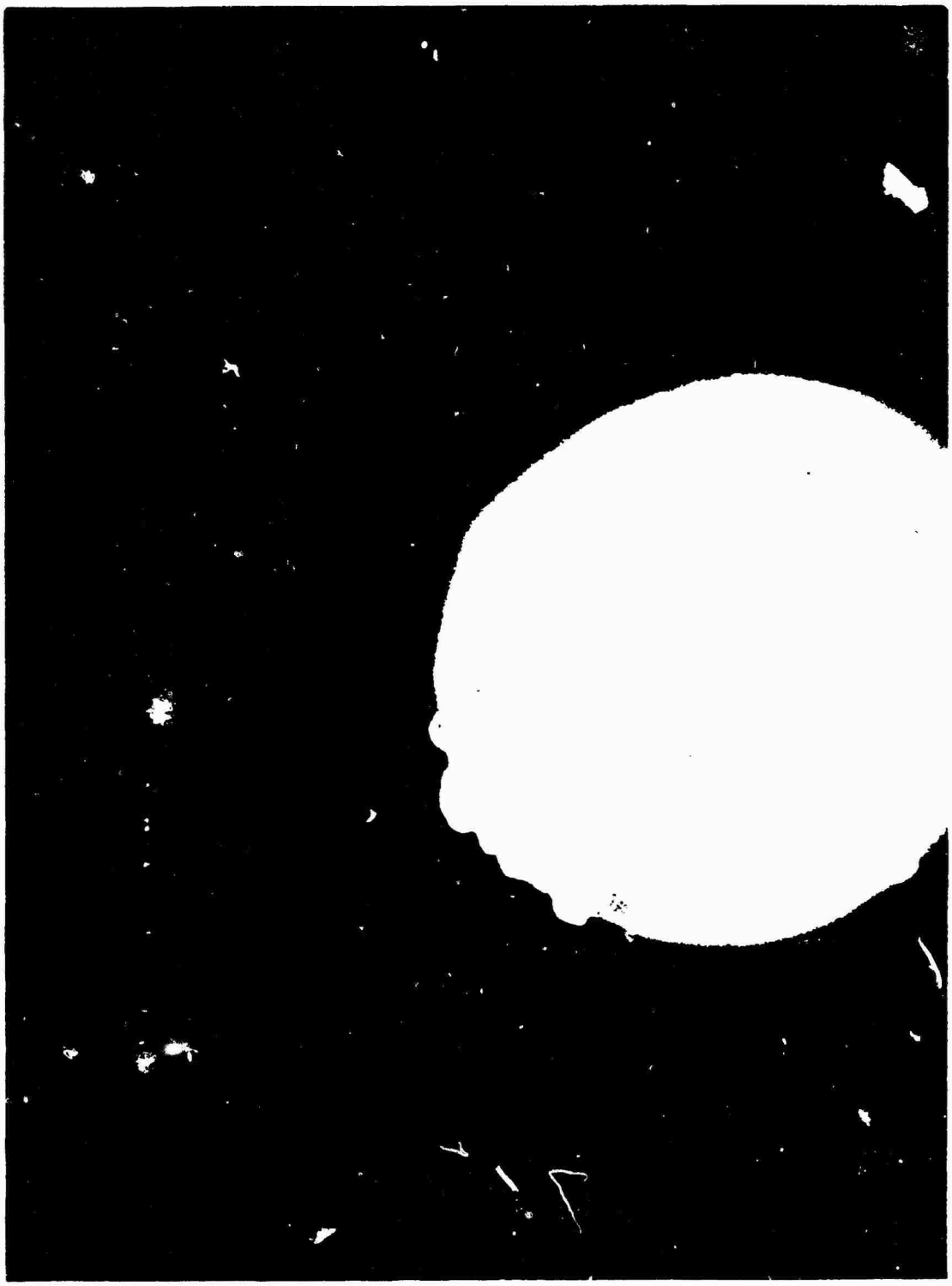

Figure 4.39 Check Mate; debris surrounded by expanding shock at 3.5 seconds, taken from Aircraft 60376. Film 94222, Frame 3.

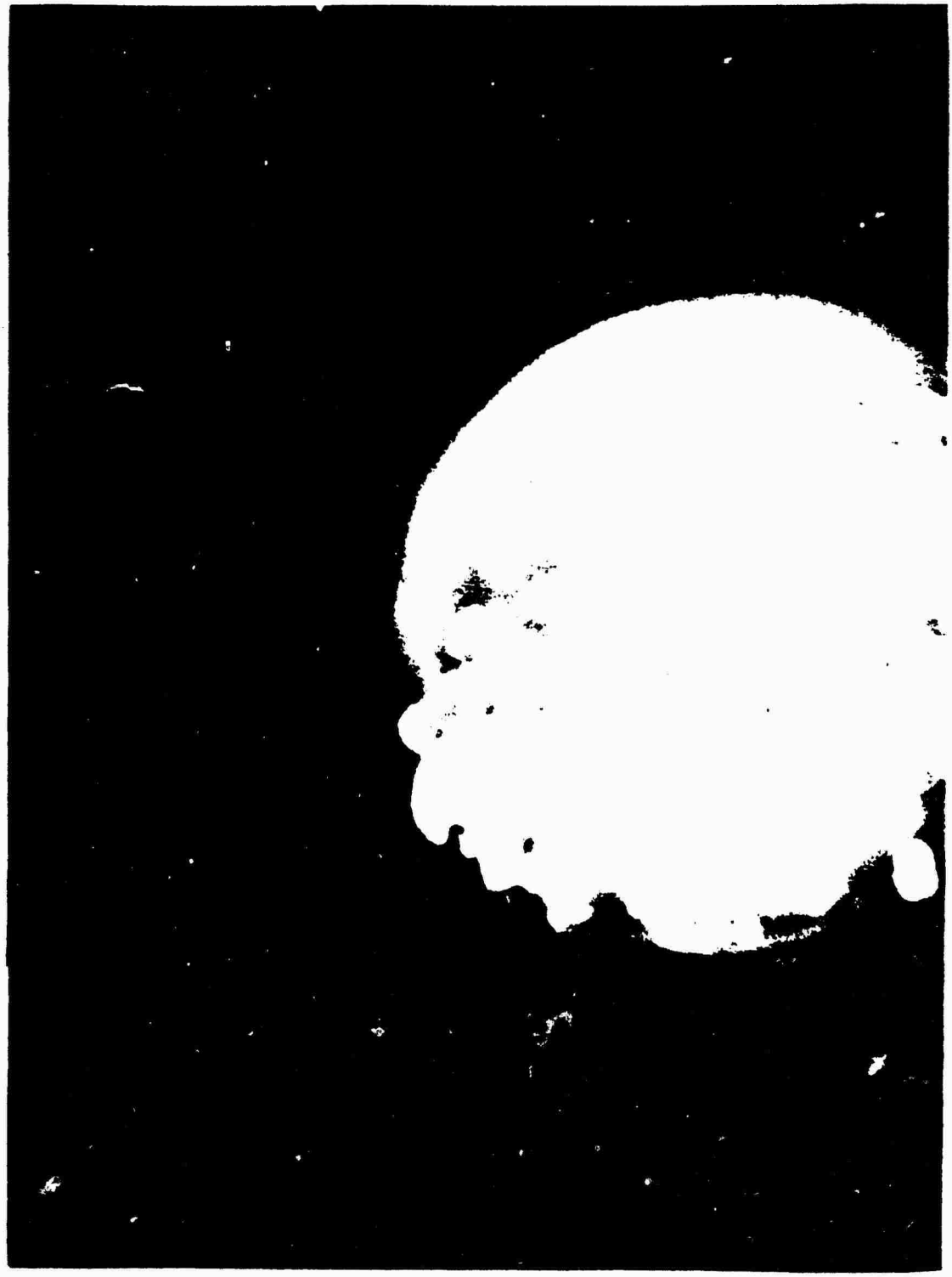

Figure 4.40 Check Mate; debris surrounded by expanding shock at 5.5 seconds, taken from Aircraft 60376. Film 94222, Frame 5.

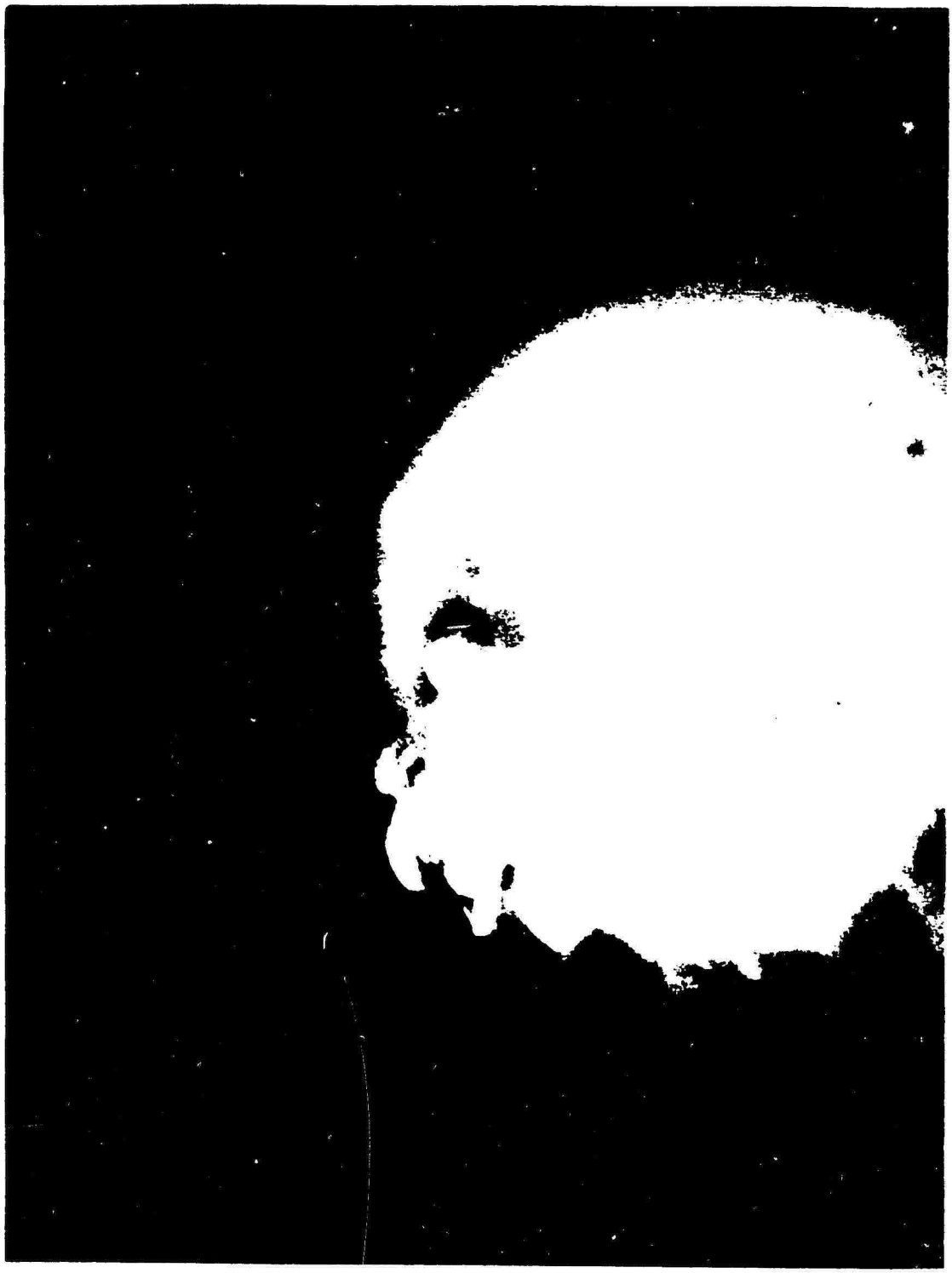

Figure 4.41 Check Mate; debris surrounded by expanding shock at 7.5 seconds, taken from Aircraft 60376. Film 94222, Frame 7.

Figure 4.42 Check Mate; debris surrounded by expanding shock at 9.5 seconds, taken from Aircraft 60376. Film 94222, Frame 9.

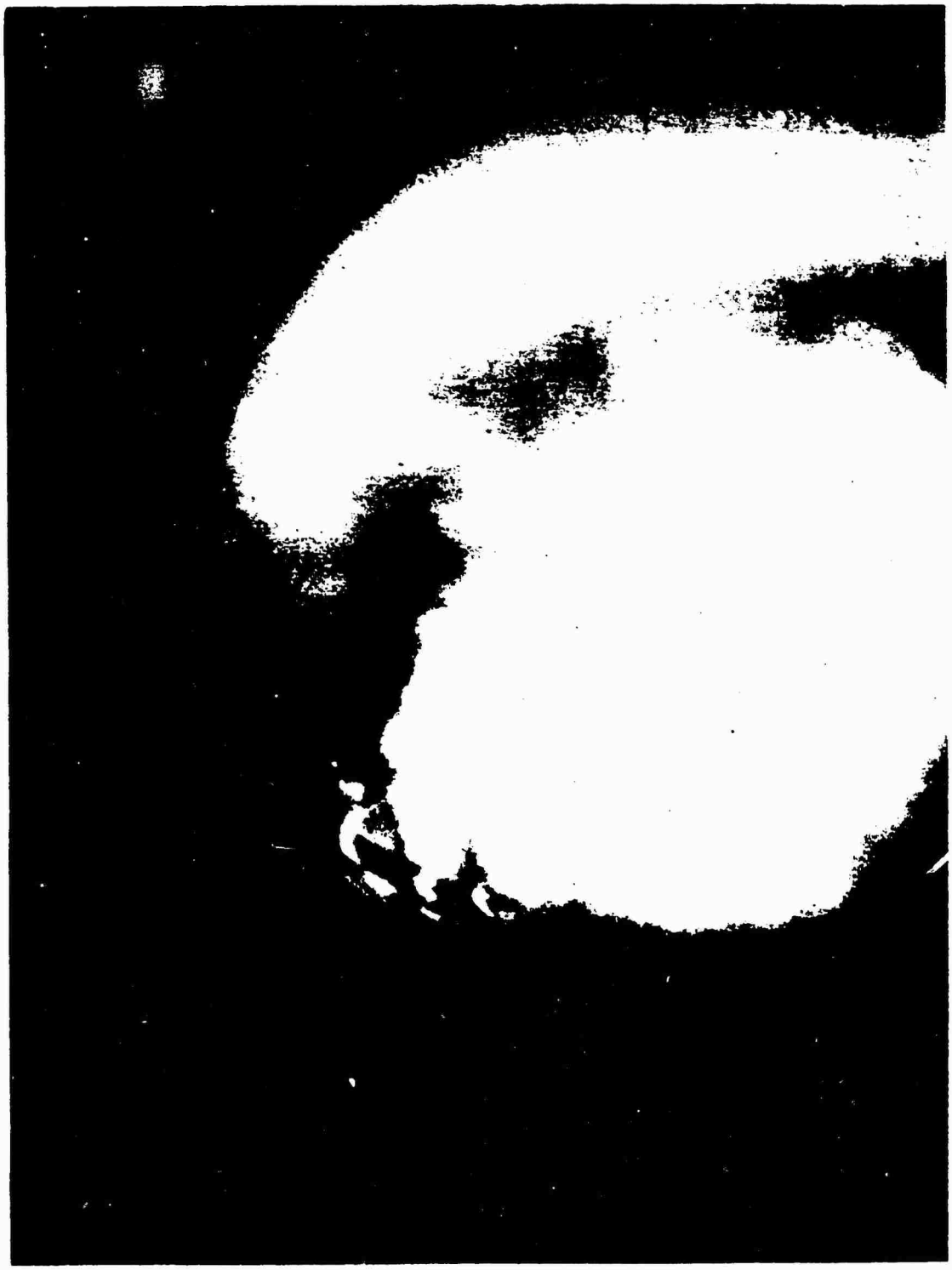

Figure 4.43 Check Mate; debris surrounded by expanding shock at 14.5 seconds, taken from Aircraft 60376. Film 94222, Frame 12.

Pages 162 and 163 deleted.

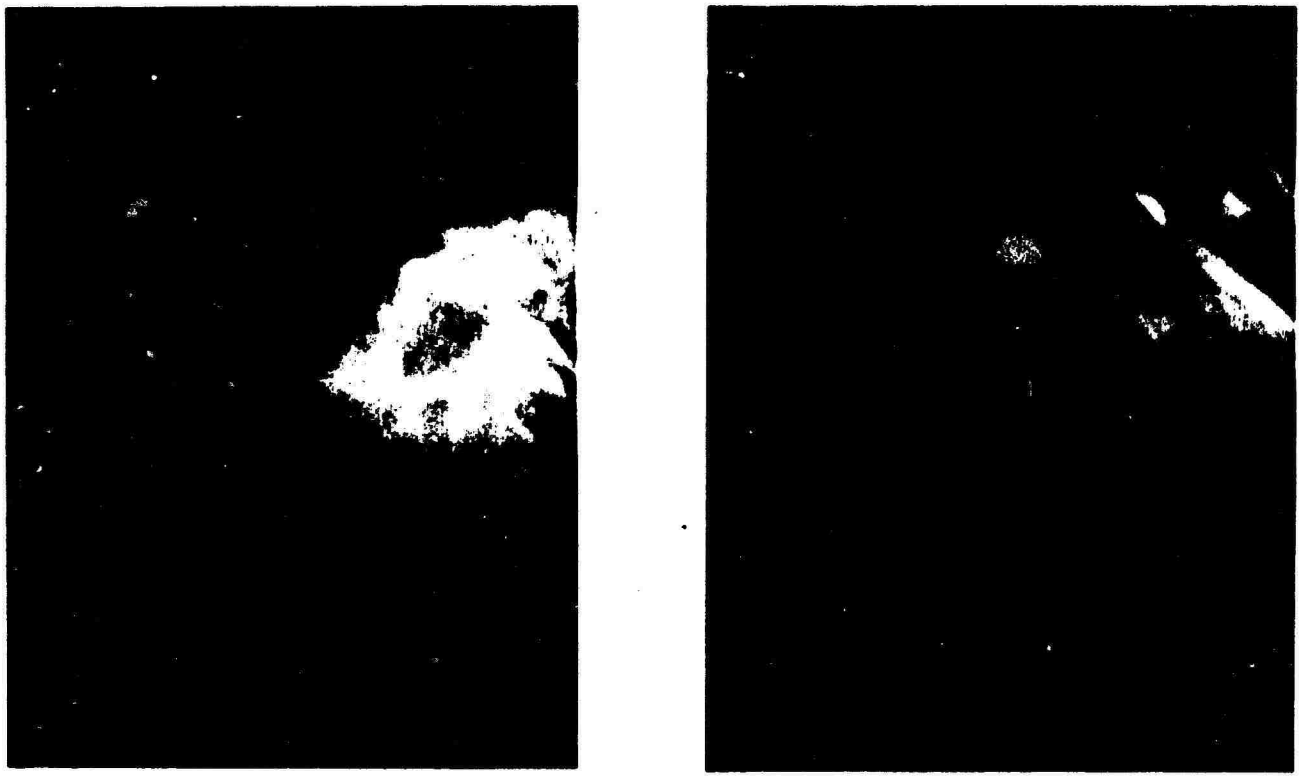

22.5 sec

40.5 sec

Figure 4.46 Check Mate; initial debris alignment along geomagnetic field, taken from Aircraft 60376. Film 94221, Frames 16 and 25.

Figure 4.47 Check Mate; late debris expansion and beta-ray aurora at 8 seconds, taken from Aircraft 53120. Film 94109, Frame 4.

Figure 4.48 Check Mate; late debris expansion and beta-ray aurora at 16 seconds, taken from Aircraft 53120. Film 94109, Frame 8.

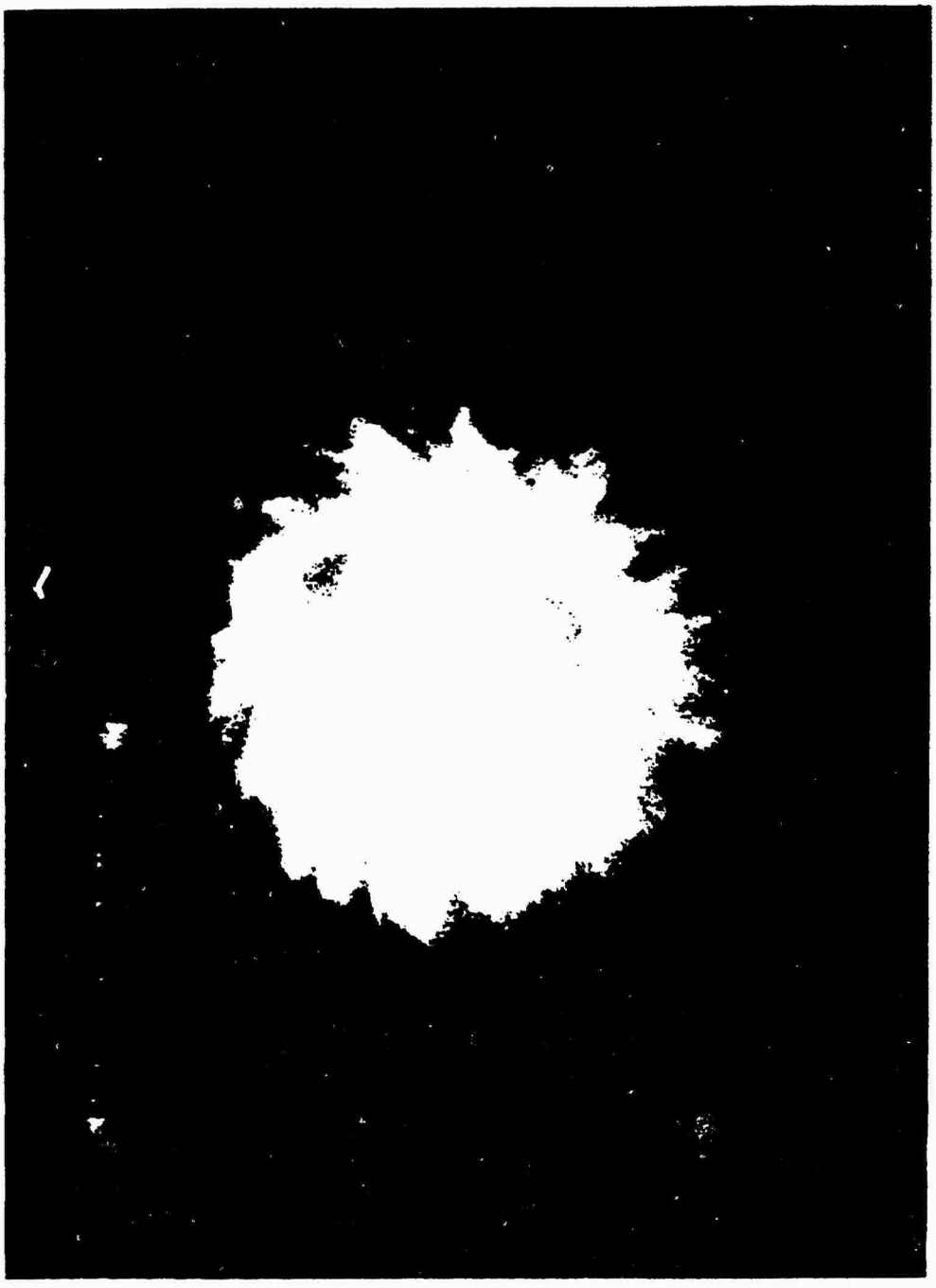

Figure 4.49 Check Mate; late debris cloud at 19.5 seconds, taken from Aircraft 53120. Film 94117, Frame 312.

Pages 168 through 170 deleted.

40 sec

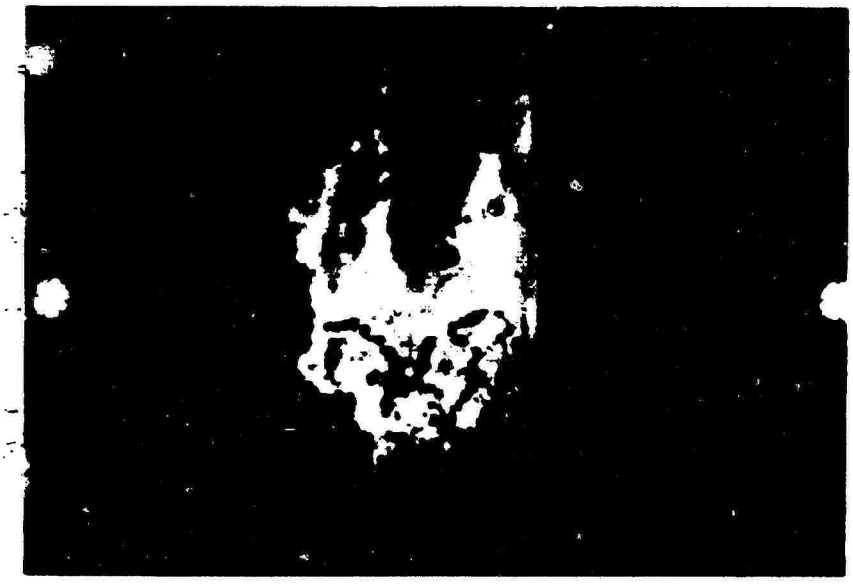

60 sec

Figure 4.52 Check Mate; extension of debris cloud along geomagnetic field lines, taken from Johnston Island. Film 94309, Frames 8 and 12.

90 sec

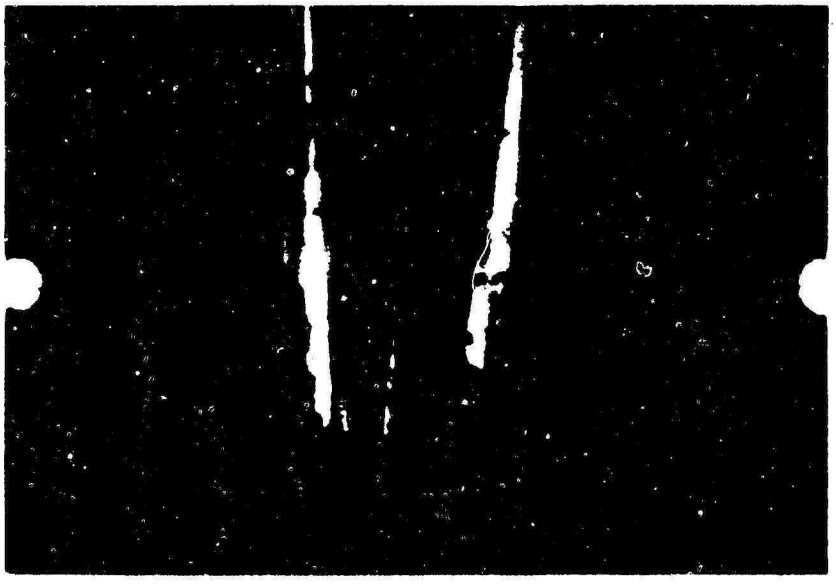

125 sec

Figure 4.53 Check Mate; extension of debris cloud along geomagnetic field lines, taken from Johnston Island. Film 94309, Frames 18 and 24.

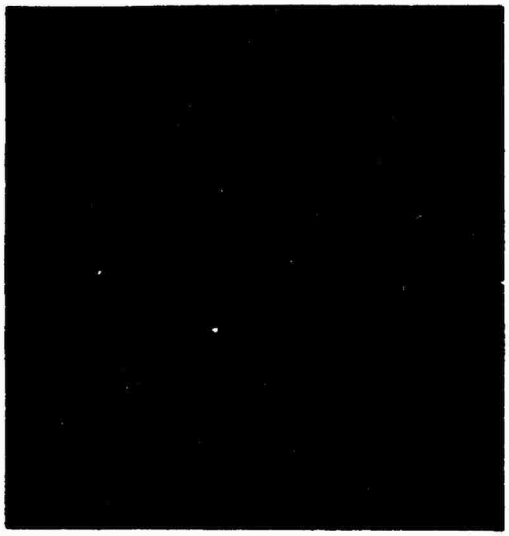

30 sec

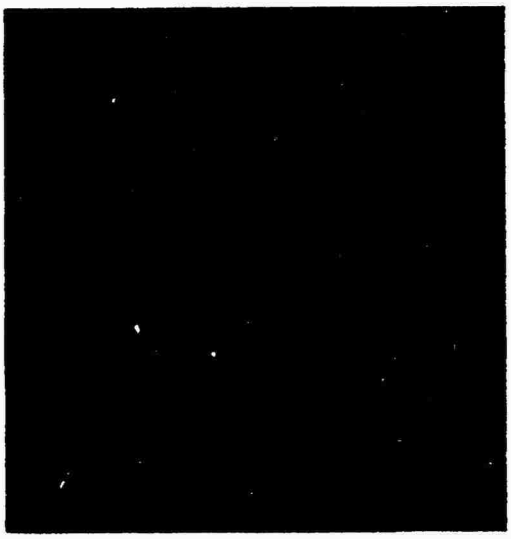

60 sec

90 sec

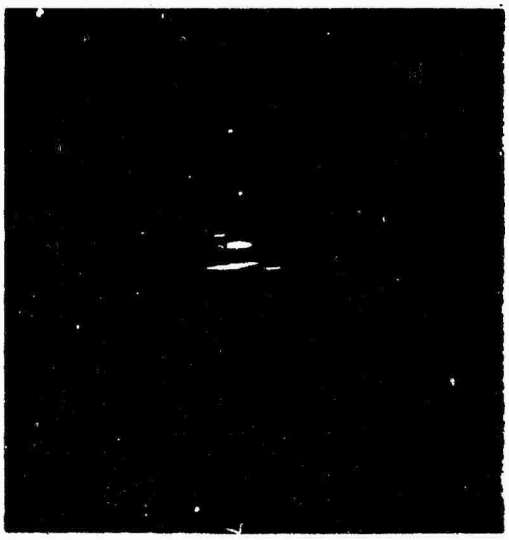

120 sec

Figure 4.54 Check Mate; rise of debris above horizon at Mauna Loa, taken from Mauna Loa. Film 94709, Frames 0, 1, 2, and 3.

3 min

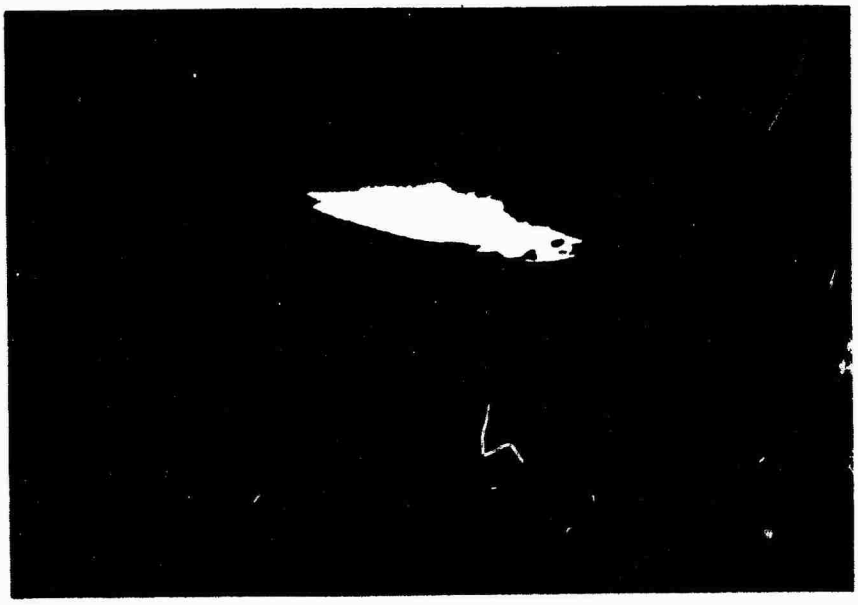

5 min

Figure 4.55 Check Mate; extension of debris along geomagnetic field lines, taken from Mauna Loa. Film 94709, Frames 4 and 5.

6 min

8 min

Figure 4.56 Check Mate; extension of debris along geomagnetic field lines, taken from Mauna Loa. Film 94709, Frames 6 and 7.

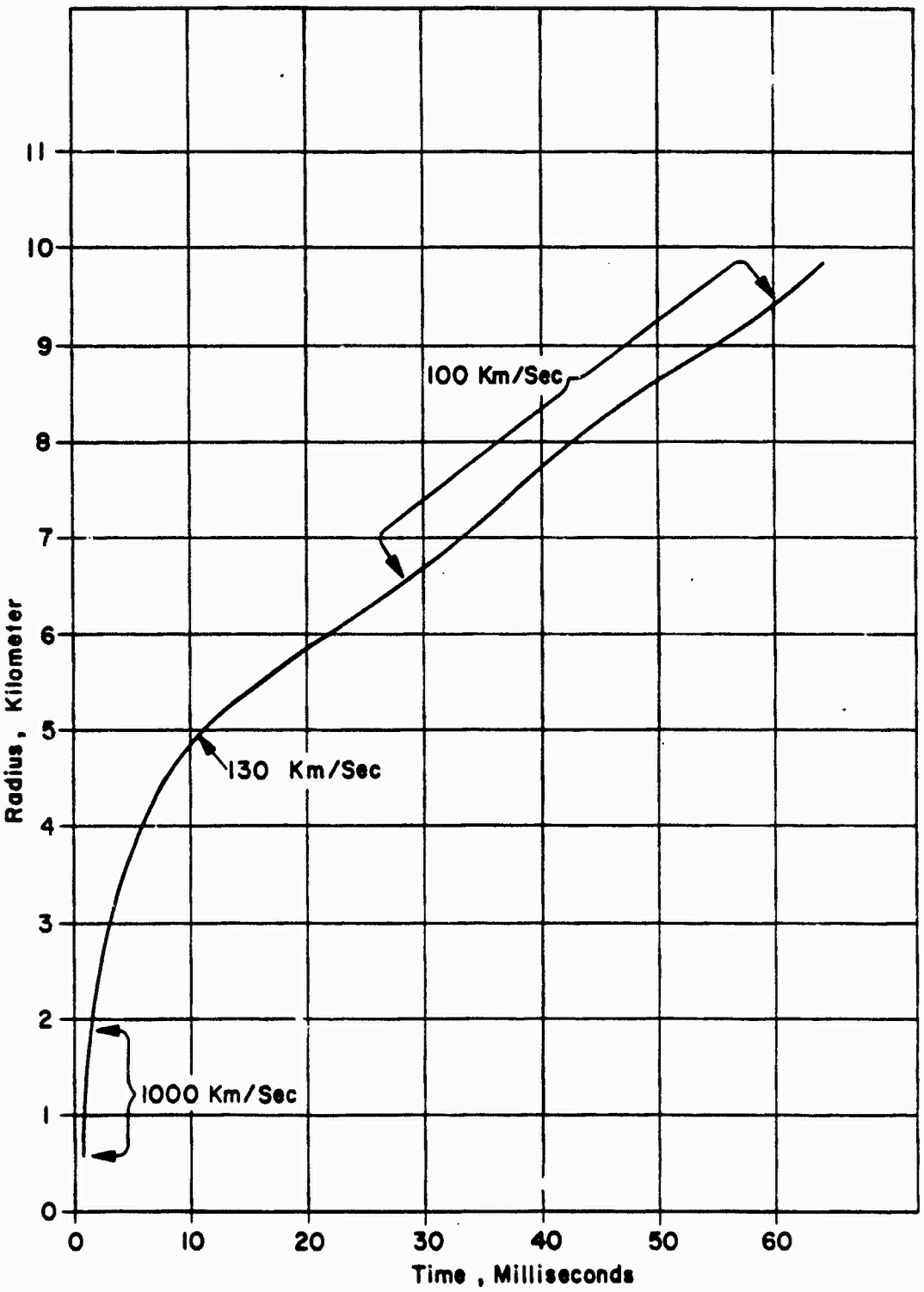

Figure 4.57 Check Mate; debris radius versus time.

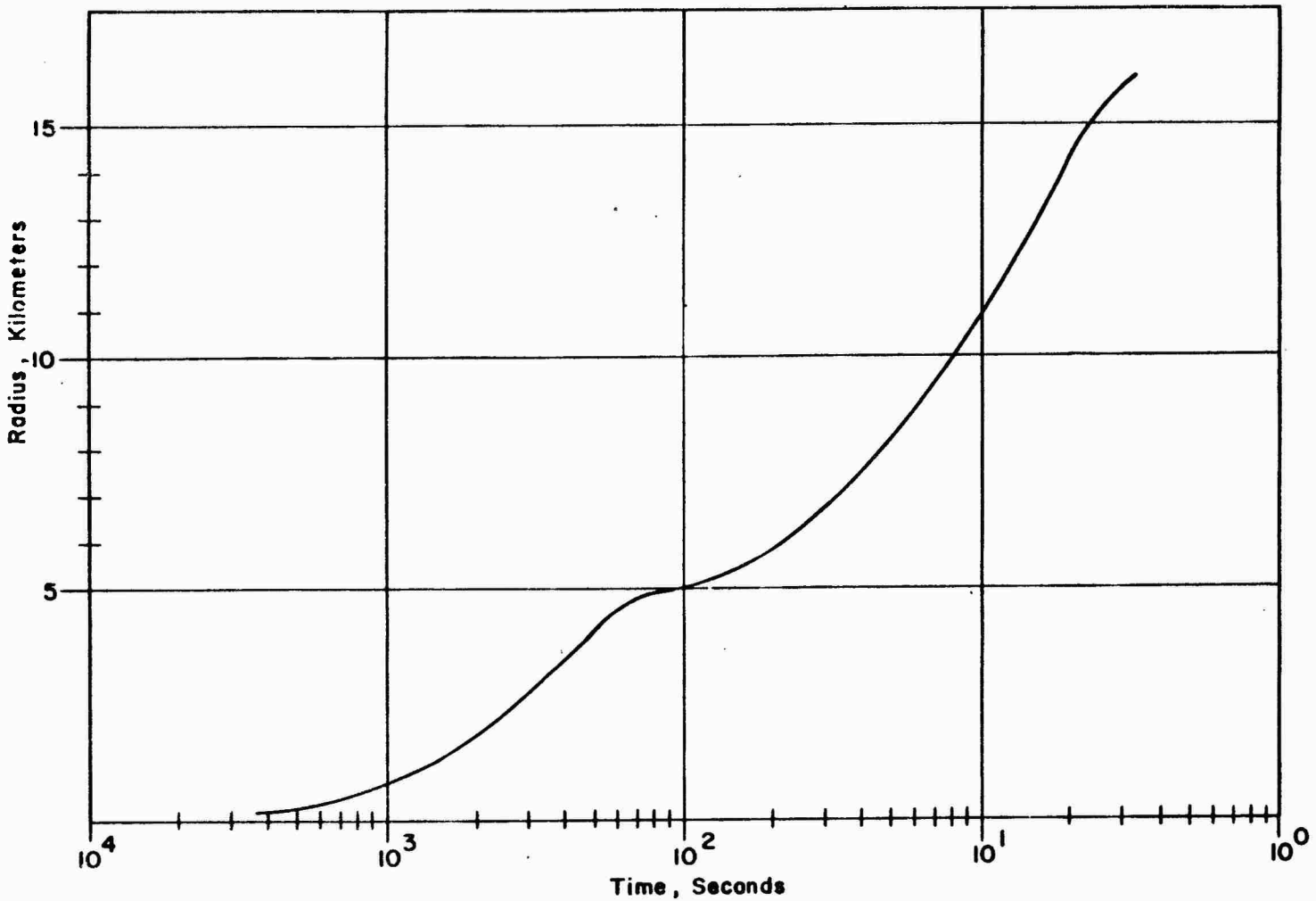

Figure 4.58 Check Mate; debris radius versus time, from 400 μsec to 300 msec.

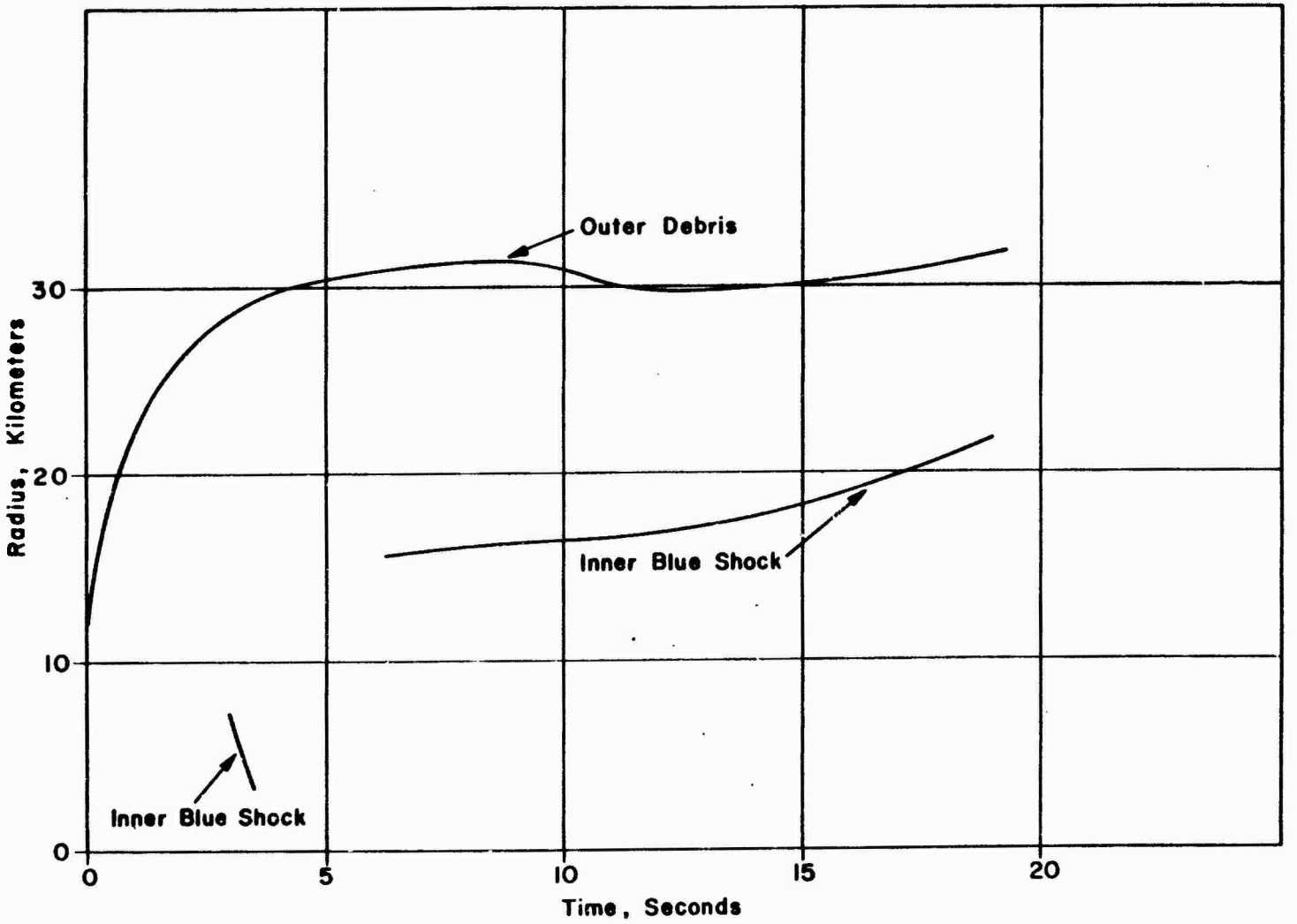

Figure 4.59 Check Mate; debris radius versus time, from 0 to 20 seconds.

179

Pages 180 and 181 deleted.

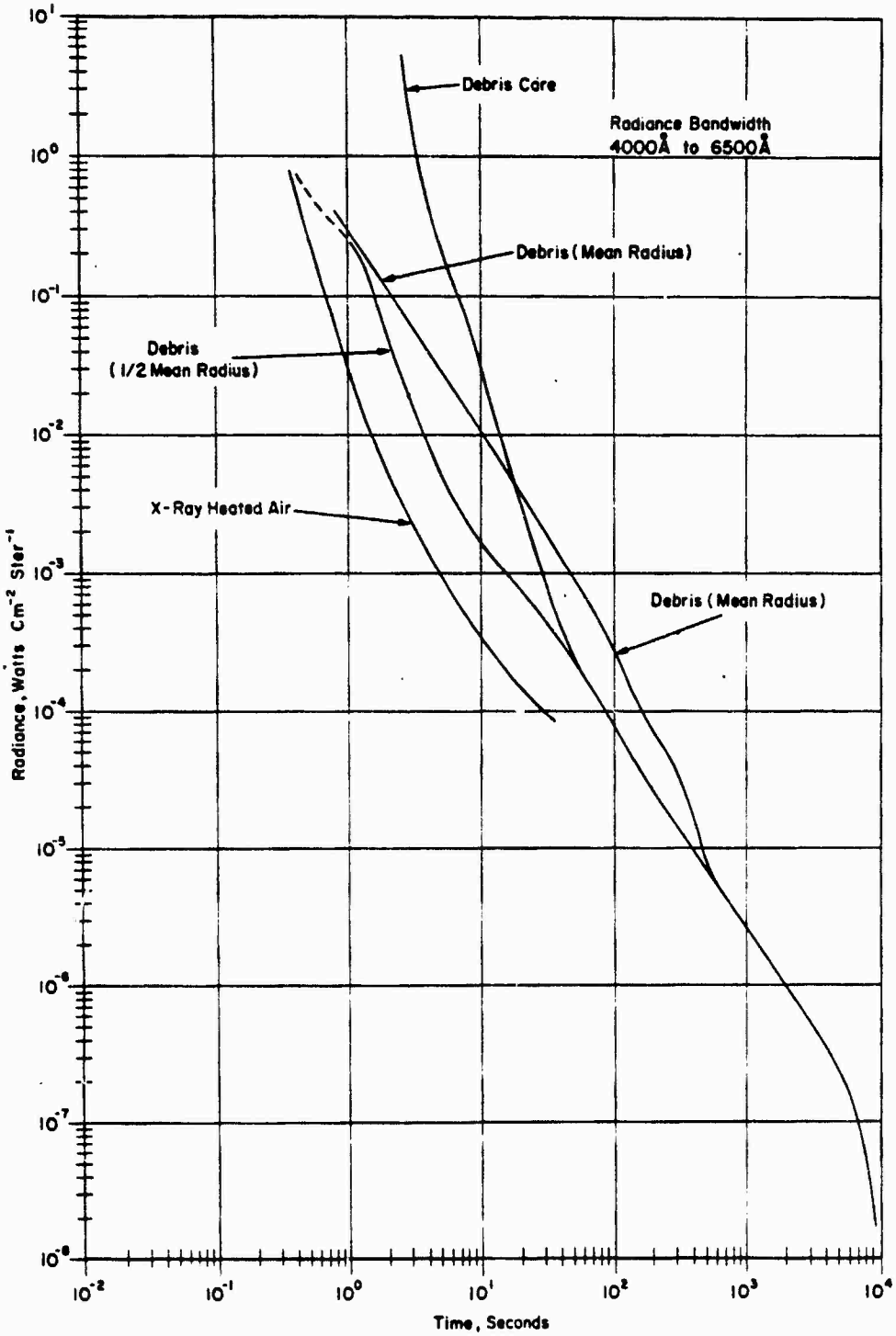

Figure 4.62 Check Mate; radiometric history of debris and X-ray-heated air.

CHAPTER 5

BLUE GILL TRIPLE PRIME PHOTOGRAPHIC RESULTS

Blue Gill Triple Prime was the detonation of a warhead at 0959:48.4753Z hours on 26 October 1962. Three prior attempts had ended in failure. The warhead was carried by a Thor missile whose trajectory reached an apogee of about 900 km before returning to the burst altitude. At main engine cutoff, three instrument pods weighing 1200 pounds each were released from their positions on the missile body. They followed separate trajectories and were at altitudes slightly below the burst point at detonation. The following additional information, extracted from Reference 18, is included to complete the description of the missile system.

The predicted burst position was determined from calculated trajectory data supplied by Douglas Aircraft Company. The actual burst position was determined by measured trajectory data obtained by Sandia Corporation. These positions are listed below:

	Planned	Actual
Latitude	16° 25' 15.60" N	16° 24' 56.64" N
Longitude	169° 35' 48.84" W	169° 36' 11.26" W

Table 5.1 presents the positions of the three instrument pods relative to the re-entry vehicle at burst time (**Reference 13**). These positions are given in the Bravo coordinate system which is a rectangular Cartesian system whose origin is the burst point and whose positive x-axis, y-axis, and z-axis points, respectively, in the direction of east, north, and the zenith.

5.1 INSTRUMENTATION

5.1.1 Camera Parameters. Tables 5.2 through 5.4 present listings of the cameras and their parameter settings used on Aircraft 53120, Aircraft 60376, and Johnston Island for Blue Gill Triple Prime. This instrumentation plan differs from that originally planned for Blue Gill because of experience gained during Star Fish Prime, and because of the changes in instruments caused by the loss of Aircraft 53144. Although one-for-one replacements of instruments was not possible, the replacement instrument complement had almost the same time and intensity range as the original instruments. A more important change in the camera plan was the more extensive use of color film and XR film. Evaluation of Star Fish Prime records showed that not only was reasonably accurate color rendition obtained, but many new phenomena could be discerned more easily. Several XR film records which had been exposed at Christmas Island pointed up the desirability of using it extensively in the remainder of Fish Bowl.

5.1.2 Aircraft Positions. The planned and actual positions for Aircraft 53120 and Aircraft 60376 for Blue Gill Triple Prime are given in Table 5.5. These positions were selected

so that the burst would be photographed from positions approximately parallel with, and perpendicular to the magnetic field of the earth, with Aircraft 53120 north of the burst and Aircraft 60376 east. Figure 5.1 is a sketch of an elevation section through the predicted burst point, Johnston Island, and one of the predicted aircraft positions. The bearings from the predicted ground zero to each of the three stations are shown.

Figure 5.2 is a plot of the aircraft positions from H-hour to H+378 seconds. These positions were plotted from the Aircraft Flight Log prepared by each navigator after the shot.

5.1.3 Instrument Pointing. The predictions of the effects of nuclear explosions indicated that the height of burst of each event would greatly influence both the extent and magnitude of the phenomenology produced. For Blue Gill it was predicted that the burst and debris would be contained by the atmosphere, with the formation of a well-developed cloud. The effect of the magnetic field on the cloud was predicted to be insignificant. However, well-formed local auroral streamers were expected to be produced by the action of the magnetic field on the delayed fission electrons.

The

size of the desired field of view of instruments recording this phase of the explosion dictated the focal length of the camera lenses tc be used. Aircraft aiming uncertainties demanded somewhat larger fields of view than those used on the Johnston Island station. Predicted late-time phenomenology indicated a considerably larger field of view would be required for cameras recording the debris and cloud motion.

Typical fields of view projected from the cameras on the two aircraft and Johnston Island onto a plane at the burst point are shown in Figures 5.3 through 5.5. To cover the rise of the debris cloud with a single camera would require a large field of view resulting in a small image. By using two cameras whose fields of view overlap in a vertical direction the entire rise can be followed and a larger image can be obtained. This technique is illustrated in Figure 5.3 by Film Number 95217 and 95220. Although Film Number 95109 and 95120 in Figure 5.4 have approximately the same field of view, the image on Film Number 95109 is about 4 times larger because it is 70-mm film, and consequently, less magnification is used to obtain the same field of view. Figure 5.5 shows similar fields of view for Johnston Island cameras. These fields of view are generally smaller than those on the two aircraft, because they only have to be large enough to

account for uncertainties in burst position. The instrument pointing angles used at Johnston Island are given in Table 5.6 with the angles to the actual burst position.

5.2 RECORD SUMMARY

A total of 66 cameras were used to record scientific photographic data on Blue Gill Triple Prime. These cameras covered the time range of microseconds to minutes with approximately one-third of the cameras recording in color. A high degree of success was attained on this shot as shown in Table 5.7.

All of the records have been examined and qualitatively evaluated for possible data content. The list of comments of this evaluation for each record is presented in Tables 5.8, 5.9, and 5.10. The comments as noted are terse and should therefore be regarded as little more than guide lines for gross data potential.

5.3 PICTORIAL HISTORY

The Project 8A.2 photographic coverage on Blue Gill Triple Prime was successful in obtaining an extensive evolutionary time history of that event. The earliest recordings were obtained by a KFC-600 camera on Johnston Island. Five photographs taken on XR film by this camera are shown in Figure 5.6. The

exposure time of each was 0.1 microsecond and the interframe time between them 1.0 microsecond. On the basis of predicted brightness values, attenuation by neutral density filters was used to set the exposure midway in the film sensitivity range. The very early time phenomena were substantially less bright than predicted, and as a result, the films were grossly under-exposed. The phenomena seen in the five frames of Figure 5.6 were recorded on the most sensitive layer of the XR film, which because of its fast speed has considerable emulsion grain. This grainy structure shows up clearly on these enlarged photographs. No record was obtained on the second of the six frames from the KFC-600, because the Kerr cell shutter failed in that optical channel.

The first frame of the KFC-600 camera was taken at 0.1 microsecond, within an uncertainty of 0.1 microsecond due to triggering delays.

the warhead had propagated a distance of 25 meters as measured

The X-rays were manifested optically by X-ray-induced air fluorescence which in turn gave rise to the 50-meter diameter sphere shown in **Frame 1.**

Had **Frame** 2 recorded, it would have shown an X-ray-induced sphere of air fluorescence about half the size recorded on

Frame 3.

From 3.1 to 5.1 microseconds the diameter remained constant. Harder components of the X-ray spectrum deposited energy at greater distances, but no evidence of them was recorded by this camera because of the diminished brightness of the X-ray-induced air fluorescence. The initial flash of air fluorescence is almost dissipated by 5.1 microseconds (**Frame 5**).

A diffuse central core slightly brighter than the air fluorescence is apparent in the last four frames of the KFC-600 record. Its dimensions are difficult to ascertain because of the small contrast between the core and the surrounding air fluorescence. Both phenomena were recorded in the toe response region of the film where a large brightness contrast produces only a small film density change. The nature of the core cannot be explained from its behavior in these five pictures.

However, the nature of the core does become obvious in the next sequence of pictures (Figure 5.7) taken by a KFC-600 camera aboard Aircraft 53120. The exposure time is ten times greater (1.0 microsecond) than in the previous sequence. Here the bright core is seen to be the radiative fireball

Two other features of this sequence are interesting. The volume of air which gave rise to the X-ray-induced air fluorescence pulse as recorded with the longer time exposure of the KFC-600 on the aircraft. The persistence of a glowing sphere indicates that a sufficient number of hard X-rays had been deposited to heat the air to incandescence after equilibration had taken place. For purposes of discussion the glowing air surrounding the radiative fireball is termed a temperature gradient "halo".

While the ellipse appeared tilted as viewed from the northern aircraft, the records from the eastern aircraft (A/C 60376) show the minor axis of the ellipse oriented in the vertical direction. A series of four Rapatronic camera photographs taken from

the eastern aircraft are shown in Figures 5.8 and 5.9. Three of these records lie between the previous KFC-600 camera records. The Rapatronic camera takes a single frame exposure of 5-microsecond duration. Only the radiative fireball is apparent in these four pictures, although the halo is apparent in the original records. The reader is cautioned not to rely upon the comparative exposures among the various records for purposes of interpretation. A photographic print has only a range of about fifty to one as contrasted to the many decades of photographic film; in this particular case the film is of the eight decade XR variety. In many cases the prints have been made to emphasize a particular phenomenon, and as a result, details of other phenomena are lost.

Figure 5.10 taken by a Rapatronic camera shows the radiative sphere from the northern aircraft (A/C 53120) at 510 microseconds. Again, the ellipse shows the slight tilt which was characteristic of the northern view. The X-ray-induced halo is obvious in this picture, but also apparent are a dark band around the halo and a tenuous envelope extending to large distances from the fireball. The latter phenomenon, which was not seen by any of the other cameras overlapping this time period, is explained on the basis of exposure times. The Rapatronic camera which took this

picture is believed to have been inadvertently set for a 40-microsecond exposure rather than for the normal 5-microsecond exposure employed with that type of camera. All other cameras which photographed this time region had either 5-or 10-microsecond exposure times. The outer nebulous envelope is seen only faintly on the original camera record and would not have been recorded at the shorter exposure times.

From Johnston Island the fireball appeared as a circular disk as seen in Figure 5.11. No trace of an elliptical shape is apparent. This photograph was taken by a Rapatronic camera at 938 microseconds and an exposure time of 5 microseconds.

The elliptical shape of the fireball was not maintained for long. Figure 5.12 taken by a Photo-Sonics 4C camera from the northern aircraft (A/C 53120) shows that during the time period from 200 to 600 microseconds the ellipsoidal shape had given way to a spherical shape. The X-ray-induced halo is still apparent with the 10-microsecond exposure time of this camera.

A long sequence of photographs taken from the same Photo-Sonics camera is presented in Figures 5.13 through 5.23, as well as the previous Figure 5.12. By 3 seconds when **Frame 7499** (Figure 5.23) was recorded the pictures suffer from a grainy

appearance due to the fact that the exposure was faint and only the most sensitive layer of the XR emulsion was able to record. However, in presenting a sequence from a single record the dimensions between all frames are rendered in their true proportions for the reader. More important, in this instance, is the fact that this particular record captured a remarkable number of shock fronts internal to the fireball.

Spectrographic records show that fireball transparency (i.e., fireball continuum with absorption line structure giving way to emission structure) occurred at about 25 milliseconds. Shortly thereafter, debris and shock front structure were seen within the fireball. At 35.8 milliseconds an outward-going shock front is clearly evident in Figure 5.15. Two other shock fronts are also seen at this time in the original record, but it was impossible to reproduce them in the photographic print. The outgoing shock front which is apparent in the picture is not spherically symmetric as one might expect but is bulged out in the downward direction, indicating a higher velocity downward.

At 63.8 milliseconds, **Frame 159**, also in Figure 5.15, it was possible to reproduce all three shock fronts. The two additional shock fronts are both spherically symmetric with larger

radii than the dominant shock which had the downward bulge. The outermost of the two shock fronts is progressing in the outward direction, while the second or middle shock front is imploding inward. In the upper fireball hemisphere, and for a portion of the lower hemisphere, the inward-going shock front is external to the innermost shock but has passed through it in the region of the bulge.

In the next two photographs (Figure 5.16) only the outward-going shock with the bulge is reproduced. On the original record the inward-going shock was not traced beyond 70 milliseconds. The outermost shock was overtaken by the dominant shock at 220 milliseconds and was not apparent thereafter.

At 250 milliseconds the only shock front remaining passes through the fireball surface and creates a shock halo external to the fireball as it proceeds outward. The shock halo is only faintly observable in the two photographs comprising Figure 5.17. Photographs taken at later times with longer exposures show the shock halo quite clearly. No further internal shock structure is seen until 0.7 second, at which time an inward-going shock leaves the fireball surface. This new shock is evident slightly inside the fireball surface in Figure 5.18, taken at 0.76 second. In Figures

5.19 to 5.21 the implosion of the shock front is followed. At 2.0 seconds (Figure 5.21) the only evidence of the imploding shock is the bright circle in the center of the photograph. This shock reflects at the origin and at 2.88 seconds (Figure 5.22) has almost reached the fireball surface. Contact with the fireball surface was made at 3.0 seconds (Figure 5.23).

A color record taken by a Photo-Sonics 4C camera from Johnston Island was successful in recording several of the shock fronts which were seen shortly after the fireball became transparent. Figure 5.24 is a single frame from that record which had an exposure time of 10 microseconds. Only one of the shocks (outgoing with downward bulge) is apparent in the reproduction.

The late-time shock fronts previously seen in the XR film record were recorded in color by a Mitchell camera on Johnston Island at 100 frames per second. Figures 5.25 and 5.26 show eight frames of this record. The first two frames shown (10 and 50) are overexposed,but the remaining six are close to normal exposure. Beginning with the frame at 0.85 second an imploding shock is seen near the boundary of the fireball; at 1.10 seconds the shock front has traveled one-third of the way to the origin, one-half the way by 1.35 seconds (Figure 5.26), and has

imploded on the origin and is returning outward at 2.10 seconds. At 2.60 seconds the shock front has progressed outward to two-thirds of the fireball diameter; and in the last frame of this sequence it has passed beyond the fireball boundary.

An interesting auroral streamer was observed from Aircraft 60376 stationed to the east. The first two frames of Figure 5.27 show this aurora which was formed by beta particles emitted by the radio-active debris. The beta particles have been constrained by the earth's magnetic field so that the aurora has the appearance of a pencil beam of light going upward to the south and downward to the north, inclined 30 degrees to the vertical. Also evident in these two frames is the outward-going shock front which passed through the fireball surface at 0.3 second. In the vicinity of the pencil aurora the shock front is enhanced, probably by its ability to further excite the air already excited by beta particles.

Three other frames taken by the same Flight Research camera are shown, two in Figure 5.27 and one in Figure 5.28. These three frames show the onset of formation of the torus from the fireball. Figure 5.29 taken from the same aircraft with a similar camera but with a greater exposure shows the torus

almost completely formed by 64 seconds. Two later frames from the same record, Figure 5.30, show the torus at 90 and 120 seconds.

The late-time history of the fireball, air shocks, aurora, and torus formation are repeated in black-and-white photographs in Figures 5.31 through 5.37. These seven photographs were all reproduced with larger magnification from the same XR film record in order to maintain proportions for the reader and to render some of the details of the phenomena which may be obscure in the color photographs. The camera was a Flight Research camera aboard the eastern aircraft.

Figure 5.31 clearly shows the shock halo, and another disturbance going outward which is visible only along the auroral streamer. The Thor booster is also evident as a small white dot some distance below the burst.

At some point in its progression the strong outward shock ceases to further excite the air, and there is no further evidence of its progression. A residual shock halo remains.

5.4 RESULTS

5.4.1 Geometric Measurements. There were two phases of Blue Gill Triple Prime during which it was difficult to assign radius values to the fireball. In both instances it was principally a question of deciding what constituted the fireball. The first phase was the time period from zero to 5 microseconds (see Figure 5.6). In the sequence of records covering that time period a halo is seen surrounding a slightly brighter core. Spectroscopic evidence (Chapter 9) indicates that this halo is X-ray-induced molecular nitrogen air fluorescence combined with emissions from dissociated nitrogen and oxygen atoms. The halo is some 400 meters in radius. At an altitude of 48.3 kilometers, the disturbed air contained therein undoubtedly equilibrates during this time period.

It is a characteristic of heated air with a uniform temperature gradient that steep brightness contours develop at points where there are discontinuities in the internal-energy deposition profile. The boundary of the halo observed from 3 to 5 microseconds is believed to be such a brightness contour.

The bulk of the X-ray energy released by Blue Gill Triple Prime is believed to be contained within a sphere of much smaller radius and is represented by the slightly brighter core seen in the

five pictures of Figure 5.6. From 2 microseconds on, this core is believed to be the isothermal sphere, growing radiatively, but masked by absorption processes within the halo that formed. At 9 microseconds the isothermal sphere is clearly evident (Figure 5.7). It is this isothermal sphere which has been called the fireball in the radius-time history shown in Figure 5.38. Measurements for the time period from 10^{-7} second to 10^{-2} second are shown in Figure 5.38, while the subsequent time period to 10 seconds is shown in Figure 5.39.

A second halo observed from 9 microseconds to 1 millisecond is believed to be caused by a gradient of temperature in the same manner as was the halo observed at the earlier times. The fact that it was not seen earlier than nine microseconds was due to its lower brightness which could not be recorded by the KFC-600 camera on Johnston Island. A third halo, only faintly recorded, was seen during the time period 10^{-4} to 1.3×10^{-3} second.

Because this third halo expanded with time, it is believed not to be of the same nature as the first two halos. Rather it is attributed to photoexcitation by ultraviolet emissions from the fireball.

The second phase of Blue Gill Triple Prime during which it was difficult to assign radius values to the fireball was the time period from 2.5 milliseconds to 0.2 second. The fireball developed two boundaries during this time period, the outermost of which was the less bright of the two. It is the outer boundary which has been identified as the fireball surface in Figure 5.39 for the time period in question.

A fourth halo appeared, at about 0.25 second for which there is no uncertainty in attributing a cause; a shock front was followed in its progress through the interior of the fireball and was seen to pass out into the surrounding air, exciting it to luminescence. Radius measurements for the halo during the time period from 0.25 to 0.35 second were difficult to make because of camera flare near the edge of the fireball; after 0.35 second the measurements were not confused by flare. It is only the latter measurements, for which accurate values were obtained, that have been plotted in the figure.

The radius measurements reported thus far were made on the horizontal dimensions of the fireball where there was symmetry. Within a few seconds after detonation a vertical asymmetry was established. Measurements of the altitude of the top, center, and bottom of the fireball as shown in Figure 5.40

reflect this asymmetry. Rates of rise of the various components of the fireball are indicated only in the vicinity of 55 seconds after detonation.

Rates of rise at other times and the approach to a stabilization altitude are shown in Figure 5.41. The mean position of the center of the fireball, and the torus once it formed, is indicated by this figure. The uncertainty in values of data points indicates the amount of error present due to lack of exact knowledge of the aircraft attitude at the time of the measurement. An extrapolation of the data indicates that stabilization occurred at an altitude between 92 and 95 kilometers.

Figure 5.42 gives the angular dimensions vs. time for Blue Gill Triple Prime as seen from Johnston Island. This figure may be of use to those interested in determining the radar target provided by the fireball and torus.

5.4.2 Shock Waves. Blue Gill Triple Prime displayed more shock phenomena than any of the other Fish Bowl detonations. The large number of shocks observed can be attributed for the most part to the altitude of the detonation, which optimized the conditions for photographing both the internal and external shock fronts. In making the comparison with other Fish Bowl events

it is really not proper to include Star Fish and Check Mate, since relatively little could be expected in the way of shock phenomena Figure 5.43 shows the many shock fronts which were observed on Blue Gill Triple Prime.

Seven distinct and unambiguously defined shock fronts were observed; these are the shocks labelled Shock No. 1 through Shock No. 7 in the figure. Shock No. 8 was definitely observed travelling down the northern auroral column, but we are uncertain as to whether it represents an independent shock front or a localized manifestation of one of the other shock fronts, for example Shock No. 3. The auroral column created by beta rays (see Figure 5.27) represents air that has been raised to a higher temperature than the surrounding air at similar radial distances from the fireball. Thus, in its passage through the auroral column the speed of Shock No. 3 would be expected to increase relative to its speed in the surrounding air.

It seems unlikely that Shock No. 4 and Shock No. 8 are connected in any way. In order for them to be the same shock, the velocity of Shock No. 4 would have had to increase from an average speed of 1.6 km/sec to 14 km/sec during the time period

for which the last observation on Shock No. 4 was made and the first measurement on Shock No. 8. It is more likely that Shock No. 4 reached the fireball surface at 1.1 seconds and was responsible for the increase in fireball radius at that time. The latter interpretation is consistent with the observed speed of Shock No. 4.

Shock No. 7 is obviously the reflected shock created by Shock No. 6 imploding on the origin. Shocks No. 4 and No. 5 are seen for only a brief period of their radial growth. This limited observation period was not enough to determine the genesis of these shocks, although they are undoubtedly reflected shocks several generations removed from the parent shock or shocks.

It seems strange that the strong shock identified as No. 2 in the figure, traveling at 5 km/sec as it reached the fireball surface, did not create a sudden increase in fireball radius as did the weaker Shocks No. 4 and No. 7 when they passed through the edge of the fireball. Even more strange is the origin of Shock No. 6. Its origin is none too clear from the camera records. However, the measurements that could be made place its origin in the neighborhood of Shock front No. 3 at a time somewhere

near 0.4 second. The physical mechanism by which Shock No. 6 was born is certainly an interesting problem.

Another phenomenon offering difficulty in interpretation is the behavior of the fireball surface during the time period from 2.5 milliseconds to 0.2 second. The fireball appeared to have two boundaries during this period; the outer one was semi-transparent permitting the inner one to be discernible (see Figure 5.14, Frame 74). The outer boundary behaved as if an internal shock front had struck the fireball surface at 2.5 milliseconds. For this reason the outer boundary has been labelled the fireball surface, and for lack of any other explanation the inner boundary has been called a contact surface (i.e., a surface having a discontinuity in pressure and density but not velocity). At 20 milliseconds, as the fireball first became transparent, a weak shock front (No. 1) is seen to leave the contact surface and implode toward the origin. At the same time, the contact surface begins to increase in radius at a velocity that makes it appear as if it had been transformed into a shock front.

5.4.3 Radiometric Measurements. The KFC-600 camera records, one from Johnston Island, the other from Aircraft 53120, represent the totality of useful radiometric data for the first 100

microseconds of Blue Gill Triple Prime. From these two records eleven time-separated data points were obtained for the fireball time history. These data points are indicated in the radiance vs. time plot, Figure 5.44, which gives the complete radiance-time history of Blue Gill Triple Prime.

Unlike all other cameras (except the Rapatronic cameras), the KFC-600 cameras used a light-yellow (Wratten 12) filter whose purpose was to eliminate a blue-violet light leak in the polarizers. The radiance bandwidth of the KFC-600 cameras was thereby restricted to 1500Å as compared to the approximately 2500Å recording bandwidth for the other cameras. Radiometric values derived from calibration of the KFC-600 cameras were increased by a factor 5/3 in order to place all data points on the same bandwidth basis. Such an adjustment of bandwidth was shown in Section 2.7 to be permissible, with only a minor error, provided the source of light is a continuum.

The scatter in radiance values during the first 5 microseconds reflects the difficulty in performing measurements on the small nebulous fireball image at these times. From 9 to 109 microseconds the fireball image size was large enough to permit accurate measurements, and this accuracy is reflected in the fact that a

smooth curve could be passed through the data points. The two peaks in the radiance-time curve prior to 100 microseconds are of uncertain origin, but could be explained as follows: The fireball was all but masked by a halo until shortly after 5 microseconds, at which time the absorption by the halo ceased and the true brightness of isothermal sphere became apparent, thereby allowing the fireball radiance to increase to the first peak at 9 microseconds. Two possible causes are suggested for the second peak (at 80 microseconds), the first is the formation of an air shock at the surface of the fireball caused by the hydrodynamic expansion of the fireball. This explanation presumes that radiative growth of the fireball had given way to hydrodynamic growth by 30 microseconds, at which time the second peak is seen to begin. Thirty microseconds seems premature for the onset of hydrodynamic growth at the Blue Gill Triple Prime altitude, however. The other suggested cause of the second peak concerns itself with the snowplowing of air by bomb debris well inside the surface of the fireball. At roughly an 85-meter radius the bomb debris would have encountered and snowplowed two masses of air each equivalent to the combined mass of all material in the warhead. The slowing down of bomb debris by the snowplow effect converts an enormous

quantity of kinetic energy into internal energy which should be manifested by the release of a pulse of radiant energy flooding through the fireball to the outside surface. The second peak of the curve may be due to this pulse. The snowplow effect also creates a strong shock known as the debris shock which reaches the surface of the fireball at a later time. The debris shock is assumed to form when approximately two masses of air equivalent to the bomb mass have been snowplowed.

If one assumes an average velocity of 1 meter/microsecond during the time taken for the debris to reach an 85-meter radius, then the time of the release of the radiant energy pulse is consistent with the time of occurrence of the second peak shown in the figure.

The behavior of the halo at these times is consistent with the second explanation offered; i.e., the release of a radiant energy pulse by the snowplow effect, rather than with the first explanation—the creation of an air shock. The radiance values of the halo were measured at a point midway between the fireball and the outer boundary of the halo. If a shock passed this point, one would expect a narrower radiance pulse in the halo than was observed, the peak of which would almost certainly be displaced

toward later times. The fact that the halo increases in brightness in a manner identical in time and shape with the fireball surface strongly suggests that a single pulse of radiant energy was simultaneously responsible for the behavior of both the fireball surface and the halo.

The remainder of the peaks on the Blue Gill Triple Prime radiance vs, time curve can be interpreted in an almost straightforward manner, with shock fronts accounting for most of the minor disturbances. It is not at all clear when the strong debris-shock reached the fireball surface. On the basis of the behavior of the radiance-time curve, one would estimate that it occurred at 10^{-2} second, yet the radius-time curve (Figure 5.43) behaves as though it occurred earlier, at 2 milliseconds.

In addition to the radiance of the fireball and debris in Figure 5.44, measurements have been included of the radiance of the northern auroral column. The data were taken at a point just outside the shock halo. It is interesting to note that for the straight-line portion of the auroral radiance curve between 8 and 40 seconds the slope of the line gives a $t^{-1.18}$ decay rate for the radiance. Since the beta-particle emission rate from fission fragments follows a $t^{-1.2}$ power law, the obvious conclusion can

be drawn that all of the beta particles emitted by the debris were channeled out of the fireball in a column of fixed diameter during this time period. Had the column diameter not remained constant, the radiance would have diminished as a result of the column expansion as well as from the fission fragment beta decay law with a resultant rate of decrease which would not have matched the $t^{-1.2}$ law. After 40 seconds the diameter of the auroral column increased markedly as a result of turbulent motion of the debris and the formation of a torus (see Figures 5.35 through 5.37). The expansion of the auroral column is reflected in the greater rate of radiance decay after 40 seconds.

A further conclusion can be drawn from the behavior of the auroral column up to 40 seconds: If the diameter of the column remained essentially constant, as it apparently did, then the distribution of the geomagnetic field lines within the fireball behaved much like a magnetic bottle, allowing beta particles to escape only at the two mirror points in the bottle, the apertures of the mirrors remaining essential constant in diameter up to 40 seconds.

5.4.4 Brightness Temperature, Radiant Power, and Thermal Yield. For purposes of this report, brightness temperature is defined as that black body temperature required to produce a radiance, evaluated in the bandwidth 4000 Å to 6500 Å, equivalent to a value of photographic radiance measured in the same bandwidth. With this as a definition the radiance vs. time curves for Blue Gill Triple Prime, Figure 5.44, were used to derive brightness temperature vs. time for the fireball and debris. The brightness temperature values thus derived are given in Figures 5.45 through 5.47.

At 0.1 second, shortly after the fireball became transparent, it was possible to determine the brightness temperature of the debris as well as the fireball. Since the observed radiance of the debris after transparency was always greater than the fireball radiance, the brightness temperature of the debris remained higher than the brightness temperature of the fireball. At 1 second the fireball brightness temperature was 2300°K, while the debris brightness temperature was 3150°K. The true temperature of the fireball was higher than the brightness temperature by an amount which depended on the emissivity and the density of air within the fireball. A calculation of the true temperature was not attempted for this report due to lack of time.

The low values of fireball temperature prior to 9 microseconds reflect the low radiance values during that time period, which are accounted for by the absorbing halo of X-ray-excited air.

To determine the amount of radiant energy emitted by the fireball is an ambiguous problem without the specification of qualifying information such as the direction (i. e., up, down, or sideways) and the distance at which the determination is to be made. For example, at early times a preponderance of energy is radiated at very short wavelengths, yet this energy may radiate only a few tens of meters before being absorbed in the air outside the fireball. A value of thermal yield which included those wavelengths would not be useful. Our criteria for choosing the qualifying conditions are based on the practical use of the data which results. Values of the radiant power and energy that are received on the ground are useful from the standpoint of eye damage and incendiary hazards. Similar values obtained at distances a few kilometers from the fireball are useful in determining thermal impulse loading on re-entry vehicles. In the time available for publication of this report each of these problems could only be given a brief analysis and then only after making several simplifying assumptions.

The first assumption made was that the fireball behaved as a black body, radiating according to Planck's law at the brightness temperatures which were deduced from the radiance data. This assumption was valid because most of the energy was radiated at times when the fireball was opaque. As a consequence of the fireball being opaque the emissivity was nearly unity for all wavelengths of interest. A second assumption made was that the amount of radiant power and energy contributed by the bomb debris was negligible. This assumption is good only for early times, but it is still a valid assumption,since most of the energy is radiated at times prior to the fireball becoming transparent.

The effect of the ozone layer and atmospheric attenuation has been neglected in the calculation of the visible energy radiated by the fireball. The values of visible power radiated,and total visible yield thus obtained,pertain to the actual quantities leaving the fireball. To use these results in problems dealing with observations at sea level, the values should be corrected for ozone and atmospheric attenuations,by applying a transmission factor averaged over the visible spectral range. The visible power radiated by the Blue Gill Triple Prime fireball as given in Figure 5.48 was limited to a bandwidth of 4000 Å to 7400 Å. By integrating

the area under a linear plot of this same curve, the total visible energy radiated was determined to be 1.20×10^{14} joules or 28.7 kilotons of energy. The visible yield thus accounted for 14.4 percent of the total yield of 200 kilotons.

Rather than calculate the total thermal power at an arbitrarily fixed distance and in a specified direction from the fireball, it was decided to calculate the power radiated between those wavelengths whose mean free path was a distance of one scale height from the fireball surface. For simplicity, the scale height chosen was the scale height appropriate to the burst altitude. At the Blue Gill Triple Prime altitude the scale height is 8.4 kilometers.

The cutoff for the short wavelength end of the bandwidth was determined by the exponential absorption characteristics of molecular oxygen in air. The wavelength for which the mean free path is equal to 8.4 kilometers at the Blue Gill Triple Prime altitude was found to be λ1925 Å.

The cutoff for the long wavelength end of the bandwidth need not be determined with any degree of precision, because only a small fraction of the total yield is radiated in the infrared. For Blue Gill Triple Prime a long wavelength cutoff of 10,000 Å was chosen for purposes of calculation. The thermal power radiated

by the fireball between the wavelength limits of 1925 Å and 10,000 Å is also shown in Figure **5.48.** The total thermal energy radiated by the fireball in this same bandwidth was 3.76×10^4 joules or 90 kilotons of energy, accounting for 45 percent of the total yield of the weapon.

The previous calculation does not take into account the energy radiated by X-ray-induced air fluorescence. On the radiant power vs. time curves (Figure **5.48)** air fluorescence would have shown as a large peak between 10^{-6} and 10^{-5} second. Its power could have been roughly calculated by multiplying the area of the spherical halo by its radiance value. However, the spectral bandwidth characteristics of air fluorescence are considerably different from those for either of the two curves shown. A crude estimate of the amount of energy contained in the air fluorescence pulse shows that it would make a negligible contribution to the total thermal energy which was radiated by Blue Gill Triple Prime.

TABLE 5.1 INSTRUMENT POD POSITIONS IN BRAVO COORDINATE SYSTEM, BLUE GILL TRIPLE PRIME

Pod	ΔX	ΔY	ΔZ	Slant Range	Slant Range
	Feet	Feet	Feet	Feet	Kilometers
B1	-782	+190	-3178	3277	0.999
B2	-493	+441	-4555	4603	1.403
B3	-57	+601	-6733	6760	2.060

TABLE 5.2 SUMMARY OF BLUE GILL TRIPLE PRIME CAMERA PARAMETERS, AIRCRAFT 53120

INSTRUMENT AND STATION POSITION		FILM TYPE	FILM NUMBER	AIMING ANGLES IN DEGREES ELEV	AZIMUTH	FILTERS ND	COLOR	FOCAL LENGTH MM	LENS F/N	FRAMES PER SECOND	SHUTTER SECTOR, DEGREES	EXPOSURE TIME	MARKER RATE CPS
MAURER	W1	EDER	95121	30	0	-	-	80	2.8	5.5	-	1MUSEC	-
MAURER	W2	XR	95122	27	0	-	-	38	4.5	5.5	-	1MUSEC	-
PHOTO-SONICS 10 B	W5	EDER	95127	30	0	1.0	-	180	16	360	1	10MUSEC	200
KERR CELL E.O. 600	W6	XR	95104	30	0	2.0	WR12	305	9.5	100000	-	1MUSEC	-
RAPATRONIC	W7	XR	95103	30	0	1.0	WR12	490	22	*(A)	-	5MUSEC	-
TRAID	W8	PX	95117	45	0	1.0	-	25	16	48	7	0.4MSEC	50
TRAID	W9	KDII	95118	45	0	-	-	25	11	48	7	0.4MSEC	50
CLOUD	W10	DXN	95109	45	0	-	-	105	3.7	0.5	-	1SEC	CLOCK
FAIRCHILD HS-100	W11	KDI	95123	30	0	1.0	-B	13	16	1000	-	0.2MSEC	50
GSAP N-6	W11	KDII	95124	45	0	-	-A	9.5	16	64	133	6MSEC	-
PHOTO-SONICS 4C	W12	XR	95125	30	0	-	-	108	5.6	2500	9	10MUSEC	200
CLOUD	W13	EDER	95110	45	0	-	-	105	3.7	0.2	-	1SEC	CLOCK
ROBOT	W15	RXP	95111	50	0	-	3914A	45	2.8	1	-	250MSEC	-
ROBOT	W16	RXP	95112	50	0	-	4278A	45	2.8	1	-	250MSEC	-
ROBOT	W17	RXP	95113	50	0	-	4709A	45	2.8	1	-	250MSEC	-
TRAID	W18	EDER	95119	55	0	-	-	25	2.3	16	160	30MSEC	50
TRAID	W19	XR	95120	55	0	-	-	25	2.3	16	160	30MSEC	50
ROBOT	W21	EDER	95114	75	0	-	-	45	2.8	1	-	250MSEC	-
ROBOT	W22	RXP	95115	75	0	-	5577A	45	2.8	1	-	250MSEC	-
ROBOT	W23	RXP	95116	75	0	-	6300A	45	2.8	1	-	250MSEC	-
PHOTO PANEL CAMERA	PANEL	PX	95131	-	-	-	-	25	16	1	160	30MSEC	CLOCK
PHOTO PANEL CAMERA	PANEL	PX	95132	-	-	-	-	25	16	0.2	160	30MSEC	CLOCK

*(A) SINGLE EXPOSURE AT 510 MUSEC.
N.B. MUSEC = MUS = MICROSECOND

TABLE 5.3 SUMMARY OF BLUE GILL TRIPLE PRIME CAMERA PARAMETERS, AIRCRAFT 60376

INSTRUMENT AND STATION POSITION		FILM TYPE	FILM NUMBER	AIMING ANGLES IN DEGREES ELEV	AZIMUTH	FILTERS ND	COLOR	FOCAL LENGTH MM	LENS F/N	FRAMES PER SECOND	SHUTTER SECTOR, DEGREES	EXPOSURE TIME	MARKER RATE CPS
BEATTIE-COLEMAN	W1	EDER	95221	30	0	-	-	105	8	*(A)	-	*(B)	-
BEATTIE-COLEMAN	W2	PX	95222	30	0	-	-	105	8	*(A)	-	*(B)	-
RAPATRONIC	W3	XR	95205	30	0	1.0	WR12	490	22	*(C)	-	5MUSEC	-
PHOTO-SONICS 10 B	W5	PX	95227	30	0	-	-	180	22	360	1	10MUSEC	200
RAPATRONIC	W6	XR	95204	30	0	1.0	WR12	490	22	*(D)	-	5MUSEC	-
RAPATRONIC	W7	XR	95203	30	0	1.0	WR12	490	22	*(E)	-	5MUSEC	-
FLIGHT RESEARCH-CINE	W8	KDII	95217	30	0	-	-	35	7	20	130	20MSEC	10
FLIGHT RESEARCH-CINE	W9	XR	95218	30	0	-	-	35	2.5	20	130	20MSEC	10
RAPATRONIC	W10	XR	95223	30	0	1.0	WR12	490	22	*(F)	-	5MUSEC	-
BEATTIE-COLEMAN	W11	EDER	95209	45	AFT 10	-	-	105	3.5	*(G)	-	*(H)	-
PHOTO-SONICS 4C	W12	PX	95225	30	0	2.0	-	108	11	2500	9	10MUSEC	200
BEATTIE-COLEMAN	W13	XR	95210	45	AFT 10	-	-	105	3.5	*(G)	-	*(H)	-
PHOTO-SONICS 4C	W14	EDER	95226	30	0	2.0	-	50	11	2500	9	10MUSEC	200
FLIGHT RESEARCH-CINE	W15	EDER	95219	50	0	-	-	35	2.3	20	130	20MSEC	10
FLIGHT RESEARCH-CINE	W16	PXR	95220	50	0	-	-	35	2.3	20	130	20MSEC	10
FLIGHT RESEARCH-PULSED	W17	RXP	95211	50	0	-	3914A	35	2.3	*(I)	130	1SEC	-
FLIGHT RESEARCH-PULSED	W18	RXP	95212	50	0	-	4278A	35	2.3	*(I)	130	1SEC	-
FLIGHT RESEARCH-PULSED	W19	RXP	95213	50	0	-	4709A	35	2.3	*(I)	130	1SEC	-
FLIGHT RESEARCH-PULSED	W20	RXP	95214	75	0	-	5577A	35	2.3	*(I)	130	1SEC	-
FLIGHT RESEARCH-PULSED	W21	RXP	95215	75	0	-	6300A	35	2.3	*(I)	130	1SEC	-
PHOTO PANEL CAMERA	PANEL	PX	95231	-	-	1.0	-	25	5.6	1	160	30MSEC	CLOCK
PHOTO PANEL CAMERA	PANEL	PX	95232	-	-	1.0	-	25	5.6	0.2	160	30MSEC	CLOCK

* (A) 1 FR/SEC, 0.5 FR/SEC, 0.2 FR/SEC, 0.1 FR/SEC UP TO +10 SEC, +60 SEC, +180 SEC +1800 SEC RESPECTIVELY.
* (B) 0.5 SEC, 1.5 SEC, 4.5 SEC, 9.5 SEC, UP TO +10 SEC, +60 SEC, +180 SEC, +1800 SEC RESPECTIVELY.
* (C) SINGLE EXPOSURE AT 14 MUSEC.
* (D) SINGLE EXPOSURE AT 52.4 MUSEC.
* (E) SINGLE EXPOSURE AT 103.4 MUSEC.
* (F) SINGLE EXPOSURE AT 256.2 MUSEC.
* (G) 1 FR/SEC, 0.2 FR/SEC, 0.1 FR/SEC UP TO +10 SEC, +180 SEC, +1800 SEC, RESPECTIVELY.
* (H) 0.5 SEC, 4.5 SEC, 9.5 SEC, UP TO +10 SEC, +180 SEC, +1800 SEC, RESPECTIVELY.
* (I) 1 FR/SEC UP TO +10 SEC, 0.33 FR/SEC UP TO +30 SEC, THEN 0.1 FR/SEC TO END.

N.B. MUSEC MUS MICROSECOND

TABLE 5.4 SUMMARY OF BLUE GILL TRIPLE PRIME CAMERA PARAMETERS, JOHNSTON ISLAND

INSTRUMENT AND STATION POSITION		FILM TYPE	FILM NUMBER	AIMING ANGLES IN DEGREES ELEV	AZIMUTH	FILTERS ND	COLOR	FOCAL LENGTH MM	LENS F/N	FRAMES PER SECOND	SHUTTER SECTOR, DEGREES	EXPOSURE TIME	MARKER RATE CPS
KFC-600	A1	XR	95304	54	192	ND2	WR12	254	9	1000000	-	0.1MUSEC	-
PHOTO-SONICS 4C	A2	EDER	95324	54	192	ND2	-	108	22	2500	9	10MUSEC	200
PHOTO-SONICS 4C	A3	PX	95323	54	192	ND3	-	150	22	2500	9	10MUSEC	200
PHOTO-SONICS 10B	A4	PX	95325	54	192	ND2	-	250	22	360	1	10MUSEC	50
RAPATRONIC	A5	XR	95303	54	192	-	WR12	490	22	*(A)	-	5MUSEC	-
MAURER	A7	XR	95319	54	192	-	-	150	6.3	5.5	-	0.5MSEC	-
MAURER	A8	EDER	95320	54	192	-	-	150	32	5.5	-	0.5MSEC	-
TRAID	A9	PX	95317	54	192	ND1	-	35	16	48	7	0.93MSEC	10
MITCHELL	A10	PX	95326	57	192	ND2	-	35	16	100	15	0.24MSEC	100
FAIRCHILD HS-100	A12	KO1	95321	54	192	ND2	-	13	16	900	-	0.22MSEC	100
GSAP	A13	KDII	95322	65	192	-	-	9.5	2.2	16	133	37MSEC	-
KC-18	A14	TXA	95332	79	192	-	-	153	6.3	0.2	-	5SEC	-
CLOUD	C1	EDER	95309	70	192	-	-	105	3.7	0.25	-	0.5SEC	-
CLOUD	C2	EDER	95310	85	192	-	-	105	3.7	0.25	-	1SEC	-
TRAID	C3	XR	95318	70	192	ND3	-	25	2.3	16	160	14MSEC	-
MITCHELL	C4	KDII	95327	57	192	ND1	-	35	16	100	15	0.24MSEC	100
BELL AND HOWELL	C5	XR	95329	70	192	-	-	25	2.0	12	160	18.5MSEC	10
MITCHELL LS	C6	EDER	95328	70	192	-	-	18.5	2.2	2.5	170	180MSEC	10
ROBOT	C7	RXP	95311	65	192	-	4278A	45	2.8	0.33	-	1.2SEC	-
ROBOT	C8	RXP	95312	65	192	-	4709A	45	2.8	0.33	-	1.2SEC	-
ROBOT	C9	RXP	95313	65	192	-	5228A	45	2.8	0.33	-	1.2SEC	-
ROBOT	C11	RXP	95314	78	192	-	6300A	45	2.8	0.33	-	1.2SEC	-
ROBOT	C12	RXP	95315	65	192	-	3914A	45	2.8	0.33	-	1.2SEC	-
ROBOT	OUTSIDE	EDER	95334	VAR.	VAR.	-	-	45	2.8	0.33	-	VAR.	-
DYNAFAX	D1	MF	95335	54	192	-	-	813	9	25000	-	5MUSEC	-
DYNAFAX	D2	HSIR	95336	54	192	-	-	76	2.8	25000	-	5MUSEC	-

*(A) SINGLE EXPOSURE AT 900 MUSEC.
N.B. MUSEC = MUS = MICROSECOND

TABLE 5.5 BLUE GILL TRIPLE PRIME H-HOUR AIRCRAFT POSITIONS

	Planned Values		Actual Values	
	Aircraft 53120	Aircraft 60376	Aircraft 53120	Aircraft 60376
Latitude	17° 0' 44.5'' W	16° 28' 18.6'' W	17° 0' 30'' N	16° 26' 00'' N
Longitude	169° 39' 2.4'' W	168° 59' 2.4'' W	169° 39' 00'' W	168° 58' 30'' W
Magnetic Heading	75°	165°	74.5°	170.3°
Altitude (feet)	37,500	37,500	37,500	37,500

TABLE 5.6 POINTING INFORMATION FOR JOHNSTON ISLAND, BLUE GILL TRIPLE PRIME

Station Location:	Latitude 16° 44' 04.79'' N
	Longitude 169° 31' 36.59' W

TABLE 5.7 STATISTICAL SUMMARY OF BLUE GILL TRIPLE PRIME CAMERA RECORDS FROM THE BURST AREA

Station	J-820	Aircraft 53120	Aircraft 60376	Totals
Number of Cameras	26	20	20	66
Number of Useful Records	23	16	20	59
Reasons for No Records:				
Mechanical failure	3	4	0	7
Inappropriate camera parameters	0	0	0	0
Error in shot location	0	0	0	0
Reasons for Poor Records:				
Inappropriate camera parameters	0	0	0	0
Error in shot location	0	0	0	0
Other	0	0	0	0
Percent Success	88	80	100	—
Overall Success: 89 percent				

TABLE 5.8 SUMMARY OF BLUE GILL TRIPLE PRIME FILM RECORDS, AIRCRAFT 53120

FILM NUMBER	FILM TYPE	CAMERA	RESULTS
95103	XR	RAPATRONIC	FIREBALL RECORD OBTAINED.
95104	XR	KFC-600	GOOD SEQUENCE OBTAINED.
95109	DXN	CLOUD	GOOD LATE STAGE CLOUD RECORD.
95110	EDER	CLOUD	NO RECORD.
95111	RXP	ROBOT	69 FEET OF RECORD
95112	RXP	ROBOT	18 FEET OF RECORD.
95113	RXP	ROBOT	40 FEET OF RECORD.
95114	EDER	ROBOT	INITIAL BLUE GLOW FOR THIRTY-TWO FRAMES, YELLOW-WHITE CLOUD RISES INTO FIELD AND PERSISTS TWENTY-EIGHT FRAMES UNTIL AIRCRAFT BANKS.
95115	RXP	ROBOT	4 FEET OF RECORD.
95116	RXP	ROBOT	NO RECORD.
95117	PX	TRAID	BURST APPEARS AT BOTTOM OF FRAME AND RISES.
95118	KDII	TRAID	SIMILAR TO SEQUENCE IN 95117.
95119	EDER	TRAID	366 FEET OF RECORD. TURBULENT CLOUD APPEARS AT +11 SECONDS AND DEVELOPS INTO TOROID. BLUE GLOW ALWAYS PRESENT. AURORA OBSERVED.
95120	XR	TRAID	360 FEET OF GOOD RECORD.
95121	EDER	MAURER	NO RECORD.
95122	XR	MAURER	NO RECORD.
95123	KDI	FAIRCHILD HS-100	GOOD RECORD.
95124	KDII	GSAP	GOOD RECORD TO END OF FILM.
95125	XR	PS-40	EXCELLENT RECORD 540 FEET. FIRST FRAME HALO. MANY SHOCK WAVES. GOOD INTERNAL FIREBALL DETAIL.
95127	EDER	PS-108	FIREBALL DETAIL STARTS AT 0.1 SECOND. GOOD RECORD TO 1 SECOND.

TABLE 5.9 SUMMARY OF BLUE GILL TRIPLE PRIME FILM RECORDS, AIRCRAFT 60376

FILM NUMBER	FILM TYPE	CAMERA	RESULTS
95203	XR	RAPATRONIC	RECORD OBTAINED SHOWING CENTRAL CORE AND HALO.
95204	XR	RAPATRONIC	RECORD OBTAINED SHOWING CENTRAL CORE AND HALO.
95205	XR	RAPATRONIC	RECORD OBTAINED SHOWING CENTRAL CORE PLUS TWO OUTER CONCENTRIC RINGS.
95209	EDER	BC	BURNHOLE ON FIRST FRAME. RECORD EXTENDS TO LATE TIME GLOW. LONG EXPOSURE TIMES SHOW IMAGE BLUR.
95210	XR	BC	RECORD FOR ENTIRE RUN. SHOWS FIREBALL GROWTH AND RISE PLUS TORUS DEVELOPMENT.
95211	RXP	FR PULSED	200 FEET OF RECORD.
95212	RXP	FR PULSED	RECORD OBTAINED.
95213	RXP	FR PULSED	46 FEET OF USEFUL RECORD.
95214	RXP	FR PULSED	RECORD SIMILAR TO OTHER FLIGHT RESEARCH RECORDS.
95215	RXP	FR PULSED	48 FEET OF RECORD.
95217	KDII	FR CINE	SUPERB RECORD OF FIREBALL, DEBRIS CLOUD DEVELOPMENT, VORTEX FORMATION, AND BLUE AURORA.
95218	XR	FR CINE	EXCELLENT RECORD 380 FEET. BURNHOLE ON FIRST FRAME.
95219	EDER	FR CINE	VERY LONG RECORD. AURORA FIRST SHOWS AT +5.6 SECONDS.
95220	PX	FR CINE	144 FEET OF RECORD BEAUTIFULLY SHOWING CLOUD RISE, EXPANSION, AND AURORA OUT OF TOP OF CLOUD.
95221	EDER	BC	BURNHOLE FIRST FRAME. GOOD AURORA COLOR. SHOWS COLOR DIFFERENCE BETWEEN AURORA AND OUTER FIRE BALL.
95222	PX	BC	DENSE EXPOSURE OF FIREBALL AND AURORA.
95223	XR	RAPATRONIC	RECORD SHOWS CENTRAL CORE PLUS OUTER HALO.
95225	PX	PS-4C	FIREBALL SURROUNDING STRUCTURED DEBRIS CLOUD OBSERVED. FIREBALL DIES LEAVING DEBRIS.
95226	EDER	PS-4C	LONG, PERSISTENT RECORD OF CENTRAL CORE. SHOWS EARLY FIREBALL DISSIPATION. SMALL IMAGE.
95227	PX	PS-10B	EXCELLENT RECORD SHOWING FIREBALL, DEBRIS, AND VARIOUS SHOCKS.

TABLE 5.10 SUMMARY OF BLUE GILL TRIPLE PRIME FILM RECORDS, JOHNSTON ISLAND

FILM NUMBER	FILM TYPE	CAMERA	RESULTS
95303	XR	RAPATRONIC	CENTRAL CORE.
95304(1-6)	XR	KFC-600	RECORD ON ALL FRAMES EXCEPT NO. 2.
95309	EDER	CLOUD	OVEREXPOSED FOR FIRST 30 SECONDS. GOOD LATE CLOUD TO 2 MINUTES.
95310	EDER	CLOUD	NOT IN VIEW FOR FIRST 30 SECONDS. EXCELLENT AURORA FROM 1 TO 12 MINUTES.
95311	RXP	ROBOT	18 FEET OF RECORD SHOWING BURST AND AURORA. 4278 A FILTER
95312	RXP	ROBOT	NO RECORD EXCEPT ROCKET TRAILS. 4709 A FILTER.
95313	RXP	ROBOT	APPROXIMATELY 55 FEET OF RECORD FIREBALL, DEBRIS, AURORA, AND TOROIDAL DEVELOPMENT. 5228 A FILTER.
95314	RXP	ROBOT	GDOD RECORD. BURST GROWS INTO FIELD OF VIEW FROM LEFT SIDE OF FRAME. 6300 A FILTER.
95315	RXP	ROBOT	28 FEET OF RECORD SHOWING AURORA PLUS FAINT TOROID. 3914 A FILTER.
95317	PX	TRAID	RECORD OBTAINED, ALBEIT SMALL IN SIZE.
95318	XR	TRAID	GOOD RECORD BUT BURST IS LOW IN FRAME. SHOWS MANY SHOCK WAVES.
95319	XR	MAURER	FOGGED FILM.
95320	EDER	MAURER	GOOD RECORD FOR 17 SECONDS. SHOWS INTERNAL FIREBALL STRUCTURE.
95321	KD-I	FAIRCHILD HS-100	EARLY FIREBALL RECORD.
95322	KDII	GSAP	GOOD RECORD OF LATE FIREBALL AND VORTEX RINGS.
95323	PX	PS-4C	94 FEET OF RECORD. PARTICULARLY GOOD FIRST FRAME
95324	EDER	PS-4C	21 FEET OF RECORD SHOWING VARIOUS SHOCKS.
95325	PX	PS-108	GOOD RECORD SHOWING FIREBALL EXPANSION.
95326	PX	MITCHELL	SHOWS EARLY FIREBALL GROWTH.
95327	KDII	MITCHELL	LIKE 95326 EXCEPT IN COLOR.
95328	EDER	MITCHELL	LONG RECORD. BURST OVEREXPOSED EARLY. AURORA AND YELLOW-GREEN CLOUD SEEN LATER.
95329	XR	B AND H	GOOD RECORD. SHUTTER OUT OF SYNCH CAUSES IMAGE TAILING.
95332	TXA	KC-1	5 GOOD LATE CLOUD PICTURES.
95334	EDER	ROBOT	42 FEET OF RECORD SHOWING BURST, WHITE TOROID, AND AURORA. CLOUD FILLS FIELD.
95335	MF	DYNAFAX	NO RECORD.
95336	HSIR	DYNAFAX	RECORD BUT OVEREXPOSED. POSSIBLE CAPPING SHUTTER LIGHT LEAK.

Page 224 deleted.

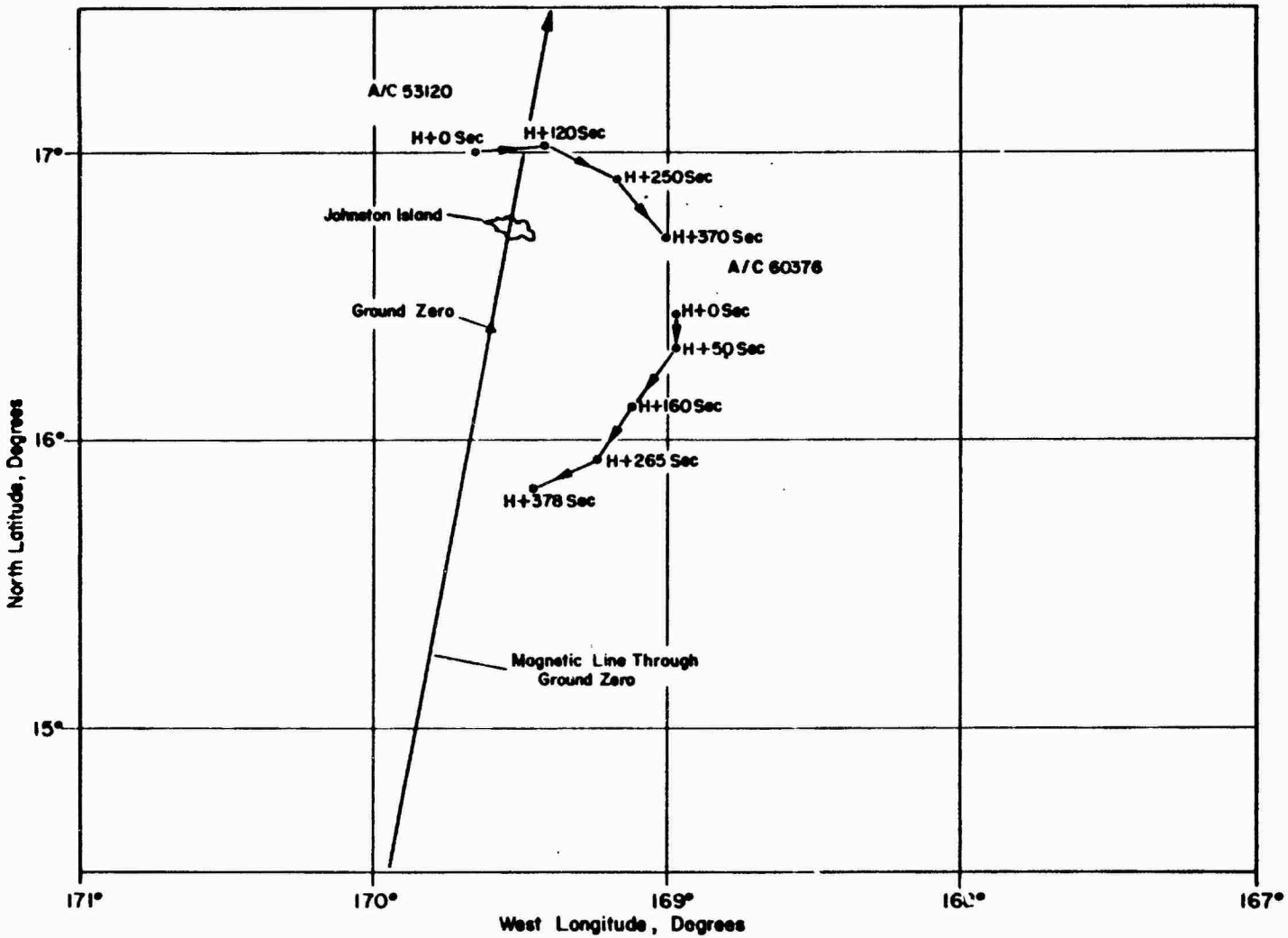

Figure 5.2 Aircraft flight paths from H-hour to 6½ minutes, Blue Gill Triple Prime.

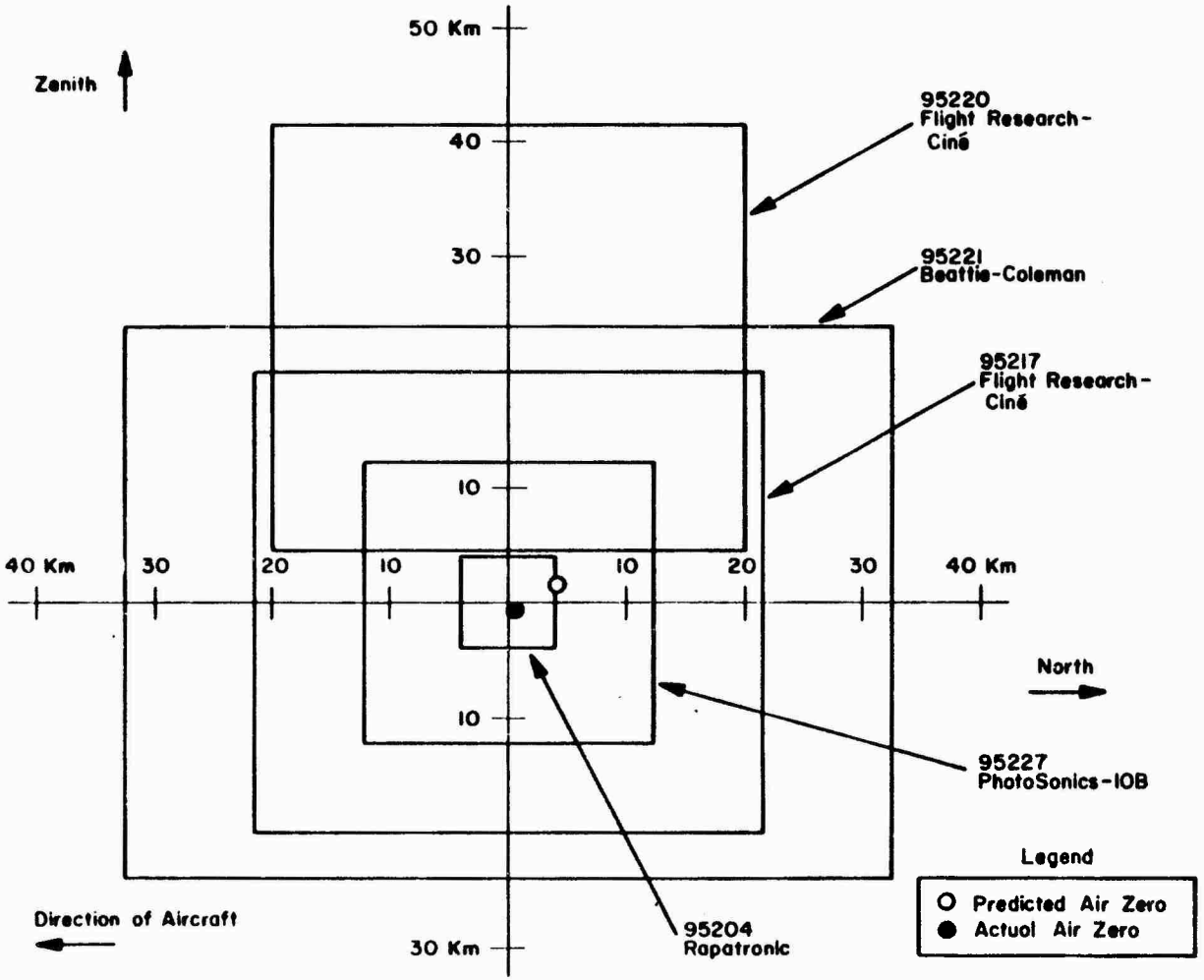

Figure 5.3 Fields of view for five Aircraft 60376 cameras with predicted and actual air zero indicated.

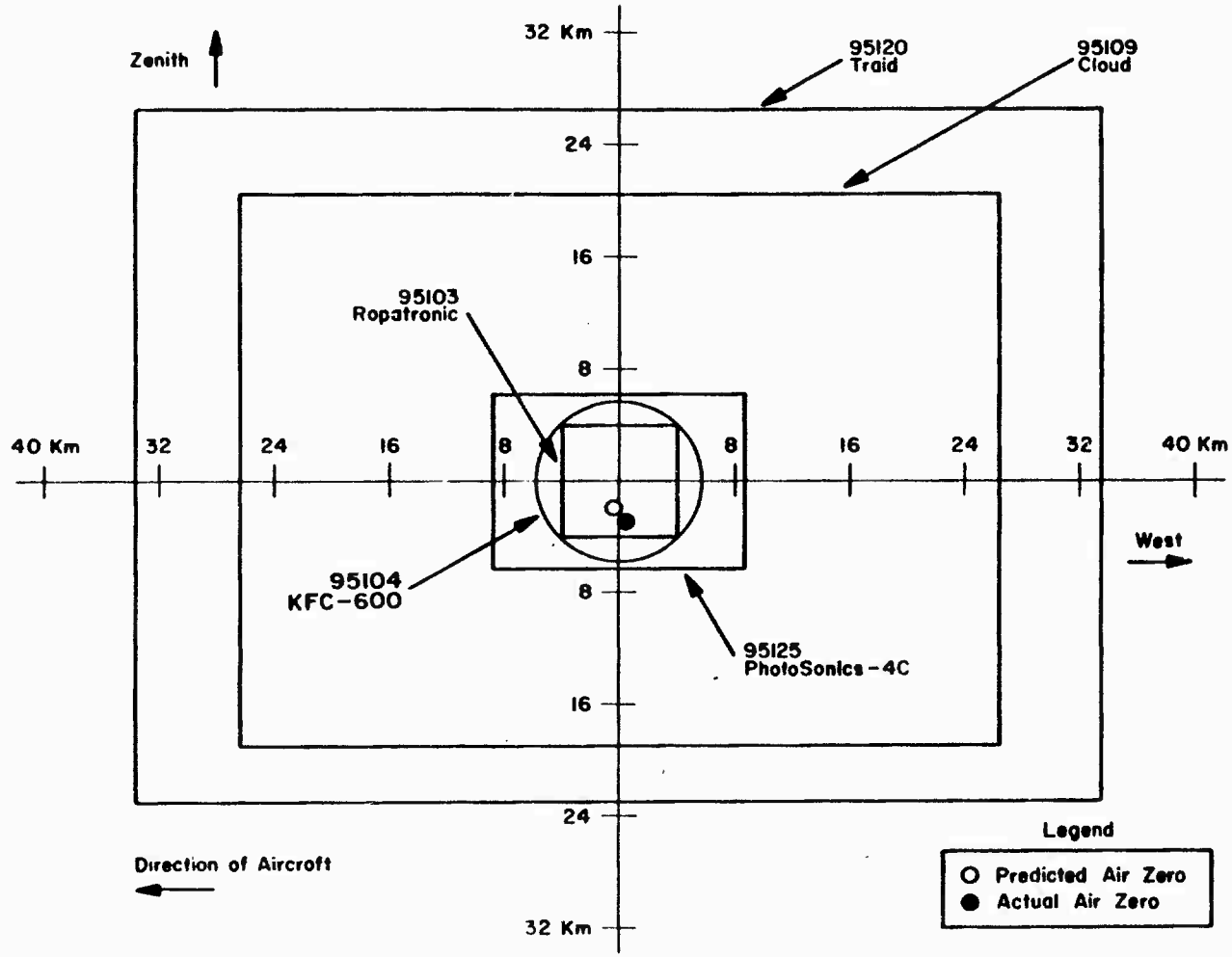

Figure 5.4 Fields of view for five Aircraft 53120 cameras with predicted and actual air zero indicated.

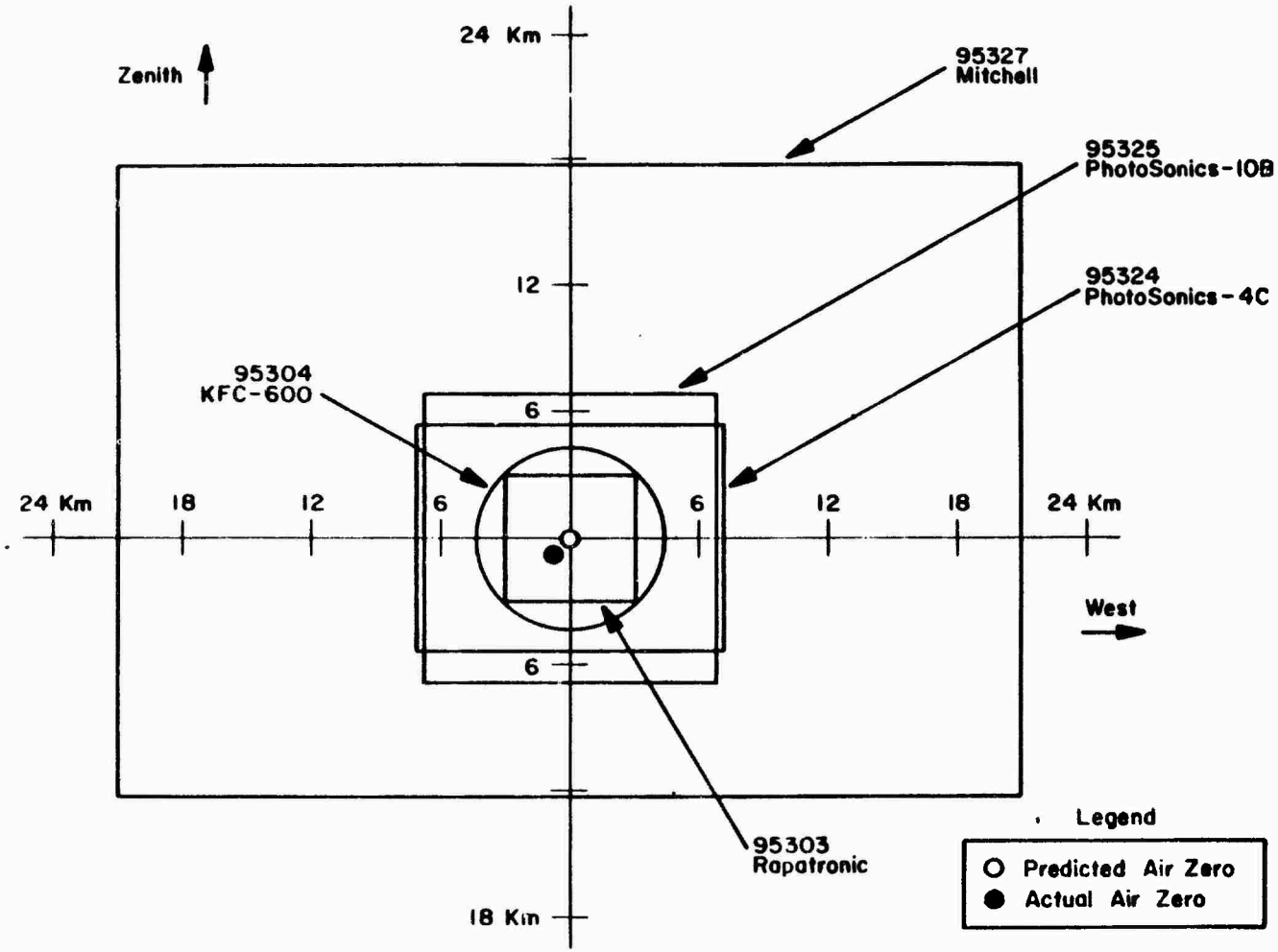

Figure 5.5 Fields of view for Johnston Island cameras with predicted and actual air zero indicated.

Pages 229 through 235 deleted.

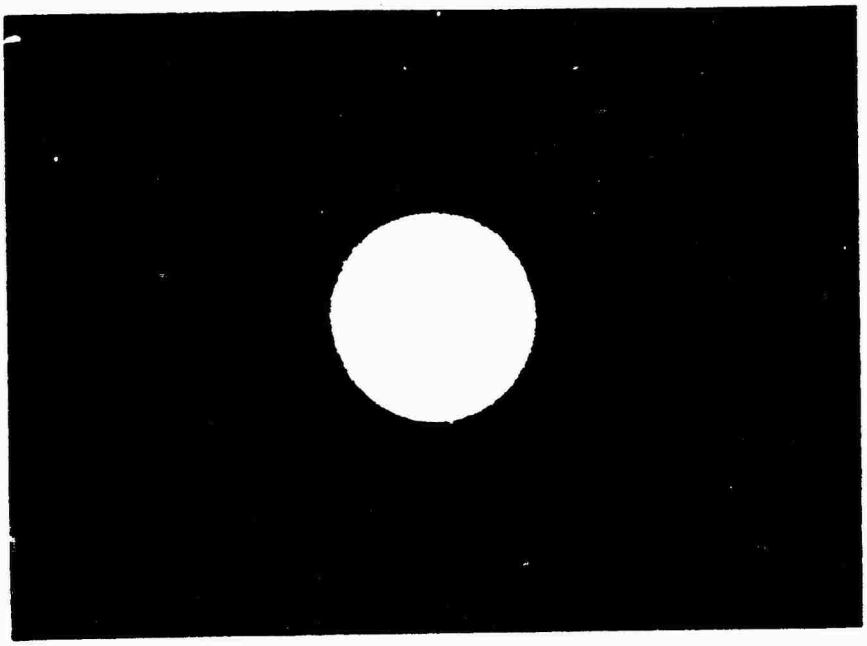

1.0 msec

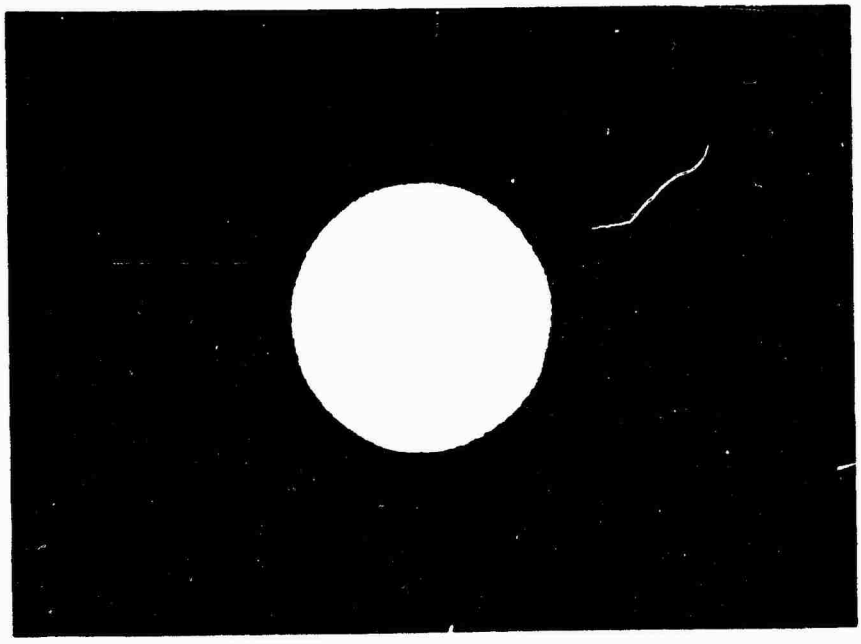

9.8 msec

Figure 5.13 Blue Gill Triple Prime; fireball growth, taken from Aircraft 53120. Film 95125, Frames 2 and 24.

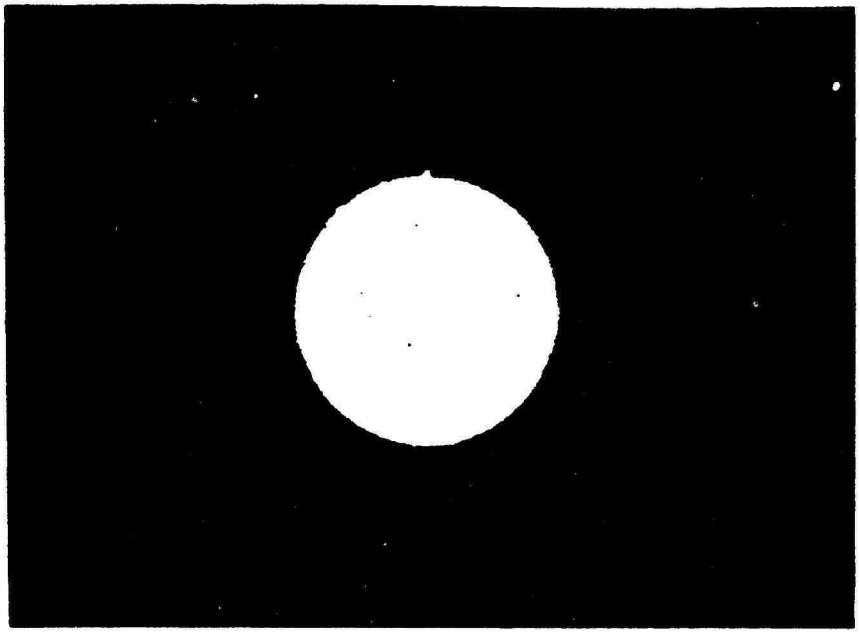

18.8 msec

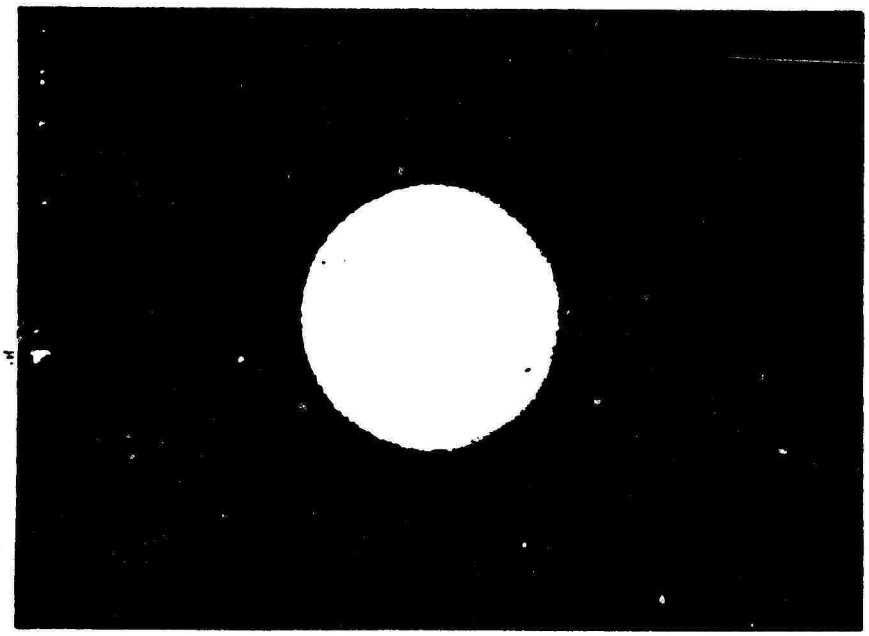

29.8 msec

Figure 5.14 Blue Gill Triple Prime; fireball growth, taken from Aircraft 53120. Film 95125, Frames 49 and 74.

Pages 238 through 241 deleted.

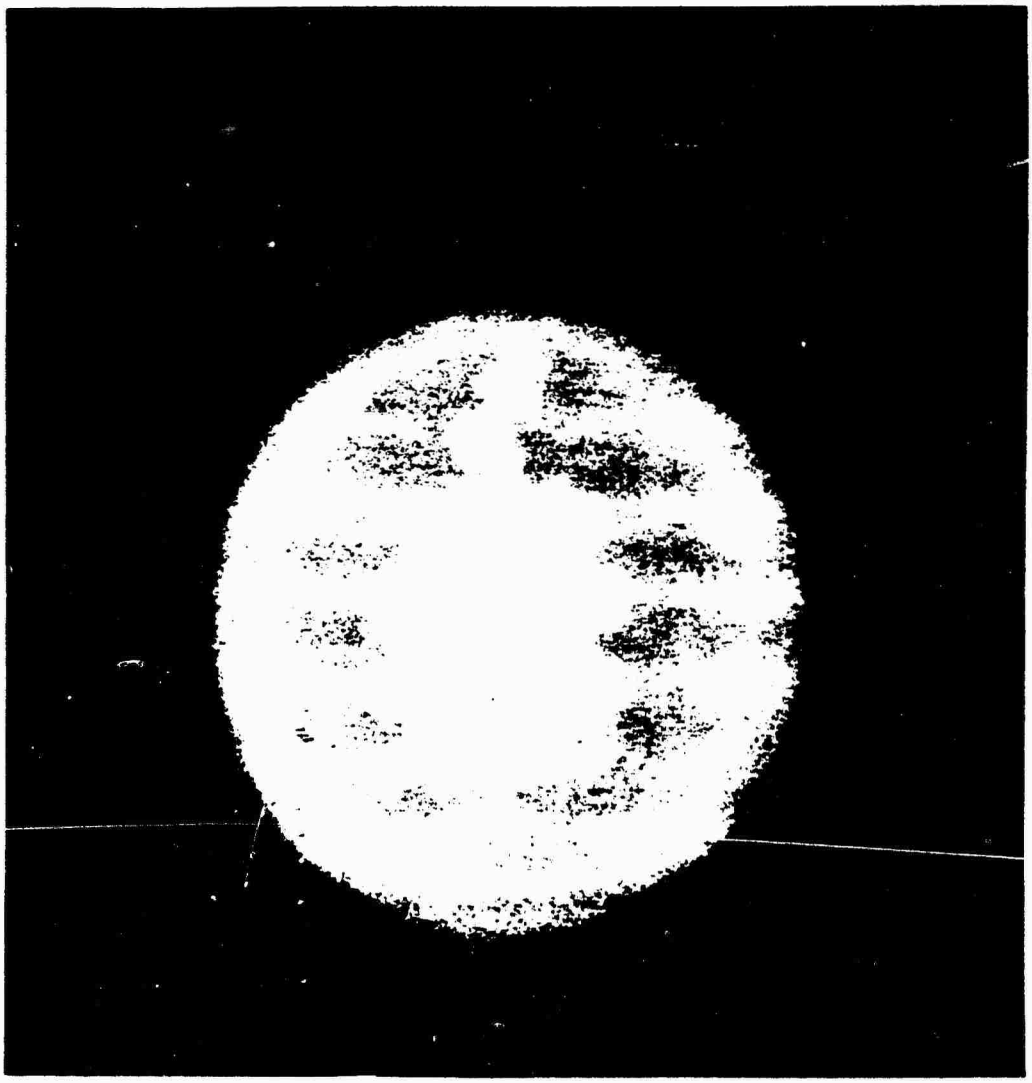

Figure 5.19 Blue Gill Triple Prime; debris and fireball with external outgoing and internal ingoing shock fronts at 1.00 second, taken from Aircraft 53120. Film 95125, Frame 2499.

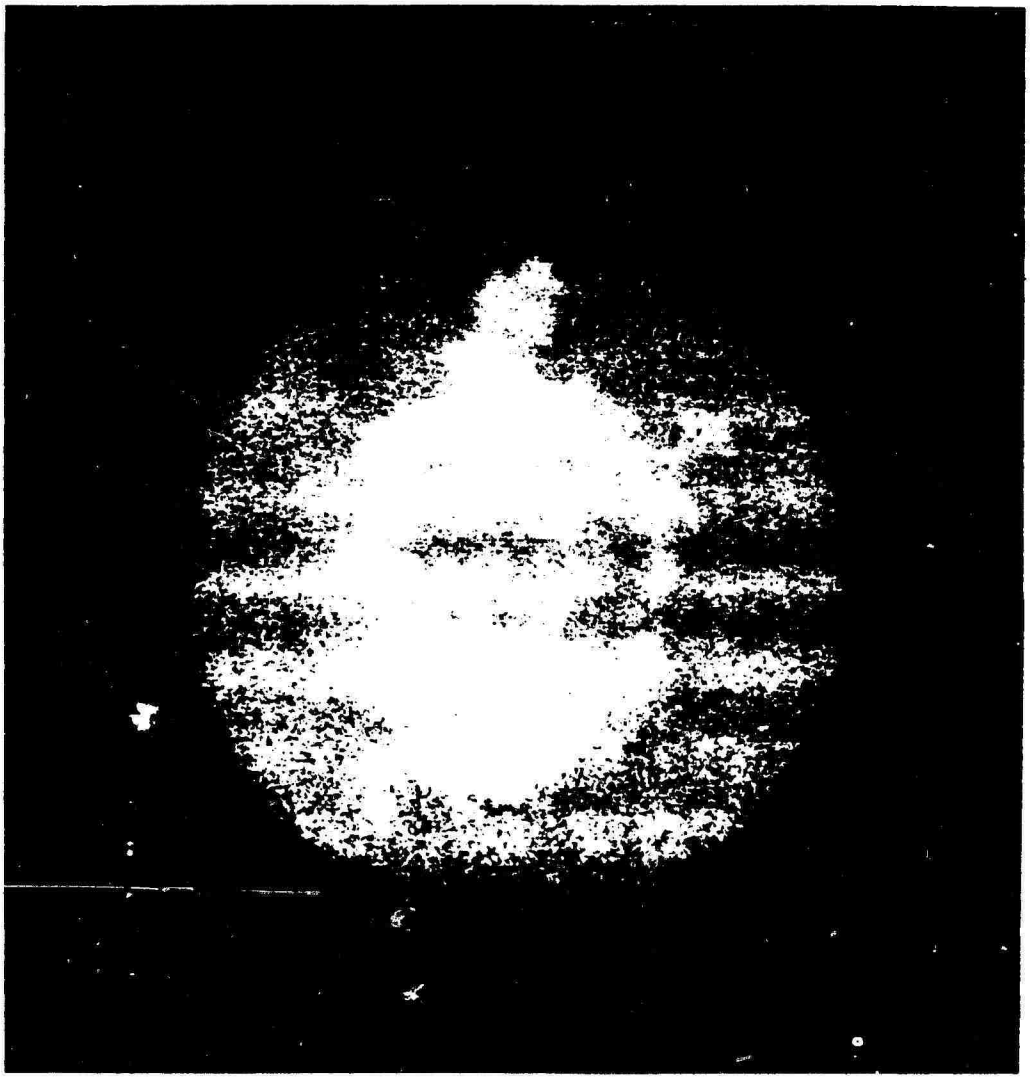

Figure 5.20 Blue Gill Triple Prime; debris and fireball with internal ingoing shock front at 1.50 seconds, taken from Aircraft 53120. Film 95125, Frame 3749.

Pages 244 through 270
deleted.

CHAPTER 6

KING FISH PHOTOGRAPHIC RESULTS

King Fish was detonated at 1210:06.12632Z on 1 November 1962. General information concerning the warhead configuration and yield as given in References 19 and 20 is summarized as follows.

The planned and actual burst coordinates as given in Reference 14 are listed in the following summary.

	Planned	Actual
Latitude	16° 06' 28.8"	16° 06' 48.61"
Longitude	169° 39' 50.04"	169° 40' 46.02"

The Thor vehicle carried three pods whose primary mission was to carry passive X-ray and thermal instrumentation. The pods were released between main engine cutoff and vernier engine cutoff so as to be placed at predetermined distances below the burst. Positions of the pods with respect to the re-entry vehicle at the time of detonation are given in Table 6.1, as taken from Reference 13. The x-axis is positive East, the y-axis is positive North (True), and the z-axis is positive upward. All values are referred to a coordinate system centered at the burst.

6.1 INSTRUMENTATION

6.1.1 Camera Parameters. The instrument parameters for King Fish are summarized in Tables 6.2 through 6.4. There are many similarities in camera parameters between King Fish and Blue Gill Triple Prime. However, the phenomena associated

with King Fish were expected to be less bright than those of Blue Gill Triple Prime; therefore, exposure times were longer, and less neutral-density attenuation was used.

For the other four Fish Bowl events, interference filters were used extensively on the Robot and Flight Research cameras, while for King Fish about half the usual number of interference filters were used. Ektachrome-Extended Range film (EDER) was generally used in the cameras from which the interference filters had been removed.

The predicted rate of rise for King Fish was larger than that for other events; therefore, the camera fields of view at Johnston Island and aboard the aircraft were staggered to cover a wider range of elevation angles and altitudes.

6.1.2 Aircraft Positions. In addition to the fast rate of rise for King Fish the geometric dimensions were expected to grow to very large proportions. For both reasons the aircraft were positioned at a considerable distance from the burst. Table 6.5 summarizes the aircraft position information at H-hour.

The aircraft were flown in a series of chords on a circular flight path similar to the pattern followed in the other events. Except for the first leg, the flight along each chord lasted for about 120 seconds, during which time the fireball, as viewed by

the cameras, would move from one edge of the field of view to the other. At the end of the chord the plane turned so as to return the fireball to the initial edge of the fields of view. Each chord was flown with a roll estimated to be ±1 degree. Figure 6.1 shows the aircraft flight paths for several minutes after H-hour.

6.1.3 Instrument Pointing. The King Fish phenomena as seen from Johnston Island and the two aircraft were expected to begin with the energy deposition by X-rays, which would quickly lead to large fireball proportions with a subsequent rapid rise of the fireball from the burst point. In order to obtain reasonable image sizes at very early times it was necessary to employ long-focal-length lenses on the fastest cameras. To cover the large phenomena at later times, and to follow the fireball rise, short focal lengths with wide fields of view were used on the slow-framing and sequence cameras.

The procedure used in pointing the Johnston Island cameras is described in Section 2.5. The methods employed for pointing cameras with long focal lengths were expected to give an accuracy of better than 10 minutes of arc. To check the accuracy with which these cameras were pointed, the position of the actual

burst with respect to the center of the frame was used. From this information, and from a knowledge of the relation of the actual burst point to the predicted burst point, it was found that in every case the optical axes of the cameras were within 30 minutes of arc from the predicted burst location.

Figure 6.2 shows the fields of view for five typical cameras located at Johnston Island. The optical axes of three long-focal-length cameras are shown centered on the predicted burst point for convenience of illustration, although there was a small dispersion of these axes around the predicted burst point. The actual burst point is shown in relation to the predicted point. Two cameras were pointed above the burst to photograph the late-time phenomena. Both the predicted and actual elevation and azimuth angles from Station J-820 to the King Fish burst point are given in Table 6.6. The actual burst occurred roughly 1° 39' west and 42' below the planned position.

The problems in camera pointing were more severe for the two aircraft stations. This was due to the fact there was no convenient way to align all cameras to a common target with any great accuracy. The method used for aligning the aircraft cameras is described in Section 2.5. Although the method was fairly

crude, a post-operation check of the pointing accuracy of selected cameras, using the actual burst point, indicated that most cameras were pointed to within 2 degrees, and a few to within 1/2 degree.

The second difficulty in pointing the aircraft cameras was one of positioning the aircraft. The problem of aircraft positioning was twofold. First, there was the navigational problem of positioning the craft so as to be within narrow prescribed limits of latitude and longitude from a given geographic point at H-hour. Second, the aircraft had to cross this point with a precise true heading to within $\pm$10 seconds of time and be in level flight to within a fraction of a degree.

Figures 6.3 and 6.4 show the fields of view for five typical cameras on each of the aircraft projecting onto predicted burst point at the H-hour positions of aircraft. The optical axes of those cameras pointed at the burst are shown coincident with the predicted air zero, although this again was not quite the case. As in the case of Johnston Island many cameras were pointed well above the burst to follow the fireball rise; and in the case of Aircraft 60376 two Beattie-Coleman cameras were pointed aft 10 degrees in order to photograph the northern auroral phenomena. Figure 6.5 shows the positions of the two aircraft and the Johnston

Island station with respect to the predicted air zero. Curvature of the earth is not indicated although it was taken into account in positioning of the aircraft.

6.2 RECORD SUMMARY

A summary of the Project 8A.2 records for King Fish event is presented in Tables 6.7 through 6.9. This summary presents pertinent comments on the film records obtained from the two aircraft and Johnston Island station.

The statistical success in useful camera records achieved by Project 8A.2 on King Fish is summarized in Table 6.10. Of the total of 66 cameras which were operated at Johnston Island and on the two aircraft, 59 obtained useful records for an overall success of 89.4 percent. The poorest showing occurred on Aircraft-60376 where inappropriate camera parameters caused the loss of four records.

6.3 PICTORIAL HISTORY

King Fish

itself to accurate scaling from Shot Teak which was at 76 km.

was not amenable to theoretical predictions of new phenomena. Consequently, a number of unsuspected optical

phenomena were observed. The present pictorial history of King Fish will show representative photographic records of these unexpected phenomena as well as the other more easily understood processes which took place.

The first five microseconds of records in Figure 6.6 illustrate the first unexpected optical phenomena which King Fish generated. These six pictures of concentric luminous rings were recorded by a KFC-600 camera on Johnston Island. The exposure time was 0.1 microsecond, and the interframe time was 1 microsecond. Frame 1 has an uncertainty of 0.1 microsecond in its assigned value of real time caused by uncertainties in triggering and cable delays.

A qualitative analysis is sufficient to establish that the ring phenomenon of King Fish could only have been produced by thermal X-rays emitted by the warhead. There are two remarkable features of the X-ray energy deposition, however; the first is the ability to optically record the crisp spherical shell structure of the X-ray pulses that were emitted by the bomb; the second is the number and comparative brightnesses of the X-ray-induced light pulses. The three rings are an optical manifestation of the X-ray deposition caused by some combination of excitation,

ionization, and dissociation of the atmospheric constituents. X-rays are normally manifested optically by air fluorescence which embodies the same physical processes but in a known specific combination. At the King Fish altitude the lifetimes of the optical radiations from X-ray-induced air fluorescence would be expected to time-smear any shell structure. Thus, normal air fluorescence seems unlikely as a fast emission process at this altitude. Also the X-ray energy deposition is too great at the close-in ring distances to allow normal air fluorescence as an emission process. A non-equilibrum process, of yet unidentified nature, is assumed to be the origin of the rings.

Briefly, the ring phenomenon is interpreted as follows. The outermost ring, seen most distinctly at 1 microsecond but progressively more diffuse at later times, is created by a shell of soft X-rays emitted by the warhead just prior to detonation of the secondary-stage. In effect it amounts to leakage or penetration of some of the primary-stage energy through the weapon case. The middle ring, seen clearly until 5 microseconds, is the thermal X-ray pulse normally associated with the bulk of energy release by a nuclear explosion. The third, or inner, ring must, by deduction, be attributed to a second case-temperature maximum.

A slight second case-temperature maximum is predicted by radiation-hydrodynamic calculations such as the LASL HENRE code (see Reference 21). A surprising feature of the third ring is its comparatively equal brightness in relation to the middle ring, which can be interpreted in either of two ways: either the second case-temperature maximum is stronger than theory predicts, or the deposition of energy by the preceding pulses has pre-excited the air and rendered it capable of optical emission with only a comparatively small amount of re-excitation.

A continuation of the X-ray deposition sequence may be seen in Figure 6.7, four pictures taken by another KFC-600 camera aboard Aircraft 53120. This KFC-600 camera had an exposure time of 1 microsecond and an interframe time of 20 microseconds. The 1-microsecond exposure time was not short enough to isolate the rings at 3 microseconds as had the 0.1-microsecond exposure from the Johnston Island KFC-600 camera; therefore, a time smearing resulted which blended the three rings. Normal errors in positioning of the aircraft resulted in the image of the burst occurring near the edge of the camera's circular field of view. Some details were lost as a result of this but probably nothing significant. Much of the general background light in the 20-, 80-,

and 100-microsecond exposures was probably due to air fluorescence in the altitude range around 75 to 80 km to which the harder component of thermal X-rays were capable of penetrating. One X-ray ring (which probably corresponds to the inner ring of the Johnston Island photographs) is faintly seen at 20, 80, and 100 microseconds within the boundary of the bright central region. A distinct envelope of unknown origin is apparent farther away in the downward direction. The small bright central spot is the weapon debris.

A vertical asymmetry in the X-ray energy deposition, is seen in the next sequence of pictures, Figure 6.8. These two color photographs, the first two frames recorded by a Photo-Sonics 4C camera from Johnston Island at 200 and 600 microseconds, show the asymmetry in X-ray deposition caused by the exponential variation of atmospheric density. Remnants of X-ray air fluorescence remain at 200 microseconds but disappear by 600 microseconds. The debris has expanded considerably by 600 microseconds, and two temperature profiles are apparent within the fireball, one at two-thirds of the fireball radius and a less obvious diffuse profile at one-half the fireball radius. At 200 microseconds the fireball is marked by a very sharp boundary which is not apparent

in the 600-microsecond photograph.

Figure 6.9, a Rapatronic picture taken from Johnston Island at 963 microseconds, shows another unusual phenomenon associated with King Fish. Because of the long focal length of this camera lens, the fireball image is quite large. The central core representing the debris is in the form of two overlapping toroids, and not spherical as one might expect. This feature of explosion asymmetry was also seen on Star Fish Prime and Check Mate.

The debris was 1 km in diameter and moving at a velocity of 0.52 meter /microsecond (averaged from zero time). In addition to the interesting double torus formation of the debris, numerous jet-like instabilities are seen forming on the toroids at this early time. King Fish was not the first event to display a debris-jetting phenomenon. Debris jetting also occurred in Check Mate.

Another phenomenon seldom observed on nuclear explosions is seen in Figure 6.10, the first frame of a Photo-Sonics 10B record from Aircraft 60376. At 1.5 milliseconds a shock front has already separated from the fireball. Its formation at this early time on King Fish indicates that its origin could not be associated with the hydrodynamic motion of the debris but rather was caused by the hydrodynamic expansion of the fireball itself. This shock then is the so-called air shock of nuclear detonation phenomenology.

The remaining five pictures from the Photo-Sonics 10B record show the rapid expansion of bomb debris and the decay of the fireball brightness. A single fast jet of debris has penetrated almost to the fireball edge by 18 milliseconds. At 43 milliseconds many more debris jets have penetrated large distances within the fireball.

Figures 6.11 and 6.12 show eight frames of a Maurer camera record taken on Johnston Island; the first two frames (at 0.27 sec and 0.45 sec) overlap the Figure 6.10 records which were taken by the Photo-Sonics 10B. Because of the longer exposure time of the Maurer camera, the air shock is again recorded. The fireball expansion is seen to be almost keeping pace with the air shock. At 0.45 second another shock becomes

apparent on the fireball edge, and at 0.63 second is seen to be rapidly overtaking the first shock. Although the motion of this shock was not distinctly observed within the fireball on any records, there is sufficient evidence to suggest that the shock was generated internal to the fireball. In the fourth frame of Figure 6.11, the remnant of the second shock is barely visible. and the first shock has disappeared entirely. The remaining four frames of this sequence, Figure 6.12, show the debris essentially having ceased its rapid expansion. Another outward-going shock is evidenced by the central white circle which is expanding irregularly through the debris. The imploding shock which must have given rise to this third observed shock is not evident in any of the records.

The remaining King Fish phenomena of interest are associated with auroral effects. The first auroral display is apparent in a heavily over-exposed sequence of four black-and-white photographs shown in Figures 6.13 and 6.14. These photographs were taken by a Flight Research Cine camera from Aircraft 60376 located southeast of the burst point. The beta-ray-induced auroral streamer is pointing downward and to the north. The approximate 30-degree inclination of the auroral

column is distorted by the perspective of the aircraft view. This sequence of photographs is included to show the early appearance and configuration of the King Fish northern-going aurora. The brightness of the fireball at this time was still significant,and in order to reproduce the aurora in the pictures the fireball detail was sacrificed. Photographs showing the upward-going auroral column are discussed in Section 6.4.4.

From Johnston Island the early beta-ray-induced aurora gave rise to the pictures reproduced in Figures 6.15 and 6.16. The streamers above the fireball are actually inclined downward and pass overhead of the Johnston Island station. These four photographs were recorded by a Bell & Howell camera with an exposure time of 0.04 second.

Much longer exposure times were required to photograph the late-time debris motion and aurora. An excellent color sequence of pictures was taken by a Beattie-Coleman camera from the southeastern aircraft (60376), with exposure times of 0.5 to 5 seconds. Six frames of this record are reproduced in Figures 6.17 through 6.19. The last frame (at 63 seconds) had a 5-second exposure.

The first two frames of this series show the fireball, aurora, and two shock fronts proceeding outward from the fireball. The outermost of the two shocks is evident only by the enhanced optical emission it produces on the auroral streamers, while the other shock is characterized by the dominant orange-red halo surrounding the fireball. At later times the shock fronts are apparent only as they progress through the auroral streamers.

Three striking features are evident in these photographs beginning at 12.5 seconds: the first is the obvious kink that develops in the auroral streamers as the fireball rises rapidly away from its origin. The kink is suggestive of either trapped magnetic field lines below the fireball (i.e., field lines frozen within an ionized medium), or alternatively, a stretching of field lines below the fireball due to the upward motion of the fireball where frozen field lines are being dragged along. The second striking feature is the narrowness of the auroral column. The beta rays are confined by their Larmor radius to rather tight spirals down the geomagnetic lines. Thus, under normal circumstances one would expect an auroral streamer associated with each position of debris. The extent of debris was enormous

by 18.5 seconds (Figure 6.18), yet the beta rays remained confined to a fairly narrow column. Such a constraint could be explained if field lines were trapped in the plasma formed by the deposition of X-ray energy to form the initial fireball. The expansion of the ionized hot air of the fireball would then have created a form of magnetic bubble. The bubble would have had two narrow openings, or mirrors, through which beta particles could have escaped, the openings being at opposite ends of the bubble, where the geomagnetic field lines return to their positions of parallelism with respect to each other.

The third striking feature which this sequence of photographs portrays is the green glow which formed at some distance below the fireball. Due to insufficient exposure, it was first apparent in this record at 63 seconds. It was recorded much earlier on a more sensitive black-and-white film. It has been suggested that the green glow is air excitation caused by the passage of a shock front. Results to be presented in Section 6.4.4 indicate the cause is more likely due to photo-excitation. Careful measurements have determined that the green glow was formed well outside the vicinity of the fireball and that the fireball never extended down to the 75-kilometer altitude where the glow formed. The yellow-green color is probably due to the forbidden auroral oxygen line $\lambda 5577$ [OI].

Six late-time photographs taken by a Cloud camera on Johnston Island are shown in Figures 6.20 through 6.22. The fireball, if it may still be called a fireball at these late times, showed strong evidence of surface magnetic phenomena in the time period from 40 to 70 seconds. The periphery of the fireball during that time period is feathered with a multitude of streamers oriented in the north-south direction. Their appearance suggests that the geomagnetic field originally excluded from within the magnetic bubble is starting to leak back in. By 88.5 seconds (Figure 6.22) the magnetic bubble had almost collapsed. The caustic curves within the fireball are an illusion seen from Johnston Island, resulting from the midriff bulge of the fireball.

The final sequence of pictures presented on King Fish were taken from Mauna Loa by a Leica camera, Figures 6.23 through 6.25, first with 10-second exposures, changed at late times to 30-second exposures. At zero time (Frame 0), only a glow on the horizon was apparent. A half minute later the shock front appeared over the horizon exciting the red forbidden auroral line λ6300 Å of atomic oxygen, [OI]. The upper limb of the fireball appeared over the horizon at 40 seconds as seen in Frame 1. The change from the fireball phase to the auroral phase transpires after 75 seconds. Debris motion is seen to progress along the geomagnetic field lines at later times.

6.4 RESULTS

6.4.1 Geometric Measurements. The early-time history of King Fish to 100 microseconds exhibited such unusual features that it is not possible to present the customary fireball radius vs. time history for this period. It will be described instead as a separate topic in Section 6.4.3.

The fireball time history after 100 microseconds is shown in Figures 6.26 and 6.27. Because of the marked fireball asymmetry, the horizontal and vertical dimensions are shown independently, Figure 6.26 gives the horizontal radius and Figure 6.27 the vertical radius. The vertical radius shown pertains to the upper half of the fireball.

A shock halo was formed external to the King Fish fireball prior to 2 milliseconds, and another was formed at 0.35 second. Both are shown in the horizontal fireball radius plot (Figure 6.26). For times up to 30 milliseconds, there was a strong brightness profile internal to the fireball, the vertical dimension of which is indicated in Figure 6.27. This profile may be seen in Figures 6.8 through Figure 6.10 and is attributed to a temperature gradient in the heated air comprising the fireball.

Fireball dimensions after 10 seconds are shown in Figure 6.28. In this figure the horizontal and vertical diameters of the fireball

are plotted as well as the horizontal and vertical diameters of the shock halo.

The altitude of the top and bottom of the fireball, as well as the altitude of the upward-moving shock front, are given in Figures 6.29 and 6.30. Figure 6.29 is an expanded version of the early time portion of Figure 6.30. This was done in order to show the rapid change in rise rate during the first 30 seconds. The extent and motion of the bomb debris during these late-time periods has not been indicated due to the difficulty in portraying such an irregular cloud of material by a simple pair of lines. The reader may crudely determine the debris position and motion by using Figure 6.29 to scale appropriate photographs of the fireball. The top of the King Fish fireball is seen to have an initial rise rate of 6.8 km/second. A line drawn midway between the top and bottom of the fireball would indicate a rise rate of approximately 4 km/second for the vertical center of the fireball. The speed of the upward-going shock front is 7.5 km/second at early times.

The angular dimensions of the King Fish fireball as seen from Johnston Island are shown in Figure 6.31. The fireball attained such a great height that at 45 seconds it appeared to shrink in size. Dimensions given in Figures 6.26 through 6.28 are not

influenced by the angular behavior, since they have been corrected for the change in altitude of the fireball.

6.4.2 Shock Waves. King Fish produced a remarkable demonstration of the formation of an air shock by the hydrodynamic motion of the fireball itself. As early as 1.5 milliseconds (see Figure 6.10) a shock-excited region of air surrounded the fireball. In fact, by 1.5 milliseconds the shock had clearly separated from the fireball, indicating that its formation had taken place earlier in time. The time history of this and other shock fronts observed on King Fish are shown in Figures 6.32 and 6.33. Figure 6.32 gives the radial dimensions of the shock fronts as measured in the horizontal direction; similarly, the vertical measurements are given by Figure 6.33. The air shock is labelled Shock No. 1.

Four distinct shock fronts were observed in the horizontal direction. One shock (No. 4) was too faint to be recorded in the vertical direction. Shock No. 2 was inadvertently omitted from Figure 6.33. Its vertical behavior was somewhat similar to its horizontal counterpart in Figure 6.32. When first observed in the horizontal direction, Shock No. 1 was traveling at the phenomenal rate of 330 km/second. By 0.35 second its speed had slowed to

2 km/second. When Shock No. 2 broke through the fireball surface, Shock No. 1 received an impulse of unknown origin which increased its speed to 4.7 km/second. After 1.5 seconds Shock No. 1 appears to be no longer capable of exciting air to luminescence. The shock continues to expand outward unseen, except for the excitation it produces in the auroral column (see Figure 6.17), leaving behind a red halo of constant radius. The halo boundary remains stationary for only a brief period before Shock No. 2 passes through it and continues the growth of the halo.

The rate of growth of the fireball at early times was equally as remarkable as the speed of Shock No. 1.

This expansion rate exceeded that of the bomb debris which is also shown in Figures 6.32 and 6.33 for the time period up to 0.07 second. The lines indicating the growth of bomb debris represent the motion of the central core. Jets of debris shot out ahead of the bulk of debris (see Figure 6.10) also at phenomenal speeds. The position of the farthermost jet is indicated in Figure 6.33 for comparison with the position of the core of debris.

The onset of debris jetting occurred prior to 1 millisecond as recorded by the Rapatronic photograph shown in Figure 6.34.

The bulk of the debris was contained in what appear to be two overlapping toroids slightly greater than 1 kilometer in diameter. At the time of this photograph the average expansion velocity of the debris toroids was 0.52 meter /microsecond. Comets of debris can be seen at a distance of 0.9 kilometer from the center of the explosion. Their velocity was then 0.93 meter/microsecond. These comets undoubtedly become the spikes which are seen at later times.

Because of the short exposure time, 5 microseconds, all that recorded was that portion of the fireball inside the steep temperature gradient. The radial position of the temperature gradient as a function of time is indicated in Figures 6.32 and 6.33.

Although the debris was observed at all times throughout the history of King Fish,no evidence of the debris shock was observed internal to the fireball. Shock No. 2 has all the characteristics of the debris shock,since one would expect the debris shock to be quite strong and capable of exciting the air external to the fireball. Other than the air shock (No. 1) no other observed shock exhibited this capability. Shocks No. 3 and No. 4 are reflected shocks related to either the parent air or debris shocks, or possibly the nuclear shock described in Reference 22.

6.4.3 X-Ray Phenomenon. Records obtained during the first 5 microseconds of King Fish show a phenomenon never before observed on a nuclear detonation. The KFC-600 records taken from Johnston Island, Figure 6.6, show a series of rings expanding with the velocity of light, and obviously associated with the deposition of the X-ray yield of the weapon. Frame 0 of the record was taken within the first few tenths of a microsecond and shows no ring structure. All rings plus the bomb debris are contained within a small sphere at that time. Frames 1, 2, and 3 show three rings, the outermost of which rapidly diminishes in brightness and diffuses in width. In the last two frames, 4 and 5, only two rings remain. At some time between 5 and 20 microseconds (see Figure 6.7), nearly all evidence of the ring structure disappears, and only a glowing sphere of heated air remains. A faint background of light extending well beyond the rings is evident in the original records during the 1- to 5-microsecond time period. This background illumination is readily apparent in the reproduction of Frame 0, at 3 microseconds, in Figure 6.7. The background illumination is believed to have been created at a lower altitude than the ring phenomenon which occurred at the burst altitude.

Figures 6.35 through 6.40 are radiance profiles of the ring phenomenon made with a scanning microphotometer. The

camera resolution at the burst point is 25 meters. The radiance contour of the earliest frame, Figure 6.35, shows a width considerably larger than the camera resolution. Half-peak radiance values are assumed to represent the pulse width, since camera flare and image spread in the emulsion tend to broaden the width of a small image. Assuming this, and using the velocity of light as the growth rate, it can easily be determined that the first record was actually taken at +0.2 microsecond rather than at +0.1 microsecond as indicated. The radial dimensions of the rings as shown in the figures are based on the assumption that they occurred precisely at the burst altitude. The segment of the X-ray shell that was actually recorded may have been at a slightly lower altitude. However, the error in radial measurements caused by the altitude difference should be negligible.

Peak radiance values of the rings at 1.1 microsecond, Figure 6.36, show that Ring 1 was brighter than Ring 2 and Ring 2 brighter than Ring 3 at that time. By 2.1 microseconds (Figure 6.37) Ring 1 had decreased considerably in brightness, while Rings 2 and 3 showed slight increases. Ring 2 was then the dominant peak.

At 1.1 microseconds the half-peak width of Ring 1 is estimated to be 250 meters and the half-peak width of Ring 2 to be

100 meters. Corresponding time widths are 25 and 10 shakes respectively (1 shake = 10^{-8} second). The structure of Ring 3 at 1.1 microseconds is too weak to make any determination of its width.

By 3.1 microseconds (Figure 6.38), Ring 3 had become the dominant peak and remained dominant until the ring phenomenon disappeared. From 3.1 microseconds on (Figures 6.38 through 6.40), Ring 1 was not discernible on the microphotometer traces, but was faintly distinguishable on the original records.

Figure 6.41 is a plot of the angle subtended by the three X-ray rings as a function of time. The angle θ, in radians, was measured by taking the ratio of ring radius on the film to the camera focal length. The velocity of light is shown for comparison purposes. It should be stressed that the measured ring velocities are only apparent velocities and can exceed the velocity of light. An apparent velocity greater than the velocity of light means, in this case, that the light emitted by the X-ray energy deposition and subsequently observed by the camera was not produced along a line perpendicular to the line of sight but rather along a line slightly inclined toward the line of sight. From the data contained in Figure 6.41 the altitude of the rings can be established.

To understand how the altitude can be determined, the geometry of the situation is shown in Figure 6.42. This figure attempts to portray the conditions which existed 5 microseconds after the detonation. An ellipse (the so-called equi-time ellipse), has been drawn with the camera on Johnston Island at one focal point, and the burst point as the other focal point. An ellipse has the property that the sum of two radii from each focus to a common point anywhere on the surface is a constant. In the ellipse shown in Figure 6.42, the time difference for light to travel a straight path between foci and a path say $R_1 + R_2$ is 5 microseconds. The path length $R_1' + R_2'$ is similarly only 5 microseconds longer than the straight path between foci.

When X-rays leave the region along path R_1 and produce light by air fluorescence or other physical processes, then that fraction of the light which follows path R_2 will reach the camera simultaneously with light that is produced by X-rays which traveled down path R_1' and created light which subsequently followed path R_2'. Although there are an infinite number of X-ray and light-path combinations which would yield signals that arrive at the camera simultaneously, only those which subtended the measured angle θ could have resulted in the rings. As a

consequence, the location of the rings in space may be determined by finding where a line drawn from the camera at angle θ intersects the equi-time ellipse for the particular record under study. In Figure 6.42 the line labeled R_2 subtends the proper angle at 5 microseconds. The extended area which was illuminated outside the rings can now be explained. It could only have originated at a lower altitude (in the 70-to 80-km region) and was caused by the harder component of X-rays penetrating to large distances below the burst.

Although only a geometric solution to the problem of ring location has been presented for the sake of clarity, an analytic solution was also obtained. The results of the latter solution confirm the fact that the ring phenomenon took place very close to the burst altitude.

The problem of determining the true time-separation of the X-ray shells when they were radiated is more complex. Figure 6.41 demonstrates that the spatial distance between the rings increased as time progressed. Thus the true time-separation in bomb time could not be deduced on the basis of the spatial separation measured from any individual photograph. An extrapolation of the Figure 6.41 data to the time axis would

have a considerable error associated with it because of the uncertain curvature required of the extrapolation. An analytic solution was not possible, because rigorously, an equi-time ellipse could pertain only to a single ring at any given instant of time. For example, a 5-microsecond equi-time ellipse would have meaning only for a ring radiated precisely 5 microseconds earlier. The ellipse would have no meaning for a ring radiated 20 shakes prior, or 30 shakes later. To analytically satisfy the experimental data contained in a single photographic record, three independent equi-time ellipses would be required. The time separations between the equi-time ellipses, however, are just the true time-separations between radiation of the X-ray pulses. In effect one would need the solution to derive the solution analytically.

The true time-separation of the rings was deduced by plotting the measured time-separations as a function of the time at which the records were taken (Figure 6.43). The plot of time-separations between Rings 1 and 2 and between Rings 2 and 3 resulted in straight lines which could easily be extrapolated. The abscissa in Figure 6.43 is the time at which the data points were recorded. The ordinate is the measured time-separation

between any pair of rings as determined by dividing the spatial separation by the velocity of light. Zero time is slightly uncertain; it probably has no true physical significance in that none of the three rings were radiated precisely at that time. If this method of deducing true separation-times is correct, then Ring 2 was radiated 19 shakes after Ring 1, and Ring 3 was radiated 18 shakes after Ring 2.

The following interpretation of the three rings is suggested, based on the true time-separations that have been determined. Ring 1 was produced by energy from the primary detonation which reached the outside of the weapon just prior to detonation of the secondary. This identification is substantiated by reasoning that the case temperature would be low, resulting in a very soft X-ray pulse which would be absorbed near the burst point and would dissipate quickly, as Ring 1 was observed to do. Ring 2 is assumed to be the main X-ray energy pulse released by the weapon case after detonation of the secondary and should represent thermal X-ray radiation from a source of approximately 1-kev temperature. The third ring is assumed to result from the re-heating of the weapon surface induced by impact

A temperature increase occurs as a result of

this interaction, as has been demonstrated by the LASL HENRE code predictions. The LASL HENRE code prediction for Blue Gill, in which a similar weapon was used, predicted a 20-shake time-separation between the two temperature peaks which is in close agreement with the 18 shakes observed.

The time interval between detonation of the primary and secondary is in no way associated with the ring phenomenon.

An argument against the suggested explanation of the X-ray rings can be made on the basis of the dominance of the third ring after 3 microseconds. The second temperature maximum predicted by the HENRE code is a minor temperature maximum compared with the temperature maximum during which the bulk of the energy is released. Ring 2, which corresponds to the first temperature maximum, would contain most of the energy plus the harder X-ray components, and as a result, should have been the dominant ring at all times.

The early time spectra of King Fish (Chapter 9) indicate that the light emitted by the rings was due mainly to atomic

emissions of highly ionized air. The spectra of atomic oxygen and nitrogen from the neutral species through OV and NV were observed. The light actually measured by the KFC-600 camera was restricted almost entirely to the spectra of NI, NII, OI and OII, because these emissions dominated that portion of the spectral region to which the camera was sensitive.

Little evidence of ring structure existed in any other camera records. A KFC-600 camera aboard Aircraft 53120 took a series of six pictures (Figure 6.7) separated by 20 microseconds, the sequence commencing at 3 microseconds. In the photographs beginning at 20 microseconds a hint of a single ring is apparent, but microphotometer traces indicate that it is probably a brightness profile due to the temperature gradient within the fireball.

Five microphotometer traces made from the aircraft KFC-600 record are given in Figures 6.44 through 6.48. The camera was mispointed due to a slight error in aircraft attitude. The mispointing caused the fireball image to appear near the edge of the field of view where considerable vignetting occurs in the KFC-600 camera. Because of the vignetting, the absolute radiance values shown in the figures are subject to question, as well as the shape of the radiance profiles. Sharp drops in radiance near the boundary of the fireball are almost certainly due to strong vignetting.

6.4.4 Green Glow. Beneath the King Fish fireball a green glow appeared which remained long after the fireball had dissipated. Several suggestions have been made as to its nature and cause, but for lack of spectral data the exact processes which gave rise to the green emission are still uncertain. An excellent set of photographs of the green glow were obtained with a Beattie-Coleman camera aboard Aircraft 60376 located southeast of the burst point. Sixteen selected frames of this very long record are shown in Figures 6.49 through 6.52. It is to be hoped that the data collected from this record can be of use in furthering the understanding of the green glow.

The exposure times of the camera were automatically programmed so that progressively longer exposures were made, beginning with a 1-second exposure at zero time, and changing at predetermined intervals to 2-, 5-, and 10-second exposures.

One suggested cause of the green glow, i.e., excitation of the air beneath the fireball by the passage of a shock front, can be eliminated on the basis of these photographs. It is quite clear from the record that the green glow formed prior to the arrival of any shocks; in fact the shocks are seen to increase

the brightness of the glowing air as they pass through it. In the picture taken at 10 seconds the first shock that left the fireball (the air shock) is seen to enter the glowing region. At 14 and 18 seconds the shock is progressing through the region and at 24 seconds is about to leave it. Other shocks follow behind the first shock. The beta-ray-induced auroral column appears to pass through the green glow region without disturbing it.

Measurements place the center of the green glow region at an altitude of 70 kilometers with a thickness of approximately 10 kilometers. Although the fireball expanded downward initially, it never reached the region of the green glow. The early frames of this Beattie-Coleman record have been deliberately over-exposed in their printing to favor the green glow. As a result, the shock-induced halo around the fireball has blended with the fireball in the early pictures, giving added dimensions to the fireball which in reality do not exist. The photographic record lasts for 19 minutes, during which time the green glow diminished in brightness by two orders of magnitude.

The radiance vs. time curve for the green glow is shown in Figure 6.53. Several peaks disturb the basic shape of the curve, so that it is difficult to determine a decay rate with any degree of

certainty. The first peak, occurring between 12 and 25 seconds, was due to the passage of the air shock through the region of the glow. It is unlikely that the remaining two peaks were similarly created by shocks, because of the late times of their occurrence. The peak commencing at 60 seconds is coincident with what appears to be the release of sodium vapor in the vicinity of the glow (see Figure 6.51).

If the green glow was due to the forbidden line λ5577 Å of atomic oxygen [OI], the decay in brightness should have proceeded much faster than the average decay rate which was actually observed. The radiative lifetime for the transition giving rise to λ5577 Å is 0.78 second, hardly in agreement with the very slow decay of the green glow, even with allowances made for the shock and other apparent disturbances. A repopulation mechanism could be at work, such as excitation by fireball radiation; however, after 60 seconds the brightness of the remnants of the fireball becomes less than that of the green glow, thereby ruling out that mechanism as a source of repopulation. Ohmic heating due to currents induced by strong magnetic disturbances has also been suggested as a possible repopulation mechanism. This mechanism must also be ruled out because the geomagnetic field has returned to normal by 400 seconds. An accurate estimate has not yet been made on the total amount of visible energy released by the green glow.

6.4.5 Radiometric Measurements. The King Fish fireball was transparent after a few tenths of microsecond, allowing the brightness of the debris to be measured throughout the entire time history. In addition to the debris and fireball a number of lesser phenomena were observed, which when their radiance histories were measured, resulted in the complex radiance vs. time presentation shown in Figure 6.54.

The radiance time-history for the first five microseconds was derived from the radiance profile curves shown in Figures 6.35 through 6.40. The curve labeled "Inner Fireball Region" during this time period refers to the radiance values measured in the region between Ring 3 and the debris on the profile plots. Rings 2 and 3 and the inner-fireball-region all exhibit the same behavior; a rise to a maximum at 2 microseconds followed by a monatonic decrease thereafter. The bomb debris was not observable at 10^{-7} second, since it was masked by Ring 1; however, the trend of data points indicates a common origin for both Ring 1 and the debris. The curve for Ring 1 is broken to avoid confusion with the curves for the other rings.

The radiance of the bomb debris shows a marked decrease in the vicinity of 4 microseconds, followed by a sudden rise to a

plateau. The cause of this dip in radiance is unexplained. It is unlikely that it was caused by a systematic error in the measurements, since the curves for all other phenomena measured from the same records show no such behavior. Data points are shown on all curves for the first five microseconds of the radiance time history, in order that the reader may judge for himself the most probable radiance behavior.

A gap in the data, indicated by dotted lines, exists between 5 and 20 microseconds. The data for the time period 20 to 100 microseconds was taken from the radiance contour plots shown in Figures 6.44 through 6.48. The data in this time region shows some inconsistencies due to vignetting in the camera. A curve has been drawn indicating the best estimate of the radiance history consistent with a smooth transition to the Photo-Sonics 4C camera records beginning at 200 microseconds. From that point on, sufficient data was obtained to accurately determine the radiance behavior of all phenomena.

Beginning at 20 microseconds, the curve labeled "Inner Fireball Region" refers to the radiance inside the strong temperature gradient seen in Figures 6.7 and 6.8. The curve labeled "Outer Fireball Region" refers to the radiance midway between the

temperature profile and the fireball boundary (see for example Frames 0 and 6 of Figure 6.10).

The radiance of the bomb debris is a prominent spike during the time period 20 to 100 microseconds (see Figures 6.44 through 6.48). From 200 microseconds on, the average radiance of the debris mass was taken. The radiance of the inner and outer fireball regions blended together in the vicinity of 0.6 second, as did the fireball and average bomb debris radiance values at 3 seconds. Beginning at 1 second, a bright shock (Internal Shock 1) was followed until it disappeared. This shock is seen clearly in the photographs of Figure 6.12. Radiance values are also shown for other phenomena which are clearly identifiable in the pictorial history.

6.4.6 Brightness Temperature, Radiant Power, and Thermal Yield. For times earlier than 200 microseconds no single specification of brightness temperature for the fireball would have significance, since a strong temperature profile existed within the fireball. The fireball brightness temperature curve shown in Figures 6.55 through 6.57 begins at 200 microseconds when a single value can be used to give a rough estimate of the brightness temperature. The fireball brightness temperature shown in these three figures refers to the outer fireball region. A similar problem

did not exist for the debris whose brightness temperature is given from 10^{-7} sec to 70 seconds.

In deriving the brightness temperature curves the same assumptions were used that were made on Blue Gill Triple Prime (Section 5.4.4). The King Fish fireball does not have a high brightness temperature even at early times, because it was quite transparent and therefore had a low emissivity. Or, more correctly, it had a low emissivity and was therefore quite transparent.

On Blue Gill Triple Prime and Tight Rope the assumptions used for calculating the thermal and visible power radiated by the detonation are fairly valid because the bulk of the energy is radiated while the fireball is opaque. On King Fish these same assumptions are inappropriate for two reasons: first, because of the transparency, which allowed the debris to radiate large quantities of energy to the outside world; and second, the temperature gradient within the fireball which invalidates the use of a single temperature association with a sphere having the radius of the fireball.

To accurately determine the thermal or visible power emitted by King Fish would have required the use of fast-responding thermal energy detectors in the case of the thermal power

measurement and photoelectric detectors for the visible power measurement. However, with the information available from the photographic measurements, a lower limit could be found for both the thermal and visible powers. A mean fireball radius was chosen from the horizontal and vertical fireball radius vs time curves (Figures 6.26 and 6.27). The contribution from the debris was neglected (a poor assumption), and the temperature of the outer fireball region was assumed to apply for the whole fireball. The thermal, visible, and photographic power vs. time curves which resulted are shown in Figure 6.58.

The visible and thermal power curves were integrated to give lower limits for the total thermal yield and the total visible yield of King Fish. The contribution from times earlier than 200 microseconds was neglected The contribution from this time period would be negligible, even if the true thermal and visible power rates were known.

6.4.7 Magnetic Phenomena. The sequence of pictures containing an excellent time history of the green glow (Figures 6.49 through 6.52) also contained the best recordings of the King Fish auroral column obtained by Project 8A.2. It is only in this sequence of pictures that on the upper half of the fireball a faint continuation of the auroral column is seen. A large change in ambient air density between the bottom and top of the fireball is undoubtedly responsible for the great difference in brightness between the upper and lower auroral columns. One obvious conclusion to be drawn from the narrow size of the auroral column is that beta rays from fission fragments are trapped by a magnetic bottle within the fireball and can only escape through apertures in the magnetic mirrors at the top and bottom of the fireball. Upon escaping from the fireball the beta rays are constrained to move in a column oriented in the direction of the geomagnetic field, the diameter of the column being approximately equal to the apertures in the magnetic mirrors.

The marked bending of the auroral column that occurred once the fireball began to rise indicates that other large scale magnetic phenomena are associated with the fireball. The bending of the column below the fireball raises numerous questions

about the shape of the auroral column above the fireball. The size, shape, and position of the upper auroral column holds the key to the distribution of trapped magnetic field lines within the fireball. From a careful analysis of the original film records of the pictures shown in Figures 6.49 and 6.50 the geometric relationship between the upper and lower auroral columns has been established. Two frames were selected to portray this relationship, one was selected at as early a time as possible (Frame 4 at 4 seconds), when the fireball had not moved significantly. In that frame the upper and lower auroral columns were found to be parallel and coaxial. The other frame (Frame 14 at 18 seconds) was chosen such that the fireball had moved upward appreciably, but the shape and position of the upper auroral column could still be determined. Figures 6.59 and 6.60 are pictorial representations of the fireball and auroral columns at 4 and 18 seconds, respectively. Figure 6.61 is an overlay of Figures 6.59 and 6.60 in which the indicated positions of the fireball and auroral column bear a true relationship to their relative positions on the original records.

A very interesting fact is clearly established by the overlay drawings. The position of the auroral column above the fireball

remains fixed in space. The position of the auroral column below the bend is seen to have shifted only a very small amount. Photographs taken at later times (Figure 6.51) show a definite northerly drift to the lower auroral column, but this may be due entirely to aircraft motion with respect to the fireball and auroral column.

It is interesting to speculate on the position of the upper auroral column at times much later than 18 seconds, for example, when the fireball has risen from its 18-second position in Figure 6.61 to a distance equivalent to its full diameter. It is suggested that at some time during such a transition the upper auroral column would develop a bend and finally end up protruding from the bottom of the fireball.

At 18 seconds the distribution of magnetic field lines within the fireball must indeed be a complex geometric pattern. The ring currents flowing on the surface of the fireball must be equally as complex.

As an aid to anyone attempting to form a qualitative, or quantitative, description of the magnetic behavior of King Fish, a Varian magnetometer record of the change in the geomagnetic field at Johnston Island is presented in Figure 6.62. This record was obtained by an EG&G electromagnetic pulse (EMP) monitoring station on Johnston Island (Reference 24). The behavior of the

geomagnetic field during the time period up to 500 seconds after detonation is measured in units of $\Delta\gamma$, where $\gamma = 10^{-5}$ gauss. Undoubtedly, there are direct correlations between the large changes in amplitude and such things as the rise of the fireball and the loss of ionic conductivity within the fireball which leads to the restoration of the original geomagnetic field distribution. Time has permitted only brief speculations as to the correlation of the observed phenomena and the measured changes in field strength.

TABLE 6.1 INSTRUMENT POD POSITIONS IN BRAVO COORDINATE SYSTEM, KING FISH

Pod	ΔX	ΔY	ΔZ	Slant Range	Slant Range
	feet	feet	feet	feet	kilometers
K-1	-82	+281	-8,143	8,149	2.484
K-2	+1,003	+1,897	+12,391	12,576	3.833
K-3	+374	+289	-9,628	9,640	2.938

TABLE 6.2 SUMMARY OF KING FISH CAMERA PARAMETERS, AIRCRAFT 53120

INSTRUMENT AND STATION POSITION		FILM TYPE	FILM NUMBER	AIMING ANGLES IN DEGREES ELEV	AZIMUTH	FILTERS ND	COLOR	FOCAL LENGTH MM	LENS F/N	FRAMES PER SECOND	SHUTTER SECTOR, DEGREES	EXPOSURE TIME	MARKER RATE CPS
MAURER	W1	DXN	96122	30	0	-	-	80	11	5.5	-	0.5MSEC	-
MAURER	W2	EDER	96121	27	0	-	-	38	11	5.5	-	1.0MSEC	-
PHOTO-SONICS 10B	W5	PX	96127	30	0	-	-	180	5.6	360	1	7.7MUS	200
KFC-600	W6	XR	96104	30	0	-	WR12	301	9.5	50000	-	1 MUS	-
RAPATRONIC	W7	XR	96103	30	0	-	-	490	22.	*(A)	-	5MUSEC	-
TRAID	W8	PX	63117	45	0	-	-	25	8.0	48	7	0.4MSEC	50
TRAID	W9	KDII	96118	45	0	-	-	25	3.5	48	7	0.4MSEC	50
CLOUD	W10	DXN	96109	45	0	-	-	105	3.7	0.2	-	0.2 SEC	CLOCK
FAIRCHILD HS-100	W11B	KD I	96123	30	0	1.0	-	13	11.	1000	-	0.2MSEC	50
GSAP N-6	W11A	KDII	96124	45	0	-	-	9.5	11.	64	133	5.8MSEC	-
PHOTO-SONICS 4C	W12	XR	96125	30	0	-	-	80	5.6	2500	9	10MUS	200
CLOUD	W13	EDER	96110	45	0	-	-	105	3.7	0.5	-	0.04 SEC	CLOCK
ROBOT	W15	RXP	96111	50	0	-	5577A	45	2.8	*(B)	-	250MSEC	-
ROBOT	W16	EDER	96112	50	0	-	-	45	2.8	*(B)	-	250MSEC	-
ROBOT	W17	RXP	96116	50	0	-	6300A	45	2.8	*(B)	-	250MSEC	-
TRAID	W18	EDER	96119	55	0	-	-	25	2.3	16	160	28MSEC	10
TRAID	W19	XR	96120	55	0	-	-	25	8	16	160	28MSEC	10
ROBOT	W21	EDER	96114	75	0	-	-	45	2.8	*(B)	-	200MSEC	10
ROBOT	W22	RXP	96115	75	0	-	-	45	2.8	*(B)	-	250MSEC	-
ROBOT	W23	RXP	96116	75	0	-	-	45	2.8	*(B)	-	250MSEC	-
PHOTO PANEL CAMERA	PANEL	PX	96131	-	-	-	-	25	16	1	160	30MSEC	CLOCK
PHOTO PANEL CAMERA	PANEL	PX	96132	-	-	-	-	25	16	0.2	160	30MSEC	CLOCK

*(A) SINGLE EXPOSURE AT 510 MICROSECONDS.
*(B) 1 FR/SEC UNTIL +60 SEC, THEN 0.5 FR/SEC TO END.
N.B. MUSEC = MUS = MICROSECOND

TABLE 6.3 SUMMARY OF KING FISH CAMERA PARAMETERS, AIRCRAFT 60376

INSTRUMENT AND STATION POSITION		FILM TYPE	FILM NUMBER	AIMING ANGLES IN DEGREES ELEV	AZIMUTH	FILTERS ND	COLOR	FOCAL LENGTH MM	LENS F/N	FRAMES PER SECOND	SHUTTER SECTOR, DEGREES	EXPOSURE TIME	MARKER RATE CPS
BEATTIE-COLEMAN	W1	EDER	96221	30	0	-	-	105	3.5	*(A)	-	*(B)	-
BEATTIE-COLEMAN	W2	PX	96222	30	0	-	-	10	3.5	*(A)	-	*(B)	-
RAPATRONIC	W3	XR	96205	30	0	1.0	WR12	490	22	*(F)	-	5MUSEC	-
PHOTO-SONICS 10B	W5	EDER	96227	30	0	-	-	135	16	360	1	0.01MSEC	200
RAPATRONIC	W6	XR	96204	30	0	1.0	WR12	490	22	*(G)	-	5MUSEC	-
RAPATRONIC	W7	XR	96203	30	0	1.0	WR12	490	22	*(H)	-	5MUSEC	-
FLIGHT RESEARCH-CINE	W8	EDER	96219	30	0	-	-	35	22	20	130	20MSEC	10
FLIGHT RESEARCH-CINE	W9	XR	96218	30	0	-	-	35	8	20	130	20MSEC	10
RAPATRONIC	W10	XR	96223	30	0	-	WR12	490	22	*(I)	-	5MUSEC	-
BEATTIE-COLEMAN	W11	EDER	96209	45	AFT 10	1.0	-	105	16	*(C)	-	*(D)	-
PHOTO-SONICS 4C	W12	PX	96225	30	0	1.0	-	108	16	2500	9	10MUSEC	200
BEATTIE-COLEMAN	W13	DXN	96210	45	AFT 10	-	-	105	3.5	*(C)	-	*(D)	-
PHOTO-SONICS 4C	W14	EDER	96229	30	0	-	-	58	9	2500	9	10MUSEC	200
FLIGHT RESEARCH-CINE	W15	KDII	96217	50	0	-	-	35	2.8	20	130	20MSEC	200
FLIGHT RESEARCH-CINE	W16	PX	96220	50	0	3.0	-	35	22	20	130	20MSEC	10
FLIGHT RESEARCH-PULSED	W17	EDER	96211	50	0	-	-	35	2.3	*(E)	130	1 SEC	-
FLIGHT RESEARCH-PULSED	W18	RXP	96212	50	0	-	-	35	2.3	*(E)	130	1 SEC	-
FLIGHT RESEARCH-PULSED	W19	EDER	96213	75	0	-	-	35	2.3	*(E)	130	1 SEC	-
FLIGHT RESEARCH-PULSED	W20	RXP	96214	75	0	-	5577A	35	2.3	*(E)	130	1 SEC	-
FLIGHT RESEARCH-PULSED	W21	RXP	96215	75	0	-	6300A	35	2.3	*(E)	130	1 SEC	-
PHOTO PANEL CAMERA	PANEL	PX	96231	-	-	10.	-	25	5.6	1	160	30MSEC	CLOCK
PHOTO PANEL CAMERA	PANEL	PX	96232	-	-	1.0	-	25	5.6	0.2	160	30MSEC	CLOCK

*(A) 1 FR/SEC, 0.5 FR/SEC, 0.2 FR/SEC, 0.1 FR/SEC UP TO + 10 SEC, +60 SEC, +180SEC
1800 SEC, RESPECTIVELY.
*(B) 0.5 SEC, 1.5 SEC, 4.5 SEC, 9.5 SEC, UP TO +10 SEC, +60 SEC, +180 SEC, +1800
SEC, RESPECTIVELY.
*(C) 1 FR/SEC, 0.2 FR/SEC, 0.1 FR/SEC UP TO +10 SEC, +180 SEC, +1800 SEC,
RESPECTIVELY.
*(D) 0.5 SEC, 4.5 SEC, 9.5 SEC, UP TO +10 SEC, +180 SEC, +1800 SEC,
RESPECTIVELY.
*(E) 1 FR/SEC UP TO +10 SEC, 0.33 FR/SEC UP TO +30 SEC, THEN 0.1 FR/SEC TO END.
*(F) SINGLE EXPOSURE AT 14 MUSEC.
*(G) SINGLE EXPOSURE AT 52.4 MUSEC.
*(H) SINGLE EXPOSURE AT 103.4 MUSEC.
*(I) SINGLE EXPOSURE AT 256.2 MUSEC.
N.B. MUSEC = MUS = MICROSECOND

TABLE 6.4 SUMMARY OF KING FISH CAMERA PARAMETERS, JOHNSTON ISLAND

INSTRUMENT AND STATION POSITION		FILM TYPE	FILM NUMBER	AIMING ANGLES (IN DEGREES) ELEV	AZIMUTH	FILTERS ND	COLOR	FOCAL LENGTH MM	LENS F/N	FRAMES PER SECOND	SHUTTER SECTOR, DEGREES	EXPOSURE TIME	MARKER RATE CPS
KFC-600	A1	XR	96304	53	191.95	-	WR12	301	9	106	-	0.1MUSEC	-
PHOTO-SONICS 4C	A2	EDER	96324	53	191.95	1.0	-	80	16	2500	9	10MUSEC	200
PHOTO-SONICS 4C	A3	PX	96323	53	191.95	-	-	108	16	2500	9	10MUSEC	200
PHOTO-SONICS 108	A4	PX	96325	53	191.95	-	-	180	16	360	1	7.7MUSEC	50
RAPATRONIC	A5	XR	96303	53	191.95	-	WR12	490	20	*(A)	-	5MUSEC	-
MAURER	A7	XR	96319	53	192	-	-	150	4	5.5	-	0.5MSEC	-
MAURER	A8	EDER	96320	53	192	-	-	150	22	5.5	-	0.5MSEC	-
TRAID	A9	PX	96317	55	192	-	-	35	11	48	7	0.4MSEC	10
MITCHELL	A10	PX	96326	55	192	1.0	-	35	11	100	15	0.4MSEC	50
FAIRCHILD HS-100	A12	KD I	96321	53	192	-	-	13	16	650	-	0.3MSEC	50
GSAP	A13	EDER	96322	53	192	-	-	9.5	16	16	133	23MSEC	-
KC-18	A14	TXA	96332	79	192	-	-	152	6.3	*(B)	-	*(C)	-
CLOUD	C1	EDER	96309	70	192	-	-	105	3.7	*(B)	-	*(C)	CLOCK
CLOUD	C2	EDER	96310	58	192	-	-	105	3.7	*(B)	-	*(C)	CLOCK
TRAID	C3	XR	96318	63	192	1.0	-	25	16	16	160	0.028SEC	10
MITCHELL	C4	KD11	96327	53	192	ND1	-	35	16	100	15	4.0MSEC	50
BELL AND HOWELL	C5	XR	96329	58	192	-	-	25	2.0	12	160	0.037SEC	10
MITCHELL LS	C6	EDER	96328	63	192	-	-	18.5	*(D)	2.5	170	0.2SEC	10
ROBOT	C7	RXP	96311	63	192	-	4278A	45	2.8	*(B)	-	*(C)	-
ROBOT	C8	EDER	96312	78	192	-	-	45	2.8	*(B)	-	*(C)	-
ROBOT	C9	EDER	96313	63	192	-	-	45	2.8	*(B)	-	*(C)	-
ROBOT	C11	RXP	96314	63	192	-	6300A	45	2.8	*(B)	-	*(C)	-
ROBOT	C12	RXP	96315	63	192	-	3914A	45	2.8	*(B)	-	*(C)	-
DYNAFAX	D1	MF	96335	53	191.95	-	-	813	9.0	25000	-	5MUSEC	2000
DYNAFAX	D2	HSIR	96336	53	191.95	1.0	-	76	2.8	25000	-	5MUSEC	2000
ROBOT OUTSIDE		EDER											

*(A) SINGLE EXPOSURE AT 963 MICROSECONDS.
*(B) 0.33 FR/SEC FROM -30 SEC TO +120 SEC, THEN 0.033 FR/SEC TO END.
*(C) 1-SEC EXPOSURE FROM -30 SEC TO +120 SEC, THEN 30-SEC EXPOSURE TO END.
*(D) F/16 FROM -30 SEC TO +60 SEC, THEN F/2.2 TO END.
N.B. MUSEC = MUS = MICROSECOND

Page 319 deleted.

TABLE 6.7 SUMMARY OF KING FISH FILM RECORDS, AIRCRAFT 53120

FILM NUMBER	FILM TYPE	CAMERA	RESULTS
96103	XR	RAPATRONIC	GOOD RECORD OF X-RAY FIREBALL.
96104	XR	KFC-600	EXCELLENT SERIES OF PICTURES.
96109	DXN	CLOUD	BEAUTIFUL SERIES OF TWENTY-EIGHT FRAMES SHOWING RAPID FIREBALL RISE AND AURORA.
96110	EDER	CLOUD	NO RECORD.
96111	RXP	ROBOT	ABOUT 10 FEET OF GOOD RECORD SHOWING DEBRIS EXPANSION AND SHOCKS. INITIAL FRAMES OVER-EXPOSED.
96112	EDER	ROBOT	BEAUTIFUL RECORD SHOWING RAPID RISE AND GROWTH OF BURST, AS WELL AS RED SHOCK AND AURORA WHOSE ORIGIN REMAINS FIXED.
96113	RXP	ROBOT	ABOUT 10 FEET OF GOOD RECORD SHOWING SHOCKS, SOME AURORA, AND DEBRIS EXPANSION.
96114	EDER	ROBOT	BURST OCCURS INITIALLY OUT OF FIELD OF VIEW BUT LATER GROWS IN. RED SHOCK OBSERVED.
96115	RXP	ROBOT	BURST INITIALLY OUT OF THE FRAME, THEN RISES TO FILL IT. SEVERAL FEET OF GOOD RECORD.
96116	RXP	ROBOT	BURST INITIALLY OUT OF THE FRAME, THEN RISES TO FILL IT. THERE ARE SEVERAL FEET OF GOOD RECORD.
96117	PX	TRAID	25 FEET OF RECORD SHOWING FIREBALL, AURORA, AND REMAINING DEBRIS.
96118	KDII	TRAID	13 FEET OF RECORD SHOWING OUTER RED SHELL, AURORA AND BLUISH-WHITE DEBRIS REMAINING AFTER FIREBALL DISSIPATION.
96119	EDER	TRAID	BURST INITIALLY OUTSIDE FIELD OF VIEW. BURST AND AURORA RISE INTO VIEW, AURORA REMAINS FIXED WHILE FIREBALL CONTINUES TO RISE.
96120	XR	TRAID	SEVERAL FEET OF GOOD RECORD SHOWING DEBRIS AND AUROPA. INITIALLY OUT OF FRAME THEN RISING TO FILL IT.
96121	EDER	MAURER	ABOUT 3 FEET OF RECORD SHOWING FIREBALL AND DEBRIS.
96122	DXN	MAURER	GOOD RECORD OF ASYMMETRIES IN FIREBALL SHAPE.
96123	KD I	FAIRCHILD HS-100	GOOD RECORD OF INITIAL FIREBALL.
96124	KDII	GSAP	GOOD FIREBALL RECORD.
96125	XR	PS-4C	BEAUTIFUL RECORD OF FIREBALL AND DEBRIS. NO AURORA.
96127	PX	PS-10B	FIREBALL ASYMMETRIES AND DEBRIS JETTING OBSERVED.

TABLE 6.8 SUMMARY OF KING FISH FILM RECORDS, AIRCRAFT 60376

FILM NUMBER	FILM TYPE	CAMERA	RESULTS
96203	XR	RAPATRONIC	GOOD RECORD OF X-RAY FIREBALL.
96204	XR	RAPATRONIC	GOOD RECORD OF X-RAY FIREBALL.
96205	XR	RAPATRONIC	GOOD RECORD OF X-RAY FIREBALL.
96209	EDER	BC	ABOUT 7 GOOD PICTURES IN THE CORNER OF THE FRAME. THESE SHOW THE FIREBALL AND DEBRIS.
96210	DXN	BC	ABOUT 30 PICTURES OF X-RAY FIREBALL AND RISING DEBRIS CLOUD NEAR BOTTOM FRAME EDGE.
96211	EDER	FR PULSED	FIREBALL GROWS INTO FRAME FROM BELOW.
96212	RXP	FR PULSED	SHORT BUT FAIR RECORD. INITIALLY OUT OF FRAME BUT RISES TO FILL THE FIELD OF VIEW.
96213	EDER	FR PULSED	NO RECORD.
96214	RXP	FR PULSED	NO RECORD.
96215	RXP	FR PULSED	NO RECORD.
96217	KDII	FR CINE	OVER 35 FEET OF RECORD. BURST IS INITIALLY BELOW FIELD OF VIEW BUT LATER GROWS IN. DEBRIS APPEARS BLUE.
96218	XR	FR CINE	SEVERAL FEET OF EXCELLENT RECORD SHOWING AURORA AND DEBRIS.
96219	EDER	FR CINE	SEVERAL FEET OF RECORD SHOWING X-RAY FIREBALL, EXPANDING DEBRIS, AND RED SHOCK.
96220	PX	FR CINE	NO RECORD.
96221	EDER	BC	ABOUT 30 GOOD PICTURES STARTING IN THE CENTER OF THE FRAME THEN RISING OUT OF IT. GOOD AURORA PICTURES.
96222	PX	BC	EXCELLENT SERIES OF PICTURES SHOWING FIREBALL RISE AND AURORAL DISTORTION.
96223	XR	RAPATRONIC	GOOD RECORD OF X-RAY FIREBALL AND DEBRIS.
96225	PX	PS-4C	79 FEET OF RECORD SHOWING ASYMMETRICAL SHAPE OF X-RAY FIREBALL AS WELL AS DEBRIS JETTING.
96226	EDER	PS-4C	OVER 350 FEET OF GOOD RECORD. PERSISTENT CENTRAL DEBRIS CORE.
96227	EDER	PS-10B	SEVERAL FEET OF GOOD RECORD SHOWING THE INITIAL FIREBALL WHICH FADES TO DEBRIS AND THEN TO A CENTRAL SPOT.

TABLE 6.9 SUMMARY OF KING FISH FILM RECORDS, JOHNSTON ISLAND

FILM NUMBER	FILM TYPE	CAMERA	RESULTS
96303	XR	RAPATRONIC	GOOD RECORD OF X-RAY FIREBALL AND DEBRIS.
96304	XR	KFC-600	EXCELLENT SERIES OF PICTURES SHOWING X-RAY DEPOSITION AND DEBRIS.
96309	EDER	CLOUD	ABOUT 3 FEET OF GOOD RECORD SHOWING THE FIREBALL, AUROPA, AND THEN DEBRIS.
96310	EDER	CLOUD	ABOUT 1 FOOT OF RECORD SHOWING THE FIREBALL, AURORA, AND THEN DEBRIS.
96311	RXP	ROBOT	SIMILAR TO COLOR ROBOT RECORDS. STRONG AURORA. FIREBALL RISE AND GROWTH WELL OBSERVED. 4278A FILTER.
96312	EDER	ROBOT	SEQUENCE SIMILAR TO 96313.
96313	EDER	ROBOT	SEVERAL GOOD PICTURES SHOWING X-RAY FIREBALL, AURORA, AND DEBRIS.
96314	RXP	ROBOT	SEVERAL GOOD PICTURES SHOWING X-RAY FIREBALL, AURORA, AND DEBRIS.
96315	RXP	ROBOT	FIVE FRAMES, ONLY SHOW INITIAL AURORA. 3914A FILTER.
96317	PX	TRAID	19 FEET OF RECORD SIMILAR TO 96326.
96318	XR	TRAID	SEVERAL FEET OF EXCELLENT RECORD SHOWING FIREBALL AND DEBRIS.
96319	XR	MAURER	FEW FEET OF GOOD RECORD SHOWING FIREBALL, SHOCK, AND EXPANDING DEBRIS.
96320	EDER	MAURER	FOURTEEN FRAMES SHOWING THE INITIAL FIREBALL, EXPANDING DEBRIS, AND A SHOCK.
96321	KD I	FAIRCHILD HS-100	SEVERAL FEET OF EXCELLENT RECORD SHOWING THE INITIAL DETONATION, FADING FIREBALL, EXPANDING DEBRIS, AND A FINAL REMAINING CENTRAL CORE.
96322	EDER	GSAP	A FEW FEET OF BEAUTIFUL RECORD CENTERED ON THE FRAME SHOWING THE FIREBALL AND DEBRIS.
96323	PX	PS-4C	325 FEET OF RECORD SHOWING FIREBALL EXPANSION AND DEBRIS JETTING.
96324	EDER	PS-4C	43 FEET OF RECORD. BURST CENTERED IN FRAME.
96325	PX	PS-10B	SEVERAL FEET OF GOOD RECORD SHOWING THE INITIAL FIREBALL, DEBRIS EXPANSION WHICH THEN FADES TO A CENTRAL CORE. THE CENTRAL CORE THEN EXPANDS AND FADES.
96326	PX	MITCHELL	18 FEET OF RECORD SHOWING DEBRIS, MAIN FIREBALL, OUTER SHELL, AND DEBRIS JETTING.
96327	KDII	MITCHELL	A FEW FEET OF GOOD RECORD SHOWING THE FIREBALL AND DEBRIS.
96328	EDER	MITCHELL	10 FEET OF EXCELLENT RECORD. STRONG AURORA
96329	XR	B AND H	SEVERAL FEET OF EXCELLENT RECORD SHOWING THE FIREBALL, DEBRIS, AND AURORA.
96332	TXA	KC-1B	SEVERAL GOOD RECORDS SHOWING FIREBALL, AURORA, AND DEBRIS.
96334	EDER	ROBOT	SEQUENCE SIMILAR TO 96312 AND 96313.
96335	MF	DYNAFAX	NO RECORD.
96336	HSIR	DYNAFAX	SMALL FAINT RECORD.

TABLE 6.10 STATISTICAL SUMMARY OF KING FISH CAMERA RECORDS FROM THE BURST AREA

Station	J-820	Aircraft 53120	Aircraft 60376	Totals
Number of Cameras	26	20	20	66
Number of Useful Records	24	19	16	59
Reasons for No Records:				
Mechanical failure	0	1	0	1
Inappropriate camera parameters	0	0	4	4
Error in shot location	1	0	0	1
Reasons for Poor Records:				
Inappropriate camera parameters	1	0	0	1
Error in shot location	0	0	0	0
Other	0	0	0	0
Percent Success	92	95	75	—
Overall Success: 89 percent				

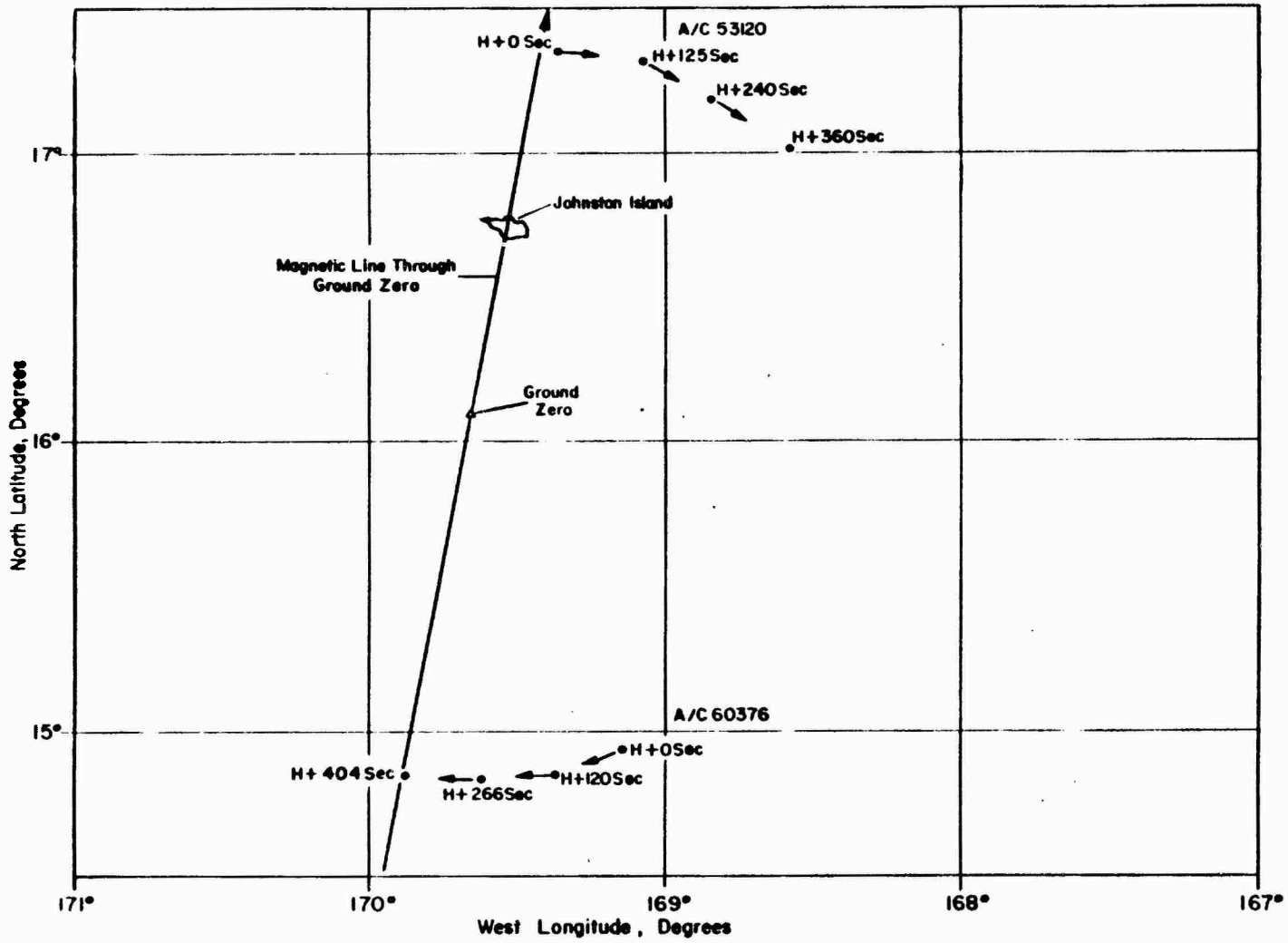

Figure 6.1 Aircraft flight paths from H-hour to + 6½ minutes, King Fish.

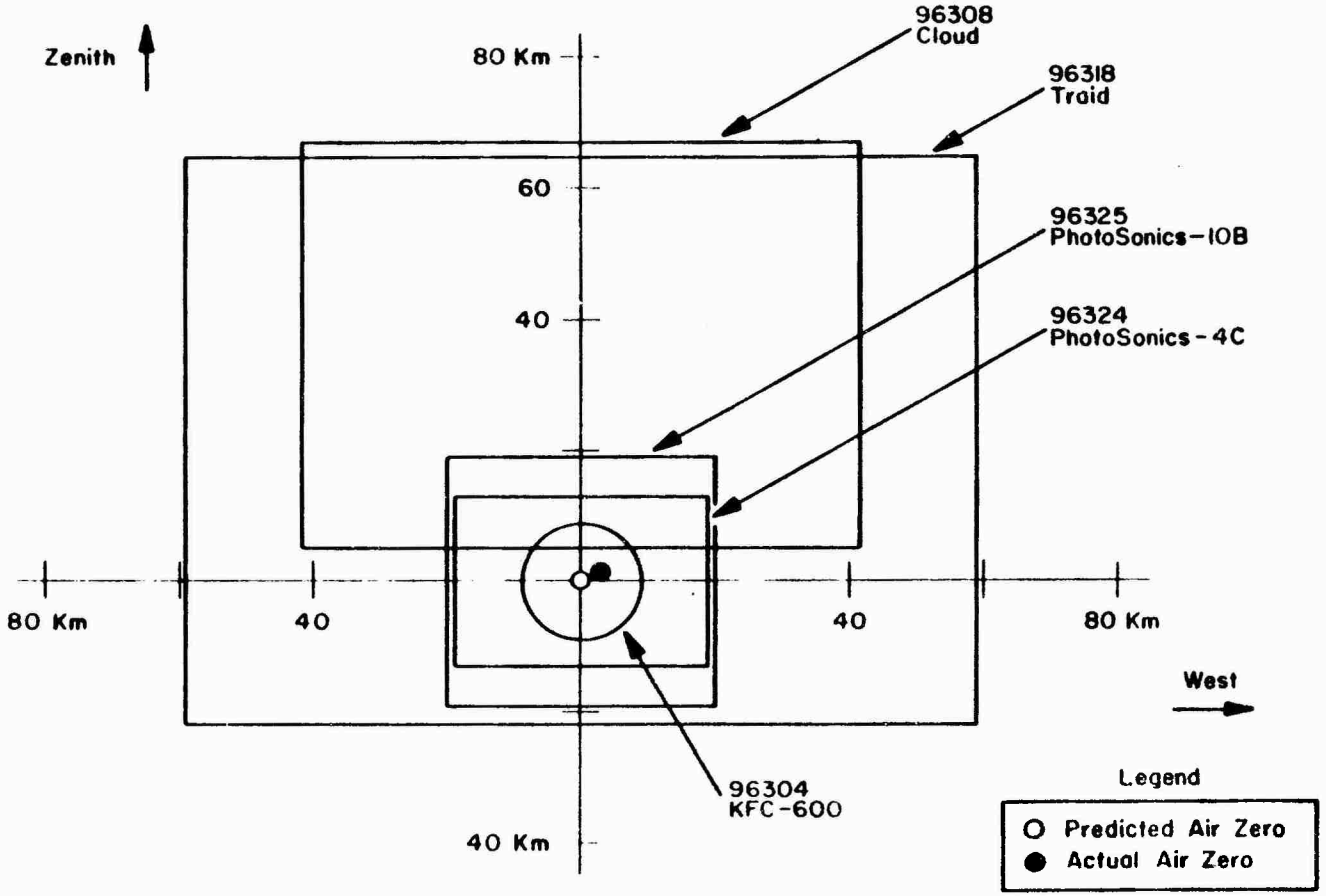

Figure 6.2 Fields of view for five cameras located on Johnston Island with predicted and actual air zero indicated.

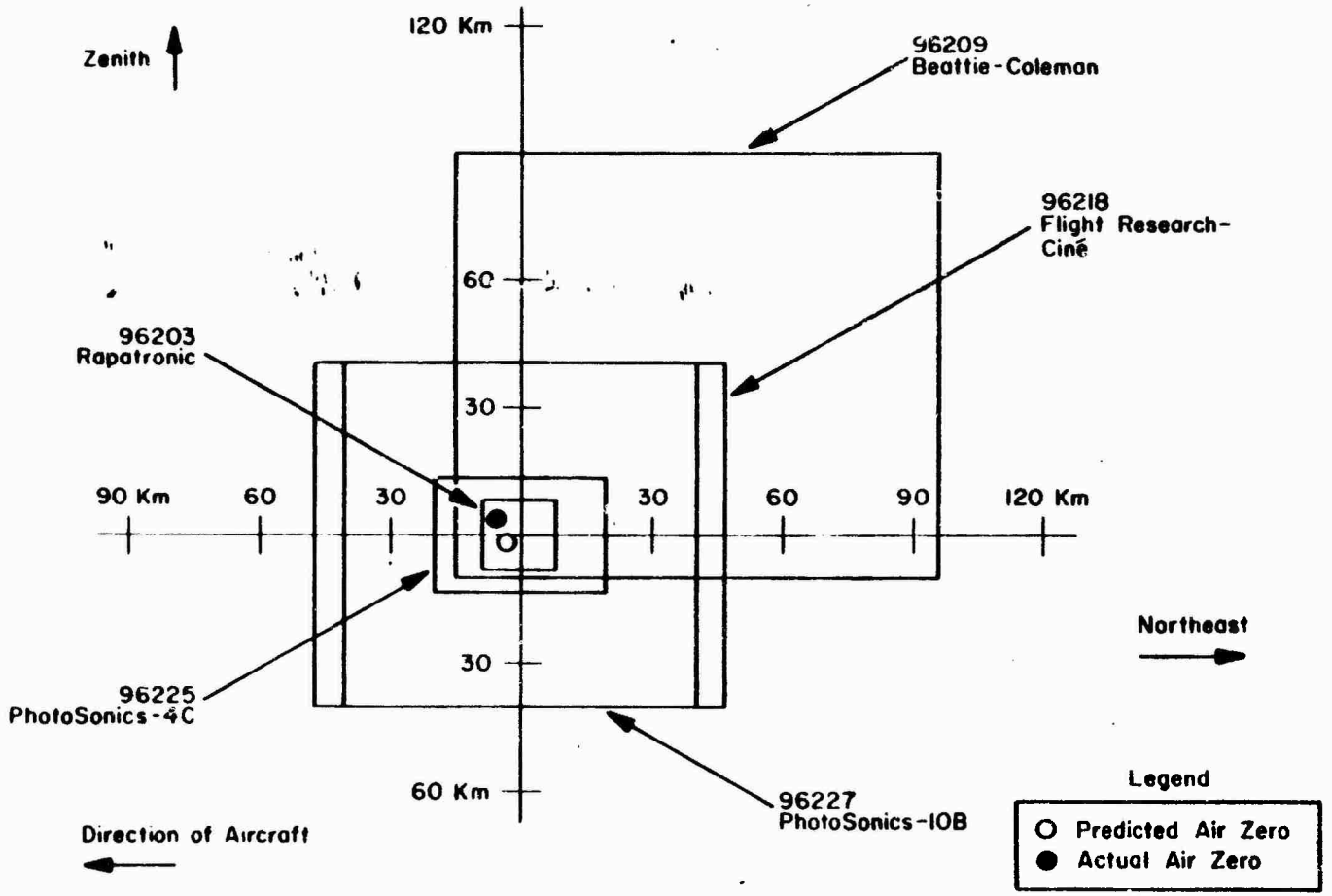

Figure 6.3 Fields of view for five Aircraft 60376 cameras with predicted and actual air zero indicated.

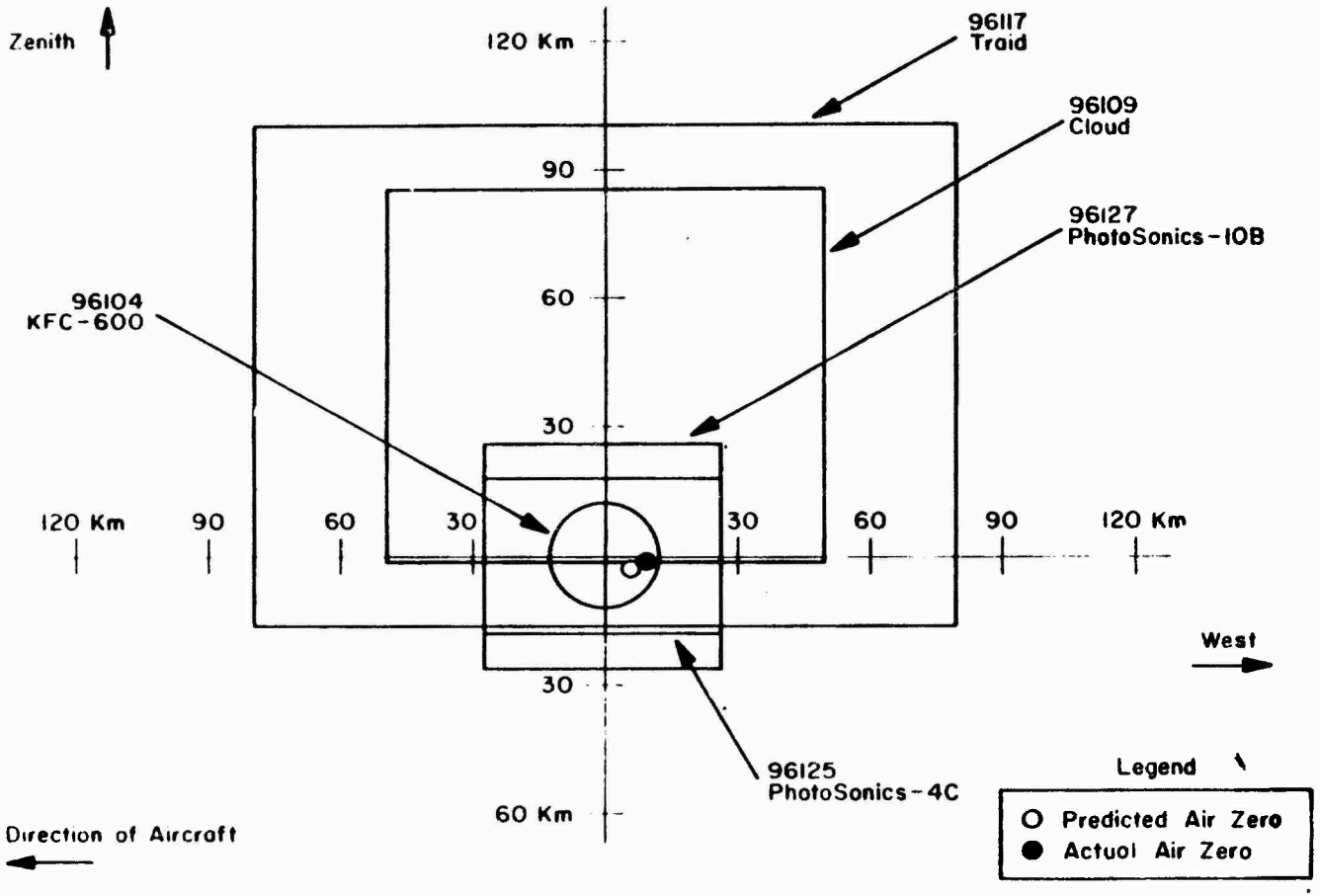

Figure 6.4 Fields of view for five Aircraft 53120 cameras with predicted and actual air zero indicated.

Pages 328 through 348 deleted.

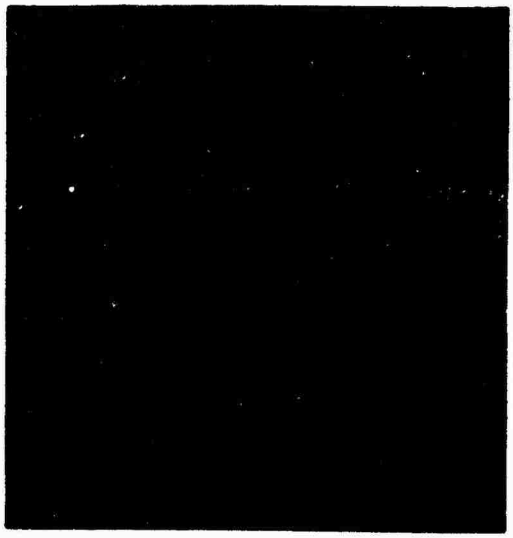

0+ sec

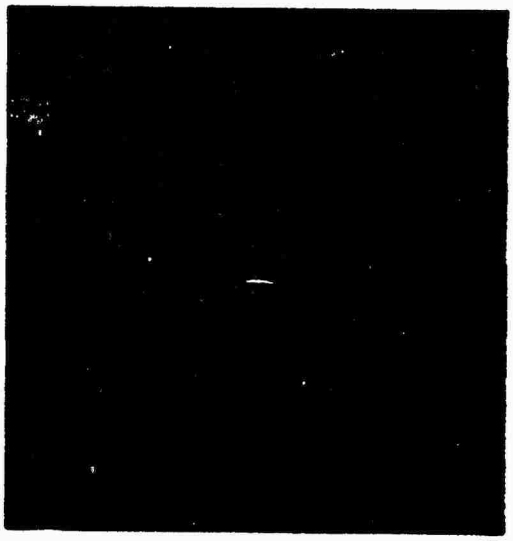

40 sec

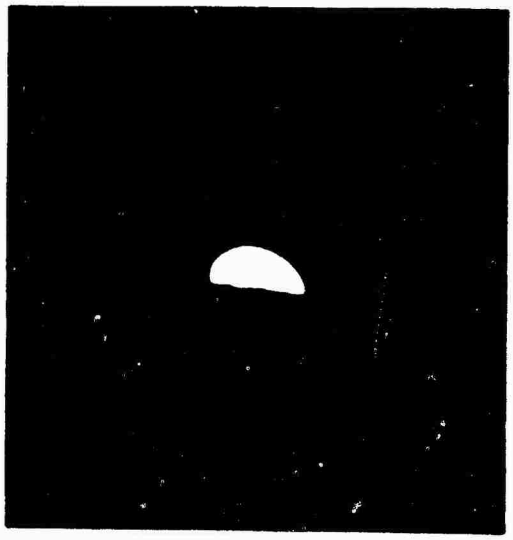

50 sec

75 sec

Figure 6.23 King Fish; residual fireball and shock front, taken from Mauna Loa. Film 96708, Frames 0, 1, 2, and 3.

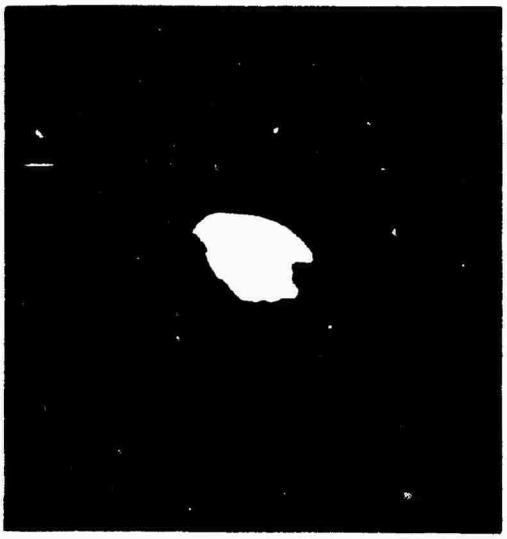

105 sec

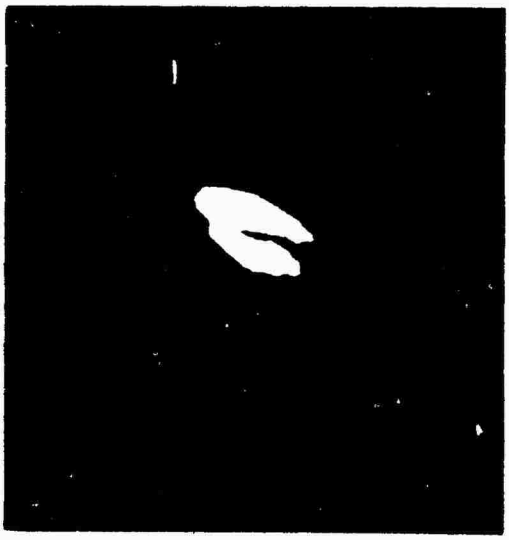

115 sec

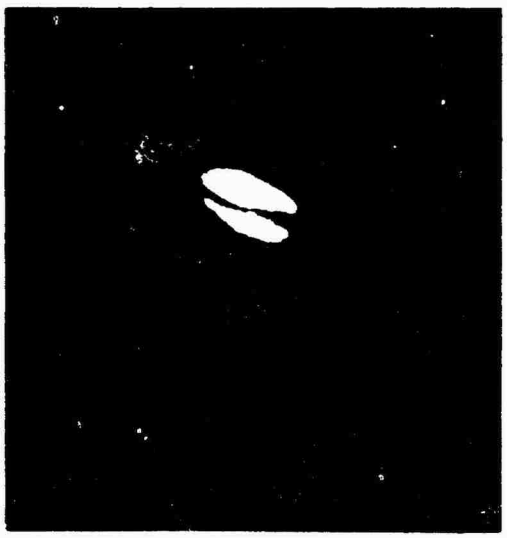

165 sec

185 sec

Figure 6.24 King Fish; transition of residual fireball to aurora, taken from Mauna Loa. Film 96708, Frames 4, 5, 6, and 7.

255 sec

315 sec

Figure 6.25 King Fish; aurora extending along geomagnetic field, taken from Mauna Loa. Film 96708, Frames 9 and 11.

351-352 Pages 353 through 361 deleted.

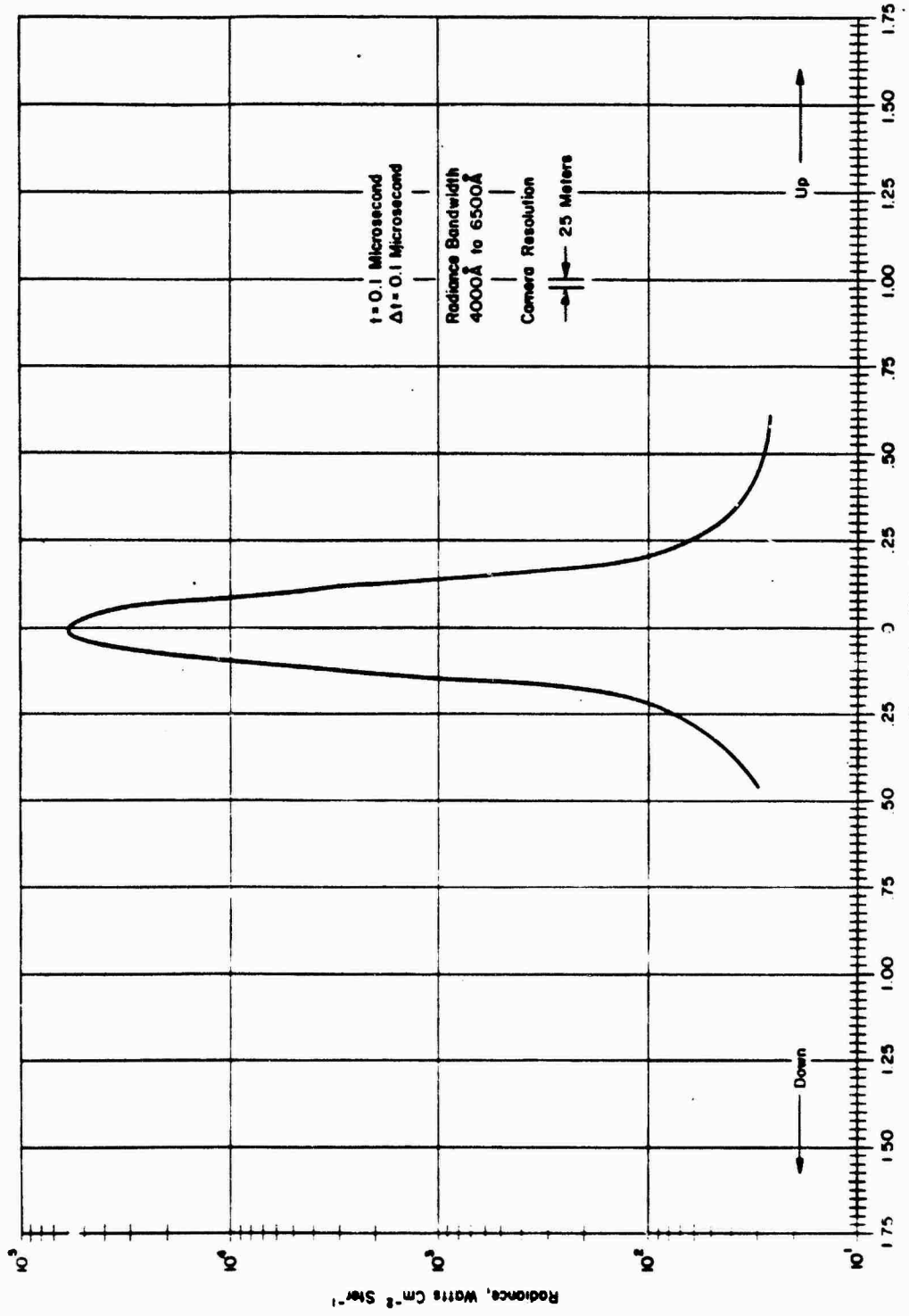

Figure 6.35 King Fish; radiance profile at 0.1 μsec.

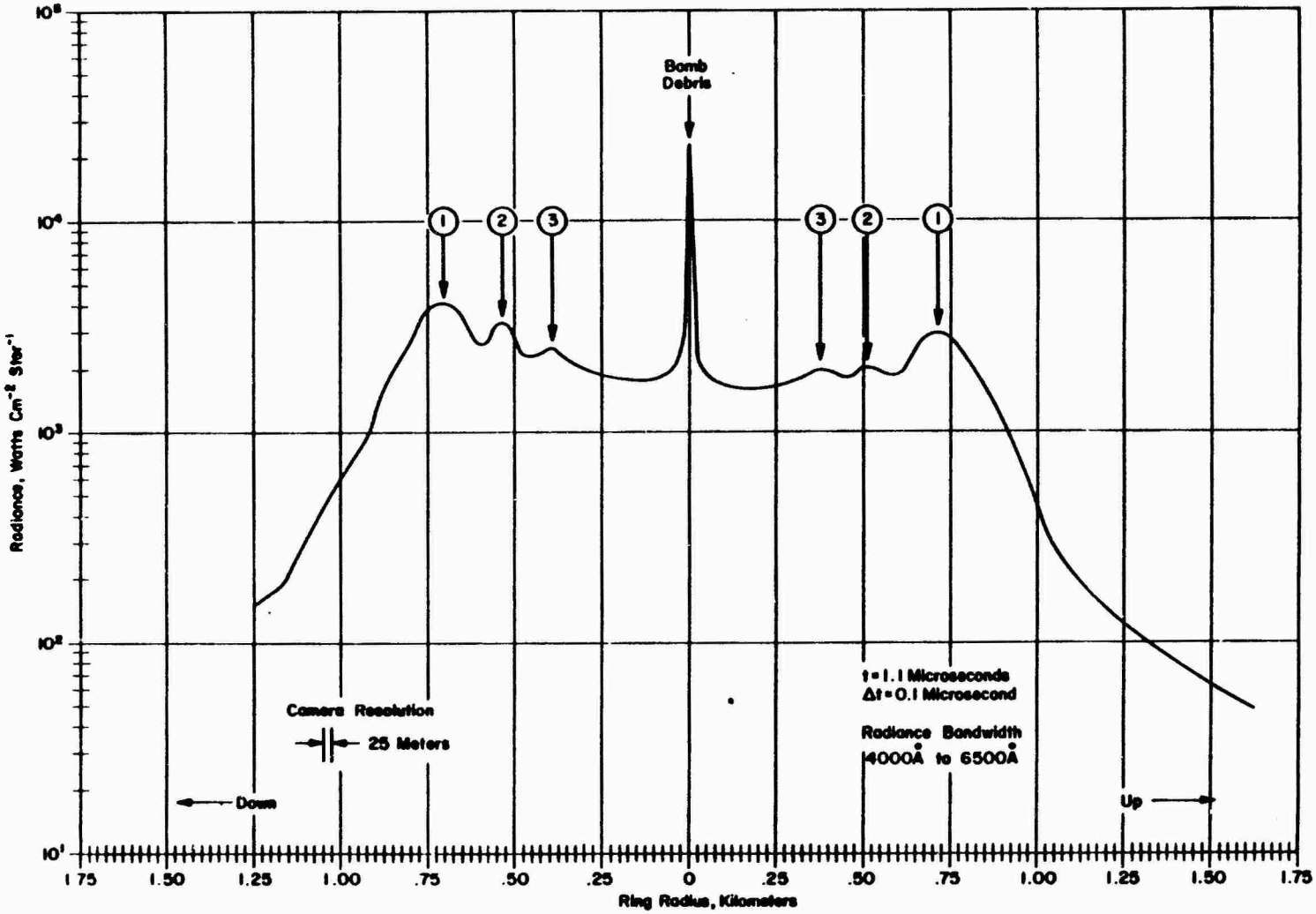

Figure 6.36 King Fish; radiance profile of bomb debris and X-ray rings at 1.1 μsec.

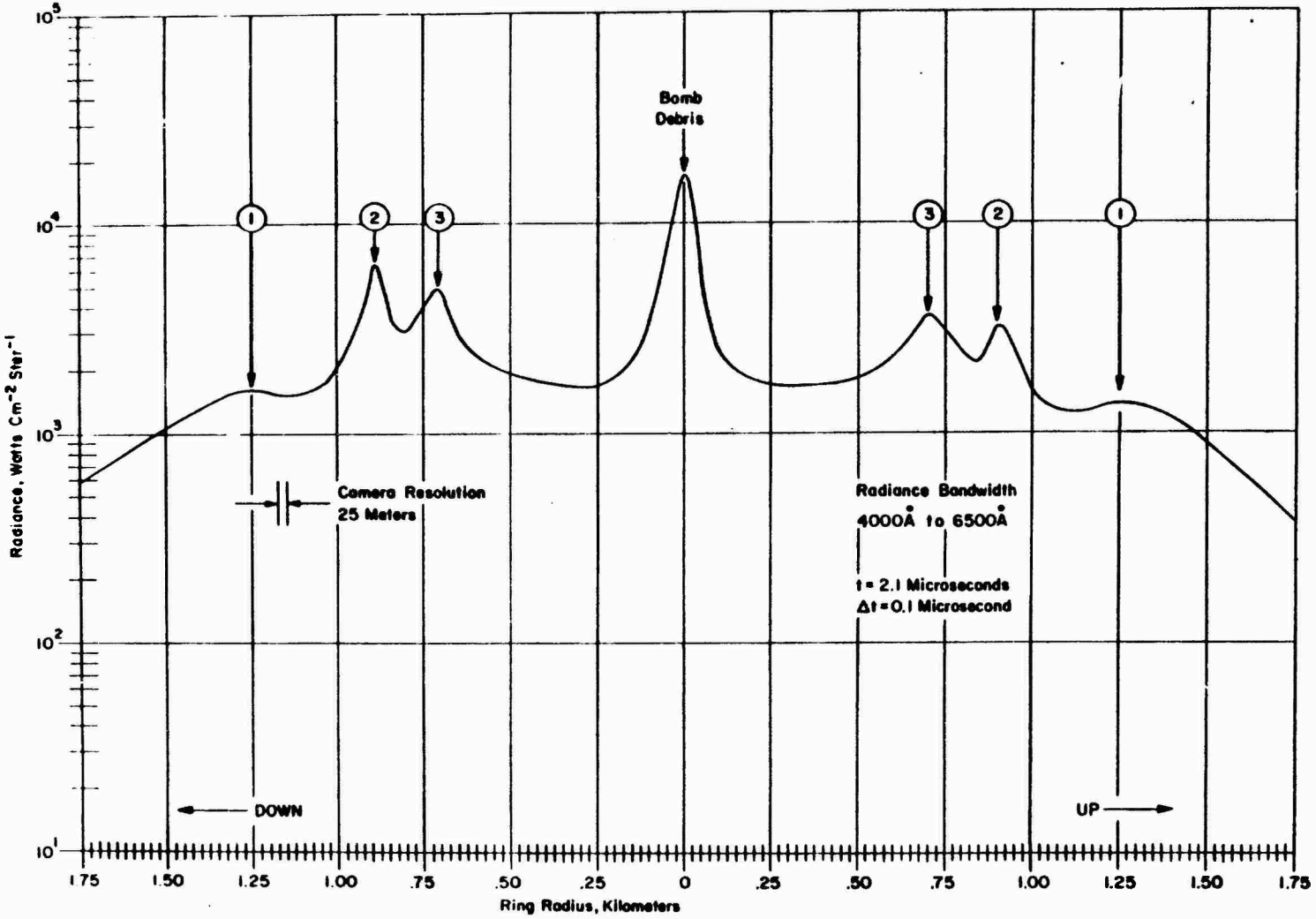

Figure 6.37 King Fish; radiance profile of bomb debris and X-ray rings at 2.1 μsec.

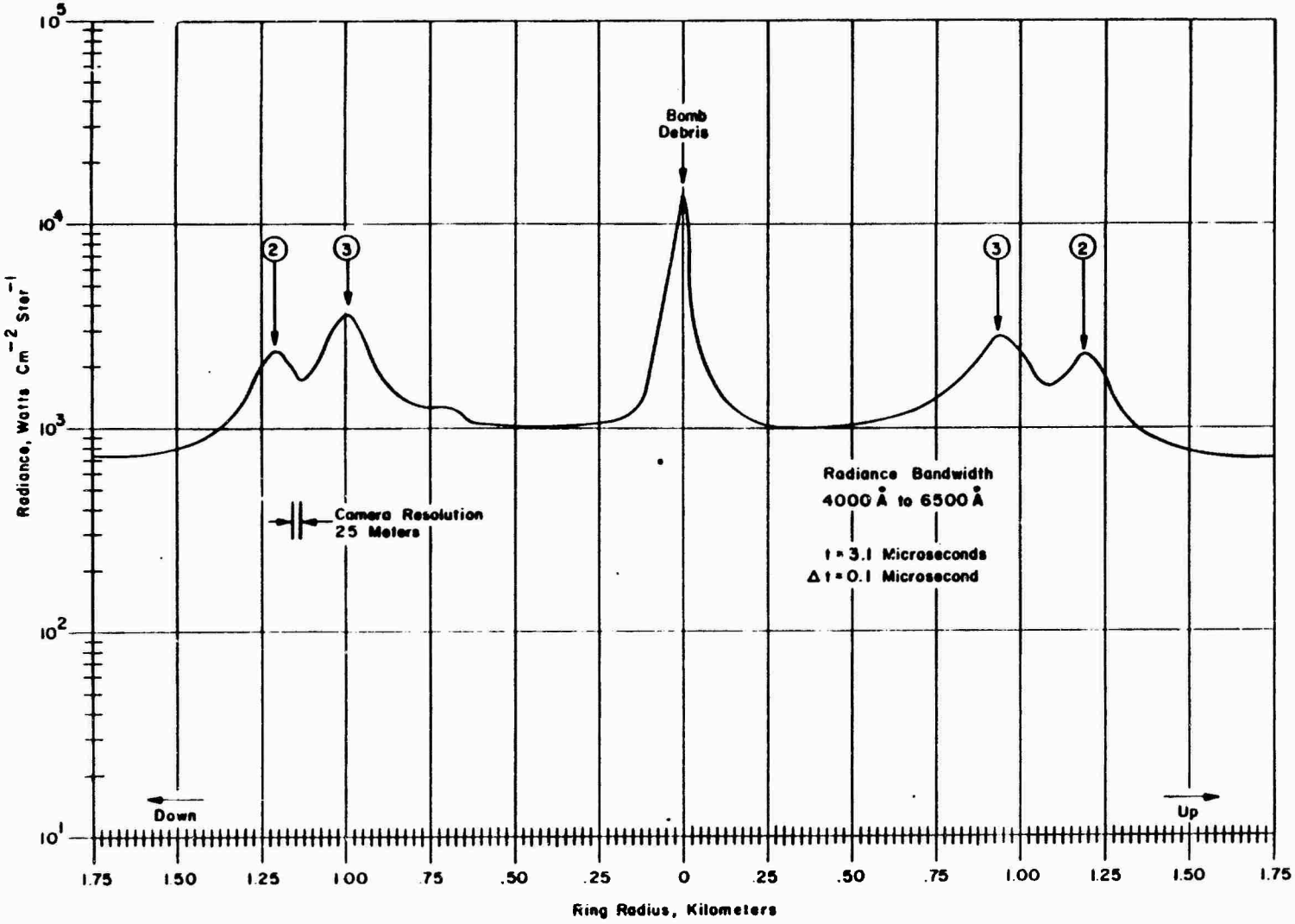

Figure 6.38 King Fish; radiance profile of bomb debris and X-ray rings at 3.1 μsec.

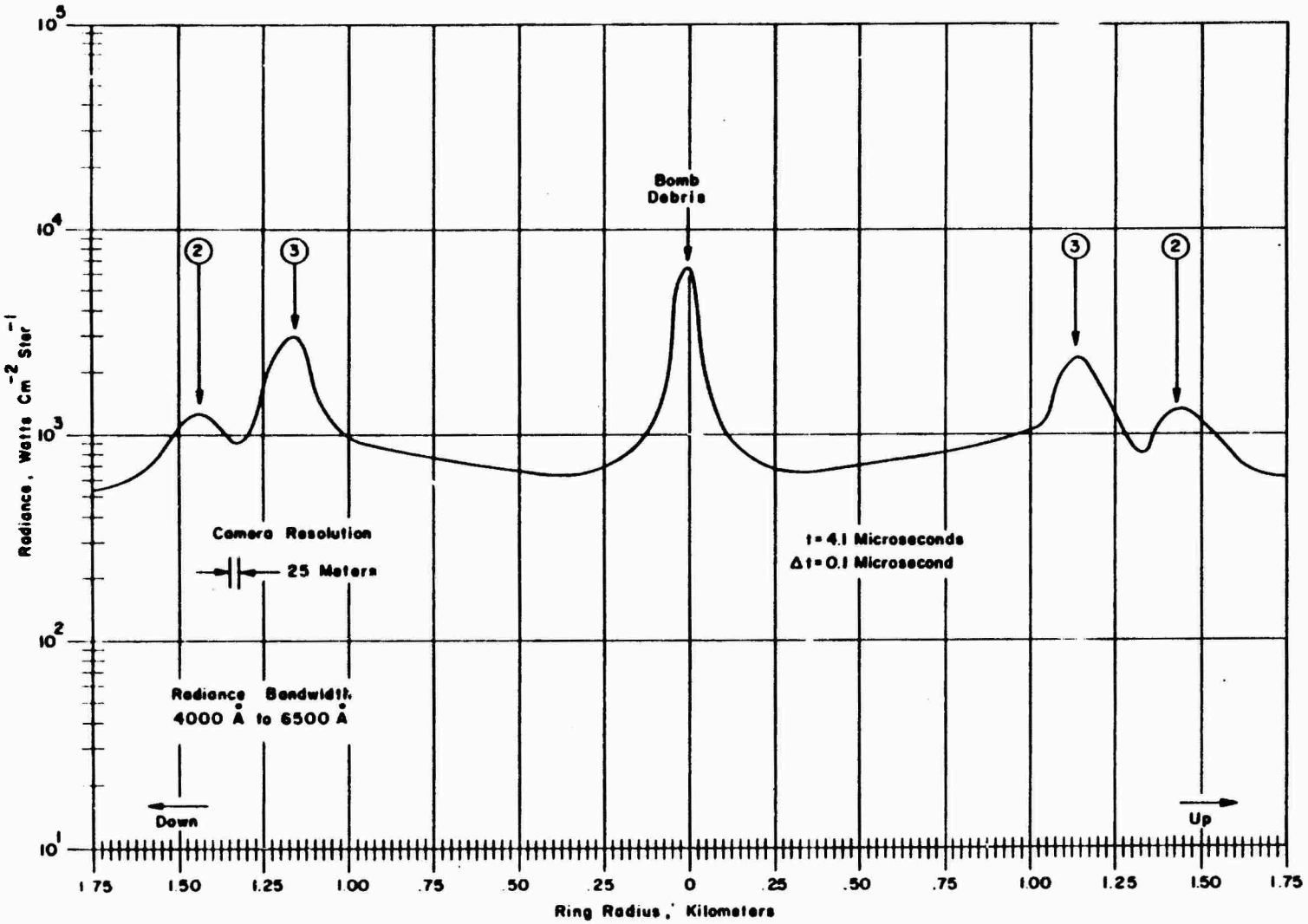

Figure 6.39 King Fish; radiance profile of bomb debris and X-ray rings at 4.1 μsec.

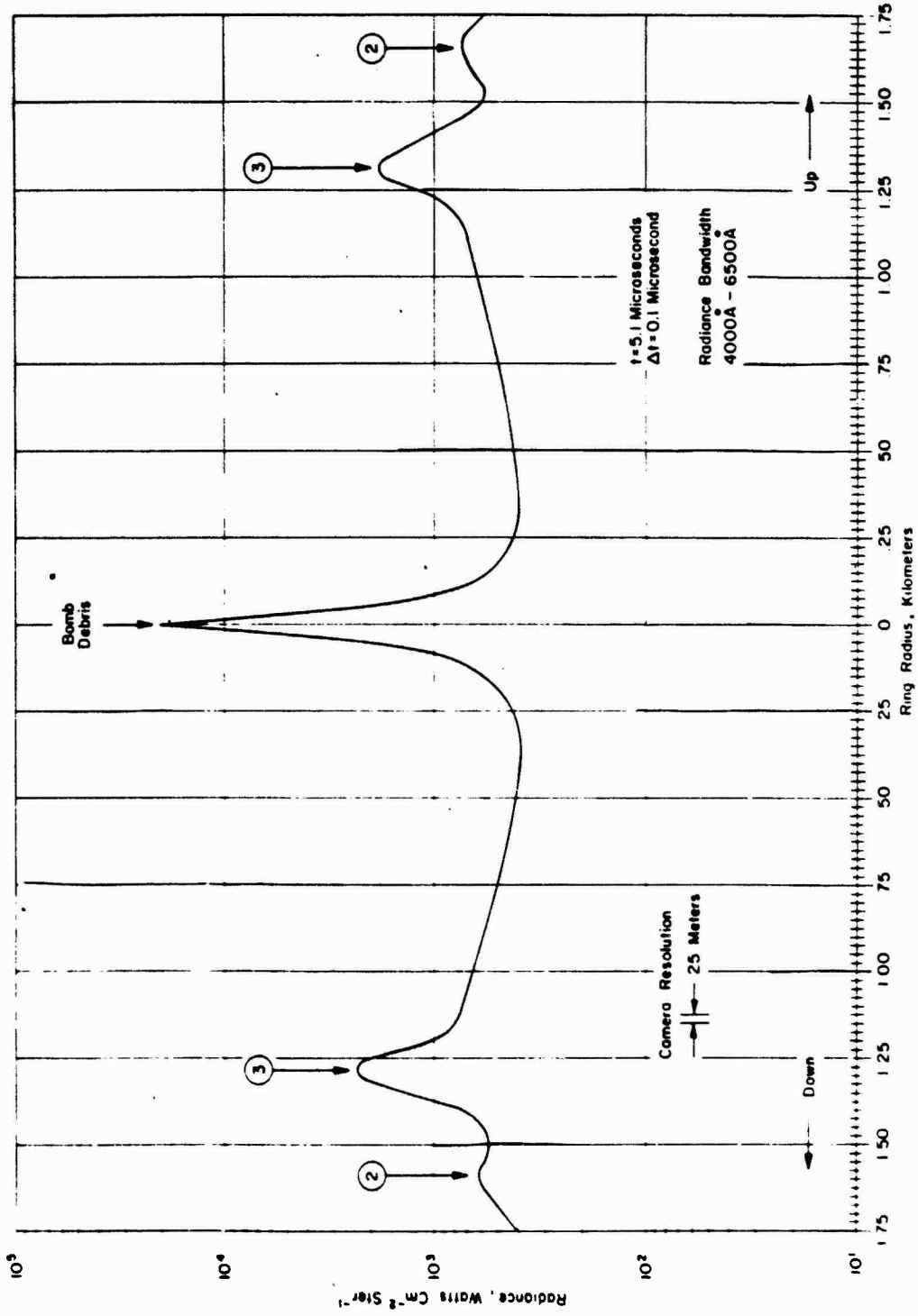

Figure 6.40 King Fish; radiance profile of bomb debris and X-ray rings at 5.1 μsec.

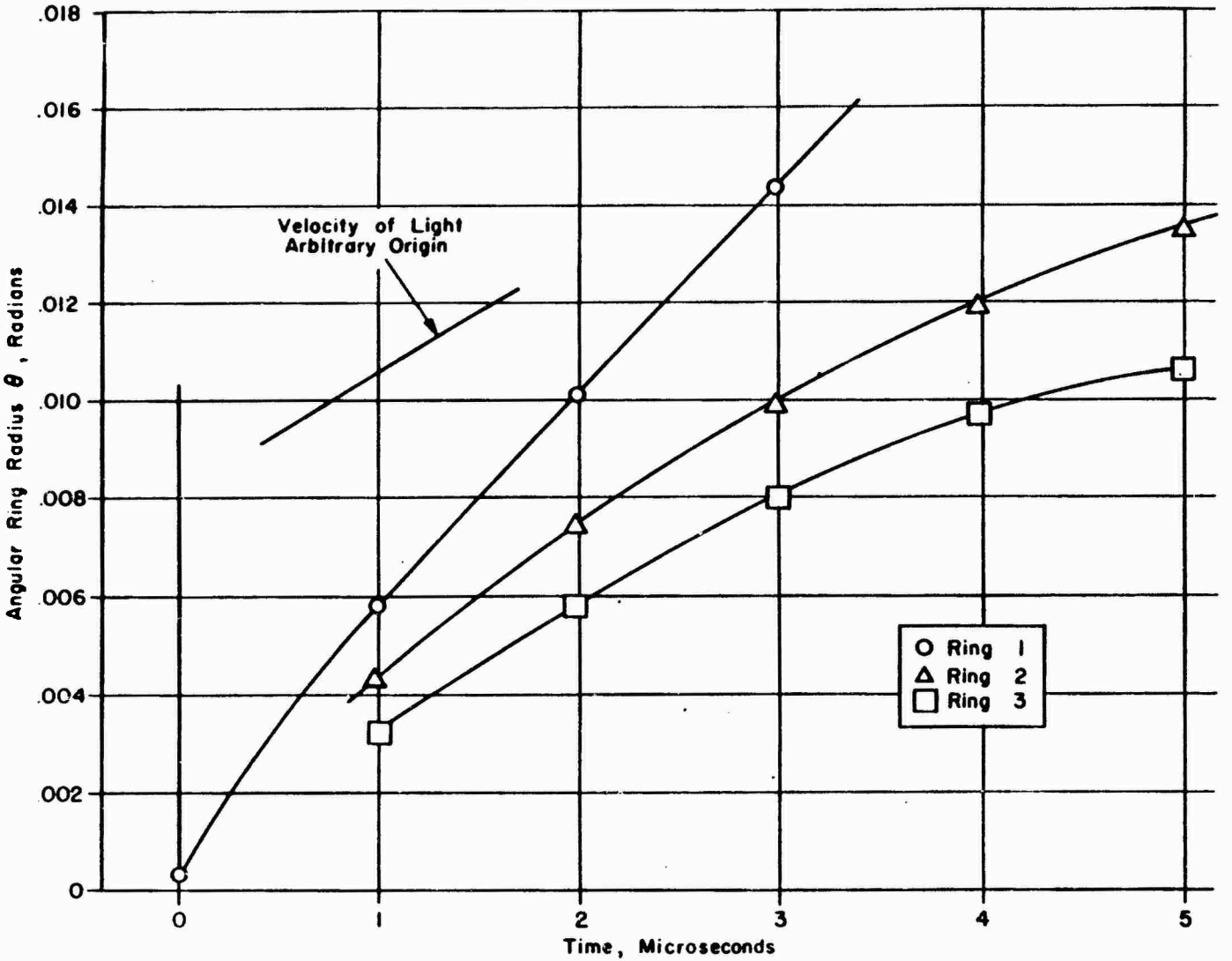

Figure 6.41 King Fish; angular radii versus time for the three X-ray rings.

Page 369 deleted.

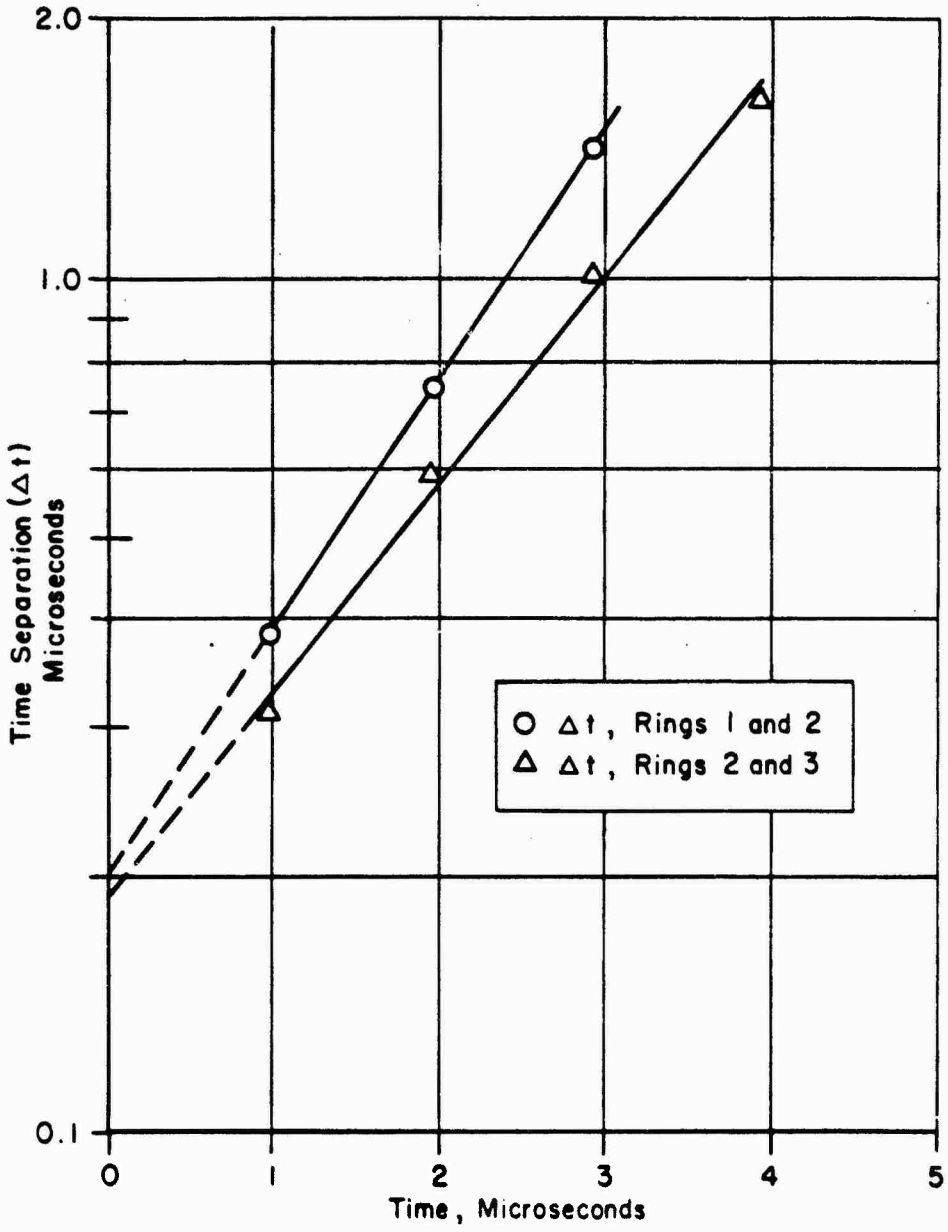

Figure 6.43 King Fish; apparent time separation between the X-ray rings versus the time at which the records were obtained.

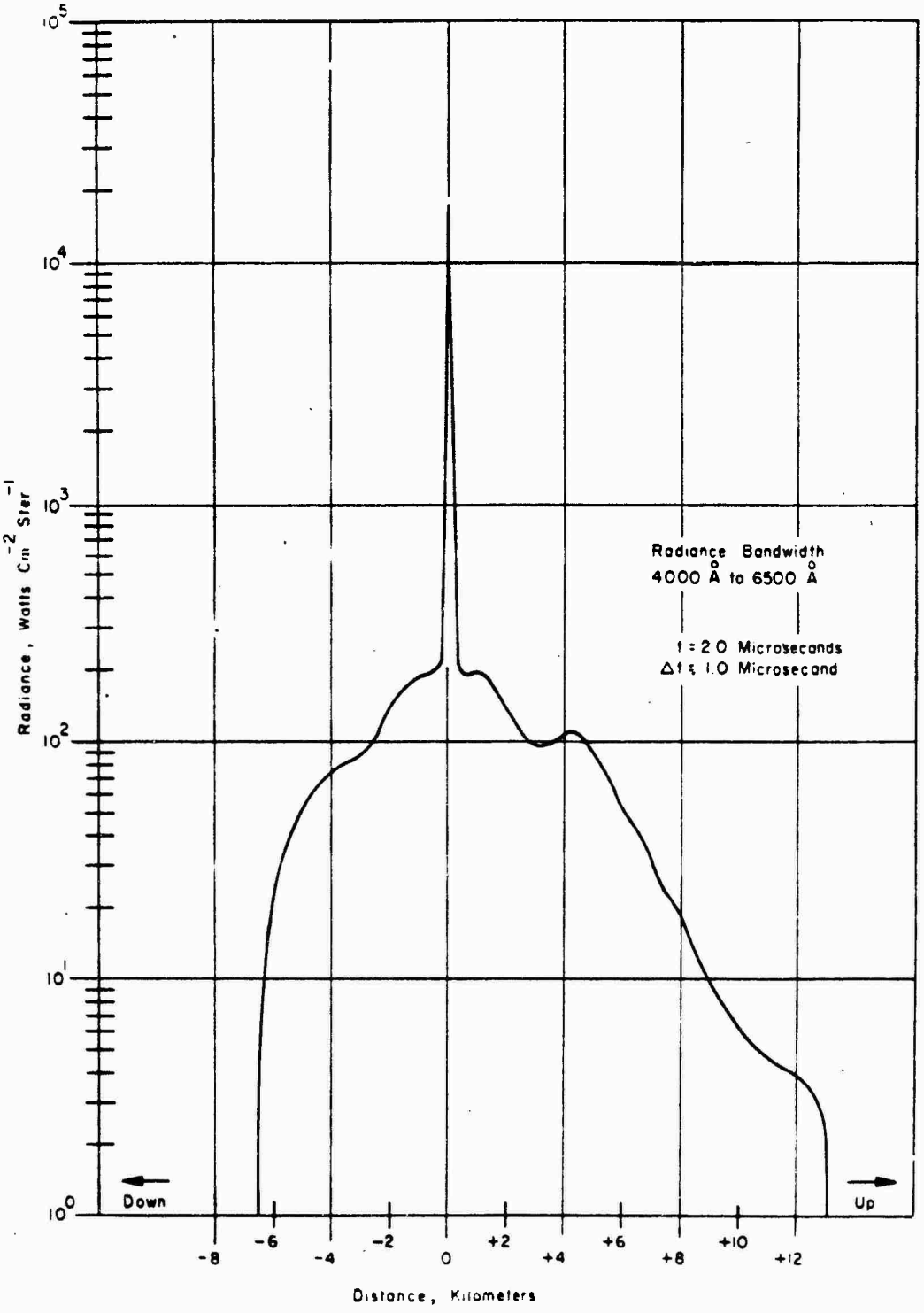

Figure 6.44 King Fish; radiance profile of fireball at 20 μsec.

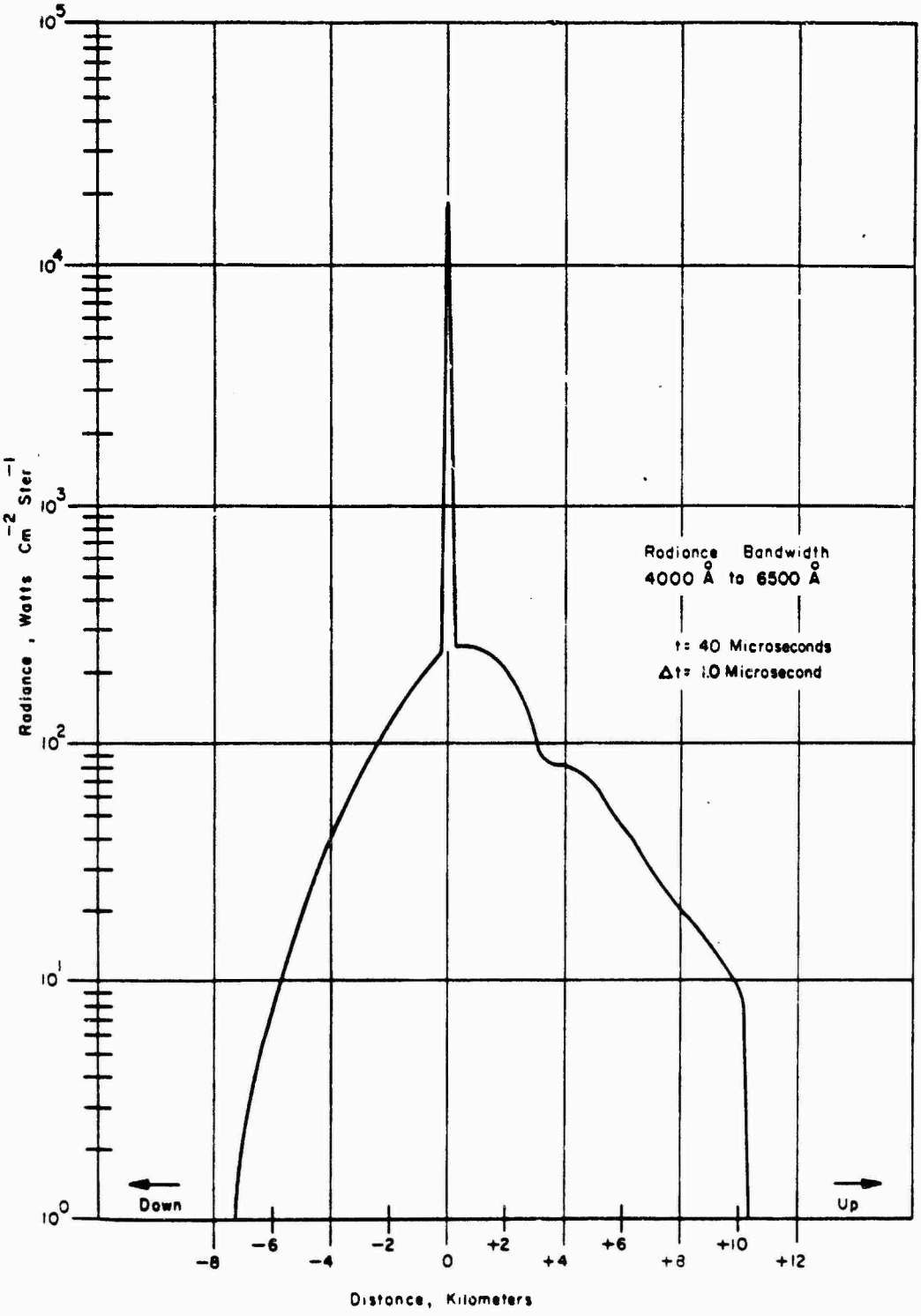

Figure 6.45 King Fish; radiance profile of fireball at 40 μsec.

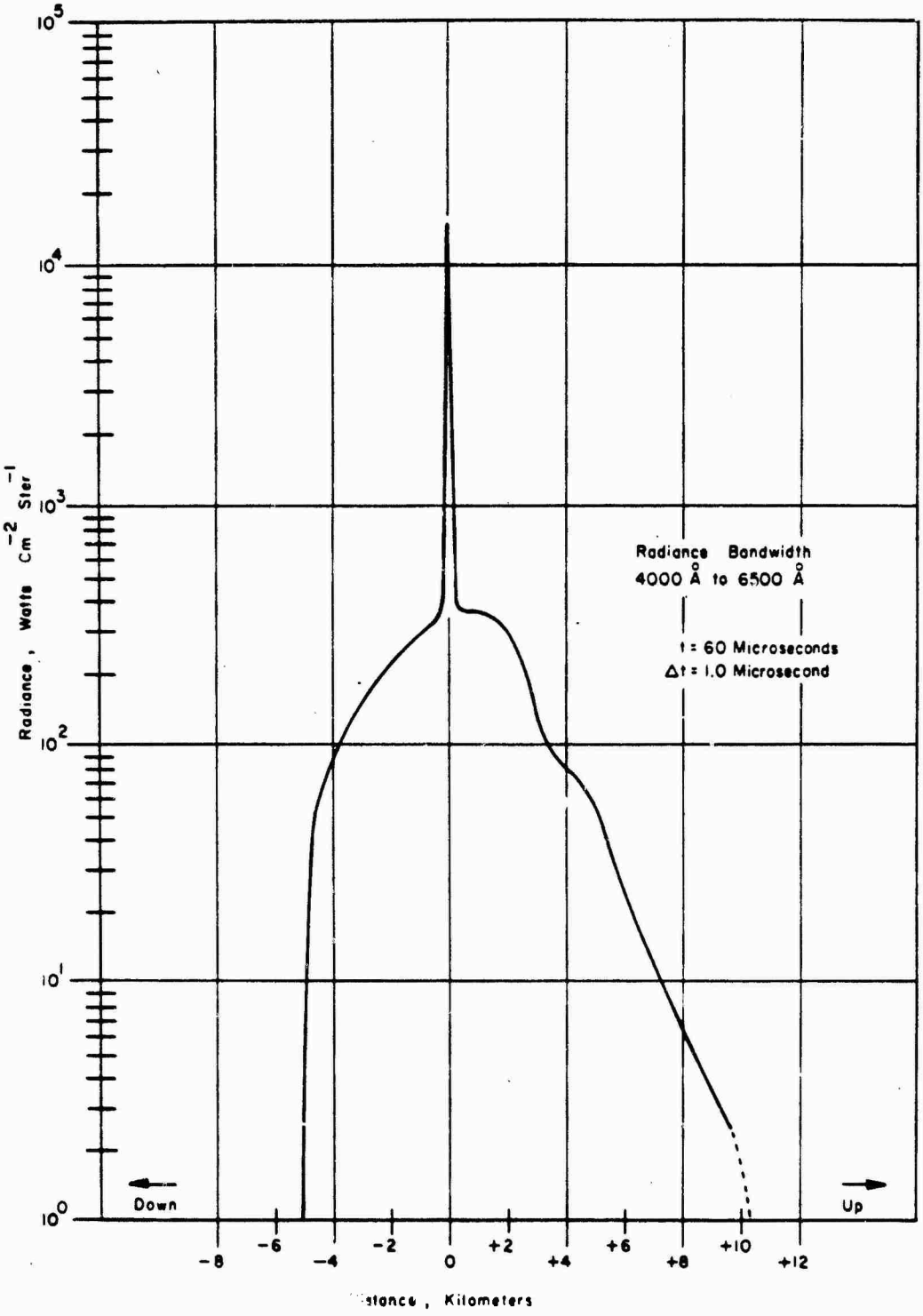

Figure 6.46 King Fish; radiance profile of fireball at 60 μsec.

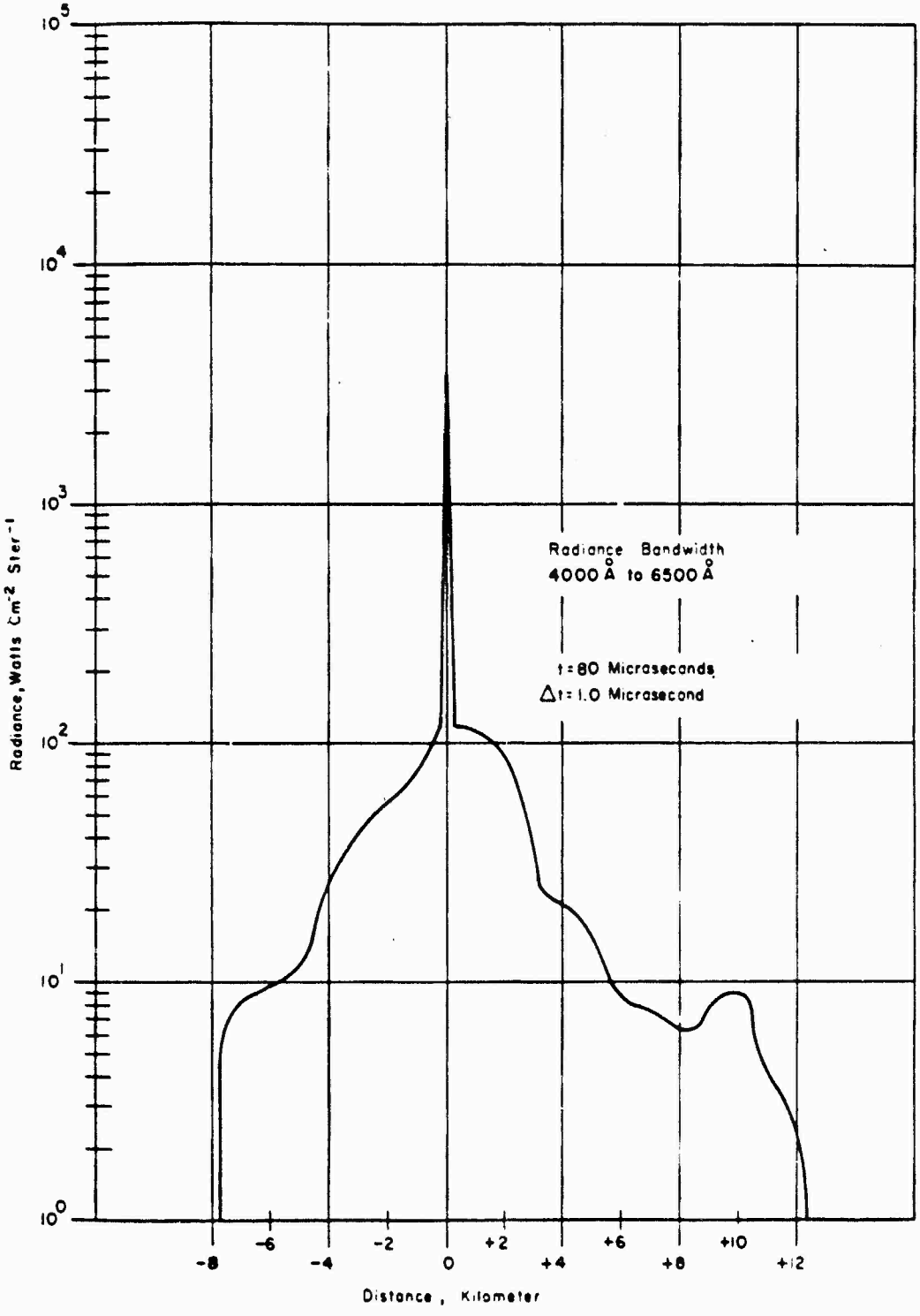

Figure 6.47 King Fish; radiance profile of fireball at 80 μsec.

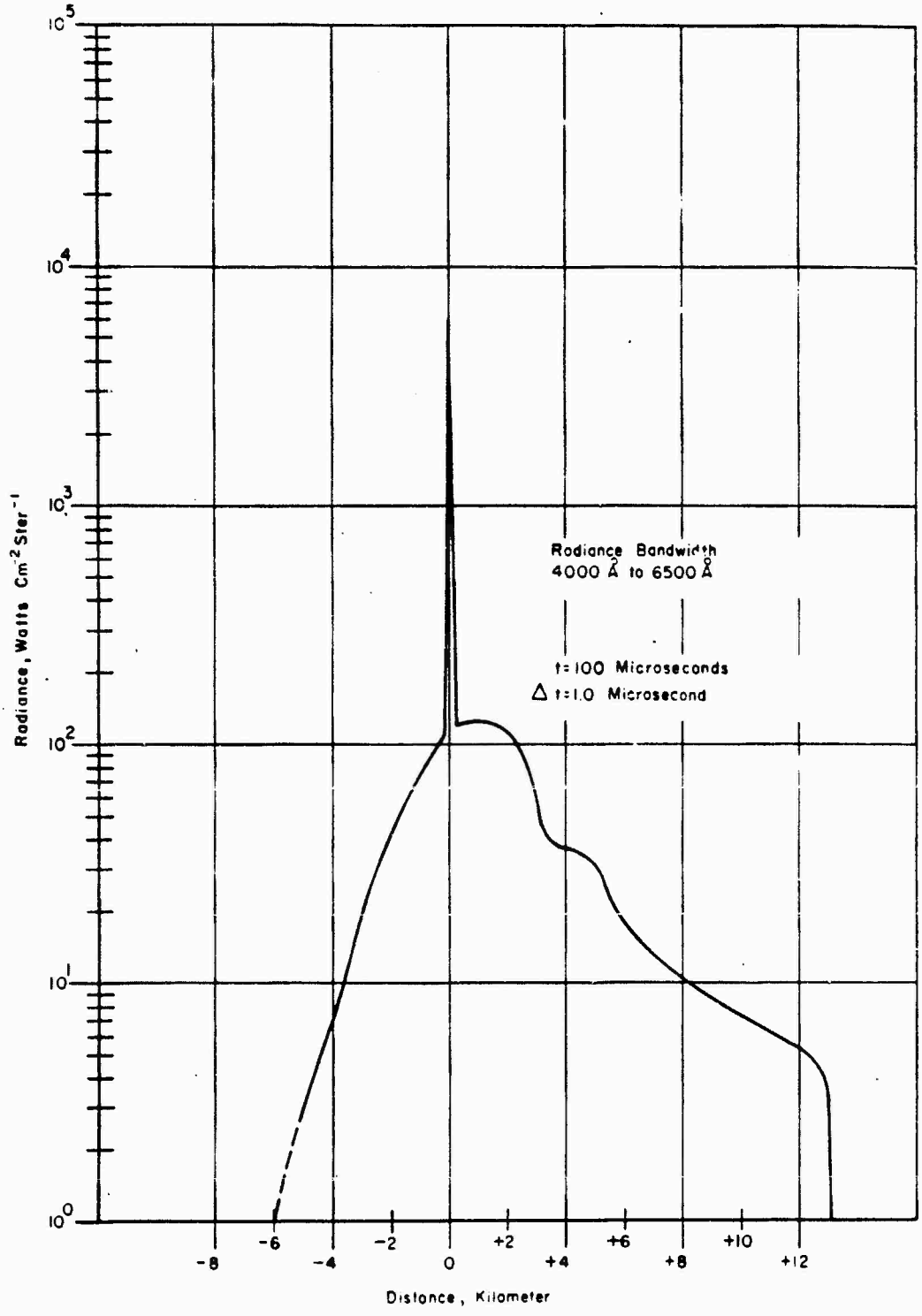

Figure 6.48 King Fish; radiance profile of fireball at 100 μsec.

Pages 376 through 378 deleted.

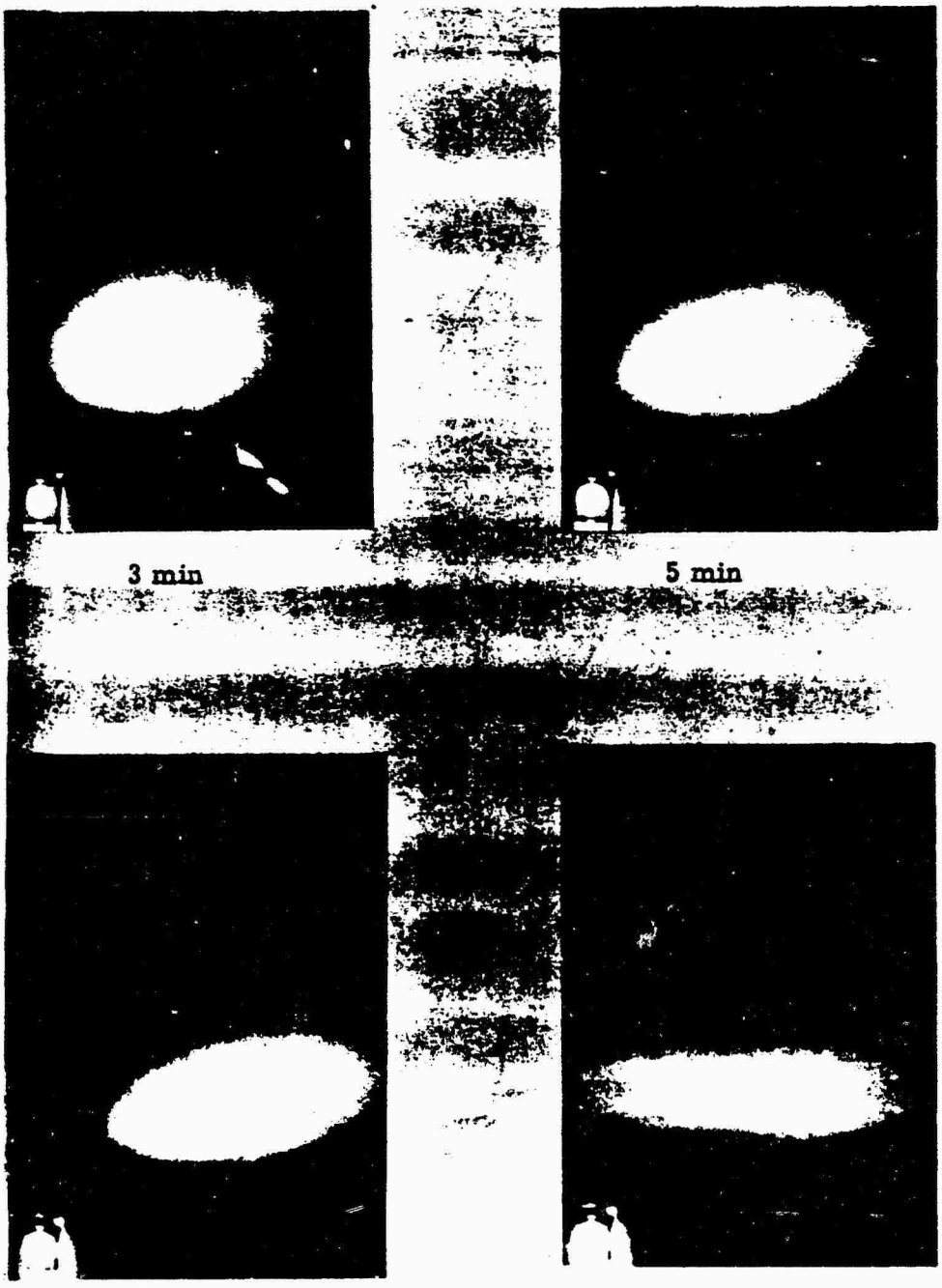

Figure 6.52 King Fish; green glow, taken from Aircraft 60376. Film 96222, Frames 60, 72, 79, and 121.

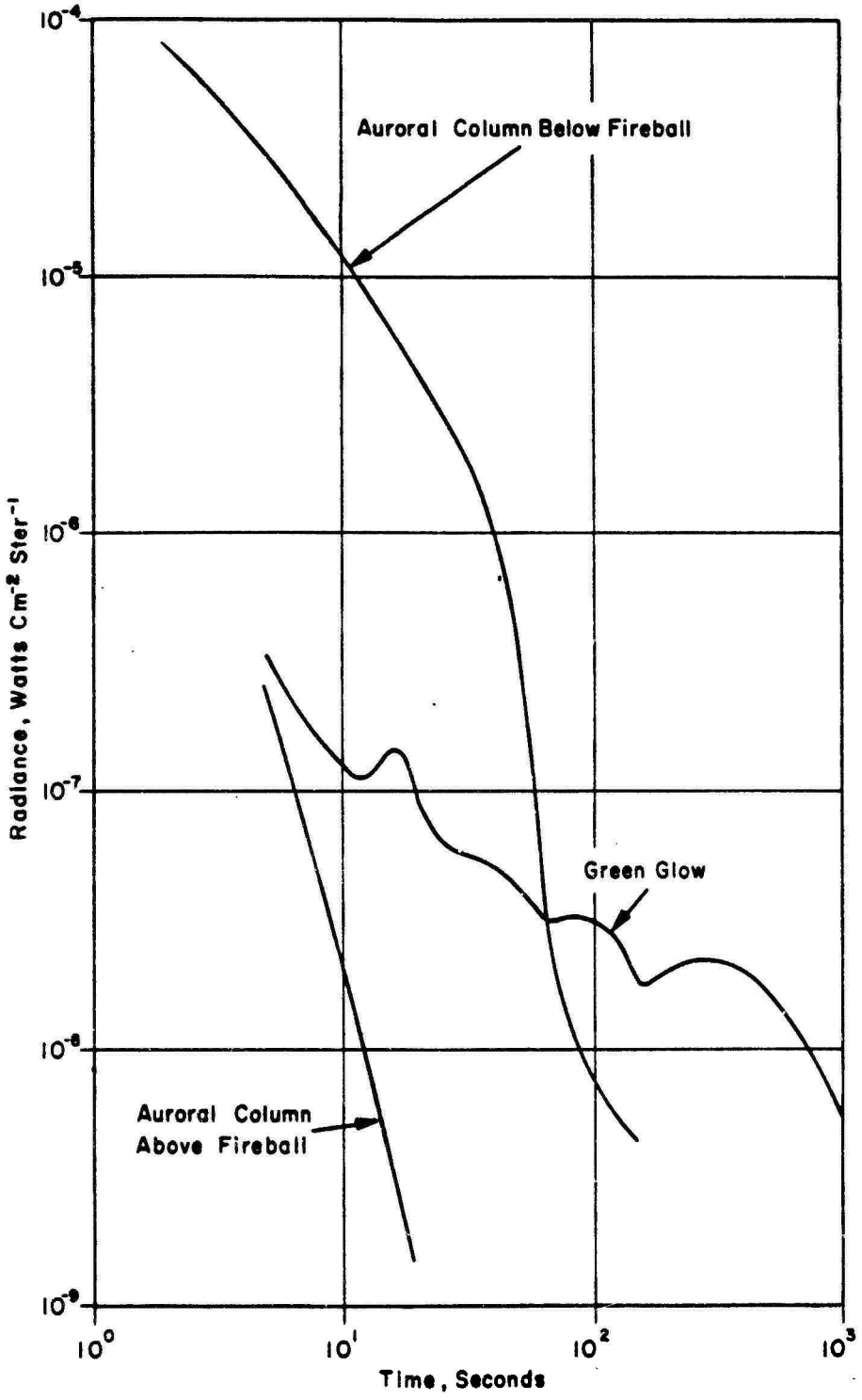

Figure 6.53 King Fish; radiance versus time for green glow and auroral column.

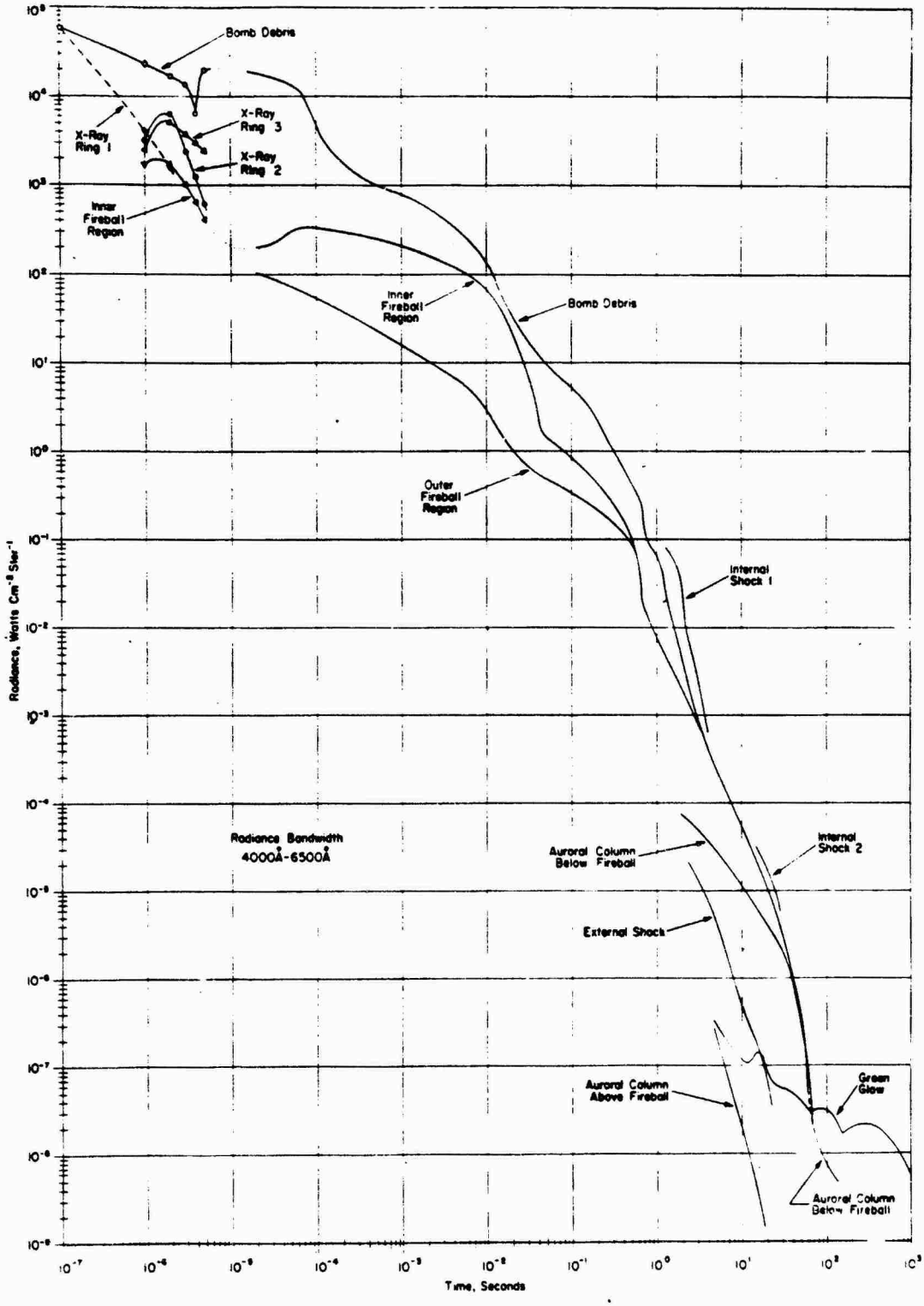

Figure 6.54 King Fish; radiance versus time curves.

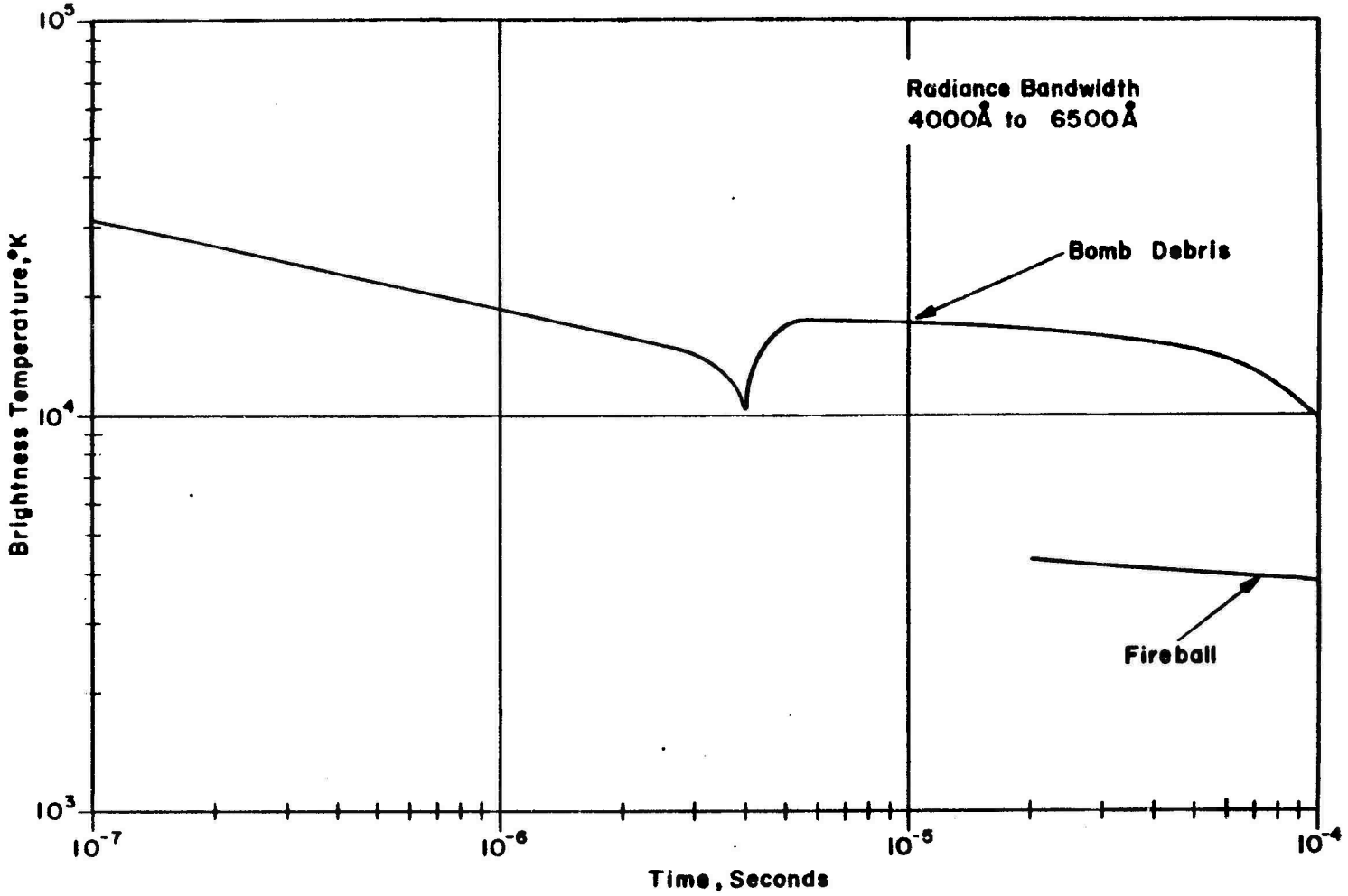

Figure 6.55 King Fish; fireball and bomb debris brightness temperature versus time from 10^{-7} to 10^{-4} second.

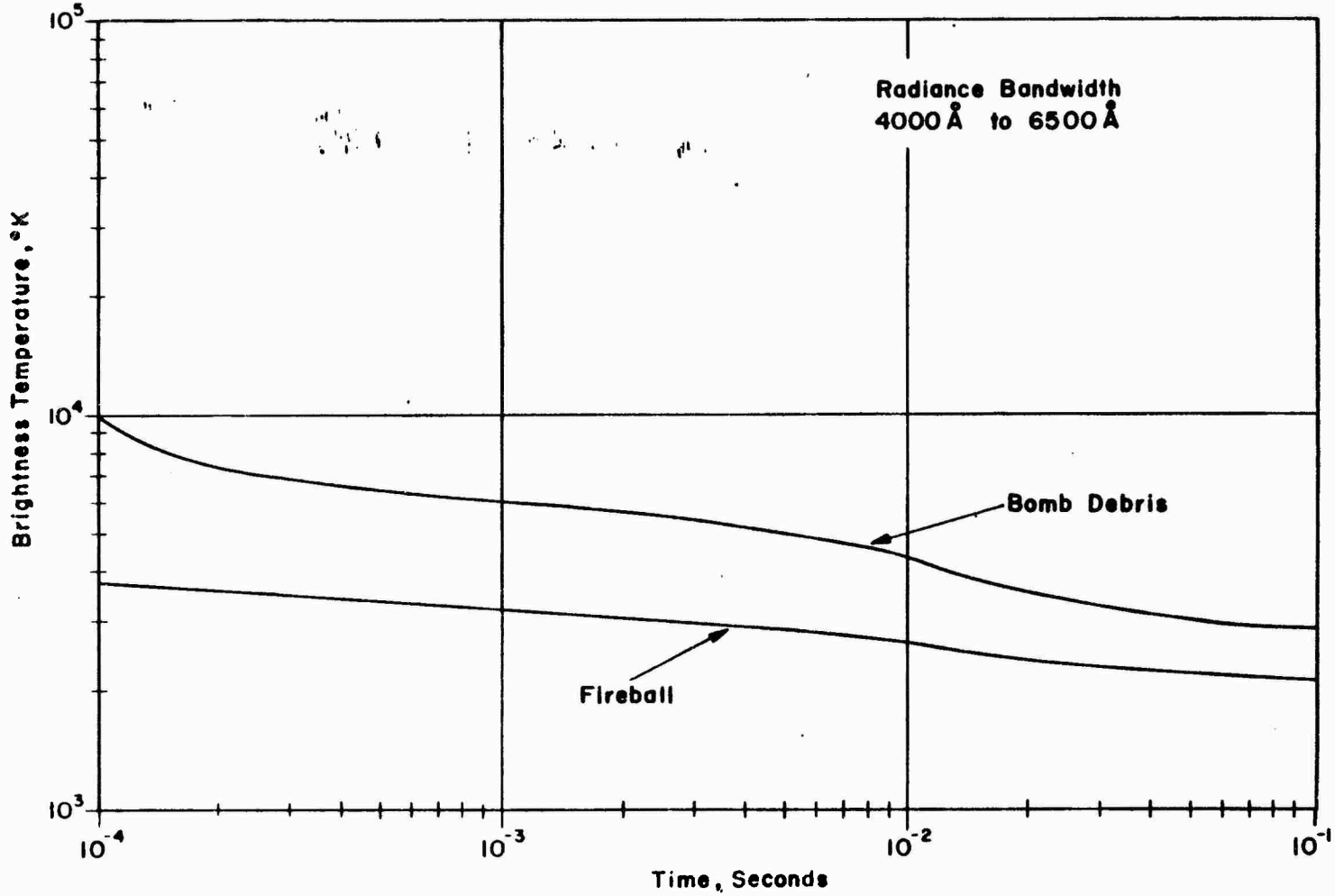

Figure 6.56 King Fish; fireball and bomb debris brightness temperature versus time from 10^{-4} to 10^{-1} second.

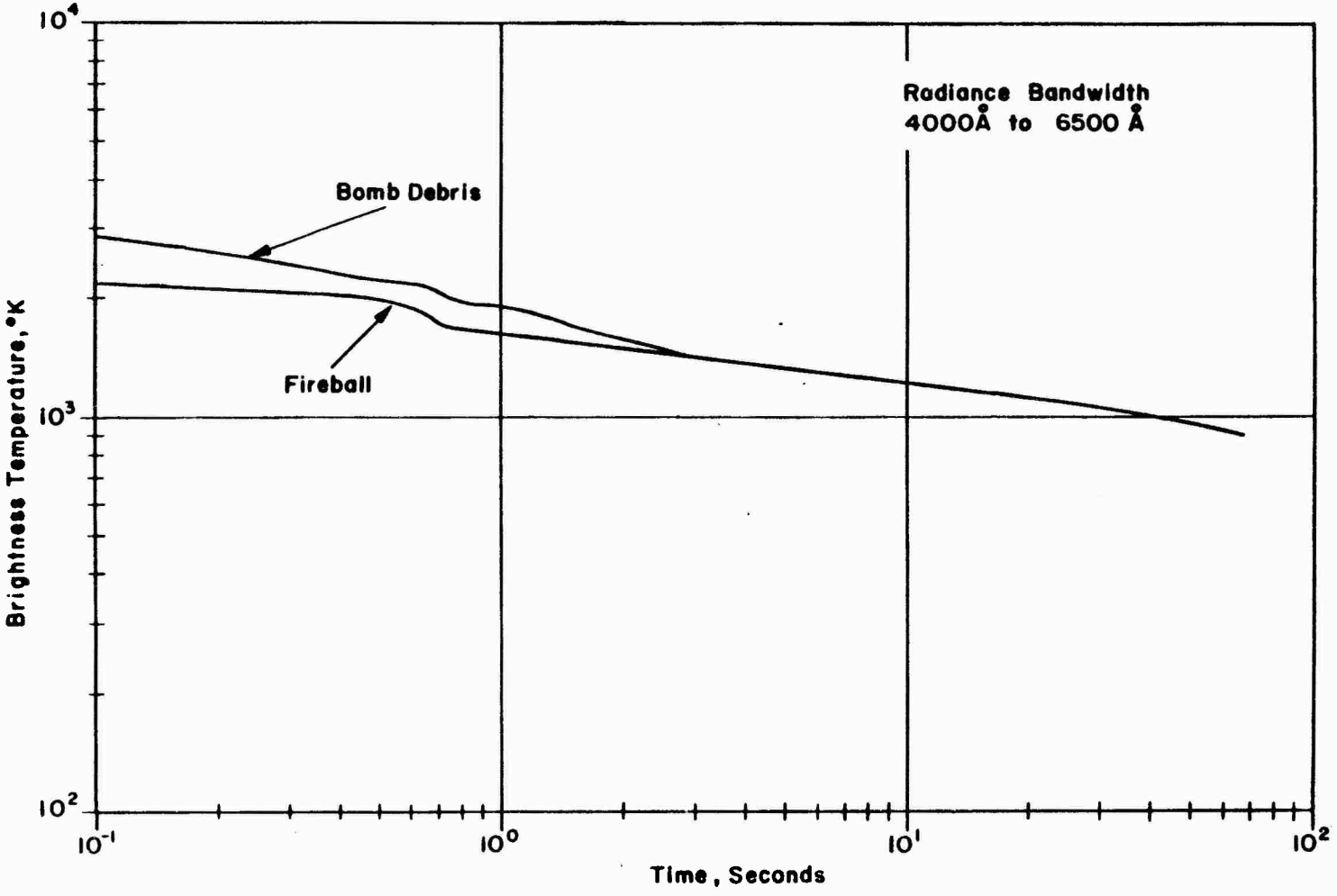

Figure 6.57 King Fish; fireball and bomb debris brightness temperature versus time from 10^{-1} to 10^2 seconds.

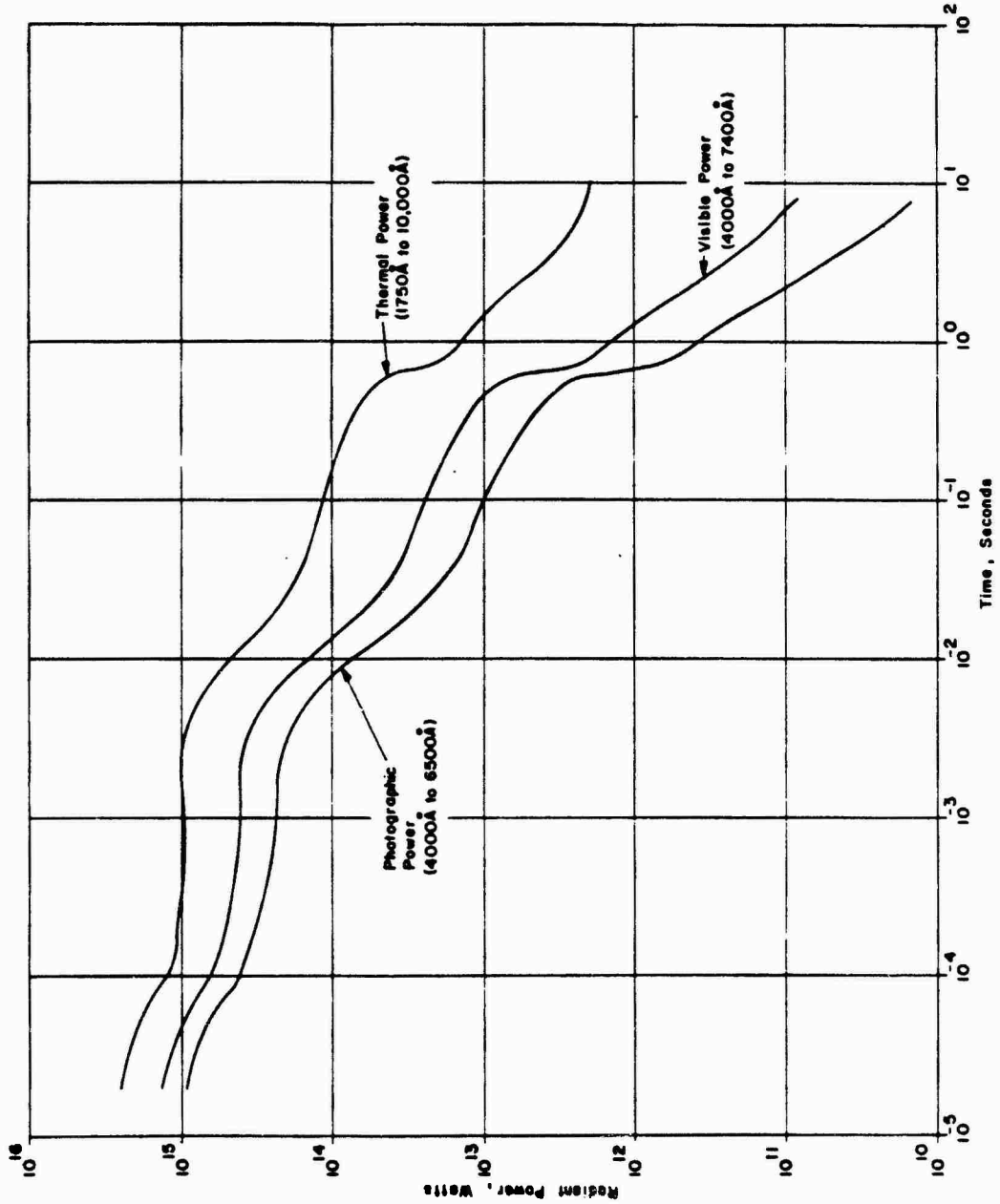

Figure 6.58 King Fish; radiant power versus time curves.

Pages 386 through 388
deleted.

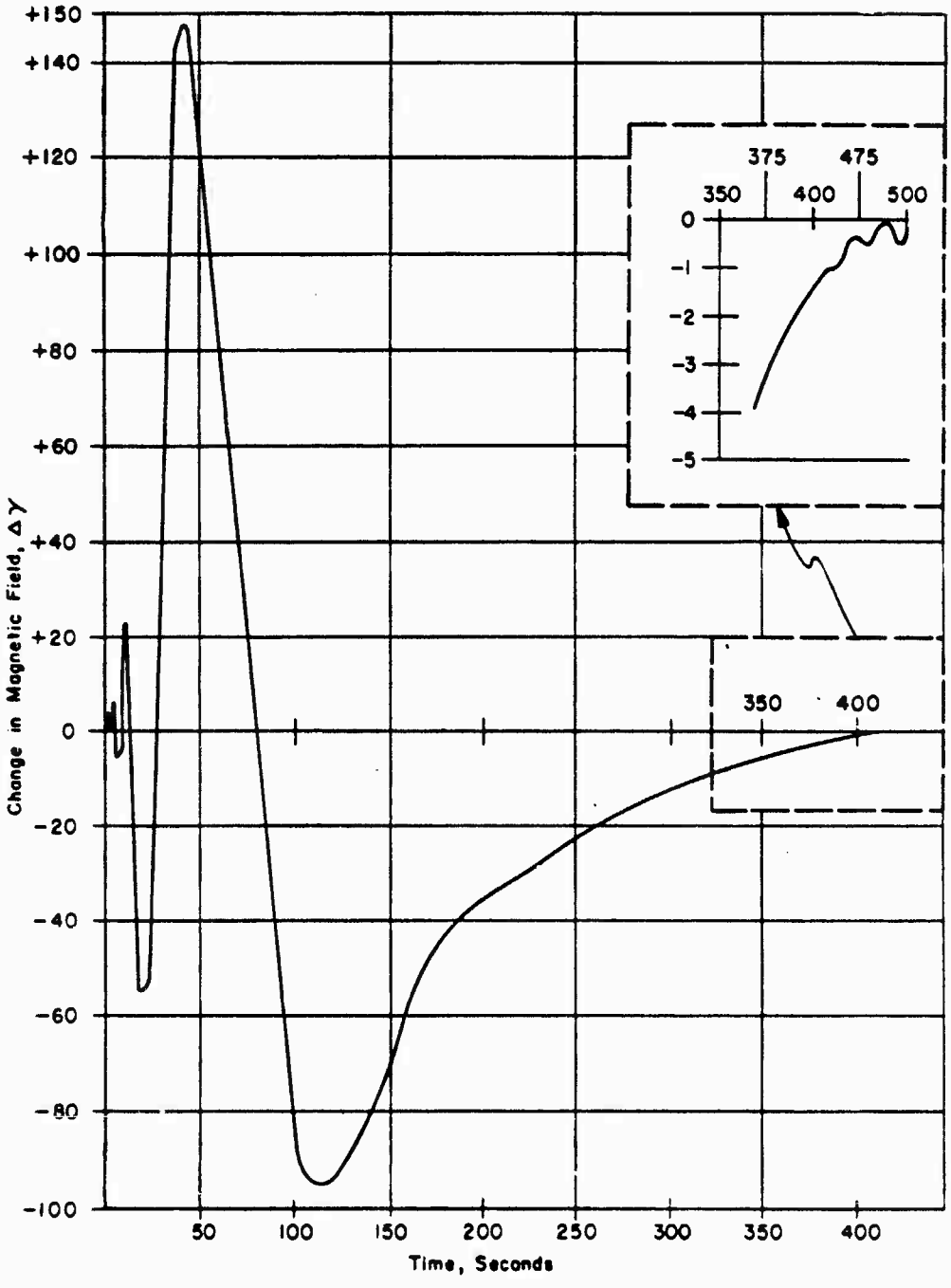

Figure 6.62 King Fish; magnetometer record of change in geomagnetic field at Johnston Island.

CHAPTER 7

TIGHT ROPE PHOTOGRAPHIC RESULTS

Tight Rope was detonated at 0730:00.0678 Z on 4 November 1962

head weight of 902 pounds. Planned and actual burst positions as given by Holmes & Narver, Inc., in Reference 25 are listed in the following summary.

	Planned	Actual
Latitude	16° 42' 04.14" N	16° 42' 26.71" N
Longitude	169° 32' 35.16" W	169° 32' 32.66" W

Further general information on Tight Rope may be found in Reference 26.

7.1 INSTRUMENTATION

7.1.1 Camera Parameters. Both the yield and altitude of Tight Rope limited the fireball to comparatively small dimensions and eliminated any auroral phenomena. Photographing details of a

small fireball requires long-focal-length lenses, which have small fields of view. This requirement was particularly appropriate for the Johnston Island Station. Long-focal-length lenses were also used on many cameras aboard the aircraft, but due to the error in burst altitude few records were obtained with these cameras aboard the aircraft.

Predictions of the radiance vs. time of Tight Rope were scaled from the Yucca shot as shown in Figure 7.1. In order to cover the large dynamic range in radiance of Tight Rope, the exposure values of the full complement of Project 8A.2 cameras were staggered in time and sensitivity. Figure 7.1 also illustrates how this was accomplished. The coverages of only five cameras as shown. The vertical (i.e., radiance) range on the graph of any camera is a function of the capabilities of the film used; saturation defines the upper end, and insensitivity the lower end. The coverage block assigned to any camera is shifted up or down depending upon parameters such as the frame rate, exposure time, f/number, and neutral density filters used. The horizontal extent of the coverage block is defined at the early time end by the interframe time (the left edge of the block being drawn one interframe time from zero) and at the late time end by the length of

film used in the camera.

The camera coverage from two stations is shown in the figure to illustrate how the cameras at various stations were interwoven to cover the full dynamic range and to provide backup in case of failure at any one station. Three of the cameras shown in the illustration used XR film, and from their coverage blocks it is easy to understand the usefulness of this film on nuclear detonations. The large exposure range of XR film can be used either to provide for great uncertainties in predicted radiance values, or to allow one camera to record for long periods of time even though large excursions in radiance may be taking place. Graphic plots similar to this were used to set exposures for all cameras on every event. For comparison purposes, radiance values of the sun, moon, and other natural phenomena are indicated in the figure.

The parameter settings for all cameras used on Tight Rope are given in Tables 7.1 through 7.3. Spectrograph parameters used on Tight Rope are given in Chapter 9. Section 2.6 provides a list of the abbreviations used for the various film types.

Where color film or conventional black-and-white films were used on intermediate-speed cameras, the exposure range of the film is quickly used up as the fireball radiance rapidly drops in value. A

typical intermediate-speed camera is the Mitchell camera which operates at 100 frames per second. If the camera is set to expose properly in the early frames, its exposure latitude is exhausted before a few seconds have elapsed. As an experiment on Tight Rope, the neutral density filters were removed and relative aperture opened to the lowest possible f/number within plus 20 seconds after zero time (Film No's. 97326 and 97327 from the Johnston Island Mitchell camera). This experiment worked quite successfully. The film was properly exposed at early times, ceased to be exposed after 5 seconds, and was again properly exposed after 20 seconds. A similar experiment was tried on the Maurer cameras on Johnston Island (Film No's 97319 and 97320) with equal success.

7.1.2 Aircraft Positions. The technique used by Projects 8A.1 and 8A.2 to determine the fixed elevation angles for the aircraft instruments had been formulated with Star Fish and Blue Gill in mind. The comparatively low altitude of Tight Rope and the fixed minimum elevation angles (25 degrees with respect to horizontal flight) posed extremely difficult requirements on the flight patterns that could be used. To have the aircraft fly in level flight using the lowest possible instrument elevation angles would have placed them within the danger zone surrounding Johnston Island. The best

compromise solution was based on the performance characteristics of the KC-135 aircraft. A plot was made of the turn radii as a function of bank angle and air speed. An overlay plot was then made of the elevation angle to the burst as a function of ground range to air zero. The family of solutions was found for the combination of bank angle and elevation angle which would allow the aircraft to maintain a continuous fixed angle of bank, while pointing the cameras to the burst and holding a constant radius from air zero. This approach gave two graphical solutions to the problem which were compatible with the fixed pointing angles provided by the camera mounts of the aircraft. The solution chosen was a 7-degree bank for the aircraft and the minimum (25-degree) elevation angle for the instruments. Figure 7. 2 portrays the aircraft positions and bank angle to accomplish the pointing to the predicted burst point at 25 kilometers.

The actual flight pattern flown by the aircraft on Tight Rope in an attempt to accomplish their mission is shown in Figure 7. 3. Strong winds hampered the attempts of the flight crews to maintain the conditions of constant bank and fixed radius from ground zero, necessitating slight departures in bank angle at times in their attempts to hold the constant radius. Nevertheless, had the burst occurred at

the altitude intended, success of the aircraft mission would have been achieved. Pertinent data regarding the aircraft positions at **H-hour** are given in Table 7.4. Both planned and actual values are shown.

7.1.3 Instrument Pointing. Although the Tight Rope detonation was 4 kilometers lower in altitude than planned, its actual azimuth and elevation angles from Johnston were close to the predicted values. This fortunate circumstance arose because the detonation occured within 10 degrees of the zenith at Johnston Island. The cameras located at the Johnston Island station were thus able to score a considerable success in recording the event. Very few early time records were obtained from the aircraft because of the error in burst altitude.

Figure 7.4 shows the fields of view of four Johnston Island cameras with relation to predicted and actual air zero. The fields of view are in a plane perpendicular to the optical axes of the cameras and passing through the predicted burst point. Table 7.5 lists the pertinent pointing information for the Johnston Island station.

Project 8A.2 was unable to obtain the vertical rise rate of the Tight Rope fireball and torus even though a small group of aircraft cameras collectively recorded the complete time history. The continuous banking maneuver of the aircraft rendered the gyro systems

inoperative, and as a consequence, no meaningful aircraft attitude data was obtained with which to correct for the roll of the aircraft. Because of high winds, the aircraft could not hold the planned 7-degree bank but was required to alter the bank angle over several degrees. Without knowledge of the precise bank angle as a function of time, it has been impossible to obtain rate-of-rise information.

7.2 RECORD SUMMARY

A summary of the Project 8A.2 records for Tight Rope is presented in Tables 7.6 through 7.8. This summary presents, in a brief form, pertinent comments on the films obtained from the two aircraft and from the Johnston Island Station. The Mauna Loa Station did not operate on Tight Rope, since no optical phenomena were expected to be visible from that site.

The statistical success in useful camera records achieved by Project 8A.2 on Tight Rope is summarized in Table 7.9. Of the 66 cameras which were operated at Johnston Island and on the two aircraft, 34 obtained useful records for a success of 51 percent. The largest single contribution to this poor showing was the error in burst location, which caused the aircraft to lose a high percentage of records.

7.3 PICTORIAL HISTORY

With the limited time available for preparation of this report it was impossible to apply quantitative data reduction procedures to all the phenomena of interest on Tight Rope. In order to provide information on all the observable features of the detonation, at least in a qualitative way, a pictorial evolutionary history is presented. The interpretation placed on any features previously unobserved on nuclear explosions is tentative and must await further study and deliberation before definite conclusions can be reached as to their physical nature, or as may be the situation in one case, it must be determined if there is instrumental influence on the records.

The Johnston Island KFC-600 camera recorded the earliest data taken by Project 8A.2 on Tight Rope. Figure 7.5 presents the six pictures recorded by this camera. The bright central core which appears in Frames 1, 2, and 6 is the isothermal sphere, growing by radiative diffusion during this time period. The exact time at which Frame 1 was taken is uncertain by approximately 0.1 microsecond, which time represents cable and electronic delays and delay in photoelectric triggering of a fiducial unit. The exposure time of each of these pictures is 0.1 microsecond, and the interframe time is 1.0 microsecond.

The dark narrow pie-shaped sector in the photographs is the rocket exhaust trail from the Nike-Hercules missile which delivered the warhead. Surrounding the core is a halo some 100 meters in diameter.

There are several possible explanations for the halo around the bright core in these six photographs. First of all, it could be an instrumental (i. e., false) image produced by the camera. If it is real, it could be due to one of many phenomena: thermal X-rays, ultraviolet photoexcitation of the air, scattering of fireball light from free electrons, photodissociation of ozone with radiative excitation, or even some combination of these phenomena. A more complete discussion of the probable source of the halo is presented in Section 7.4.

Both aircraft failed to obtain any records earlier than 1 millisecond on Tight Rope because of the large error in the altitude of the burst. Consequently, a time gap exists in the data from 5 microseconds to approximately 200 microseconds which would normally have been covered by the KFC-600 and Rapatronic cameras aboard the aircraft stations.

The next record in the Tight Rope time sequence was obtained by a Photo-Sonics 4C camera from Johnston Island, beginning at approximately 0.2 millisecond (with a typical uncertainty in zero time of $\pm$200 microseconds because of the interframe time). Eight frames of this record are presented in Figures 7.6 through 7.13. Exposure times are 10 microseconds for each frame.

A number of peculiar features are observed in the Photo-Sonics 4C camera record. In Frames 1, 2, and 3 (Figures 7.7, 7.8 and 7.9) for example, there are small but distinct protuberances scattered over the surface of the fireball. Similar disturbances appear on low-altitude fireballs at the time of separation of the cold air shock, but since the Tight Rope fireball is still in the hydrodynamic growth stage prior to shock separation, the origin of these protuberances is unknown.

Inside this circle is a bright core which has a small dark circle around it. The origin of these circles is an instability on the fireball surface associated with the Nike-Hercules rocket exhaust trail. The development of the instability is shown in a later sequence of photographs from Aircraft 60376.

In Figures 7.10 through 7.13 the continued growth of the fireball is shown by the same Photo-Sonics 4C record. Figure 7.13 (Frame 24) shows crater-like instabilities on the fireball surface in what appears to be a regular pattern.

Figures 7.14 through 7.21, taken by a Photo-Sonics 10B camera from Johnston Island, show the continued development of the Tight Rope fireball. Time resolution of these frames is 7.7 microseconds. At approximately 70 milliseconds, as determined from spectrographic records, the onset of fireball transparency began. Shortly thereafter, the debris cloud is seen within the fireball. Figure 7.16, taken at 96 milliseconds, and the remaining figures of this group show the irregular debris expansion.

On the original film records an outward-moving shock front is seen as early as 77 milliseconds, and an inward-moving shock is first apparent at 88 milliseconds. The shocks are difficult to reproduce from the original records because of the small brightness contrast between the shock front and the fireball. An outward-moving shock is clearly evident in Figure 7. 18, midway between the debris and the edge of the fireball at 169 milliseconds. This shock was the inward-moving shock, first seen at 88 milliseconds, having imploded on the origin and reflected outward again. In Figure 7. 19, at 185 milliseconds, this same outward-moving shock is almost coincident with the edge of the fireball. Contrasted to Blue Gill Triple Prime, there is no evidence of a reflection of this shock at the fireball surface, nor is there evidence of any other shocks after this shock disappears at 200 milliseconds. The fireball brightness diminishes rapidly with respect to the debris brightness after the disappearance of the last shock as seen in the remaining two frames of the Photo-Sonics 10B record (Figures 7. 20 and 7. 21).

A sequence of four color photographs taken from Johnston Island by a Maurer camera with an exposure setting of 0. 5 millisecond is shown in Figure 7. 22. Since the exposure latitude of

color film is short, the fireball was deliberately overexposed in the first few frames in order to expose it properly on later frames. By 1 second, (Frame 5) the exposure is normal, and the heated air within the fireball is seen to have pink color, while the weapon debris is white. Since colors are sometimes rendered distorted in the reproduction process, the reader is cautioned not to place great emphasis on the particular shades of color shown in these or subsequent photographs.

Figure 7.23 shows two frames of a Mitchell camera record taken from Johnston Island. These two pictures are interspersed in the time span of the previous four color photographs to show the fireball and debris under slightly larger magnification.

Figures 7.24 and 7.25 continue the sequence of Maurer pictures shown in Figure 7.22. The fireball rapidly changes from a spherical to toroidal shape during the 5- to 10-second period. Frames 46, 49, and 53 were inadvertently reproduced with a slightly larger magnification than the other nine photographs of this Maurer sequence. The reader is cautioned to allow for this disproportion in his study of these particular pictures. In the time period between 10 and 20 seconds it appears that the light emitted by the torus is predominantly

that of heated debris, whereas by 30 seconds the torus glow is due to beta-ray-induced air fluorescence.

The time period from 30 to 310 seconds is shown in Figure 7.26 which presents a series of time exposures taken by a cloud camera from Johnston Island. At 206 seconds (Frame 14) the torus is beginning to dissipate, and by 310 seconds (Frame 17) the dissipation of the torus is complete.

Figure 7.27 is a view of Tight Rope from Aircraft 53120 taken at 0.2 second by a Maurer camera. This picture is interesting in that the fireball has illuminated the surface of the ocean, and Johnston Island is visible directly beneath the burst. An engine nacelle of the aircraft is visible in the foreground.

The Tight Rope torus seen from Aircraft 60376 at 65 seconds is shown in Figure 7.28. The actual color of the torus at this time is blue-violet, but the color film is comparatively insensitive to the violet radiations.

Going back in time to the early growth of the Tight Rope fireball, the instability associated with the Nike-Hercules vapor trail will now be commented on. A sequence of eight photographs taken from Aircraft 60376 by a Photo-Sonics 10B camera is shown

in Figures 7.29 and 7.30. The exposure time of each frame is 7.7 microseconds, and the elevation angle to the burst from the aircraft is 18 degrees.

The instability is seen to be initially quite similar to the spikes which occur on sea level detonations where the spikes propagate along tower or balloon guy wires ahead of the fireball. Here however, there is no solid material involved, only the reaction products of the rocket exhaust. Close observation of the record reveals the presence of the instability as early as 1.4 milliseconds. At 3 milliseconds it is propagating at Mach 70 with respect to the ambient speed of sound. Until 25 milliseconds it has a solid appearance, but by 29 milliseconds it has become detached, with the shape of a glowing conical apex followed by a Mach cone. It continues to have the latter appearance for some 150 milliseconds after zero time, at which time it became too faint to photograph.

7.4 RESULTS

7.4.1 Geometric Measurements. Of the five Fish Bowl events, Tight Rope gave the least number of problems in defining the geometric dimensions of the photographically observable phenomena. This was due to the fact that the number of unusual physical phenomena were few, and the fireball had surface characteristics

not unlike the sharply defined features of surface detonations. Because of the low altitude the radiative and early hydrodynamic growth phases produced an opaque fireball with a well-defined boundary. No shock fronts excited the air external to the fireball to luminescence thereby lending any ambiguity to the interpretation of the geometric measurements. After formation of the debris torus, at late times, precise dimensional measurements became impossible because of the irregular cloud-like boundary of the ring.

Radius vs. time plots of the Tight Rope fireball and torus as measured from Johnston Island photographic records are given in Figures 7.31 and 7.32. The measurements cover the time period from 2×10^{-7} second to 90 seconds, and all values have been corrected for the vertical rise of the fireball during the 90-second time period.

Rate-of-rise information was impossible to determine on Tight Rope from the Johnston Island records because of the high elevation angle at which the shot was detonated. Furthermore, because of the error in burst position and the failure of the gyro systems aboard the two aircraft stations to indicate aircraft attitude while in a continuous bank, Project 8A.2 was unsuccessful

in obtaining altitude vs. time measurements on Tight Rope. From another aircraft operating in level flight at a greater distance from the event, an EG&G-LASL group (Reference 27) were able to obtain a rough altitude vs. time plot for Tight Rope which is shown in Figure 7.33. The altitudes shown refer to the top of the fireball and torus rather than to their centers. An initial rise rate of 0.17 km/sec was measured from this plot. At two minutes the rate of rise had dropped to 0.042 km/sec. Stabilization altitude was not reached during the 205-second time period over which the measurements were made.

The radar target provided by the photographically defined fireball and torus, in angular dimensions, as seen from Johnston Island is given in Figure 7.34 for the time period 10^{-1} second to 90 seconds. There is no photographic evidence of shock excitation or photo excitation of air external to the fireball which could create a larger radar target than is defined by the fireball and torus as shown in this figure.

7.4.2 Shock Waves. Two optical measurement techniques are available for determining when fireball transparency begins. The two techniques are fairly crude and do not necessarily agree.

One method relies on time-resolved spectrographic observations. By this method, transparency is said to begin at the time when the absorption line spectra which are superimposed on the fireball continuum change to omission spectra. This spectrographic technique seems to indicate a time when fireball transparency is well advanced, rather than the onset. On Tight Rope, the spectroscopic technique indicated transparency at 70 milliseconds, and shortly thereafter (Figure 7.35) internal shocks were photographed deep within the fireball. Bomb debris, however, was faintly discernible earlier at 50 milliseconds.

The second technique for determining the onset of fireball transparency relies on radiance measurements across the profile of the fireball. When limb darkening sets in, the trend toward transparency is assumed to have begun. Limb darkening began at about 30 milliseconds on the Tight Rope fireball. This latter technique seems to be a premature indicator for seeing to any significant depth within the fireball, since debris was not seen until 50 milliseconds, and internal shocks were not actually seen until 78 milliseconds. The radiance-profile technique probably indicates the onset of transparency, while the spectroscopic method indicates a more advanced stage.

Three shock waves were photographed which were internal to the Tight Rope fireball. No external shocks were made visible by the process of shock excitation of cold air, but two external shocks were clearly evident by refraction as they progressed down the XM-33 rocket exhaust trail.

It is not obvious that the three shocks shown in Figure 7.35 are in any way related, although the shock labelled No. 3 may possibly be the reflected shock created by Shock No. 2 which imploded on the origin. No attempt has been made to classify the shock by the physical processes which gave rise to them. It seems likely, however, that all three shocks are related to the original debris shock created by the snowplowing of air by bomb debris.

Shock waves are manifested by the behavior of the fireball surface even when the shock fronts themselves are not apparent. One usual effect of a shock front as it passes through the surface of the fireball is an accompanying increase in the fireball radius. Such an increase is apparent at the time Shock No. 1 passes through the fireball surface. An increase in fireball radius does not always accompany the passage of a shock through the fireball surface, however, as may be witnessed in the case of Shock No. 3. In the case of the two shocks in question it is difficult to understand

why Shock No. 1 increased the fireball radius and Shock No. 3 did not, since Shock No. 3 is obviously the stronger of the two having an average velocity in the neighborhood of 2600 meters/sec as opposed to 1500 meters/sec for Shock No. 1.

Another observable effect accompanies the passage of a shock wave through the fireball surface; a marked brightening occurs as the shock front reaches the surface. In the case of Tight Rope, surface brightening accompanied both Shocks No. 1 and No. 3.

The passage of shocks through bomb debris is also easily observed by the increased brightening of the debris as the shock passes through it.

7.4.3 Vapor Trail Instability. The physical process by which the vapor trail instability (Figures 7.29 and 7.30) was created and the mechanism by which it propagates are unknown at this time. The underlying cause appears to be hydrodynamic rather than radiative in nature, since the instability detaches completely from the fireball.

Figure 7.36 gives the position of the vertex of the instability as a function of time. Two positions are shown, one related to the fireball surface, the other to the fireball center. Velocities of the vertex with respect to a reference frame situated at the center

of the fireball are indicated in the figure.

Under the assumption that the air in the vicinity of the fireball exterior has not been heated or otherwise disturbed, the speed of the vertex is supersonic for the entire time period during which it was photographed.

7.4.4 Early Time Veil. It was first thought that the veil phenomena seen in the KFC-600 pictures during the first 5 microseconds of Tight Rope (Figure 7.5) was not real; rather it was attributed to light leakage by the Kerr cell shutters which are used with that camera. The Kerr cell shutters transmit a small amount of light in the crossed position; thus, it was thought that the halo could represent light emanating from the fireball at a later time (up to 500 microseconds) when the size was much greater. At 500 microseconds a magneto-mechanical shutter positively caps the lens. This explanation is still a remote possibility, but on the basis of other evidence we are now inclined to favor the probability that the veil is real.

Similar halos are clearly evident on Blue Gill Triple Prime, not only on two KFC-600 cameras but on many Photo-Sonics 4C cameras and Rapatronic cameras as well. Leakage is an impossible cause of the halo (or veil) in these latter two types of cameras.

The veil was not observed on the much smaller number of Rapatronic and Photo-Sonic cameras which observed the burst on Tight Rope. There is a reasonable explanation however. Not all cameras observed the halos on Blue Gill either. Whether or not it was observed was function of the exposure time. The radiance-time history of Tight Rope is not so different from that of Blue Gill Triple Prime that it would have caused light leakage where Blue Gill Triple Prime did not.

The Tight Rope veil is some 50 meters in radius, and in appearance, not unlike the X-ray veil accompanying the surface detonation of high yield to mass ratio nuclear devices. A hard thermal X-ray component is responsible for the veil observed on surface detonations, where the hard X-rays are a result of very high case temperatures (of the order of 1.5 kev).

Rough calculations demonstrate that it is virtually impossible to attribute

the Tight Rope veil to any hard component of even the 0.3-kev case temperature. Only an insignificant amount of X-ray energy could have penetrated to 50 meters from a device of that temperature.

It is suggested that a photo-excitation or photo-dissociation process was responsible for the Tight Rope veil, and that ozone may possibly have played a role in its formation, since the detonation occurred in the bottom third of the ozone layer. Whatever its origin, it was semi-transparent for the first microsecond, almost opaque from 2 to 4 microseconds, and semi-transparent again at 5 microseconds. During the 2- to 4- microsecond time period, the bright isothermal sphere is only barely distinguishable, indicating that a continuum wavelength absorption mechanism was present in the veil.

7.4.5 Radiometric Measurements. The early time radiometric history of Tight Rope suffered considerably, as did all the early time Tight Rope measurements, through lack of data caused by the error in burst position. Figure 7.37 gives the radiance time history of the fireball and debris from 10^{-7} second to 200 seconds. These are composite curves representing measurements taken from the records of many cameras. A

significant gap exists in the data between 5 and 200 microseconds which would have been filled by the KFC-600 camera aboard Aircraft 53120 had the burst not been low. An interpolation of data from adjoining records has been extended through the time period for which data is missing. There is no reason to believe that the interpolated curve actually represents the behavior of the Tight Rope fireball during this time period. In fact it is quite likely that a slight radiance minimum occurs as evidenced by the Yucca data (Figure 7.1).

Radiance measurements were performed at three distinct points on each of the Tight Rope fireball records beginning at 200 microseconds: the center of the fireball, one-half of the fireball radius, and two-thirds of the fireball radius. No differences were observed until approximately 4 milliseconds when the center of the fireball showed a slight drop in radiance compared to measurements at the other two points.

Beginning at 200 microseconds photographic data points exist at 400-microsecond intervals. Because of the small number of data points from 200 microseconds to 1 millisecond, details of a slight radiance maximum during that time period could not be realized from the photographic data. A streak spectrograph record from Aircraft 60376 was used to fill in the missing information. After 1 millisecond

a sufficient number of data points exists to determine a precise radiance-time history for Tight Rope.

For part of the time span (30 to 50 milliseconds) during which fireball transparency set in and was completed (50 to 70 milliseconds) it was difficult to perform the fireball radiance measurement at two-thirds of the radius and avoid contamination of the measurement with radiance from the debris. The dotted line in Figure 7.37 during this time period indicates the best estimate of radiance values for this time period. After 50 milliseconds when the debris was distinguishable, the radiance values shown are those of heated air with no contribution from debris. Once the debris was distinguishable, the one-half radii measurements were shifted to follow the behavior of a particular protuberance of debris.

The radiance behavior of bomb debris at the times that shock fronts are approaching the surface of the fireball is unusual. Shock fronts are seen (Figure 7.35) approaching the surface at approximately 1 and 2 milliseconds. Radiance values of the debris show a marked drop just prior to these times with an increase shortly thereafter. At 2 milliseconds this effect may be due to the increased radiance values of the fireball, but this

does not explain the situation at 1 millisecond where no such increase in fireball radiance is observed.

After 8 seconds it was impossible to obtain separate measurements of heated air and debris. From that time on to the end of the measurements, only the outer debris radiance values were obtained, since the debris torus evolved in that region.

7.4.6 Brightness Temperature, Radiant Power, and Thermal Yield. The brightness temperature of the Tight Rope fireball and debris were derived from the measured radiance values using the same assumptions made in Section 5.4.4 for Blue Gill Triple Prime. Figures 7.38 through 7.40 show the Tight Rope brightness temperature vs. time for both fireball and debris.

The debris brightness temperature curve starts at 25 milliseconds at the onset of fireball transparency. This curve was derived from the radiance data appropriate to bomb debris near the fireball edge rather than the center (see Figure 7.37). At 1 second, the fireball has a brightness temperature of 2400°K, and the debris temperature is 2950°K. True temperatures can be derived using appropriate values of emissivity and air density within the fireball.

The low values of brightness temperature during the first 30 microseconds after the detonation are attributed to the veil which obscured the isothermal sphere.

The radiant power in various spectral bandwidths, derived under the same assumptions used on Blue Gill Triple Prime, are presented in Figure 7.41. The photographic power radiated was calculated for the bandwidth (4000 Å) appropriate to the response of the camera system used in making the measurements. Similarly, the visible power radiated was based on the visible bandwidth (4000 Å to 7400 Å).

These values represent the total visible energy leaving the fireball. Any application of these results relative to sea level conditions must take into account atmospheric and ozone attenuation. Tight Rope occurred so that the usual attenuation coefficients for the ozone layer should be modified accordingly.

Because Tight Rope took place in the ozone layer, the short wavelength cutoff for the thermal power bandwidth was

dictated by ozone absorption coefficients rather than those of diatomic molecular oxygen. In determining the wavelength mean free path equal to one scale height, 10^{12} ozone molecules/cm^3 was assumed. The actual number of ozone molecules at an altitude varies with latitude and with the seasons of the year. The wavelength with a mean free path equal to one scale height was found to be approximately 2900 Å. This wavelength is also the cutoff for solar radiation passing through the ozone layer. The cutoff wavelength in the downward direction is probably much shorter, since the burst occurred low in the ozone layer. Spectrograms obtained on Tight Rope (Chapter 9) indicate that wavelengths well below 2900 Å were recorded on Johnston Island. The upper thermal bandwidth limit was taken at 10,000 Å.

Figure 7.41 shows the thermal power between the wavelength limits of (2900 Å and 10,000 Å) as a function of time, for Tight Rope. A sphere of radius equal to the measured values shown in Figures 7.31 and 7.32 was assumed to represent the fireball at all times. After a few seconds, when the toroidal shape began to develop, this assumption was no longer valid. The thermal power values at late times are rendered higher than they

should be by the assumed spherical shape. The error does not affect the total thermal yield derived from this curve,however, since the contribution at late times is insignificant.

TABLE 7.1 SUMMARY OF TIGHT ROPE CAMERA PARAMETERS, AIRCRAFT 53120

INSTRUMENT AND STATION POSITION		FILM TYPE	FILM NUMBER	AIMING ANGLES IN DEGREES ELEV	AZIMUTH	FILTERS ND	COLOR	FOCAL LENGTH MM	LENS F/N	FRAMES PER SECOND	SHUTTER SECTOR, DEGREES	EXPOSURE TIME	MARKER RATE CPS
MAURER	W1	DXN	97122	30	0	-	-	38	5.6	5.5	-	0.5MSEC	-
MAURER	W2	FDER	97121	27	0	-	-	38	8	5.5	-	1MSEC	-
PHOTO-SONICS 10 B	W5	FDER	97127	25	0	2.0	-	135	22	360	1	7.7MUS	200
KFC-600	W6	XR	97104	25	0	-	WR12	301	9.5	50000	-	1MUOEC	-
RAPATRONIC	W7	XR	97103	25	0	-	-	482	22	*(A)	-	5MUSEC	-
TRAID	W8	PX	97117	30	0	1.0	-	25	8	48	7	0.4MSEC	50
TRAID	W9	FDER	97118	30	0	1.0	-	25	16	48	7	0.4MSEC	50
CLOUD	W10	DXN	97109	45	0	-	-	105	3.7	0.2	-	0.5SEC	CLOCK
FAIRCHILD HS-100	W11B	KDI	97123	25	0	2.0	-	13	16	1000	-	0.2MSEC	50
GSAP N6	W11A	KDII	97124	25	0	1.0	-	9.5	22	64	133	5.8MSEC	-
PHOTO-SONICS 4C	W12	XR	97125	25	0	-	-	80	11	2500	9	10MUSEC	200
CLOUD	W13	FDER	97110	45	0	-	-	105	3.7	0.2	-	0.5SEC	CLOCK
ROBOT	W15	RXP	97111	50	0	-	3914A	45	2.8	*(B)	-	250MSEC	-
ROBOT	W16	RXP	97112	50	0	-	4278A	45	2.8	*(B)	-	250MSEC	-
ROBOT	W17	RXP	97113	50	0	-	4709A	45	2.8	*(B)	-	250MSEC	-
TRAID	W18	FDER	97119	55	0	-	-	25	2.3	16	160	28MSEC	10
TRAID	W19	XR	97120	55	0	-	-	25	8	16	160	28MSEC	10
ROBOT	W21	FDER	97114	70	0	-	-	45	2.8	*(B)	-	250MSEC	-
ROBOT	W22	RXP	97115	70	0	-	5577A	45	2.8	*(B)	-	250MSEC	-
ROBOT	W23	RXP	97116	70	0	-	6300A	45	2.8	*(B)	-	125MSEC	-
PHOTO PANEL CAMERA	PANEL	PX	97131	-	-	-	-	25	16	1	160	30MSEC	CLOCK
PHOTO PANEL CAMERA	PANEL	PX	97132	-	-	-	-	25	16	0.2	160	30MSEC	CLOCK

* (A) SINGLE EXPOSURE AT 510 MUSEC.
* (B) 1 FR/SEC FOR ABOUT 1 MIN. THEN 1/2 FR/SEC TO END.
N.B. MUSEC = MUS = MICROSECOND

TABLE 7.2 SUMMARY OF TIGHT ROPE CAMERA PARAMETERS, AIRCRAFT 60376

)NSTRUMENT AND STATION POSITION		FILM TYPE	FILM NUMBER	A)MING ANGLES IN DEGREES ELEV	AZ!MUTH	FILTERS ND	COLOR	FOCAL LENGTH MM	LENS F/N	FRAMES PER SECOND	SHUTTER SECTOR, DEGREES	EXPOSURE TIME	MARKER RATE CPS
BEATTIE-COLEMAN	W1	EDER	97221	30	0	-	-	105	11	*(A)	-	*(B)	-
BEATTIE-COLEMAN	W2	DXN	97222	30	0	-	-	105	5.6	*(A)	-	*(B)	-
RAPATRONIC	W3	XR	97205	25	0	1.0	WR12	490	22	*(F)	-	5MUSEC	-
PHOTO-SON)CS 10 B	W5	PX	97227	25	0	1.0	-	180	22	360	1	7.7MUS	200
RAPATRON)C	W6	XR	97204	25	0	1.0	WR12	490	22	*(G)	-	5MUSEC	-
RAPATRONIC	W7	XR	97203	25	0	1.0	WR12	490	22	*(H)	-	5MUSEC *(H)	-
FLIGHT RESEARCH-C)NE	W8	EDER	97217	30	0	-	-	35	22	20	130	18MSEC	10
FLIGHT RESEARCH-C)NE	W9	XR	97218	30	0	-	-	35	5.6	20	130	18MSEC	10
RAPATRONIC	W)0	XR	97223	25	0	1.0	WR12	490	22	*(J)	-	5MUSEC	-
BEATTIE-COLEMAN	W11	EDER	97209	45	0	-	-	105	5.6	*(C)	-	*(D)	-
PHOTO-SONICS 4C	W12	EDER	97226	25	0	2.0	-	108	16	2500	9	10MUSEC	200
BEATTIE-COLEMAN	W13	DXN	97210	45	0	-	-	105	3.5	*(C)	-	*(D)	-
PHOTO-SON)CS 4C	W14	PX	97225	25	0	2.0	-	108	16	2500	9	10MUSEC	200
FL)GHT RESEARCH-C)NE	W15	PX	97219	50	0	-	-	35	22	20	130	18MSEC	10
FLIGHT RESEARCH-CINE	W16	EDER	97220	50	0	-	-	35	11	20	130	18MSEC	10
FLIGHT RESEARCH-PULSED	W17	PX	97211	50	0	-	3914A	35	2.3	*(E)	130	1SEC	-
FLIGHT RESEARCH-PULSED	W18	RXP	97212	50	0	-	4278A	35	2.3	*(E)	130	1SEC	-
FLIGHT RESEARCH-PULSED	W19	RXP	97213	50	0	-	4709A	35	2.3	*(E)	130	1SEC	-
FL)GHT RESEARCH-PULSED	W20	RXP	97214	50	0	-	5577A	35	2.3	*(E)	130	1SEC	-
FLIGHT RESEARCH-PULSED	W21	RXP	97215	50	0	-	6300A	35	2.3	*(E)	130	1SEC	-
PHOTO PANEL CAMERA	PANEL	PX	97231	-	-	1.0	-	25	5.6	1	160	30MSEC	CLOCK
PHOTO PANEL CAMERA	PANEL	PX	97232	-	-	1.0	-	25	5.6	0.2	160	30MSEC	CLOCK

* (A) 1 FR/SEC, 0.5 FR/SEC, 0.2 FR/SEC, 0.1 FR/SEC, UP TO +10 SEC, +60 SEC, +)80 SEC, +1800 SEC, RESPECT)VELY.
* (B) 0.5 SEC, 1.5 SEC, 4.5 SEC, 9.5 SEC, UP TO +10 SEC, +60 SEC, +180 SEC, +)800 SEC, RESPECTIVELY.
* (C) 1 FR/SEC, 0.2 FR/SEC, 0.1 FR/SEC UP TO +10 SEC, +180 SEC, +1800 SEC, RESPECTIVELY.
* (D) 0.5 SEC, 4.5 SEC, 9.5 SEC UP TO +10 SEC, +180 SEC, +)800 SEC, RESPECTIVELY
* (E) 1 FR/SEC UP TO 60 SEC, THEN 1/3 FR/SEC TO END.
* (F) SINGLE EXPOSURE AT 14 MUSEC.
* (G) SINGLE EXPOSURE AT 52.4 MUSEC.
* (H) SINGLE EXPOSURE AT 103.4 MUSEC.
* (J) SINGLE EXPOSURE AT 256.2 MUSEC.

N.B. MUSEC - MUS - MICROSECOND

TABLE 7.3 SUMMARY OF TIGHT ROPE CAMERA PARAMETERS, JOHNSTON ISLAND

INSTRUMENT AND STATION POSITION		FILM TYPE	FILM NUMBER	AIMING ANGLES IN DEGREES ELEV	AZIMUTH	FILTERS ND	COLOR	FOCAL LENGTH MM	LENS F/N	FRAMES PER SECOND	SHUTTER SECTOR, DEGREES	EXPOSURE TIME	MARKER RATE CPS
KFC-600	A1	XR	97304	BURST		-	WR12	301	9	1000000	-	0.1MUSEC	-
PHOTO-SONICS 4C	A2	EDER	97324	BURST		ND2	-	250	32	2500	9	10MUSEC	200
PHOTO-SONICS 4C	A3	XR	97323	BURST		ND1	-	360	22	2500	9	10MUSEC	200
PHOTO-SONICS 10B	A4	PX	97325	BURST		ND2	-	500	16	360	1	7.7MUS	50
RAPATRONIC	A5	XR	97303	BURST		-	WR12	482	20	*(A)	-	5MUSEC	-
MAURER	A7	DXN	97319	BURST		ND2	-	150	11	5.5	-	0.5MSEC	-
MAURER	A8	EDER	97320	BURST		*(E)	-	150	8	5.5	-	0.5MSEC	-
TRAID	A9	PX	97317	BURST		-	-	35	8	48	7	0.4MSEC	10
MITCHELL	A10	PX	97326	BURST		*(D)	-	105	*(D)	100	15	0.4MSEC	50
FAIRCHILD HS-100	A12	KDI	97321	BURST		ND3	-	13	16	650	-	.3MSEC	50
GSAP	A13	KDII	97322	BURST		-	-	9.5	2.2	16	133	23MSEC	-
KC-18	A14	TXA	97332	BURST		-	-	152	6.3	*(B)	-	*(C)	-
CLOUD	C1	EDER	97309	BURST		-	-	105	3.7	*(B)	-	*(C)	CLOCK
CLOUD	C2	DXN	97310	BURST		-	-	105	3.7	*(B)	-	*(C)	CLOCK
TRAID	C3	XR	97318	BURST		-	-	35	2.3	16	160	0.028SEC	10
MITCHELL	C4	KDII	97327	BURST		*(D)	-	150	*(D)	100	15	0.4MSEC	50
BELL AND HOWELL	C5	EDER	97329	BURST		-	-	35	8	12	160	0.037SEC	10
MITCHELL LS	C6	EDER	97328	BURST		-	-	18.5	2.2	2.5	170	0.2SEC	10
ROBOT	C7	RXP	97311	BURST		-	4278A	45	2.8	*(B)	-	*(C)	-
ROBOT	C8	RXP	97312	BURST		-	4709A	45	2.8	*(B)	-	*(C)	-
ROBOT	C9	RXP	97313	BURST		-	5228A	45	2.8	*(B)	-	*(C)	-
ROBOT	C11	RXP	97314	BURST		-	6300A	45	2.8	*(B)	-	*(C)	-
ROBOT	C12	RXP	97315	BURST		-	3914A	45	2.8	*(B)	-	*(C)	-
DYNAFAX	D1	MF	97335	BURST		-	-	813	9	25000		1MUSEC	2000
DYNAFAX	D2	MF	97336	BURST		-	-	76	2.8	25000		5MUSEC	2000
ROBOT	OUTSIDE	EDER	97334	VARIABLE		-	-	45	2.8	*(B)	-	*(C)	-

* (A) SINGLE EXPOSURE AT 936 MUSEC.
* (B) 1/3 FR/SEC FROM -30 SEC TO +30 SEC, THEN 30-SEC EXPOSURE TO END.
* (C) 1-SEC EXPOSURE FROM -30 SEC TO +30 SEC, THEN 30-SEC EXPOSURE TO END.
* (D) ND-2 AND F/22 FROM -5 SEC TO +20 SEC, NO ND AND F/2.3 FROM +20 SEC TO END
* (E) ND-2 FROM -5 SEC TO +20 SEC, NO ND FROM +20 SEC TO END.

N.B. MUSEC = MUS = MICROSECOND

TABLE 7.4 TIGHT ROPE H-HOUR AIRCRAFT POSITIONS

	Planned Values		Actual Values	
	Aircraft 60376	Aircraft 53120	Aircraft 60376	Aircraft 53120
Latitude	16° 44' N	17° 05' N	16° 42' N	17° 05' 15" N
Longitude	169° 09' W	169° 35' W	169° 08 W	169° 33' 30" W
Magnetic Heading	165°	075°	175.2°	075.7°
Altitude (feet)	37,500	37,500	37,500	37,500

TABLE 7.5 POINTING INFORMATION FOR JOHNSTON ISLAND, TIGHT ROPE

Station Location:	Latitude 16° 44' 04.79" N
	Longitude 169° 31' 36.59" W

TABLE 7.6 SUMMARY OF TIGHT ROPE FILM RECORDS, AIRCRAFT 53120

FILM NUMBER	FILM TYPE	CAMERA	RESULTS
97103	XR	RAPATRONIC	NO RECORD.
97104	XR	KFC-600	NO RECORD.
97109	DXN	CLOUD	BURST OCCURS OUTSIDE FIELD. AT LATER TIMES TORUS SHOWS AT BOTTOM OF FRAME.
97110	EDER	CLOUD	NO RECORD.
97111	RXP	ROBOT	SEVEN FRAMES RECORDED.
97112	RXP	ROBOT	INITIAL FLASH DISSIPATES AFTER EIGHT FRAMES.
97113	RXP	ROBOT	INITIAL FLASH DISSIPATES AFTER TWELVE FRAMES.
97114	EDER	ROBOT	NO RECORD.
97115	RXP	ROBOT	INITIAL FLASH DISSIPATES AFTER FIVE FRAMES.
97116	RXP	ROBOT	INITIAL FLASH DISSIPATES AFTER EIGHT FRAMES.
97117	PX	TRAID	61 FEET OF RECORD. BURST IN LOWER RIGHT CORNER. TOROID FORMS AND SMALL VORTEX RING OBSERVED.
97118	EDER	TRAID	SMALL IMAGE, OVEREXPOSED INITIALLY. SHOWS FORMATION OF TORUS.
97119	EDER	TRAID	NO RECORD.
97120	XR	TRAID	POOR RECORD.
97121	EDER	MAURER	FIRST TWO FRAMES SHOW JOHNSTON ISLAND ILLUMINATED BY BURST.
97122	DXN	MAURER	LONG RECORD. BURST OCCURS IN LOWER RIGHT CORNER. SOME GROWTH AND TORUS FORMATION OBSERVED.
97123	KDI	FAIRCHILD HS-1DO	VERY SMALL IMAGE.
97124	KDII	GSAP	VERY SMALL IMAGE.
97125	XR	PS-4C	NO RECORD.
97127	EDER	PS-10B	NO RECORD.

TABLE 7.7 SUMMARY OF TIGHT ROPE FILM RECORDS, AIRCRAFT 60376

FILM NUMBER	FILM TYPE	CAMERA	RESULTS
97203	XR	RAPATRONIC	NO RECORD.
97204	XR	RAPATRONIC	NO RECORD.
97205	XR	RAPATRONIC	NO RECORD.
97209	EDER	BC	ONLY A FEW FRAMES SHOWING TORUS. BLURRED BY AIRCRAFT MOTION.
97210	DXN	BC	RECORD NOT VERY USEFUL. ONLY A FEW FRAMES SHOW TORUS.
97211	RXP	FR-PULSED	SMALL IMAGE. TORUS AND VORTEX RING FORMATION OBSERVED.
97212	RXP	FR-PULSED	BURST OCCURRED OUTSIDE FIELD. TORUS, AND LATER, CLOUD OBSERVED.
97213	RXP	FR-PULSED	NO USEFUL RECORD.
97214	RXP	FR-PULSED	NO USEFUL RECORD.
97215	RXP	FR-PULSED	NO USEFUL RECORD.
97217	EDER	FR-CINE	FAIR RECORD SHOWING TORUS, OVER-EXPOSED ON EARLY FRAMES.
97218	XR	FR-CINE	GOOD RECORD FOR 100 SECONDS.SHOWS TORUS FORMATION AND GROWTH.
97219	EDER	FR-CINE	POOR RECORD, SMALL IMAGE. BLURRED DUE TO AIRCRAFT MOTION. 50 FRAMES.
97220	PX	FR-CINE	NO RECORD.
97221	EDER	BC	POOR RECORD, ABOUT 24 FRAMES. INITIAL FRAMES OVER EXPOSED.
97222	DXN	BC	TWELVE FRAMES OF TORUS DEVELOPMENT.
97223	XR	RAPATRONIC	NO RECORD.
97225	PX	PS-4C	500 FEET OF RECORD. BURST AT BOTTOM OF FRAME. CENTRAL CORE AND DEBRIS OBSERVED THPOUGH EXPANDING TRANSPARENT FIREBALL.
97226	EDER	PS-4C	NO RECORD.
97227	PX	PS-10B	FIREBALL GROWTH AND DEBRIS.

TABLE 7.8 SUMMARY OF TIGHT ROPE FILM RECORDS, JOHNSTON ISLAND

FILM NUMBER	FILM TYPE	CAMERA	RESULTS
97303	XR	RAPATRONIC	GOOD FIREBALL RECORD.
97304	XR	KFC-600	EXCELLENT SEQUENCE OF PICTURES.
97309	EDER	CLOUD	SEVERAL GOOD LATE-TIME PICTURES SHOWING TORUS GROWTH.
97310	DXN	CLOUD	GROWTH OF TORUS OBSERVED. FIRST FRAMES OVER-EXPOSED.
97311	RXP	ROBOT	TWENTY-FIVE FRAMES SHOWING TOROID GROWTH AND BREAK-UP. 4278 A FILTER.
97312	RXP	ROBOT	EIGHT FRAMES SHOWING GROWTH OF VORTEX RING. 4709 A FILTER.
97313	RXP	ROBOT	TWELVE FRAMES SHOWING GROWTH OF VORTEX RING. 5228 A FILTER.
97314	RXP	ROBOT	TEN FRAMES SHOWING TORUS GROWTH. 6300 A FILTER.
97315	RXP	ROBOT	THIRTY-SIX FRAMES SHOWING GROWTH OF TORUS. 3914 A FILTER.
97317	PX	TRAID	90 FEET OF RECORD SHOWING FIREBALL GROWTH, BREAKUP, AND TOROID DEVELOPMENT.
97318	XR	TRAID	EXCELLENT RECORD SHOWING TORUS FORMATION AND GROWTH. OVEREXPOSED INITIALLY.
97319	DXN	MAURER	118 FRAMES SHOWING GROWTH OF FIREBALL AND TORUS.
97320	EDER	MAURER	GOOD RECORD SHOWING TORUS.
97321	KD I	FAIRCHILD HS-100	VERY SMALL FIREBALL IMAGE.
97322	KDII	GSAP	GOOD LATE-TIME RECORD. OVEREXPOSED INITIALLY.
97323	XR	PS-4C	EXCELLENT RECORD.
97324	EDER	PS-4C	EXCELLENT RECORD.
97325	PX	PS-10B	EXCELLENT RECORD OF FIREBALL GROWTH.
97326	PX	MITCHELL	230 FEET OF RECORD SHOWING FIREBALL TRANSPARENCY, DEBRIS, AND TOROID FORMATION.
97327	KDII	MITCHELL	17 FEET OF RECORD SHOWING FIREBALL SHOCK, DEBRIS, DEBRIS SHOCK, AND HOT CENTRAL CORE.
97328	EDER	MITCHELL	FAIR RECORD SHOWING TORUS AFTER FORMATION, OVEREXPOSED ON EARLIER FRAMES.
97329	EDER	B AND H	EARLY TIME FRAMES OVEREXPOSED. LATE TIMES SHOW TORUS GROWTH. SMALL IMAGE.
97332	TXA	KC-1	POOR IMAGES. BLURRED DUE TO FILM MOTION DURING EXPOSURE TIME.
97334	EDER	ROBOT	NO RECORD.
97335	MF	DYNAFAX	NO RECORD.
97336	MF	DYNAFAX	WEAK EXPOSURE. SMALL BUT GOOD IMAGE.

TABLE 7.9 STATISTICAL SUMMARY OF TIGHT ROPE CAMERA RECORDS FROM THE BURST AREA

Station	J-820	Aircraft 53120	Aircraft 60376	Totals
Number of Cameras	26	20	20	66
Number of Useful Records	24	5	5	34
Reasons for No Records:				
Mechanical failure	1	2	0	3
Inappropriate camera parameters	0	0	0	0
Error in shot location	1	5	6	12
Reasons for Poor Records:				
Inappropriate camera parameters	0	2	0	2
Error in shot location	0	6	9	15
Other	0	0	0	0
Percent Success	92	25	25	—
Overall Success: 51 percent				

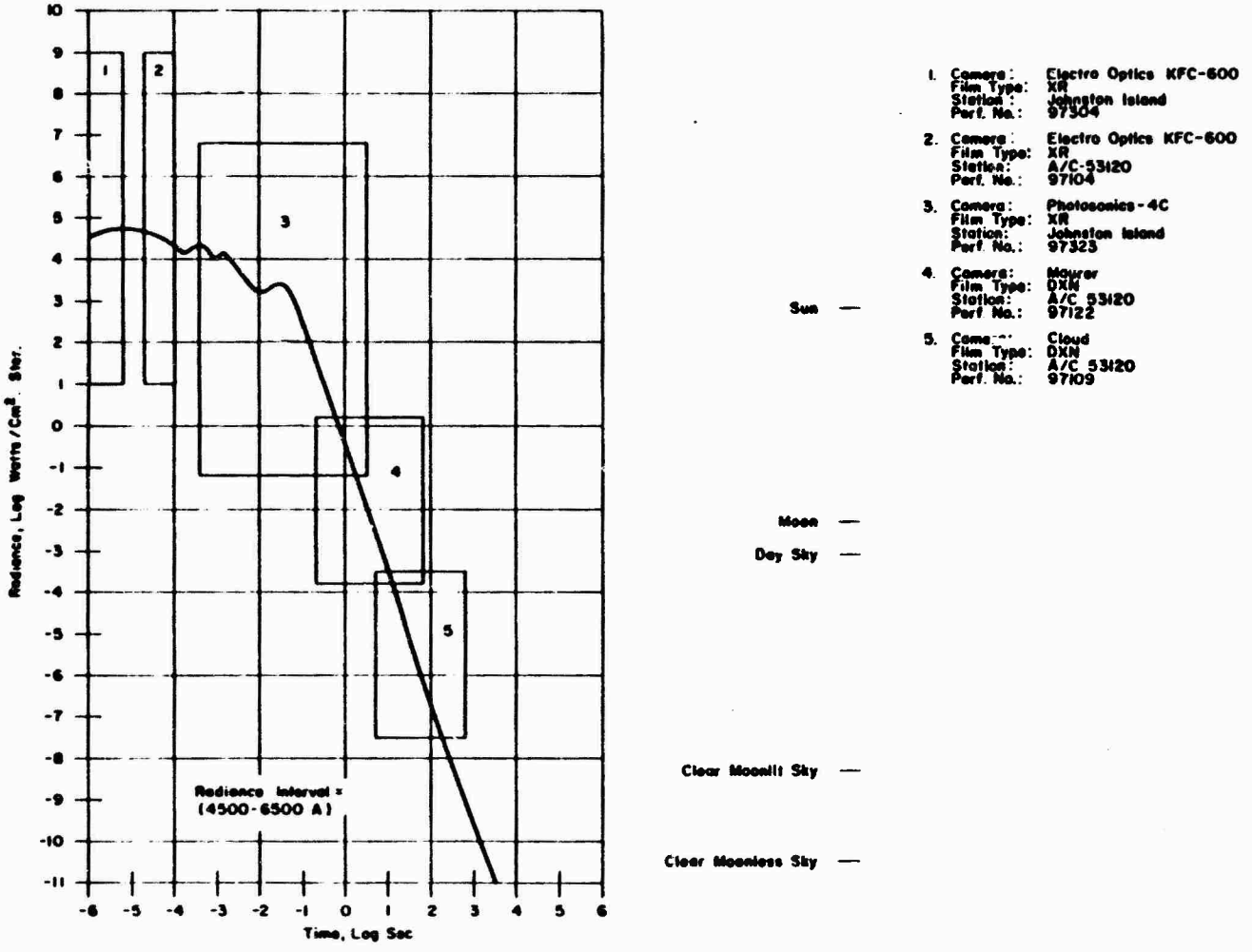

Figure 7.1 Predicted radiance versus time for Tight Rope, and the photographic coverages provided by five Project 8A.2 cameras.

Page 428 deleted.

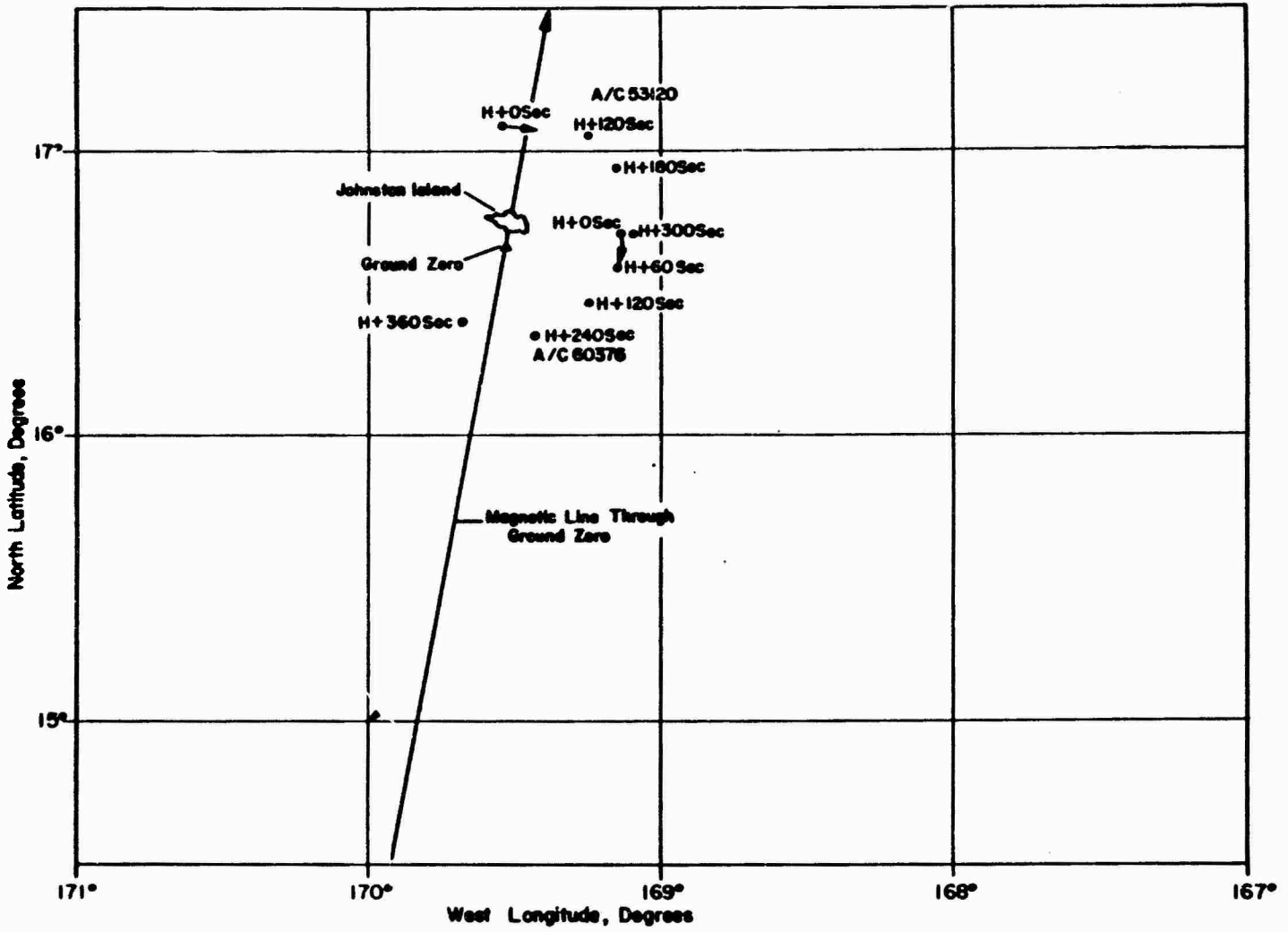

Figure 7.3 Aircraft flight paths from H-hour to + 6 minutes, Tight Rope.

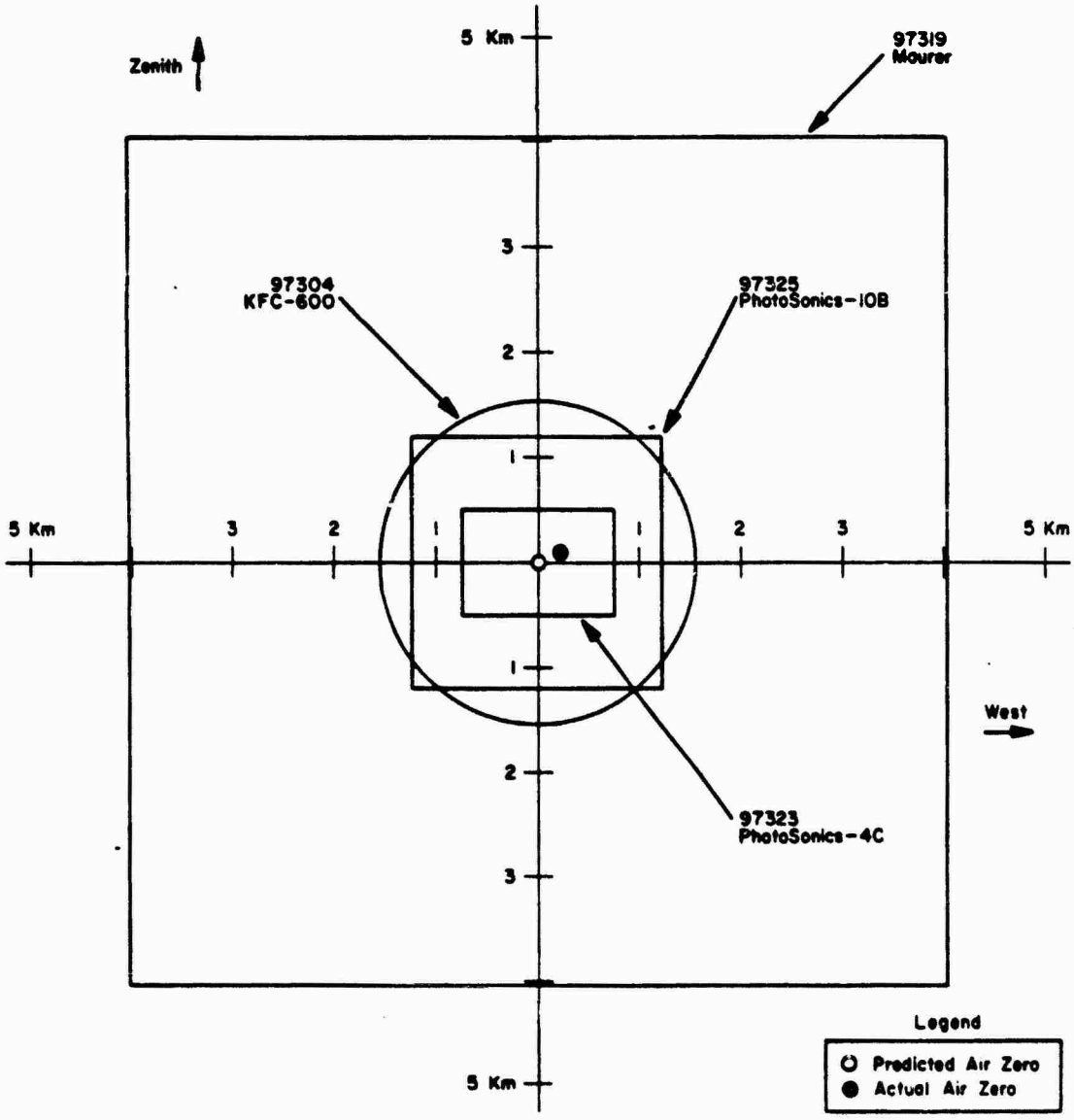

Figure 7.4 Fields of view for four Johnston Island cameras with predicted and actual air zero.

Pages 431 through 453 deleted.

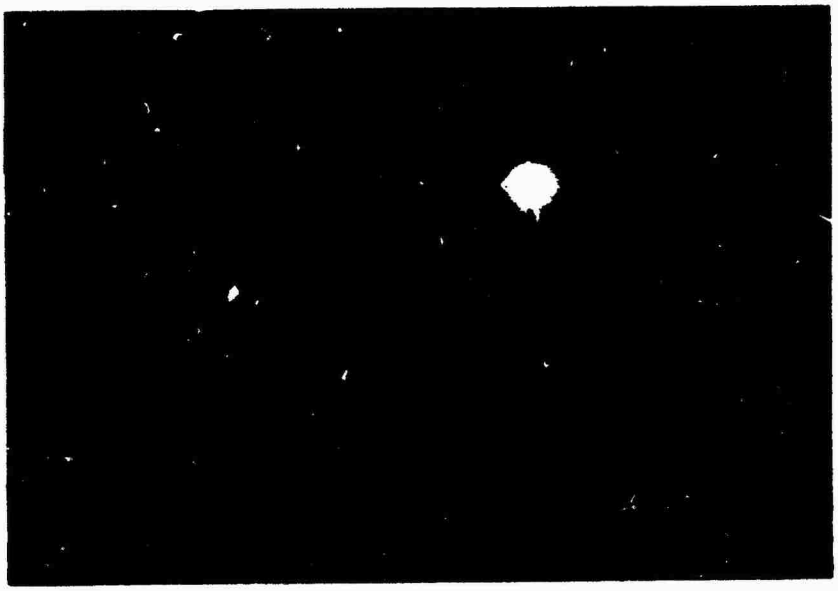

Figure 7.27 Tight Rope; fireball over Johnston Island at 0.2 second, taken from Aircraft 53120. Film 97121, Frame 1.

Figure 7.28 Tight Rope; torus at 65 seconds, taken from Aircraft 60376. Film 97209, Frame 21.

Pages 455 through 462 deleted.

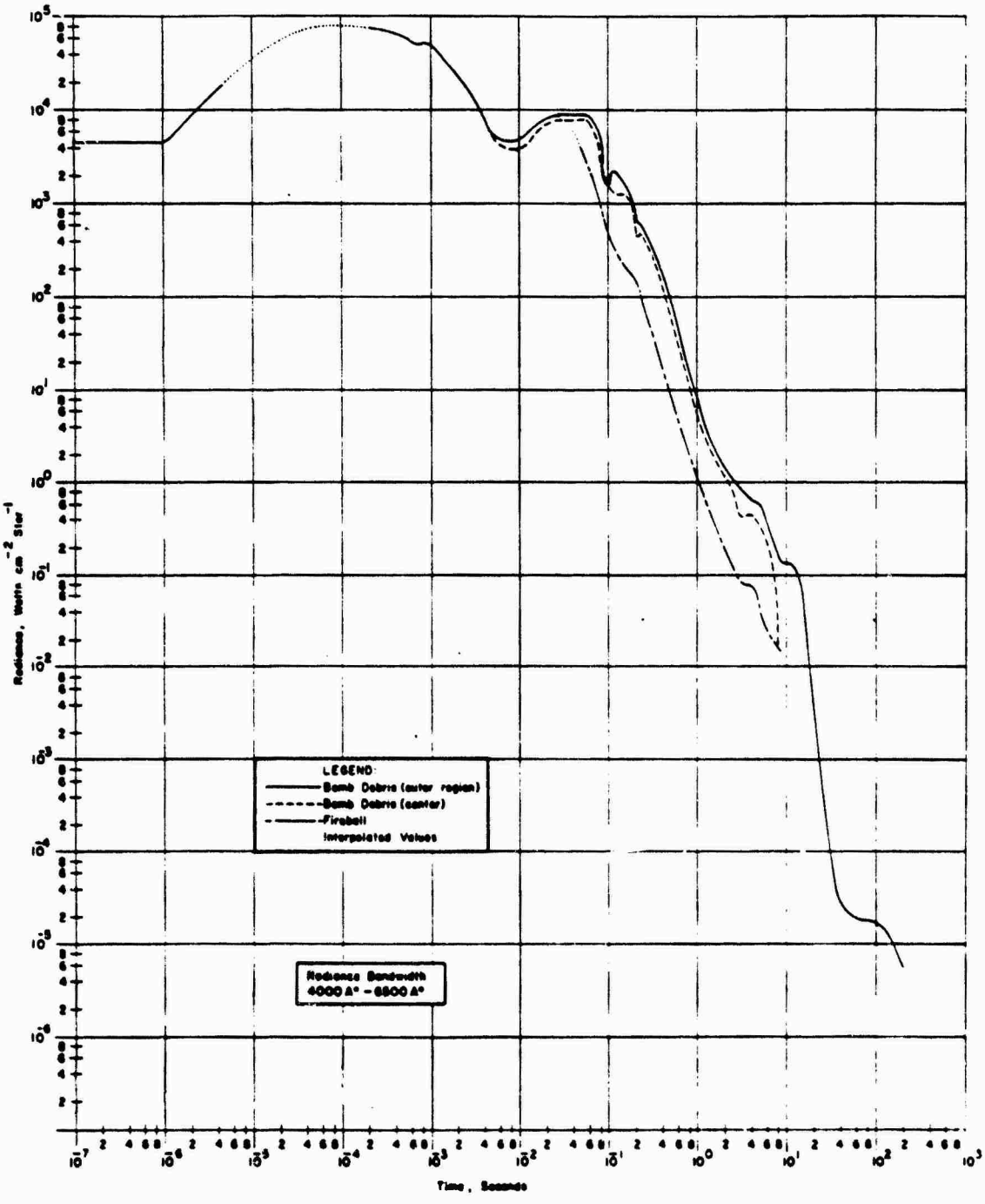

Figure 7.37 Tight Rope; radiance versus time curves.

Page 464-466 deleted.

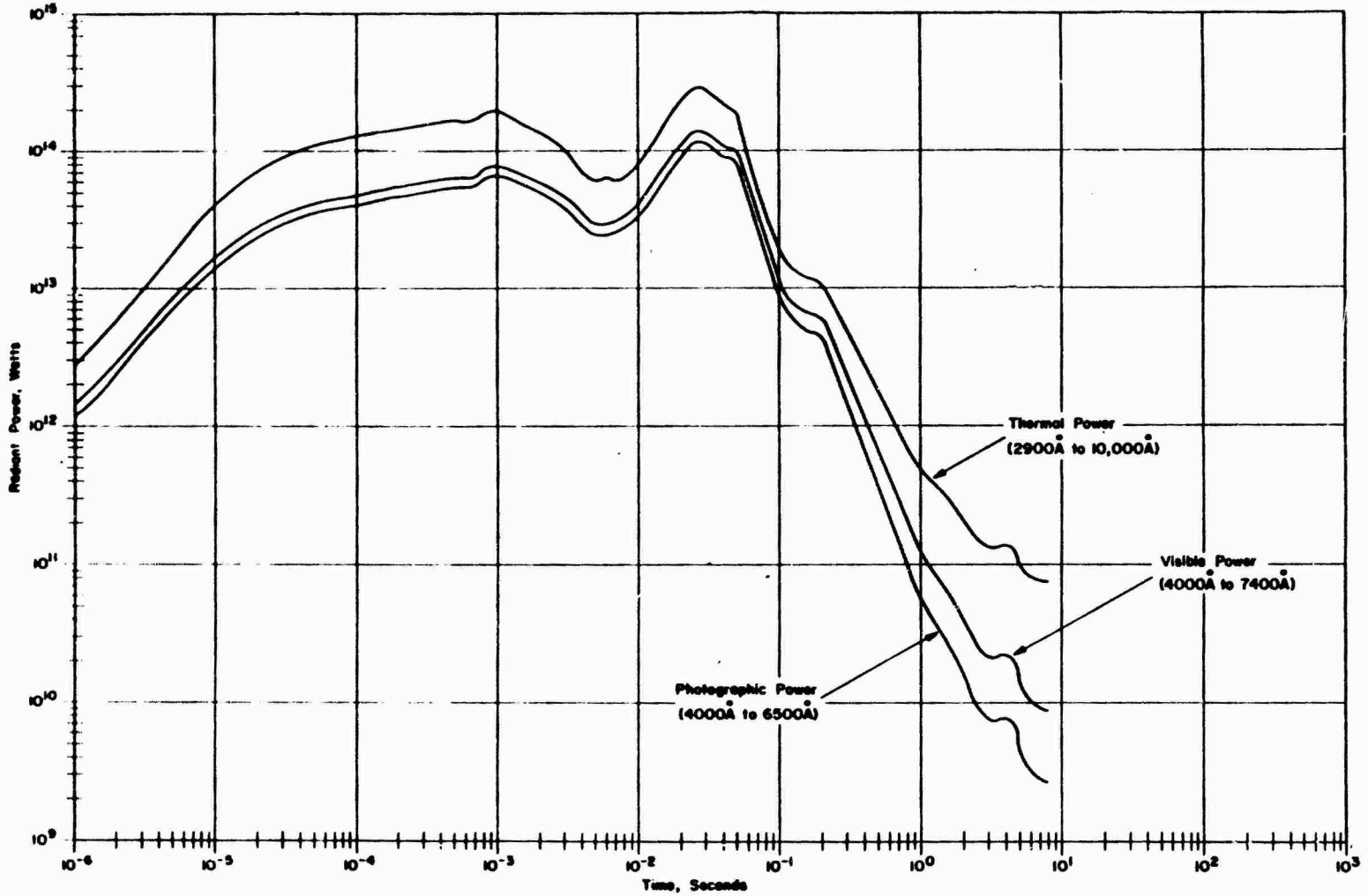

Figure 7.41 Tight Rope; radiant power versus time curves.

467-468 Pages 469 and 470 deleted.